Characterising the in vitro and in vivo function of the RhoG effector

DOCK4 during angiogenesis and ischemia.

Leander Stewart BSc

Submitted in accordance with the requirements for the degree of

Doctor of Philosophy

The University of Leeds

Leeds Institute of Cancer and Pathology

School of Medicine

Sept 2019

The candidate confirms that the work submitted is her own and that appropriate credit has been given where reference has been made to the work of others.

This copy has been supplied on the understanding that it is copyright material and that no quotation from the thesis may be published without proper acknowledgement.

The right of Leander Stewart to be identified as Author of this work has been asserted by her in accordance with the Copyright, Designs and Patents Act 1988.

Acknowledgements

I would like to express gratitude to my supervisors Dr Georgia Mavria and Prof Stephen Wheatcroft for their continued support and guidance throughout my PhD. I would also like to thank the British Heart Foundation for the funding for my PhD studies. I offer my deepest gratitude towards Dr Fiona Errington-Mais, for her patience, sage counsel, and encouragement throughout the past 4 years. The support and mentorship of multiple research fellows, PhD students, and laboratory staff across many research groups has enabled me to accomplish the research found within this thesis; including the research groups of Prof Stephen Wheatcroft and Prof Richard Bayliss. My most sincere appreciation to Dr Adam Odell, who greatly aided in developing my initial research skills throughout my first year of my PhD, and Dr Chiara Galloni, for her guidance in research but also for her friendship. To Dr Nadira Yuldasheva, for carrying out all of the HLI surgical procedures, described within this thesis, and also for her invaluable teaching and advice. And to Dr Natalie North, who also mentored me throughout my *in vivo* research training. To the staff of the FBS protein production facility, Dr Brian Jackson and Laura Wilkinson-Hewitt, for not only providing me with instrumental guidance but also friendship and support throughout the most challenging time period of my PhD.

I also wish to direct my deepest gratitude to my family for their patience, understanding, and emotional support throughout the past 4 years. Lastly to my son, Micah Stewart, who has provided me with the love and motivation to continue to persevere in my pursuit of personal and academic success.

Abstract

The RAC1 specific GEF, DOCK4, has been identified as an essential component in the Rho GTPase signalling pathway, imperative for correct vascular patterning and lumenisation during sprouting angiogenesis *in vitro*. As RAC1 has been previously implicated in the signalling events involved in vascular regrowth within a hypoxic environment, it was hypothesized that DOCK4 may be an important effector in the response to vascular injury and oxygen deprivation. To test this hypothesis, a DOCK4 depleted endothelial co-culture assay was carried out in both hypoxic and normoxic conditions. DOCK4 driven activation of RAC1 has been demonstrated under VEGF signalling, however FGF2 signalling pathways have also been strongly implicated in vascular response to blood vessel injury and hypoxia. Therefore, co-culture assays were carried out to assess sprouting angiogenesis with DOCK4 knockdown in response to FGF2 supplementation. Further, a heterozygous DOCK4 depleted murine model in ischemia studies using a model of HLI was employed together with LDI monitoring of vascular response and regrowth, comparing the response of heterozygous Dock4 KO mice and their WT littermate controls.

DOCK4 interacts with the CDC42 GEF DOCK9 but the molecular basis of the interaction is unknown, as is the role of GEF heterodimerization in cell signalling. This study aims to further understand the function of DOCK4 within a pathological sprouting angiogenesis while also investigating the mechanism of interaction between DOCK4 and DOCK9.

The two pro-angiogenic growth factors VEGFA and FGF2 drive different phenotypical growth responses during sprouting angiogenesis *in vitro*. DOCK4 was demonstrated as being an important component of FGF2 stimulated angiogenesis under hypoxia, indicating DOCK4 as important for mechanisms involved in the angiogenic response to ischemia. The specific

site of DOCK9 which interacts with the SH3 domain of DOCK4 was not elucidated during this study, however it was determined that DOCK9 proline rich regions identified as PRR 2, 3, 4, and 9 were unlikely to be involved in the interaction. The small molecule inhibitor QL-47 was demonstrated to be a potent anti-angiogenic compound with VEGFA stimulated ECs being particularly sensitive to QL-47. However, it is highly unlikely that the anti-angiogenic effects are due to disruption of the DOCK4-DOCK9 interaction, as the p.C628 cysteine residue was found to not be involved in DOCK4 SH3 domain interaction.

Understanding how Rho GTPases are regulated and mechanisms underpinning their activity will progress the understanding of events that drive blood vessel growth while gaining insight into dysregulation during angiogenic pathologies.

Table of Contents

Table of Figures

Thesis abbreviations

aFGF	Acidic fibroblast growth factor
AGK	Angiokit-tested
AP1	Activator protein-1
αVβ3	αV and integrin β 3
αVβ5	αV and integrin β 5
BPI	Branch point index
CDC42	Cell division control protein 42 homolog
CLI	Critical limb ischemia
DbL	Diffuse B-cell lymphoma
DH-PH	Dbl homology - pleckstrin homology domain
DHR1	DOCK homology region1
DHR2	DOCK homology region2
DLL1, 3, 4	Delta-like
DMEM	Dulbecco's modified eagle medium
DOCK	Dedicator of cytokinesis
DTT	Dithiothreitol
EC	Endothelial cell
ECM	Extracellular matrix
ELMO	Engulfment and Motility
eNOS	Endothelial nitric oxide synthase
ESAM	Endothelial cell-selective adhesion molecules
EV	Empty vector

F-actin	Filamentous actin
FBS	Foetal bovine serum
FGF	Fibroblast growth factor
FGFR	Fibroblast growth factor receptor
FHF1-FHF4	FGF homologous factors 1-4
G-actin	Globular proteins
GAP	GTPase activating proteins
GDI	Guanine nucleotide dissociation inhibitors
GDP	Guanine di-phosphate
GEF	Guanine nucleotide exchange factor
GF	Growth factor
GFP	Green fluorescent protein
GPCR	G protein-coupled receptor
GTP	Guanine tri-phosphate
HDAC7	Histone-deacetylase 7
HDF	Human Dermal Fibroblast
HEK 293T	Human Embryonic Kidney Cells 293T
HLI	Hind limb ischemia
HRP	Horseradish peroxidase
HSPG	Heparin sulfate proteoglycans
HUVEC	Human Umbilical Vein Endothelial Cells
IP	Immunoprecipitation
IPTG	Isopropyl β- d-1-thiogalactopyranoside
Jag-12	Jagged
JAM	Junction adhesion molecule

JNK	c-Jun N-terminal kinase
LB	Lysogeny broth
LDI	Laser Doppler Imaging
LDL	Low density lipoproteins
LVEM	Large Vessel Endothelial Medium
MAPK	P42/44 mitogen-activated protein kinases
MLCK	Myosin light-chain kinase
MLK	Mixed lineage kinase
MRCK	Myotonic dystrophy kinase-related CDC42 binding kinase
mTOR	Mammalian target of rapamycin
MYPT	Myosin light chain phosphatase
NFkB	Nuclear factor kappa-light-chain-enhancer of activated B cells
NOX	NADPH-dependent membrane oxidase
NMIIA	Non-muscle myosin IIA heavy chain
NPF	Nucleation- promoting factors
NRP	Neuropilin
NS	Non silencing
OD	Optical density
PAD	Peripheral artery disease
PAK	p21 activating kinases
PBS	Phosphate Buffered Saline solution
PDGF	Platelet derived growth factor
PH	Pleckstrin-homology

PI3K	Phosphatidylinositol-3-kinase
PlGF	Placenta growth factor
PKC	Protein kinase C
PKD	Protein kinase D
PLCγ	Phospholipase Cγ
PRR	Proline rich region
PVDF	Polyvinylidine difluoride membrane
RAC	Ras-related C3 botulinum toxin substrate
RFP	Red fluorescent protein
Rho	Ras homolog
RhoA	Rho GTPases member A
ROS	Reactive oxygen species
SGEF	Src homology 3 domain-containing Guanine nucleotide Exchange Factor
TIE1/2	Tie-like receptor tyrosine kinase
TK	Tyrosine kinase
TL	Total lysate
TVL	Total vessel length
VEGFA	Vascular endothelial growth factor A
VEGFR	Vascular endothelial growth factor receptor
VSMC	Vascular smooth muscle cells,
vWF	Von Willebrand factor
WASP	Wiskott–Aldrich syndrome protein
WAVE	WASP-family verprolin-homologous protein
WT	Wild type

Preface

The overarching aim of this thesis is to expand upon the understanding of the RhoG pathway (RhoG-DOCK4-RAC-DOCK9-CDC42) and its role in the process of angiogenesis. DOCK4 and its interaction with DOCK9 are the central components of the pathway, as together they drive some of the hallmarks of angiogenic growth, filopodia formation and sprouting (Abraham et al., 2015).

1   Introduction

1.1   The mammalian vascular system

The mammalian vascular system serves as a multifunctioning network of tubes, or hollow cords, which enables flow of blood for maintenance of cellular homeostasis, distribution of essential nutrients and oxygen in concert with removal of metabolic waste and carbon dioxide. It also allows the trafficking of growth factors (GFs), cytokines, hormones and immune cells around the body (Wacker and Gerhardt, 2011b). The vascular system is essential in maintenance of homeostasis of ionic concentration, physiological pH, body temperature, and glucose concentration (Wacker and Gerhardt, 2011b).

The cardiovascular system is an enclosed organ system composed of a contractile four chambered muscular pump, the heart, and a complex network of multicellular tubes organized into three subsystems based on structure and function; the arterial system, venous system, and the lymphatic system (Carmeliet, 2000), as is seen in figure 1.1.

The arterial system delivers blood from the heart to the other organs, tissues, and limbs of the body. Blood pumped from the right ventricle of the heart and flows through the pulmonary artery, allowing for oxygenation of the blood in concert with removal of carbon dioxide. Oxygenated blood then flows into the left atrium of the heart where it is pumped into the left ventricle. The left ventricle contracts to force the blood to flow through the aorta, the largest of the arteries. Blood flows at high pressure through the aorta into arteries, arterioles, and capillaries of decreasing diameter to the other organs, brain, and tissues of the body (Udan et al., 2013).
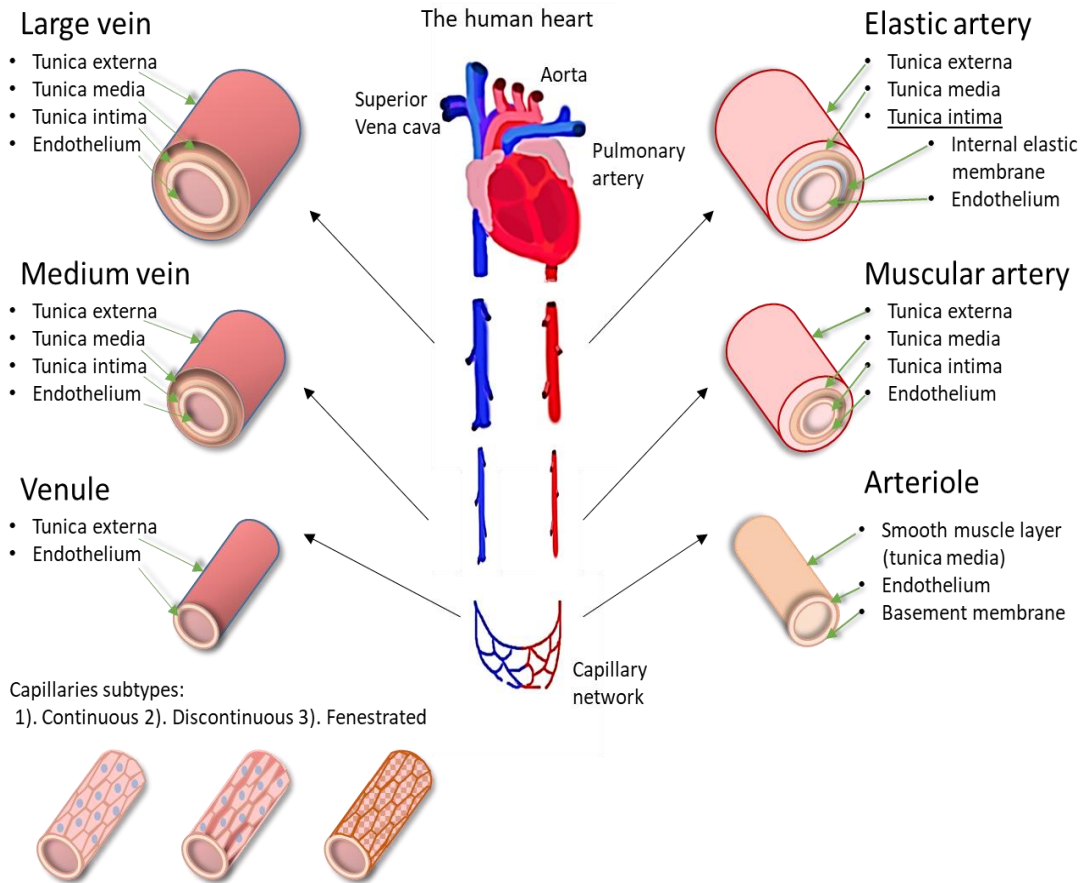
Figure 1-1 The human circulatory system

Diagram of the human circulatory system: the heart, arteries, veins and capillaries. Arteries possess three structural layers: the Tunica Adventitia, Tunica Media, and Tunica Intima. The Tunica Adventitia is the outer layer of arteries and consists of connective tissue, collagen, and elastic fibres. The middle layer, the Tunica Media, contains smooth muscle cells and elastic fibres. The Tunica Intima is the inner most layer of the arteries and is comprised of endothelial cells. There are three distinct types of arteries: elastic arteries, muscular arteries, and arterioles. Veins also have three layers; the Tunica Adventitia, Tunica Media, and the Tunica Intima. The Tunica Media of veins possesses an irregular covering of vascular smooth-muscle cells and pericytes. In the lumen of veins also lie valves which act to prevent the backflow of blood through the less pressurized vascular structures. Capillaries are small, thin vessels comprised of a single layer of flattened ECs with no muscular layer. There are three types of capillaries: continuous, fenestrated, and discontinuous.

The venous system allows blood to flow from the periphery, tissues, and organs through vessels which increase in diameter from venules to veins and then into the vena cava, the largest of the veins. Through the vena cava blood flows back to the heart, entering through the right atrium (Udan et al., 2013).

The lymphatic system serves as a system of vessels that provide passage for interstitial fluid to flow from the organs and tissue to re-enter circulation through the subclavian vein (Udan et al., 2013).

The vessels forming the three subsystems possess unique composition allowing for their distinct function. Within humans and rodents the cardiovascular system is the first organ formed during embryogenesis (Udan et al., 2013). Formation of the precursor structures of the cardiovascular system begins during the early stages of embryo development through a process called vasculogenesis (Galan Moya et al., 2009). Once formed the vascular structures may further specialize to adopt characteristics essential for the vessel's physiological function within its specified organ or tissue.

Dysregulation of endothelial cells (ECs) due to vascular injury or cellular dysfunction can contribute towards many pathological conditions including vascular disorders: atherosclerosis, peripheral artery disease, hypertension, and inflammatory disorders such as sepsis and inflammatory syndromes to name a few (Galley and Webster, 2004; Vanlandewijck et al., 2018).

1.2   Blood vessels

Vascular structures may display some variability in functional characteristics to allow for specialization within the context of their location. Despite these differences, human blood vessels retain the same histological organization of a single layer of ECs, with a luminal-abluminal polarity, located on the intima of all vessels. The layer of ECs form into hollow cords with the abluminal side of the EC layer connected to vascular basement membrane

(Lammert and Axnick, 2012) and a layer mural cells, smooth muscle cells and pericytes, at the external side of the basement membrane (Lammert and Axnick, 2012). Once blood vessels have fully formed and blood flow is established, ECs exhibit features of planar cell polarity in response to blood flow (Lizama and Zovein, 2013).

1.2.1 The endothelium

The endothelium is a heterogeneous and multi-functional disseminated organ which not only forms vascular structure but is vital in maintenance of a non-thrombogenic blood-tissue interface responsible for regulating blood flow, vascular tone, thrombosis, thrombolysis, and platelet adherence (Cines et al., 1998). ECs which form the endothelium also function in secretory, synthetic, metabolic, and immunologic roles in addition to forming a semi-permeable barrier (Cines et al., 1998).

1.2.2 Growth of blood vessels

In the healthy adult, vasculature and ECs are largely quiescent with the exception of during pregnancy, the menstrual cycle, and wound healing (Adams and Alitalo, 2007; Rizov et al., 2017). ECs may remodel their morphology, to form new vessel under pathological conditions, such as tissue ischemia, in order to meet the metabolic needs of the tissue (Egami et al., 2006).

1.2.2.1 Vasculogenesis

The vascular system first forms through vasculogenesis, a process initiated when endothelial precursor cells differentiate from blast-like bi-potential cells called angioblasts (Carmeliet, 2000), as depicted in figure 1.1. The ventral floor of the dorsal aorta gives rise to mesenchymal cells. The pluripotent mesenchymal cells differentiate into angioblasts that in turn differentiate into intermediate pre-ECs; cells capable of differentiating into either a committed haematopoietic cell line or ECs. ECs may also display plasticity to transdifferentiate into mesenchymal cells and intimal smooth muscle cells. Once the EC phenotype has been acquired, further specialisation may take place to adapt the cell to the

specific type and location of the vascular structure (Choi et al., 1998; Galley and Webster, 2004).

Forming vascular structures recruit smooth muscle expressing mural cells, such as vascular smooth muscle cell (VSMC) and pericytes. These cells form the smooth muscle layer which envelopes vascular structures on the external surfaces of the basement membrane at the abluminal side of the endothelium (Drake et al., 1998; Hirschi and D'Amore, 1996). The phenotypical features and organisation of mural cells associated with a vascular structure varies based on size and type of vascular structure.
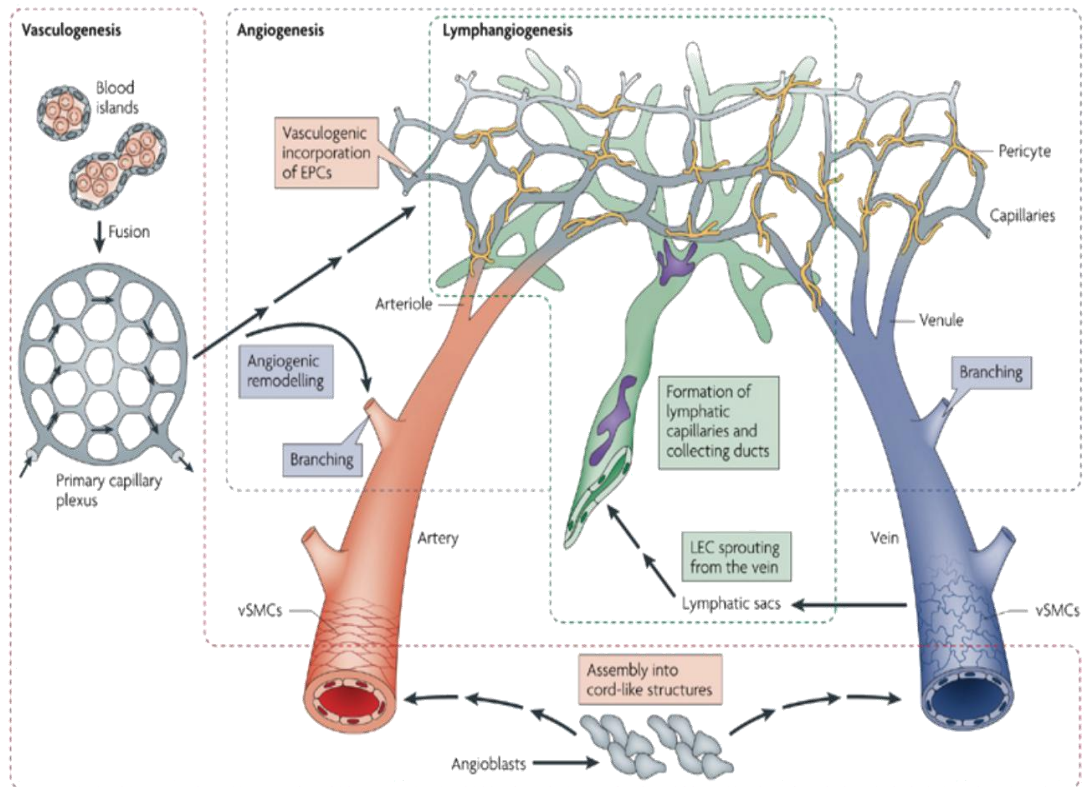
Figure 1-2 Mechanisms of vascular growth

During embryogenesis the primitive capillary plexus is formed through differentiation and expansion of angioblasts derived from the mesoderm, which assemble into cords, forming the beginning of vascular structures. Further remodelling, expansion, and recruitment of smooth muscle cells and pericytes giving rise to blood vessels and lymphatic vessels through the process of angiogenesis and lymphangiogenesis respectively. Image taken with permission from Adams & Alitalo (2007).

1.2.2.2 Mural cells

Mural cells provide scaffold to vascular structures and are responsible for contraction and dilation of blood vessels. Mural cells directly contact ECs to co-regulate vascular function via paracrine signalling and direct physical contact. Direct physical contact between mural cells and ECs allow for mechanical signalling through contractile forces via junction complexes between the two cell types; which include (but are not limited to) β-catenin-based adherent junctions, N-cadherin, cell-adhesion molecules, and extracellular matrix (ECM) components (Gerhardt et al., 2003; Vanlandewijck et al., 2018).

VSMCs have been associated with larger vessels and have not been observed to embed into the basement membrane of vascular structures, a characteristic of pericytes (Gerhardt et al., 2003). Arterioles are coated with a thick and continuous layer of VSMCs and elastic and collagenous fibres (Cleaver and Melton, 2003; Vanlandewijck et al., 2018) that control contraction and relaxation of arterioles.

Pericytes form an intermittent single cell layer over capillaries and post-capillary venules, and anchor to ECs through adhesion plaques. Unlike VSMC, pericytes embed into the basement membrane of vascular structures, allowing direct contact between pericytes and the endothelium. Pericytes extend longitudinal cytoplasmic projections along the length of blood vessels, to allow for integration of signalling along the vessel and may connect multiple capillaries within the vasculature (Rucker et al., 2000). Pericytes may also develop contacts between discontinuities in the vessel basement membrane, through peg-and-socket contacts (Rucker et al., 2000; Vanlandewijck et al., 2018).

1.2.3 **Vascular structures**

There are a number of different types of vascular structures which form the circulatory system, to allow for circulation of blood in tune to the beat of the heart. The differences in structure of each vessel type aids in the particular function required for

maintaining circulation of blood to and from the heart, regulation of blood pressure, exchange of gases and substances, and movement of immune cells.

1.2.3.1   Arteries

Arteries are the largest of the vascular structures and are constructed of concentrically arranged smooth-muscle cells, which form elastic vessel walls made to withstand higher blood pressures (Shepherd, 1983; Aaronson et al., 2012). Arteries possess three structural layers: the Tunica Adventitia, Tunica Media, and the Tunica Intima. The Tunica Adventitia is the outer layer of arteries and consists of connective tissues, collagen, and elastic fibres. The middle layer, the Tunica Media, contains the smooth muscle cells and elastic fibres, this layer regulates vascular contraction, relaxation, and vascular tone (Shepherd, 1983; Aaronson et al., 2012). The Tunica Intima is the inner most layer of the arteries and is comprised of ECs. The Tunica Intima lies directly in contact with the arterial blood flowing. A hollow lumen lies throughout the centre of the arteries, through which blood flows (Shepherd, 1983; Aaronson et al., 2012). The lumen of arteries are typically smaller than that of veins, a structural feature specialised to aid in the high pressure of blood flow from the heart (Shepherd, 1983; Aaronson et al., 2012).

There are three distinct types of arteries: elastic arteries, muscular arteries, and Arterioles. Elastic arteries, the aorta and pulmonary artery, have thin vessel walls with a high level of elastin to aid in expansion and recoil of the vessels in response to the high-pressured flow of blood from the heart. Muscular arteries contain a smooth muscle rich wall capable of modifying blood flow through the vessel via contraction and relaxation of the muscular layer. Arterioles are the smallest of the arterial vessels which contain concentric rings of smooth muscle within the tunica media layer and connect blood flow from other arteries to capillary beds (Cleaver and Melton, 2003; Sandoo et al., 2010; Aaronson et al., 2012).

9

1.2.3.2 Veins

Veins retain a similar structure to that of arteries with the same three layers; the Tunica Adventitia, Tunica Media, and the Tunica Intima (Shepherd, 1983; Aaronson et al., 2012). However, the Tunica Media layer of veins is considerable thinner when compared to arteries. The cellular structure of the Tunica Media also differs between the two vascular sub-groups, with the intermediate layer of arteries primarily being formed by a thick layer of VSMCs and veins possessing an irregular covering of VSMCs and pericytes (Aaronson et al., 2012).

Throughout the lumen of veins also lie valves which act to prevent the backflow of blood through the less pressurised vascular structures (Aaronson et al., 2012).

1.2.3.3 Capillaries

Capillaries are small, thin vessels comprised of a single layer of flattened ECs with no muscular layer. There are three types of capillaries continuous, fenestrated, and discontinuous (Shepherd, 1983; Aaronson et al., 2012; Bennett et al., 1959). While capillaries do not have an adventia layer, continuous capillaries possess intermittent pericytes. Fenestrated capillaries possess fenestrations, or pores, which aid in movement of larger molecules. Discontinuous capillaries are only found in the liver. The structure formed between the ECs and hepatocytes creates clefts through which macromolecules and blood cells to pass through (Galley and Webster, 2004; Vanlandewijck et al., 2018).

Capillaries connect arterioles to venules and facilitate passive diffusion and pinocytosis of nutrients and cellular wastes between the blood and the tissue cells. The absence of the muscular layer, thinness of the capillary walls, and distribution of intercellular junctions, aid in movement of substances and white blood cells between circulation and tissues (Galley and Webster, 2004; Vanlandewijck et al., 2018).

1.2.3.4 Collateral arteries

Collateral arteries are narrow arterioles which provide circulation interconnections between nearby arteries or arterioles (Antoniucci et al., 2002; Schaper, 2009; Faber et al., 2014; Simons and Eichmann, 2015). Networks of native collateral arteries function to divert blood flow in instances of arterial occlusion, allowing for continuation of circulation to the affected tissue and organ (Heil et al., 2006; Schaper, 2009; Simons and Eichmann, 2015; Ramo et al., 2016). Once blood flow to the collateral circulation has been initiated, sheer force of the blood flow drives arteriogenesis of the collateral arteries to develop into efficient conductance arteries (Ramo et al., 2016). The number and patterning of pre-existing collateral arteries prior to an occlusion greatly affects the adequacy of the diversion of blood flow to the affected tissue/organ (Ramo et al., 2016).

1.2.3.5 Lymphatic vessels

Lymphatic vessels make up the lymphatic component of the vascular system and are functionally and structurally unique from the blood vessel circulatory element of the vascular system. They are structurally unique from blood vessels, with features which aide in their function to uptake fluid, macromolecules, and cells. Lymphatic vessels are formed of a single layer of attenuated, non-fenestrated, ECs (Schmid-Schönbein, 1990; Aukland and Reed, 1993).

The lymphatic system serves to aid in multiple biological functions; primarily in regulation of fluid and fluid pressure within the interstitium, movement of fluid and macromolecules to and from blood circulation, as well as immunological functions involving movement of immune cells and antigens between tissues and lymph nodes (Pepper and Skobe, 2003).

1.3 Mechanisms of blood vessel growth

1.3.1 **Sprouting angiogenesis**

Expansion and remodelling of the vascular system beyond vasculogenesis is propagated via angiogenesis; either through sprouts branching (as seen in figure 1.3) from pre-existing blood vessels (sprouting angiogenesis) or through splitting of existing vessels to a larger number via intussusception (Adams and Alitalo, 2007). In adults, angiogenesis occurs typically in response to nutrient and oxygen deprivation, tissue damage, or in response to aberrant cell signalling arising from pathological stimuli (Egami et al., 2006; Potente et al., 2011). Parenchymal cells respond to hypoxia by secreting pro-angiogenic GFs such as vascular endothelial growth factor A (VEGFA; described in detail in section 1.3.6.1).

During sprouting angiogenesis, quiescent ECs lining blood vessels excrete protease to degrade the basement membrane, break away from the vessel wall, and alter their morphology while they rapidly proliferate and invade the surrounding tissue to form new sprouts (Blanco and Gerhardt, 2013). Under pro-angiogenic signalling, ECs coordinate in a migratory hierarchy of leading 'tip cells' and trailing 'stalk cells' dependent upon local chemotactic gradients and juxtacrine Notch signalling (Jakobsson et al., 2010). At the angiogenic front this organization of cells is malleable, with tip cells and stalk cells frequently changing position (Jakobsson et al., 2010).

VEGFA stimulation of the VEGF-receptor 2 on ECs induces a Delta-Notch signalling response which prompts a tip-cell phenotype (Jakobsson et al., 2010; Hellstrom et al., 2007). Within mammals the Notch signalling pathway regulates angiogenesis through multiple Notch receptors (Notch1-4) and their interactions with multiple membrane bound ligands: Delta-like (DLL1, 3, 4) and Jagged (Jag-12) (Lawson et al., 2002; Iruela-Arispe, 2017). VEGFA driven Notch receptor-ligand interaction drives proteolytic cleavage of the Notch receptor and release of the intracellular domain which relocates to the nucleus to function as a

transcription factor, binding to DNA and modulating gene expression (Lawson et al., 2002; Iruela-Arispe, 2017).

Expression of Delta-like-4 (Dll4) stimulates Notch receptors on neighbouring ECs, initiating neighbouring cells to adopt a stalk cell morphology through suppression of VEGF-receptor 2 production (Adair and Montani, 2010). Stalk cells display a much higher level of proliferation with lower migratory behaviour than that of tip cells (Adair and Montani, 2010).

Tip-cells produce multiple filopodia at the distal end of the cord (as depicted in figure 1.3) which probe the extracellular environment for growth cues aiding in organised and guided growth through detection of a gradient of pro and anti-growth signalling cues (Gerhardt et al., 2003; Wacker and Gerhardt, 2011b). Upon the meeting of two EC sprouts, the growths connect and join to create an enclosed vessel in a process termed anastomosis (Wacker and Gerhardt, 2011b). ECs wrap and form a polarised luminal-abluminal organization which initiates cord hollowing and subsequent lumenisation of the newly formed vessel (Wacker and Gerhardt, 2011b).
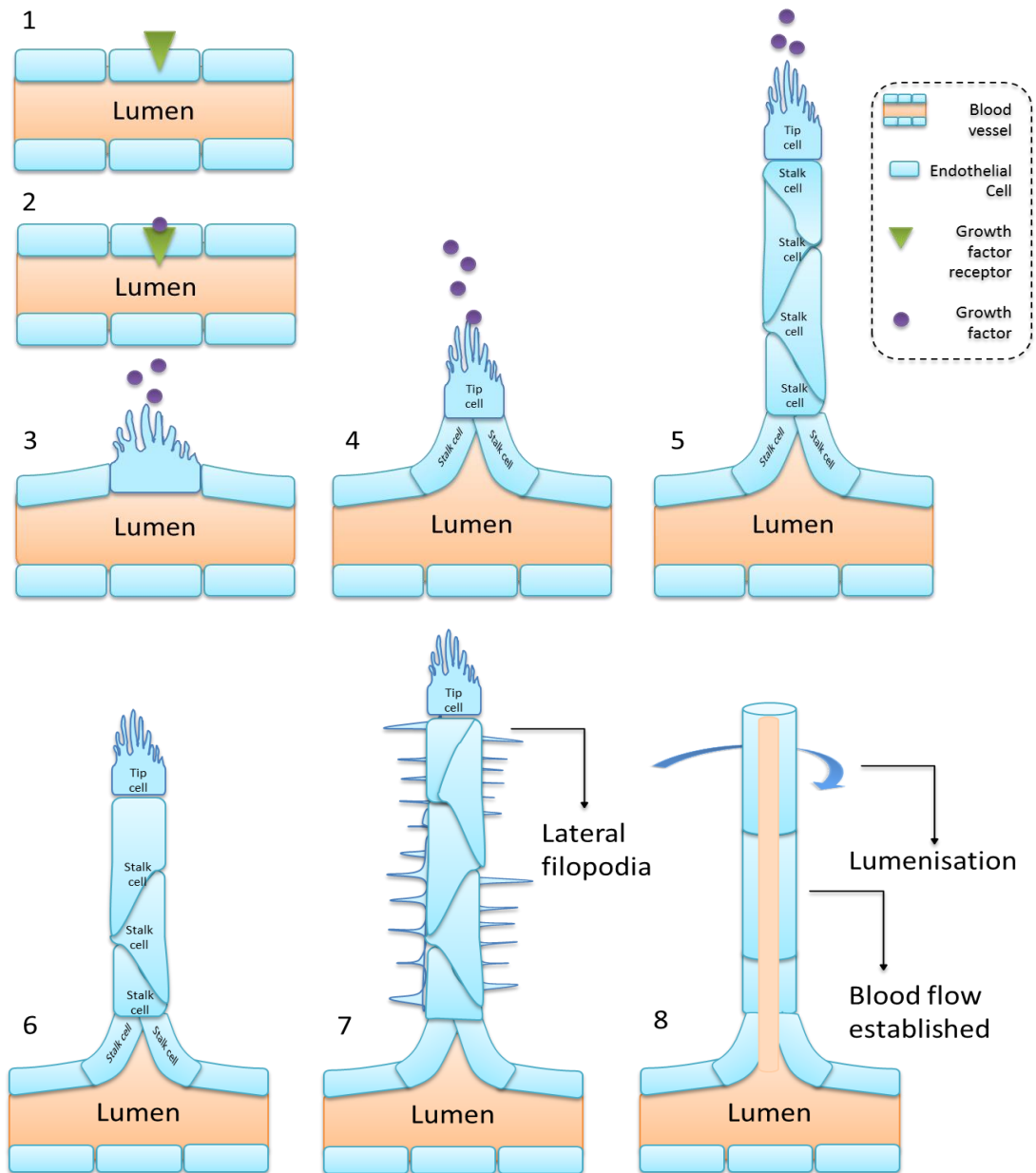
Figure 1-3 Basic schematic diagram of sprouting angiogenesis

During sprouting angiogenesis quiescent ECs within a blood vessel (1) respond to binding of an extracellular ligand or cue to a transmembrane receptor (2). This initiates tip cell selection and filopodia production at the leading edge of the tip cell (3). Intracellular signalling event within the tip cell convey a signal to adjacent cells, prompting a stalk phenotype in the neighbouring cells (4). Stalk cells rapidly proliferate to establish an elongated cord of cells (5). Depletion of GF (6; or contact with other growing cords) is hypothesized to results in extension of lateral filopodia (7). Luminal-abluminal polarity is established within ECs of the cell cord, initiating lumenisation.

1.3.2 **Endothelial cell filopodia**

Filopodia are actin-rich cytoplasmic protrusions found on actively motile cells in 3D spaces, they are also found in ECs and were initially observed on tip cells. EC filopodia probe the surrounding environment for chemical and mechanical signals and direct migration towards chemotactic signals such as VEGF. The interaction between filopodia and the ECM produces points of cell-ECM attachment allowing generation of tension necessary for propulsion towards the direction of migration (Blanco and Gerhardt, 2013). Interactions between filopodia and chemotactic cues promote rapid extension and directional growth of the vessel sprouts while guiding correct patterning of the newly forming vessels (DeLisser, 2011).

Recently filopodia have been described at lateral sites (Abraham et al., 2015) which develop along a tubule and give rise to lateral sprouts (DeLisser, 2011). Lateral filopodia are thus required for the dynamic remodelling of newly forming vessels and correct patterning prior to lumen formation (DeLisser, 2011). Once lateral junctions between ECs establish, ECs may polarize and initiate lumen formation. The formation of filopodia requires changes of the actin cytoskeleton with rapid F-actin polymerisation proceeded by actin contraction within the projections (Blanco and Gerhardt, 2013).

While filopodia promote sprouting both *in vivo* and in 3D tissue culture models (DeLisser, 2011; Hetheridge et al., 2011), lamellipodia have been shown to promote EC migration in a 2D substratum. Interestingly when filopodia are inhibited, lamellipodia-like structures may promote the growth of blood vessels *in vivo* (Gerhardt et al., 2003).

1.3.3 **Lumen Formation**

Once the blood vessels have expanded through the process of filopodia-driven sprout formation, the blood vessels have to form enclosed tubes to allow blood flow and gain functionality. During angiogenic sprouting, ECs migrate as cords that form a hollow interior, or lumen, as they grow through and invade the surrounding matrix (Iruela-Arispe

and Davis, 2009). The process of lumen formation is complex and the cellular and molecular mechanisms are only partially understood. Multiple mechanisms have been described, including cord hollowing, cell wrapping, cell hollowing, budding, and cavitation (Lammert and Axnick, 2012). Of those mechanisms cell and cord hollowing are those that have been investigated in greater detail. Cell hollowing entails formation of an intracellular vacuole which expands through neighbouring ECs in a cord, giving rise to the lumen (Lizama and Zovein, 2013). Cord hollowing involves either the invagination of unicellular membranes; a hollow centre forming between multicellular cords (Iruela-Arispe and Davis, 2009); or formation of a lumen at sites of lateral EC-cell adhesions (Strilic et al., 2009).

Before lumen formation may take place, ECs must acquire polarity through recruitment of proteins to the apical membrane. One such protein is the glycoprotein podocalyxin, the accumulation of which at the apical domain marks initiation of the process of lumen formation (Sigurbjornsdottir et al., 2014). This establishment of luminal-abluminal polarity results in accumulation of a negative charge in the apical surface and opening of the lumen via electrostatic repulsion (Sigurbjornsdottir et al., 2014; Debruin et al., 2014; Gebala et al., 2016). Cord hollowing has been more widely accepted as the process by which lumens form *in vivo*, although the latest studies in zebrafish show that within intersegmental vessels the apical membrane expands through both laterally adjacent, and single cells to form the lumen (Gebala et al., 2016).

1.3.4 Blood vessel elongation

During angiogenesis, growth of blood vessels proceeds not only through proliferation of ECs and development of new sprouts but also through elongation of a developing tubule that fuses with other growing or established blood vessel. Elongation may take place at the single cell level, or results from proliferation of cells arranged in a cord (Gebala et al., 2016). Cell elongation occurs through internally driven remodelling of the cytoskeleton which allows cells to grow in a directional fashion (Gebala et al., 2016).

Interestingly, brain microvascular cells resist cell elongation and minimize lateral cell-cell junctions in response to curvature and sheer stress, resulting in the characteristic radial arrangement of cells, as opposed to axial, within the brain micro-vessels (Merks et al., 2006). Therefore, the ability of ECs to elongate can have profound effects on the structure and function of blood vessels (Merks et al., 2006). Little is known about the molecular mechanisms underlying blood vessel elongation, at the single or multi-cellular level. Within a 3D organotypic angiogenesis model tubules stimulated with the GF fibroblast growth factor (FGF) develop an elongated phenotype (Scarcia M, unpublished data), however it is not known whether this is due to cells becoming more elongated, or that cells proliferate more at the axial orientation. However, other studies have described FGF as inducing both proliferation of ECs and elongation of individual cells (Lee and Kay, 2006; Ornitz and Itoh, 2015).

1.3.5 Arteriogenesis

Arteriogenesis describes a mechanism through which pre-existing collateral arterioles (described in 1.2.3.4) remodel from narrow vessels with little to no blood flow to become large conducting arteries, in response to sheer stress following occlusion of a secondary supply blood vessel (Antoniucci et al., 2002; Schaper, 2009; Faber et al., 2014). Unlike angiogenesis, arteriogenesis is initiated by mechanical forces and has thus far been shown to occur without stimulation of hypoxic factors (Heil et al., 2006; Grant and Karsan, 2018). Sheer stress has been seen to drive monocyte recruitment to the collateral arteries, leading to monocyte and endothelial secretion of GFs cytokines and proteases; driving matrix degradation, proliferation of smooth muscle, and enlargement of the collateral arteries (Ramo et al., 2016).

1.3.6 Growth factor signalling

Chemical stimulation which drives the growth of blood vessels integrates the activity of a diverse repertoire of proteins including GF signalling molecules, cell surface receptors,

integrins, and prostaglandins, just to name a few of the many components driving the complex process of blood vessel growth (Ucuzian et al., 2010; Simons et al., 2016). The GF signalling pathways, VEGF and FGF, are two pathways that have been described to drive angiogenesis in similar but unique ways. Canonical VEGF signalling has been well described in the context of embryogenesis and development, in addition to the vascular response to hypoxia (Ucuzian et al., 2010; Simons et al., 2016). VEGF signalling has been implicated in driving tip/stalk cell selection. Canonical FGF signalling has been strongly implicated in response to wound healing and drives a highly proliferative endothelial phenotype (Ornitz and Itoh, 2015). This section will overview the two signalling pathways in the context of vascular biology and pathologies related to dysregulation of the two pathways.
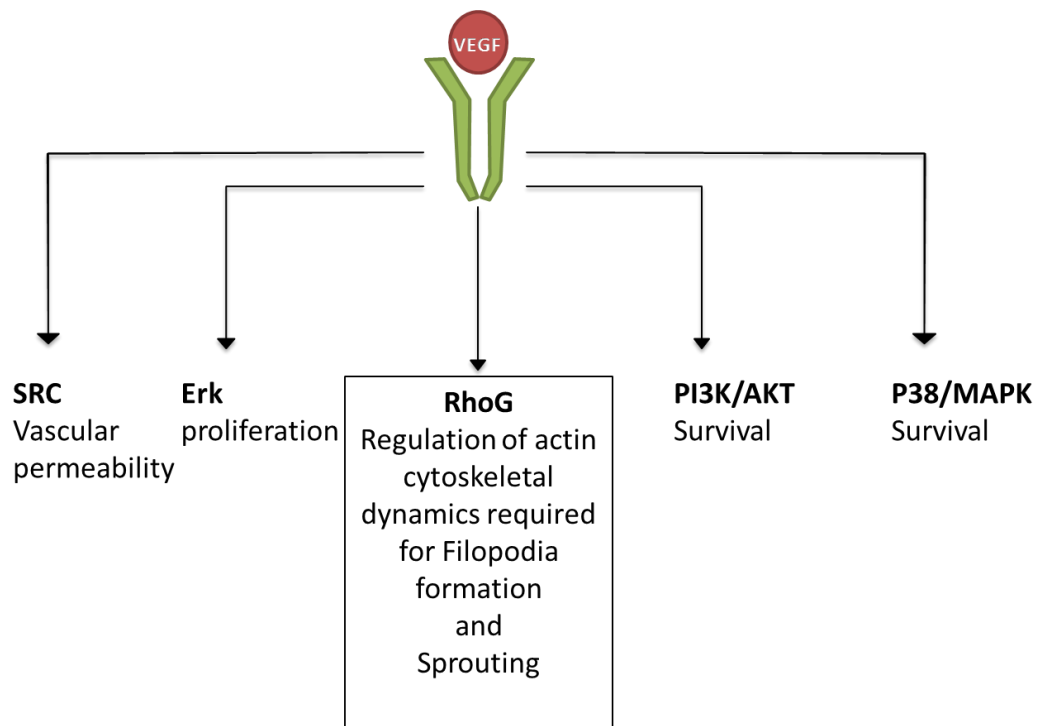
Figure 1-4 Schematic diagram of canonical VEGF signalling mechanisms in ECs

Binding of a VEGF ligand leading to homodimerisation of VEGF receptors driving intracellular tyrosine kinase activity of the receptor. Activated VEGF receptor leads to activation of signalling pathways Src, Erk, Rho GTPase, PI3K/AKT, and P38/MAPK.

1.3.6.1 Vascular endothelial growth factor

VEGF signalling is complex, with the potential to stimulate multiple cell surface receptors and subsequent activation and integration of a vast number of cell signalling pathways. For the aforementioned reasons, only VEGF characteristics and signalling components relevant to this report and the primary VEGF signalling components shall be discussed in detail within this introduction.

VEGFs are a sub-group of the platelet-derived GF family of cysteine-knot GFs (Ucuzian et al., 2010; Simons et al., 2016). VEGF is an EC mitogen that acts as a major regulator of blood vessel formation through vasculogenesis, angiogenesis, and arteriogenesis, in addition to maintenance and function of vascular structures (Ucuzian et al., 2010; Simons et al., 2016).

During sprouting angiogenesis VEGF binds to the VEGF receptor of the ECs and controls directional vascular growth through a chemotactic gradient, created via VEGF secreted by oxygen deprived cells (Gerhardt et al., 2003). Both VEGF and the VEGFR expression are upregulated within angiogenic sprout tip cells, with VEGF antibody inhibition leading to significant decrease in micro-vessel sprouting (Gerhardt et al., 2003; Brown et al., 1996b).

There are several variants of VEGF, vertebrate VEGFs A–D, placenta GF (PlGF), Parapoxvirus VEGFE and snake venom VEGFF. Each variant differs in their affinity for the different VEGF receptor subtype, of which there are 3, as well as their ability to bind co-receptors and initiate homodimerisation/heterodimerisation of receptor complex formation (Simons et al., 2016). The type of VEGF molecule driving a signalling response dictates the activity and complex formation of the target receptor, thus regulating the downstream cellular response to binding of the VEGF ligand (Simons et al., 2016).

VEGFA is the classical VEGFR activating ligand, and is often referred to simply as VEGF. VEGFA has been strongly characterised as a primary component in proliferation,

survival, and migration of ECs (Simons et al., 2016). VEGFA has multiple isoforms, each resulting from alternative splicing of the same gene product. Each isoform varies in their ability to activate the VEGF receptor, due to the differences in their affinity for binding co-receptors, such as neuropilin (NRP) family members NRP1 and NRP2 and to heparin sulfate proteoglycans (HSPGs) (Simons et al., 2016).

VEGF receptors act as receptor tyrosine kinases and binding of a VEGF ligand leads to homodimerisation of VEGF receptors driving intracellular tyrosine kinase activity of the receptor (as is seen in figure 1.4). Activated VEGF receptor leads to activation of signalling pathways Src, Erk, Rho GTPase, PI3K/AKT, and P38/MAPK (Iruela-Arispe, 2017).

Each sub-type of the VEGFR greatly differ in effect following ligand binding (Iruela-Arispe, 2017). There are numerous VEGF receptor subtypes with VEGFR1, VEGFR2, and VEGFR3 being the best characterised. VEGFR1 is a negative regulator of angiogenesis which is expressed by blood vascular ECs, macrophages, trophoblasts, tumour cells, and other cell types (Wu et al., 2006; Tsuchida et al., 2008) and can exist in a membrane bound or secreted form. VEGFA, VEGFB, and PIGF are the known canonical ligands which bind to VEGFR1.

VEGF binds to VEGFR1 with a higher affinity than to VEGFR2, however VEGFR1 has not been seen to activate a downstream signalling response and is therefore assumed to act as a decoy receptor, potentially sequestering free VEGF molecules (Hiratsuka et al., 1998; Iruela-Arispe, 2017). Constitutive knockout of VEGFR1 in a murine model is embryonic lethal on day E9 due to excessive EC overgrowth (Fong et al., 1995). VEGFR2 is expressed on blood vascular ECs and to a lesser degree on the surface of lymphatic vascular ECs (Simons et al., 2016). VEGFR2 is known as the primary endothelial receptor responsible for conferring the mitogenic signal induced by VEGF. VEGFR2 is canonically activated by VEGFA and processed VEGFC and VEGFD. VEGFR2 may also be non-canonically activated via multiple mechanisms: Shear stress due to changes in blood flow; the bone morphogenic protein antagonist gremlins, which has been seen to bind VEGFR2 with a similar affinity of VEGF and is able to

stimulate similar downstream activity (Mitola et al., 2010); Galectin-1, a β-galactoside-binding protein, which prompts phosphorylation of VEGFR2 extending cell surface retention of the receptor, with inhibition of galectin-1 greatly reducing tumour associated angiogenesis; Lactate has been observed to upregulate expression of VEGF and VEGFR2 (Kumar et al., 2007) as well as upregulating the ligands which activate the latter (Ruan and Kazlauskas, 2013); Low density lipoproteins (LDL) may negatively affect VEGFR2 activity, with presence of LDL leading to a reduced endothelial response to VEGFA and a decrease in VEGFR2 expression. Unlike VEGFR1, constitutive VEGFR2 deletion in a murine model is embryonic lethal on day E9 due to insufficient EC lineage commitment (Simons et al., 2016; Sakurai et al., 2005; Takahashi et al., 2001).

1.3.6.2 VEGFR2 functions and pathways activated

Of all receptors capable of binding VEGF, VEGFR2 has the second highest binding affinity for VEGF, second only to VEGFR1. While VEGF binds to VEGFR1 with a significantly higher affinity than to VEGFR2, the tyrosine kinase (TK) activity of VEGF bound VEGFR2 is 10-fold stronger than the TK activity of VEGF stimulated VEGFR1. Activated VEGFR2 transduces a strong positive angiogenic signal to the EC (Shalaby et al., 1995) indicating VEGF-VEGFR2 as the primary signal transducer of angiogenesis stimulation (Shibuya, 2013).

Endothelial VEGFR2 activation stimulates a multitude of intracellular signalling pathways, some of which have been better characterised than others. Activated VEGFR2 preferentially signals to phospholipase Cγ (PLCγ), protein kinase C (PKC) and p42/44 mitogen-activated protein kinases (MAPK) (Shibuya, 2013) and is essential for vasculogenesis during embryogenesis (Sakurai et al., 2005) and EC proliferation (Xia et al., 1996; Takahashi and Shibuya, 1997; Takahashi et al., 1999). The VEGFR2-PLC-γ-PKC pathway regulates EC proliferation and migration through activation of the protein kinase D (PKD)-histone-deacetylase 7 (HDAC7) pathway (Wang et al., 2008). Sase et al. (2009) demonstrated that differentiation of endothelial stem cells to ECs strongly depends on the VEGFR2- PLC-γ

pathway, while zebrafish mutants of the PLC-γ1 gene results in lethal deficiency of arteriogenesis (Sase et al., 2009; Lawson et al., 2002).

VEGFR2 activation controls vaso-motion, barrier function, and cell survival through regulation of phosphatidylinositol-3-kinase (PI3K)/Akt and mammalian target of rapamycin (mTOR) signalling pathways (Zhuang et al., 2013) while also partaking in regulation of von Willebrand factor (vWF) release from ECs, an essential component of the coagulation system (Xiong et al., 2009). Activation of the VEGFR2 also mediates tip cell selection in initiation of sprouting angiogenesis, leading to modulation of Notch signalling and initiation of the stalk cell phenotype of adjacent ECs which proliferate along a newly forming sprout. This regulation is a characteristic not described in an FGF signalling context and demonstrates the clear differences the two signalling pathways drive during angiogenesis (Xiong et al., 2009).

Activated VEGFR2 has also been described to regulate signalling via the Rho family of small GTPases driving changes to the actin cytoskeleton; activity necessary for regulation of cell shape, polarity, junction conformation, migration, and cellular growth in response to growth signalling cues (Rodrigues and Granger, 2015). Luke Hoeppner et al (2015) described how *in vitro* VEGF-VEGFR2 driven activation for the small RhoGTPase RhoC promotes a proliferating and a migratory phenotype. RhoC binds to and stabilises nuclear localised β-catenin; prompting an increase in expression of the cell cycle intermediate cyclin D. However, RhoC was also described to inhibit migration in a MAPKs and myosin light chain 2 dependent manner and downregulate the PLCγ calcium (Ca^{2+}) endothelial nitric oxide synthase (eNOS) cascade, leading to decreased vascular permeability (Hoeppner et al., 2015).

During sprouting angiogenesis VEGF-VEGFR2 driven activation of the small Rho family GTPases ras-related C3 botulinum toxin substrate (RAC) and cell division control protein 42 homolog (CDC42) drive directional migration and correct vascular patterning via regulation of the actin polymerisation required for lateral filopodia production, along cords

of newly forming vascular sprouts, in addition to lumen formation of the newly forming vessels (Abraham et al., 2015).

VEGFR2 has also been indicated in control of many other signalling pathways including: Src, p38 MAPK, STATs and G protein-coupled receptor (GPCR)-dependent signalling (Simons et al., 2016).

VEGFR3 is highly expressed on the cell surface of lymphatic ECs and blood vascular ECs (Simons et al., 2016). VEGFR3 binds and transduces signals from the ligands VEGFC and VEGFD. VEGFR3 may also be non-canonically activated by sheer stress (Byzova et al., 2000; West et al., 2012). VEGFR3 constitutive deletion within a murine model is embryonically lethal at day E9.5 as a result of vascular remodelling defects (Simons et al., 2016).
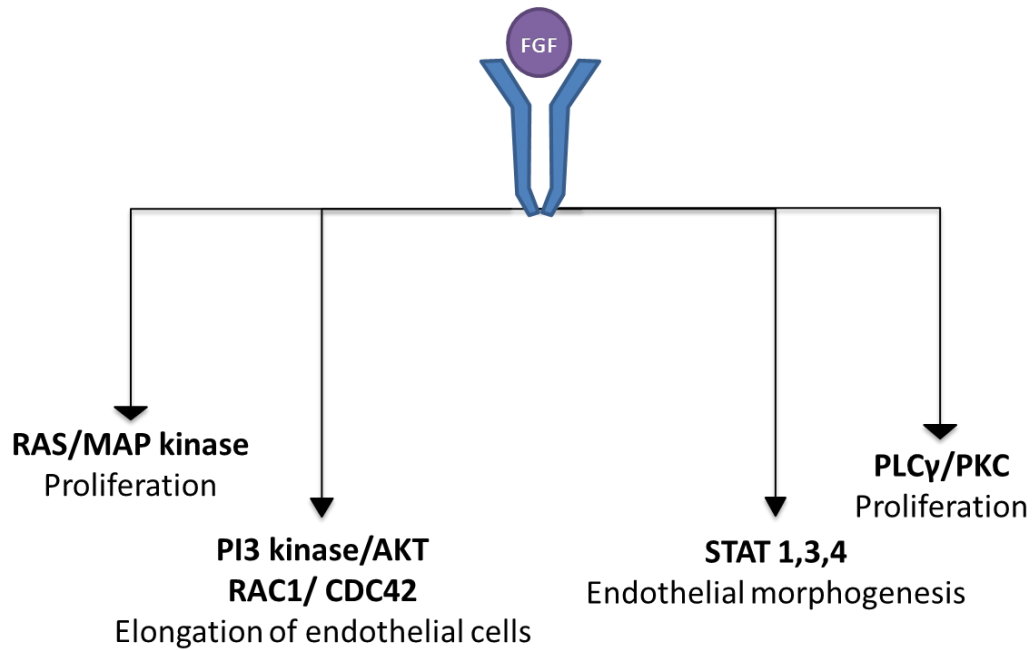
Figure 1-5 Schematic diagram of canonical FGF signalling mechanisms in ECs

Binding of an FGF ligand leading to homodimerisation of FGF receptors drives intracellular tyrosine kinase activity of the receptor. Activated FGF receptor stimulates activation of signalling pathways RAC/MAP kinase, PI3K/AKT, Rho GTPase RAC1 and CDC42, PLCγ/PKC, and STAT 1,3,4.

1.3.6.3 Fibroblast Growth Factor

The FGF family of GFs and their receptors have been implicated in many developmental and post developmental processes affecting multiple tissues and organs throughout the body. During embryogenesis and development, FGF signalling regulates tissue patterning, organogenesis, branching morphogenesis, and limb development. Within the vascular system, FGF acts as a potent endothelial mitogen (Gospodarowicz et al., 1977; Maciag et al., 1981; Thornton et al., 1983) which is stored within the vascular basement membrane and acts as an angiogenic factor during vascular development and progression (Ucuzian et al., 2010; Javerzat et al., 2002).

There are four FGF receptors (FGFR), with each subtype differing in kinase domain and ligand binding affinity (Trueb et al., 2013; Beenken and Mohammadi, 2009). As depicted in figure 1.5, binding of an FGF ligand leading to homodimerised FGF receptor molecules drives intracellular TK activity of the receptor. Activated FGFR stimulates activation of signalling pathways RAC/MAP kinase, PI3K/AKT, Rho GTPase RAC1 and CDC42, PLCγ/PKC, and STAT 1,3,4 (Beenken and Mohammadi, 2009; Dailey et al., 2005).

Stimulation of FGFRs primarily leads to intracellular regulation of two main intracellular substrates; PLCγ1 and FGFR substrate 2 (FRS2; (Beenken and Mohammadi, 2009)). Phosphorylation of FGFRs leads to PLCγ phosphorylation and activation. FRS2 associates with a juxtamembrane region of FGFR to drive constitutive activation of the FRS2, inducing activation of the Ras–mitogen-activated protein kinase (MAPK) and phosphoinositide 3-kinase–Akt signalling pathways (Beenken and Mohammadi, 2009; Dailey et al., 2005).

FGF ligands also signal through the low-affinity heparin sulphate transmembrane proteoglycan, syndecan 4 (Kitamura et al., 2008). FGF stimulation of S4 independently of FGF receptors is due to the receptor's ability to activate PKC (Horowitz et al., 1999; Partovian et

al., 2008). FGF activated S4 associates with a ubiquitous cytoplasmic protein, synectin (Gao et al., 2000).

The family of FGFs consists of 22 structurally similar signalling ligands, FGF1 -FGF23, of which 18 eighteen (FGF1-FGF10 and FGF15-FGF22) have been identified as ligands capable of binding to FGF receptor tyrosine kinases (Smallwood et al., 1996; Olsen et al., 2003). Similarly to VEGF, FGF proteins also possess heparin binding affinity (Shing et al., 1984). Due to the vast and varied activity of the FGF family of ligands and receptors, only FGF characteristics and signalling components relevant to this report and the primary FGF signalling components shall be discussed in detail within this introduction.

The FGF ligands FGF1 and FGF2, regulate vascular tone and thus blood pressure (Cuevas et al., 1991) and have been implicated in regulating NOS activity (Cuevas et al., 1996). Mice with FGF1 or FGF2 depletion are viable with no known defects and maintain normal vascularization (Miller et al., 2000) potentially due to redundancy, or action of alternative angiogenic GFs in their absence.

FGF1 is capable of binding to all FGF-receptor subtypes, a characteristic unique to FGF1. FGF1 is a potent angiogenic mitogen (Blaber et al., 1996) under the condition of hypoxia, and is able to drive the FGF1 proliferation and differentiation of the endothelial and smooth muscle cells necessary for construction of an arterial vessel (Stegmann, 1998; Khurana and Simons, 2003). FGF1 has been implicated in driving a protective response in cardiac ischemia, with higher levels of FGF1 found within pericardial fluid following an ischemic cardiac event (Iwakura et al., 2000). FGF1 treatment within cardiovascular disorders have also demonstrated FGF1 function in collateral artery growth, capillary proliferation (Schumacher et al., 1998) and in improving perfusion within the lower extremities following ischemia (Comerota et al., 2002; Nikol et al., 2008). FGF1 has also been implicated in nerve repair following injuries (Cheng et al., 1996; Takahashi and Shibuya, 1997; Lin et al., 2005;

Cheng et al., 2004). *In vitro*, FGF1 induces microvascular branching within cultured ECs (Uriel et al., 2006).

During wound healing FGF1 and FGF2 stimulate the proliferation of fibroblasts and ECs, necessary for angiogenesis, and developing granulation tissue (Ornitz and Itoh, 2001).

FGF2 plays a role in a broad spectrum of processes, regulating multiple mitogenic and cell survival activities (Ornitz and Itoh, 2001). FGF2 is a more potent stimulator of angiogenesis than either VEGF or PDGF (but not FGF1) and promotes angiogenesis through stimulating proliferation and physical organization of ECs into tube-like structures (Ornitz and Itoh, 2001).

FGF2 function has been implicated in embryonic development, morphogenesis, tissue repair, and functions in regulating migration and proliferation of ECs, mitogenesis of smooth muscle cells and fibroblasts, anti-apoptotic responses, adipogenesis, and inflammation (Ware and Simons, 1997; Yanagisawa-Miwa et al., 1992; Scholz et al., 2001; Hutley et al., 2004; Keller et al., 2008).

In vivo, FGF2 plays a role in migration and proliferation of ECs (Ware and Simons, 1997), and has been implicated in the development of large collateral vessels with adventitia (Scholz et al., 2001). Use of FGF2 as a treatment following cardiac ischemia has been demonstrated to reduce the size of ischemic regions in the myocardium, reduce the frequency of angina (Unger et al., 2000; Laham et al., 1999), and has also been established to improves peripheral circulation of people suffering from claudication; pain within the lower limbs due to obstruction of blood flow (Lazarous et al., 2000). FGF2 inhibition in tumours has been shown to impede vascularisation (Wang and Becker, 1997) but does not impact on microvessel density in tumours (Presta et al., 2005).

FGF1 and FGF2 induced vascular growth develops features distinctly different when compare to VEGF induced vascular growth; with a marked reduction in fenestrations, and

thus permeability, of blood vessels produced under FGF driven vascular growth (Cao et al., 2004; Hori et al., 2017).

1.3.6.4 FGF stimulation of RhoG, RAC1, and CDC42 activity

FGF2 binding to syndecan-4 drives RAC1 activation in a RhoG dependent mechanism (these Rho GTPases are described in detail in section 1.4), through initiating release of RhoG from an inhibitory ternary protein complex S4–synectin–RhoGDI1 (a RhoGTPase inhibitory protein described in section 1.4). FGF stimulation of RhoG activation of RAC1 leads to the activation of PKC in rat fat pad ECs (Elfenbein et al., 2009).

FGF2 stimulated endothelial activation of PI3K induces the reorganization of actin cytoskeleton to the cortex, and stimulation of changes in cell morphology, to induce and elongated phenotype in a Rho GTPase dependent manner (Lee and Kay, 2006).

Jeong Goo Lee and EunDuck P. Kay (2006) demonstrated that FGF2 stimulation of cultured corneal ECs, a type of non-vascular ECs, drives formation of protrusive processes in a CDC42/RAC1 dependent manner, in parallel with Rho inactivation. All FGF2 driven Rho GTPase regulation was observed to be blocked through administration of a PI 3-kinase inhibitor, LY294002.

RAC1 and CDC42 have also been demonstrated to be required for internalisation of FGF2 in complex with syndecan-4 on the surface of smooth muscle cells *in vitro* (Tkachenko et al., 2004)*.* FGF2 bound syndecan-4 interacts with dextran during endocytosis of the complex. *In vitro* dominant negative RAC1 within smooth muscle cells blocks internalisation of FGF2 and syndecan-4. Smooth muscle cells with dominant-negative CDC42 blocked endocytosis of FGF2, syndecan-4 and dextran (Tkachenko et al., 2004).

With consideration to the literature it can thus be considered that FGF signalling in angiogenesis drives EC proliferation and elongation during wound healing. The FGF stimulation of EC elongation occurs in a RAC1 and CDC42 specific context. As DOCK4 is an

activator of RAC1, DOCK4 may serve as a potential component in conferring the cellular response to FGF.

1.3.7 Peripheral artery disease

Peripheral artery disease (PAD) describes a pathologically driven reduction in blood flow to the lower extremities and, within the Western world, is a predominant cause of mortality (Ferraro et al., 2010; Rissanen et al., 2001). In severe cases, PAD may manifest as critical limb ischemia (CLI), which often results in a requirement for limb amputation. Limb ischemia has been attributed to insufficient neovascularisation following blood vessel occlusion (Carmeliet, 2003). While patients suffering from PAD may receive physical therapy (Gardner and Poehlman, 1995; Robeer et al., 1998), treatment is aimed to reduce underlying pathological instigators of PAD (i.e. atherosclerosis), or surgical procedures to introduce a catheter or stimulate re-vascularisation (Norgren et al., 2007). Despite the use of these interventions there is currently no effective treatments for CLI (Aviles et al., 2003).

FGF signalling ligands and receptors have been indicated as critical for neovascularisation following injury and have been indicated as potential therapeutics for treating CLI (Ferraro et al., 2010; Bobek et al., 2006).

Sunday S. Oladipupo et al (2014) utilised both FGFR1 and FGFR2 deficient mice to demonstrate that FGF signalling via either of the FGFR1 or FGFR2 TKs is not required for embryonic vascular development or maintenance of vascular integrity under homeostatic conditions. However, depletion of FGFR1/2 led to impairment of neovascularisation following injury to the skin or cornea. Analysis of post-injured murine skin samples indicated a heightened level of FGF2, VEGF, and PIGF, this finding was attributed to disruption of feedback mechanisms regulating levels of gene expression. This finding indicates FGF signalling through the FGFR1/2 primarily functions within neovascularisation during wound healing.

Bernadette Ferraro et al. (2010) found electroporation-mediated intradermal delivery of plasmid FGF2 (pFGFE+) treatment of hind limb ischemia (HLI) in rats, following occlusion of the femoral artery, was observed to significantly increase blood flow to the affected hind limb (Ferraro et al., 2010). This study supported the earlier work of Fujii, et al. (2008) which demonstrated that intramuscular injection of an FGF2 expressing plasmid greatly enhanced hind limb perfusion to an ischemic limb via VEGF driven enhancement of placental GF signalling (Fujii et al., 2008). Together these findings implicate FGF as an important mediator of the vascular response to tissue ischemia. Further, understanding the mechanisms involved in regulating downstream vascular signalling events activated by FGF signalling may lend insight into potential therapeutic targets for treatment of pathological peripheral ischemia.

1.4   The Rho family of small GTPases

The Ras homolog (Rho) family of low molecular weight proteins form a distinct group of proteins within the large Ras superfamily of regulatory guanine tri-phosphate (GTP) hydrolases (Sadok and Marshall, 2014). In parallel with other GTPase proteins, each family member possesses a conserved 20kDa GTP-binding domain (Sadok and Marshall, 2014). Activation of Rho GTPases arises through alternation in binding of GTP/GDP (guanine di-phosphate) inducing a switch-like control mechanism in activating or deactivating the Rho GTPase respectively, as is seen in figure 1.6 (Cherfils and Zeghouf, 2013). Once activated, Rho GTPases modulate multiple downstream targets that are involved in the organisation of the actin cytoskeleton and the microtubule network.

Guanine nucleotide exchange factors (GEFs) induce activation of GTPases through release of GDP enabling binding of GTP (Cherfils and Zeghouf, 2013). There are two distinct groups of Rho GEFs, both of which have GDP exchange activities but no sequence homology. Diffuse B-cell lymphoma (Dbl)-family GEFs mediate nucleotide exchange through a Dbl

homology-pleckstrin homology (DH-PH) domain (Cherfils and Zeghouf, 2013). The PH domain can be auto inhibitory and also permits binding to phospholipids allowing for localisation at the plasma membrane (Meller et al., 2008; Sadok and Marshall, 2014).

The DOCK180 family make up the second group of Rho GEFs. DOCK180 proteins possess DOCK homology region (DHR) 1 and 2 domains. The DHR2 domain controls nucleotide exchange, while the DHR1 domain is thought to control plasma membrane localisation (Cote and Vuori, 2007; Patel et al., 2011). The majority of DOCK180 proteins lack a PH domain with the exception of three members: DOCK9, DOCK10, and DOCK11 (Meller et al., 2008). DOCK1 proteins possess an SH3 domain (SH3 domains are described in section 1.4.6.4) capable of binding adaptor proteins containing a proline-rich motifs such as ELMO (Patel et al., 2011). GEF proteins will be described in more detail in section 1.4.6.
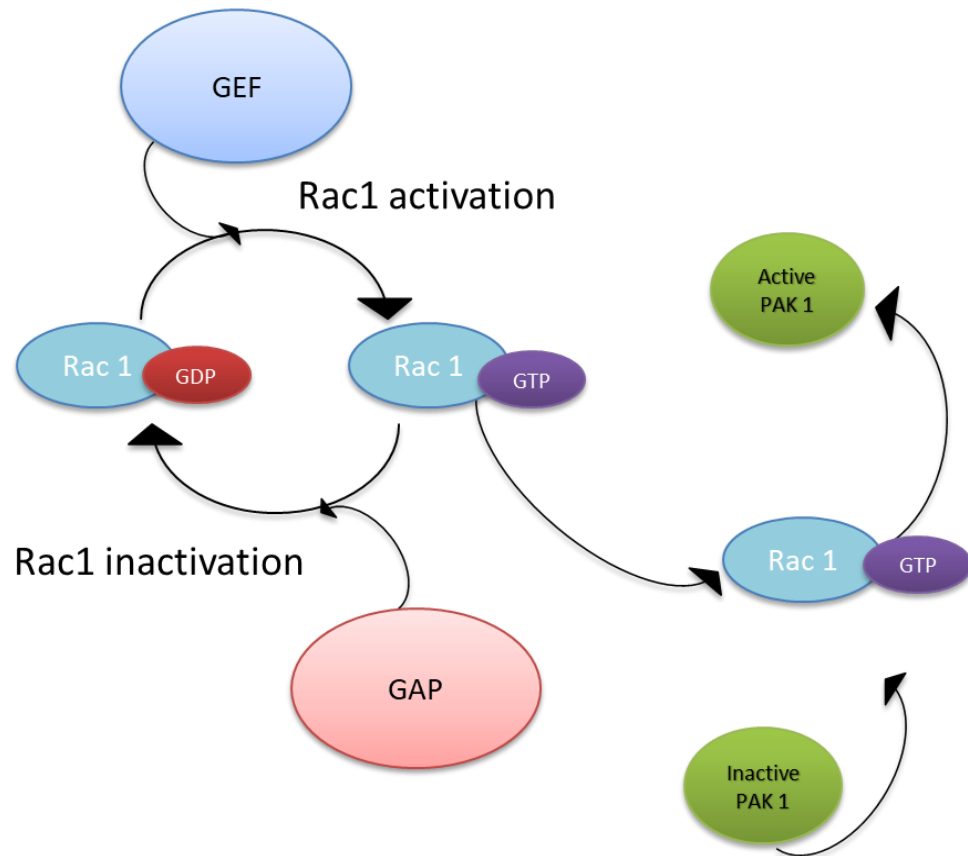
Figure 1-6 Schematic diagram of RAC1 activation and inactivation

Alternation in binding of the Rho GTPase to GTP/ or GDP induces a switch-like control mechanism in activating or deactivating the Rho GTPase respectively. Once activated Rho GTPases modulate multiple downstream targets that are involved in the organisation of the actin cytoskeleton and the microtubule network. GEFs induce activation of GTPases through mediating release of GDP enabling the binding of GTP. GAPs drive inactivation of Rho-GTPases via stimulation of GTP hydrolysis. GAPs catalyse the intrinsic GTPase activity of Rho proteins that hydrolyses GTP to GDP thus leading to inactivation of the Rho protein.

GTPase activating proteins (GAPs) drive inactivation of Rho-GTPases via stimulation of GTP hydrolysis (Sadok and Marshall, 2014). Rho guanine nucleotide dissociation inhibitors (GDIs) are also capable of regulating Rho-GTPase activity through binding to the C-terminal prenyl group, and retaining the GTPase in the cytoplasm (Sadok and Marshall, 2014; Etienne-Manneville and Hall, 2002). Interestingly, the Rho GAP, RhoGDI 1, acts as a chaperone to multiple Rho proteins, acting to facilitate correct folding and prevent ubiquitination and degradation (Etienne-Manneville and Hall, 2002).

It must also be noted that atypical Rho-GTPase proteins remain continually bound to a GTP molecule, effectively rendering the protein permanently activated yet under the control of alternative mechanism (Sadok and Marshall, 2014).

The switch-like control mechanisms of the Rho-GTPase proteins enables integration of a fast acting and local stimulus. The existence of over 70 GEFs and 80 GAPs, which have thus far been identified (Sadok and Marshall, 2014; Hall, 2012), allows for diverse and complex fine tuning of Rho GTPase protein activation and localisation. The extensive repertoire of GEFs, GAPs, and GDIs lend to the Rho GTPase capacity to modulate and integrate multiple signals and their involvement in numerous cellular responses.

Multiple signalling transduction pathways (MAPK, PI3K, PLCγ, and Rho-family of small GTPase) have been noted to regulate the dynamic plasticity of ECs (Etienne-Manneville and Hall, 2002). Of the many signalling molecules involved, the Rho family of small GTPases have been found to be integral in transmitting extracellular stimuli and converting them to cellular responses during angiogenesis (Etienne-Manneville and Hall, 2002). In ECs, Rho-GTPases are primarily essential in regulating actin cytoskeletal dynamics thereby controlling cell migration, adhesion to the ECM, and lumen formation. They are also important in cell polarity, maintenance of endothelial barrier integrity, and may influence angiogenic metabolism, transcription factor activity, and transportation pathways as reviewed in Etienne-Manneville & Hall (2002).

1.4.1 Actin cytoskeleton

The cytoskeleton of a cell is a network of fibrous elements found within the cytoplasm which provides morphological diversity, cellular structure, and migratory capabilities. The cytoskeleton is comprised of microtubules, actin microfilaments, and intermediate filaments (Fletcher & Mullins, 2010). Networks of highly dynamic actin filaments are typically found beneath the cell cortex and consist of globular proteins (G-actin) assembled into long double helix filaments (F-actin; (Fletcher and Mullins, 2010)).

Actin filament remodelling is dynamic and tightly regulated through complex mechanisms. Growth of actin filaments occurs through addition of G-actin monomers onto either the fast growing barbed end of the F-actin filaments, or the pointed slow growth end of F-actin filaments, via polymerization (Fletcher and Mullins, 2010). Depolymerisation occurs through cleaving of G-actin from either end of the F-actin filaments (Holmes et al., 1990; Oda and Maéda, 2010). Existing actin filaments are maintained in a caped state, with uncapping and nucleation of the barbed end required for initiation of polymerisation. Three major classes of actin nucleators have been identified: the Arp2/3 complex, formins, and tandem actin-binding domain nucleators (Weston et al., 2012).

Nucleation-promoting factors (NPFs) of the Wiskott–Aldrich syndrome protein (WASP)/WASP-family verprolin-homologous protein (WAVE) family activates and binds the F-actin bound Arp2/3 complex in conjunction with also binding G-actin monomers (Chesarone and Goode, 2009). This complex formation initiates creation of a nucleation core prompting actin nucleation and polymerisation of a new actin filament from a pre-existing actin filaments (Chesarone and Goode, 2009). The Arp2/3 complex also catalyses the production of branched F-actin filaments via increasing the number of barbed ends through binding to the side of filaments at the pointed end, forming the base of a new branch (Egile et al., 2005).

The Formin family of proteins also bind to the barbed ends of actin filaments to prompt the formation of linear actin filaments (Chesarone and Goode, 2009).

Cofilin is an actin binding protein capable of initiating actin nucleation via depolymerisation of actin filaments. Cofilin cleaves actin monomers from actin filaments, creating barbed ends aiding nucleation and actin polymerisation (Ichetovkin et al., 2002; Andrianantoandro et al., 2006). Gelsolin also drives depolymerisation of F-actin and increases the number of free pointed ends, with a considerably higher binding affinity than that of cofilin (Ressad et al., 1998).

The actin binding capping protein blocks actin polymerisation, terminating filament elongation, through binding to the F-actin barbed ends (Caldwell et al., 1989; Cooper and Pollard, 1985; Jo et al., 2015).

1.4.2 RhoA, RAC1, and CDC42

Of the 20 known Rho family members, member A (RhoA), RAC, and CDC42 have been the most extensively studied, with these three considered to be hallmark family members (Sadok and Marshall, 2014). These three proteins have been noted through numerous studies to each regulate different aspects of cell shape changes through interactions with the cytoskeleton (Sadok and Marshall, 2014). CDC42 and RAC1 may regulate activation of one another, dependent on the signalling context, whereas RAC1 and RhoA often act in opposition (Machacek et al., 2009). The three canonical Rho GTPases RhoA, RAC1 and CDC42 act in co-ordination with one another to regulate cytoskeleton dynamics.

Within fibroblasts, the three Rho GTPases have been observed to fluctuate in activity within sub-minute times of one another and at a micro-meter length scales apart (Martin et al., 2016). RAC and/or CDC42 influence migration in distinctly different ways despite sharing some common GEF activators, indicating that RAC and CDC42 are activated within different sub-cellular locations simultaneously while acting upon distinctly different downstream targets (Cook et al., 2013). The mechanisms occurring downstream of each Rho-GTPase may

differ greatly dependent on the proteins through which they interact and their localisation within the cell (Cook et al., 2013).

1.4.2.1 RhoA

In the most basic sense, RhoA drives bundling of actin filaments into contractile stress fibers, increases cell contractility, and initiates assembly of focal adhesions. RhoA is most commonly recognised as the Rho-GTPase responsible for inducing contractility at the trailing edge of a migrating cell in 2-D motility. However, RhoA has also been implicated in events occurring at the leading edge of migrating cells (Wacker and Gerhardt, 2011b).

There are multiple recognised mechanisms through which RhoA promotes EC migration. RhoA activation of the downstream target ROCK is the most studied activity of RhoA (Wacker and Gerhardt, 2011b). RhoA-ROCK signalling enables actomyosin contractility through phosphorylation of myosin light chain in addition to phosphorylating and inhibiting myosin phosphatase (Wacker and Gerhardt, 2011b). RhoA activation of the formin, mDia, also initiates actomyosin contractility and force generation (Sadok and Marshall, 2014). During initiation of cell migration, recruitment of RhoA from cell junctions to the leading edge of the cell, in a Rab-13-dependent manner, allows for activation of RhoA induced by the RhoGEF Syx. The p110α subunit of PI3K may also influence migration through RhoA signalling (Wacker and Gerhardt, 2011a).

Reorganisation of the actin cytoskeleton may be further controlled through RhoA-ROCK signalling via ROCK phosphorylation of LIM-Kinase, leading to phosphorylation of the actin-regulatory protein cofilin (a protein responsible for actin capping and depolymerisation) thus reducing accumulation of F-actin (Arber et al., 1998; Olson et al., 1995).

Rho signalling via ROCK has also been described in regulating EC protrusion and branching. ROCK activation during sprouting through stiffer ECM results in enhanced

directional growth and reduced EC branching (Fischer et al., 2009; Wacker and Gerhardt, 2011a).

1.4.2.2 RAC1

RAC1 is ubiquitously expressed signal transducer which integrates signals from numerous cell signalling pathways (see figure 1.7) following stimulation of receptor kinases, G protein-coupled receptors, or integrins (Bosco et al., 2009). RAC1 has been implicated to be fundamental in several cellular functions and has been well described as a primary regulator of actin cytoskeletal reorganisation, axonal guidance, as well as cell migration and cell transformation. RAC1 has also been implicated in the induction of DNA synthesis and superoxide production (Bosco et al., 2009).

RAC1 interacts with multiple proteins involved in various aspects of cytoskeletal dynamics including cytoskeleton remodelling, microtubule stability, and gene transcription (Bosco et al., 2009). Activated RAC1 binds a number of effector molecules such as IQ Motif Containing GTPase Activating Protein 1 (IQGAP), IRSp53/WAVE, PAK, and mixed-lineage protein kinases 2 and 3(MLK2/3) (Bosco et al., 2009). WASP family of verprolin-homologous proteins and the formin family of proteins promote actin nucleation downstream of RAC1 (Galan Moya et al., 2009). RAC1 may also activate cofilin and gesolin, driving actin capping and depolymerisation. RAC1 control of spectrin activation drives membrane-associated actin binding (Galan Moya et al., 2009). The described RAC1 targets may also cooperate in exportation of proteins to expanding filaments thus further promoting migration.

RAC1 effectors, protein family of p21 activating kinases (PAK), bind RAC1-GTP potently stimulating PAK kinase activity and leading to cytoskeletal dynamics, adhesion, and transcription (Frost et al., 1996; Brown et al., 1996a).. RAC1 driven activation of PAK leads to c-Jun N-terminal kinase (JNK) activation (Westwick et al., 1997) and MLK2/3 driven activation of the JNK pathway through RAC1 mediated nuclear (Nagata et al., 1998; Teramoto et al., 1996). RAC1 is also involved in canonical JNK regulated Wnt-signalling to the TCF

transcription factor (Wu et al., 2008). Also, RAC1 leads to activation of PAK transmembrane guanylyl cyclase activity and the second messenger cGMP production (Guo et al., 2007).

RAC1 may also antagonise RhoA driven actomyosin contractility via signalling through PAK. RAC1-GTP activity may also drive stabilisation of cell-cell contacts through targeting the scaffold protein Ras GTPase-activating-like protein (IQGAP). RAC1 bound IQGAP1 displacing α-catenin from the cadherin-catenin cellular adhesion complex through binding β-catenin (Noritake et al., 2005).

RAC1 accumulates at the leading edge of migrating cells and was initially identified as driving cytoskeletal changes and formation of actin-rich lamellae at the leading edge of fibroblasts in response to microtubule growth. RAC1 also promoted neurite extension through prompting lamellipodia formation within the neural growth cone (Kozma et al., 1995). E-cadherin stimulated RAC1 activity is also fundamental in actin recruitment to epithelial cell-cell adherens junctions (Vasioukhin et al., 2000; Ehrlich et al., 2002). RAC1 also drives actin polymerisation in stimulated blood platelets, lymphocytes, mast cells, and ECs (Hall, 1998) and is also involved in endocytosis/trafficking, and pinocytosis within dendritic cells (Nobes and Marsh, 2000).

RAC1 also prompts actin nucleation and polymerisation through IRSp53 dependent N-WASP activation of the Arp2/3 complex (Miki et al., 2000). RAC1 signalling is crucial within immune defence via its involvement in phagocytosis; RAC1 regulates polymerisation of actin fibres at membrane sites of micro-organism and particle uptake (Etienne-Manneville and Hall, 2002); RAC1 partakes in activation of NADPH oxidase within phagocytic cells leading to the superoxide ions production required to kill bacteria (Bokoch, 1995; Abo et al., 1992); RAC1 regulates macrophage cell immunoglobulin-receptor mediated phagocytosis; RAC1 also activates MAPK and JNK pathways enabling an inflammatory response (Caron and Hall, 1998).

RAC1 is also a prominent regulator of NADPH-dependent membrane oxidase (NOX), a primary source of reactive oxygen species (ROS). Through ROS production RAC1 signalling is also involved in senescence, p53 activity, and genomic stability (Debidda et al., 2006; Joneson and Bar-Sagi, 1998; Cheng et al., 2006) with double negative RAC1 fibroblasts unable to generate ROS (Irani et al., 1997).

RAC1 signalling may also induce cellular changes in gene transcription through activation of the activator protein-1 (AP1) transcription factors via activating nuclear factor kappa-light-chain-enhancer of activated B cells (NFkB), JNK, and MAPK (Caron, E, 1998). This modulation of transcription by RAC1 has been described to induce G1/S progression of the cell cycle through upregulating cell cycle proteins such as cyclin D1 and c-myc (Olson et al., 1995; Chiariello et al., 2001). RAC1 is essential for the growth of major blood vessels, developmental angiogenesis and formation of lymphatic vessels (D'Amico et al., 2009; Tan et al., 2008), functions which will be described in detail later on within this introduction.
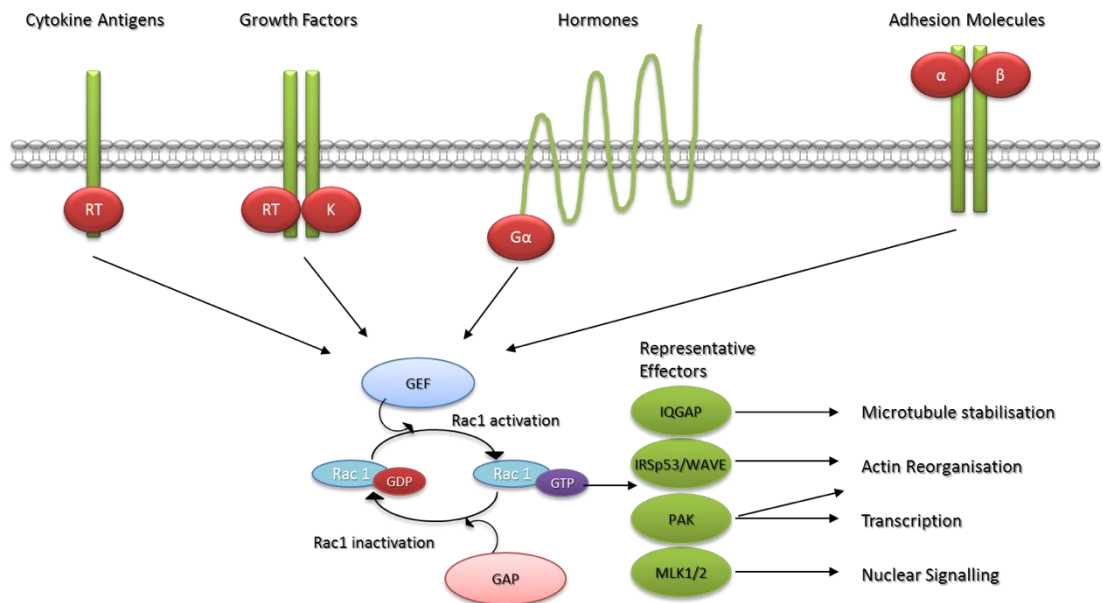
Figure 1-7 RAC1 signal transduction

RAC1 transduces external stimulus transmitted through receptor kinases, G protein-coupled receptors, or integrins via GEFs. GTP bound RAC1 targets effector molecules such as IQGAP, IRSp53/WAVE, PAK, and MLK2/3, prompting intracellular activities such as cytoskeleton remodelling, microtubule stability, and gene transcription.

1.4.2.3 CDC42

CDC42 possess similar feature to RAC1 in that this small cyclic GTPase has many downstream effectors yet is highly specific in activity, integrating signals concerning specific functions transduced via distinct pathways. This is regulated through the diverse repertoire of GEFs which drive CDC42 activation downstream of surface receptors. CDC42 signalling is crucial for regulating changes to cell morphology, as well as cell cycle progression, cell migration, and endocytosis (Barry et al., 2015).

CDC42s principal function is in conveying signals from the external environment prompting modification of the actin-cytoskeleton. CDC42 is also a predominant signalling transducer in establishing correct cell polarity in response to external signalling cues (Etienne-Manneville and Hall, 2002). CDC42's ability to modulate the actin cytoskeleton is directed via multiple downstream targets including; Pak2, Pak4; cofilin; N-WASP and Arp2/3 complex; IRSp53/Mena complex; Myosin light-chain kinase (MLCK); myotonic dystrophy kinase-related CDC42 binding kinase (MRCK); and IQGAP (Govek et al., 2005; Etienne-Manneville, 2004).

During migration CDC42 exerts much of its effects towards filopodia formation and has typically been described as an upstream regulator of RAC activation; with the exception of RAC1 dependent CDC42 activation under the control of VEGF stimulated RhoG activity within sprouting angiogenesis (Abraham et al., 2015). CDC42 function in regulating formation of filopodia has been attributed to its signalling via N-WASP and Pak2/4-mediated non-muscle myosin IIA heavy chain (NMIIA) signalling (Etienne-Manneville, 2004). CDC42 activates N-WASP in an IRSp53/Mena complex dependent mechanism inducing Arp2/3 activation and subsequent actin nucleation and polymerisation (Lim et al., 2008).

CDC42 may also act to inhibit myosin light chain phosphatase (MYPT), an activity more commonly associated with RhoA-ROCK signalling, via activation of MRCK (Zhao and Manser, 2015). Thus, CDC42 activation can cooperate with RhoA-ROCK in instigating cell

motility (Machacek et al., 2009; Zhao and Manser, 2015). However, the ability for one pathway to dominate control of MLC2 phosphorylation dictates the cell morphology displayed by the cell during migration, with Rho signalling prompting a more rounded morphology and CDC42 signalling instilling the more elongated morphology (Wilkinson et al., 2005), as is seen in EC angiogenic migration.

In quiescent ECs, CDC42 activity has been observed to influence intercellular gaps between adjacent cells and between cell-ECM (Zihni and Terry, 2015; Etienne-Manneville, 2004). CDC42 may also impact EC polarity and EC lumenisation (Etienne-Manneville, 2004).
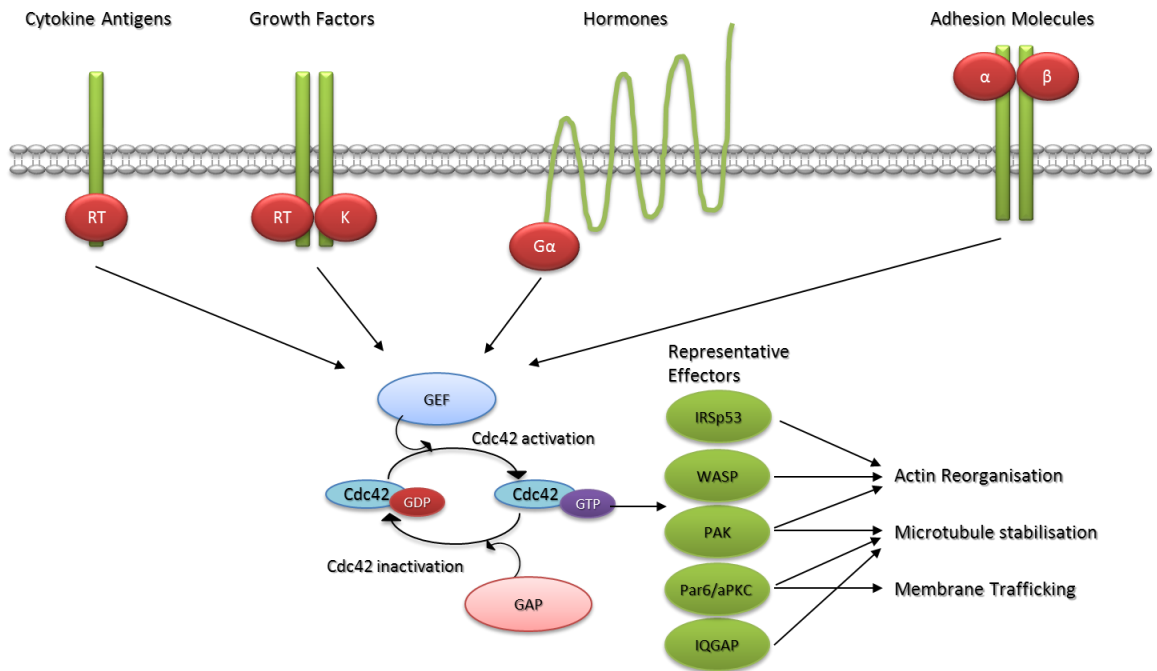
Figure 1-8 CDC42 signal transduction pathways

CDC42 transduces external stimulus transmitted through T-cell receptor, tyrosine kinase receptors, G-protein coupled receptors, integrins, Cadherins, and Nectins are all capable of transmitting extracellular stimulus inducing CDC42 activation via GEF. GTP bound CDC42 targets effector molecules such as IRSp53/Mena complex, WASP, PAKs, Par6/aPKC and IQGAP prompting intracellular activities such as cytoskeleton remodelling, microtubule stability, and membrane trafficking.

1.4.2.4 RhoG

RhoG is a ubiquitously expressed member of the RAC1 subfamily of RhoGTPase and has primarily been described to function within cell migration and regulation of macropinocytosis and caveolar endocytosis (Ellerbroek et al., 2004; Prieto-Sanchez et al., 2006). RhoG stimulates a cellular migratory morphology through activation of RAC1 (Cote and Vuori, 2007). DOCK180 activation of RhoG leads to binding of the adapter protein ELMO and subsequent activation of RAC1 (Katoh et al., 2006; Katoh and Negishi, 2003).

RhoG has been found to be regulated by a number of GEFs. TRIO driven activation of RhoG has been found to promote GF-induced neurite outgrowth in PC12 cells (Estrach et al., 2002). Within ECs the RhoG specific GEF, SGEF (Src homology 3 domain-containing guanine nucleotide exchange factor), stimulates RhoG activation of RAC1 in a VEGF dependent signalling pathway. RhoG activation of RAC1 signals via the RAC1 specific GEF DOCK4 (Cote and Vuori, 2007). DOCK4 driven RAC1 activation downstream of RhoG initiates CDC42 activation via DOCK9 activation, leading to actin cytoskeleton rearrangement and pro-growth and migratory endothelial phenotype during sprouting angiogenesis (Abraham et al., 2015). RhoG activation also induces macropinocytosis within fibroblasts (Ellerbroek et al., 2004) and apical cup assembly in ECs. Dbs, ECT2, VAV2 and VAV3 GEFs have also been implicated in RhoG activation (Wennerberg et al., 2002; Schuebel et al., 1998; Movilla and Bustelo, 1999).

1.4.3 Rho GTPase signalling in EC filopodia formation

During the initiation of migration stimulation of Rho GTPase signalling downstream of pro-angiogenic factors is a pivotal stage in inducing the dynamic remodelling of cell shape during angiogenic sprouting (Wacker and Gerhardt, 2011b). Filopodia are cytoplasmic rich actin projections which extend out from the cell to probe the extracellular space for growth signalling cues (Krugmann, 2001). Filopodia are present in abundance at the leading edge of

tip cells but have also been observed to a lesser degree along the elongating stalk of newly developing cords of ECs (Abraham et al., 2015).

During filopodia production, CDC42 induces F-actin bundles through activating actin-associated proteins, including fascin, formin (mDia2) and Ena/VASP (Mattila and Lappalainen, 2008; Chhabra and Higgs, 2007). CDC42 also regulate filopodia in a RhoG dependent manner (Abraham et al., 2015). *In vitro* CDC42 instigates actin polymerisation through cooperation with WASP and Pak2/4-mediated NMIIA signalling (Barry et al., 2015) which results in activation of Arp2/3 actin nucleation complex (Rohatgi et al., 1999).

RAC1 has also been found to be essential in filopodia formation through activation of CDC42 (Abraham et al., 2015). Abraham, et al (2015) observed disruption of lateral filopodia formation following RAC1 knockdown in a tissue culture organotypic angiogenesis assay. Suppression of lateral filopodia was also seen in ECs following knockdown of DOCK4, a known RAC1 GEF (Abraham et al., 2015). Reduction of lateral filopodia prevented lumen formation within sprouting vessels, resulting in elongated unbranched sprouts. Knockdown of either RAC1 or DOCK4 appeared to have little effect on tip filopodia, indicating that different control mechanisms are involved in the development of the two types of filopodia. Interestingly Phng LK et al. (2013) reported that *in vivo* inhibition of actin polymerisation with latrunculin B reduced the presence of tip cell filopodia and speed of EC migration while guidance was unaffected (Phng et al., 2013).

1.1   Rho GTPase signalling in blood vessel lumen formation

In addition to their role in protrusive activity and EC migration, CDC42 and RAC1 are also necessary for lumen formation (Wacker and Gerhardt, 2011b). Studies performed in tissue culture in 3D collagen matrices have shown that RAC1 and CDC42 are required for changes in EC polarity during lumen formation taking place through the process of cell

hollowing (Lizama and Zovein, 2013), which entails formation an intracellular vacuole which expands through other cells giving rise to the lumen.

RAC1 stimulation of PAK2, in addition to CDC42 activation of Pak2, Pak4, Par3, and Par6 all influence lumen formation, potentially in a protein kinase C dependent manner (Koh et al., 2008; Iruela-Arispe and Davis, 2009). Koh et al (2008) also describe potential interactions between CDC42, RAC1 and polarity protein complexes in driving lumen formation during cell hollowing. CDC42's ability to regulate vascular lumen formation *in vitro* has been linked to CDC42-Par3-Par4-PKC atypical complex (Koh et al., 2008; Hoang et al., 2011); the four proteins form a quaternary complex, with loss of any of the four components of the complex disrupting lumen formation (Koh et al., 2008). Knockdown of Pak2 and Pak3 disrupt formation lumens (Hoang et al., 2011; Barry et al., 2015). CDC42 may further promote lumenisation through phosphorylation and inhibition of glycogen synthase kinase-3β (GSK-3β) (Hoang et al., 2011).

Barry et al (2015) found deletion of CDC42, in Tie2-Cre driver line mouse model, blocked angiogenic tubulogenesis while the deletion was lethal due to blood vessel defects. Additionally, EC specific RAC1 knockout in Cre/Flox mice has been seen to disrupt correct formation of major blood vessels and resulted in an absence of small-branched vessels (Tan et al., 2008; D'Amico et al., 2009). The EC RAC1 knockout is embryonic lethal at mid-gestation (Sugihara et al., 1998).

Abraham et al (2015) described delineation of the Rho-GTPase pathway downstream of VEGF signalling essential for lateral filopodia formation, a process potentially imperative for lumenisation (as seen in figure 1.9). VEGF signalling resulting in activation of SGEF, a GEF which targets and activates RhoG, initiating a pathway which results in RAC1 activation (via binding of an ELMO and DOCK4 complex) and CDC42 activation downstream of RAC1 (through binding of DOCK9 and potential interactions with DOCK4) (figure. 1.6; Abraham et al., 2015).
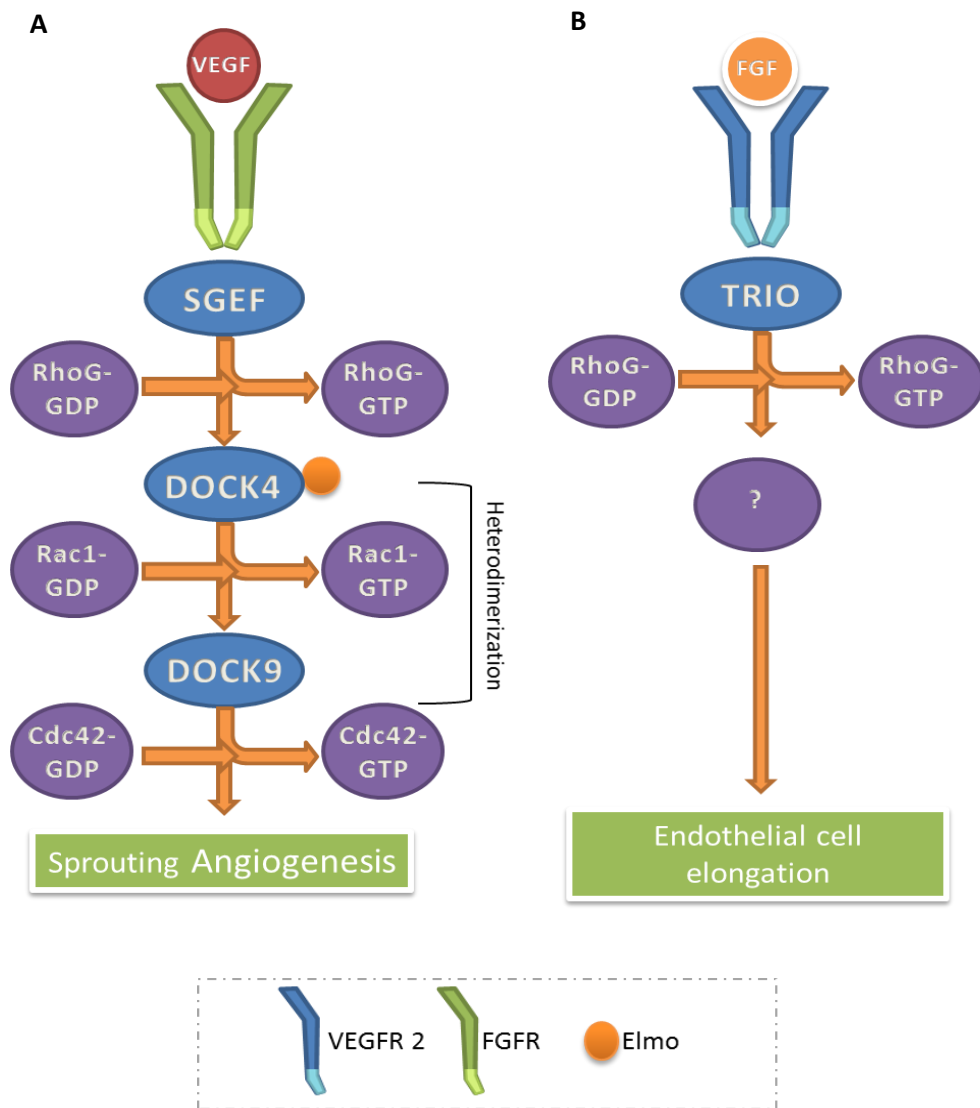
Figure 1-9 RhoG signalling in angiogenesis

Schematic diagram of intracellular signal transduction downstream of activated VEGF and FGF. (A) VEGF stimulation induce filopodia formation and sprouting angiogenesis. The Rho GEF SGEF activates RhoG, which in turn activates Rac GEF DOCK4 allowing binding of DOCK4 to ELMO. DOCK4-ELMO then translocate to the plasma membrane to activate Rac1. Abraham et al. (2015) described formation of an ELMO-DOCK4-DOCK9 complex capable of activating Cdc42 and stimulating filopodia formation. (B) Previous work in the laboratory has shown that FGF2 stimulation of ECs results in the activation of RhoG via the GEF Trio.

1.4.4 RhoGTPase in EC elongation

Little is known in regard to Rho GTPase activity in driving EC elongation. However, RAC1 has been implicated in driving EC elongation downstream of the GEF Tiam-1 through a TNF-α-mediated re-arrangement of F-actin (Cain et al., 2010). Recently, Jiahui Cao et al. (2017) described a RAC1 dependent mechanism which, in cooperation with microtubules, drives cell elongation following VEGF stimulation of ECs. This RAC1 dependent signal transduction led to an increase in cell perimeter and decrease in junctional concentration of VE-cadherin. RAC1 activity stimulated formation of an actin-driven junction-associated intermittent lamellipodia (JAIL) via regulation of the WASP/WAVE/ARP2/3 complex, thus implicating RAC1 as a potential prominent component within EC elongation (Cao et al., 2017).

SiRNA mediated knockdown of cingulin-like 1 was found to impair the elongated phenotype via loss in Tiam-1 driven Rac1 activation (Chrifi et al., 2017). Marghe Scarcia (Thesis, 2013) found supplementing EC *in vitro* with FGF2 propagated EC elongation through initiating Trio driven RhoG activation.

1.4.5 Guanine nucleotide exchange factors

GEFs, as previously described in section 1.4, can be grouped into two separate categories due to their distinct functional domains. Atypical DOCK1 related GEFs, as depicted in figure 1.10, are characterised by their evolutionary conserved DOCK homology region1 (DHR1); which has been described to bind phospholipids, and DOCK homology region 2 (DHR2), a domain which has been observed to bind target Rho GTPases and drive activation (Cote and Vuori, 2007; Meller et al., 2005; Brugnera et al., 2002).
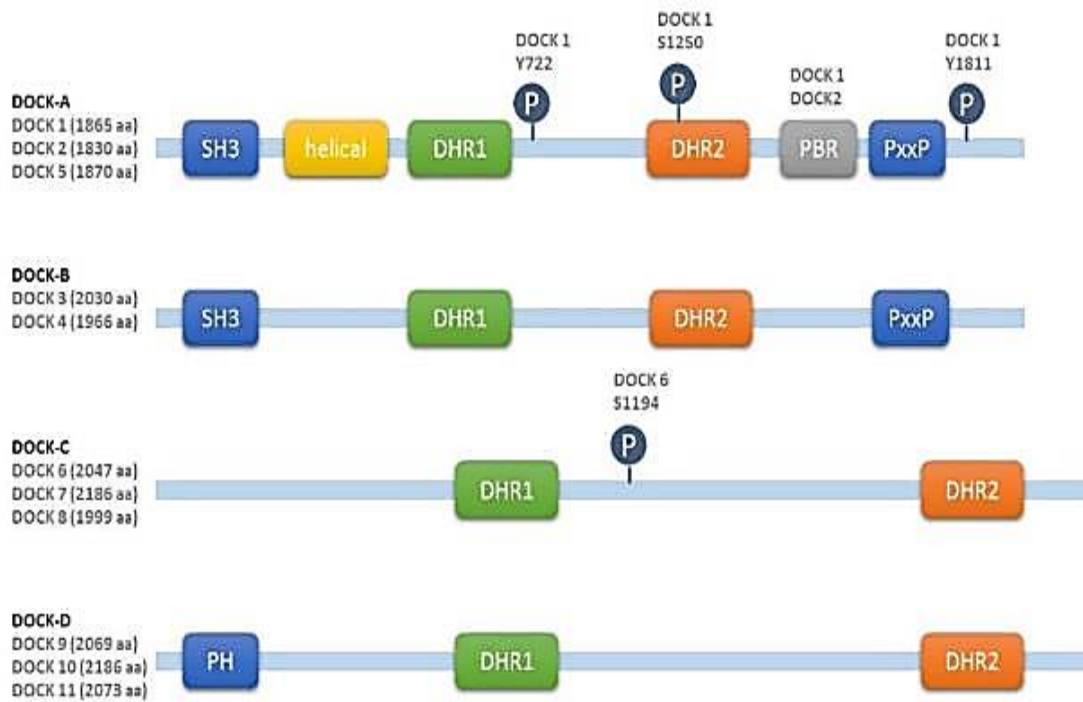
Figure 1-10 Schematic diagram of DOCK protein functional domains

DOCK1-related proteins are classified by their domain organisation and sequence similarity into four sub-groups: DOCKA (DOCK1, DOCK2, and DOCK5), DOCKB (DOCK3, and DOCK4), DOCKC (DOCK6, DOCK7, and DOCK8), and DOCKD (DOCK9, DOCK10, and DOCK11. DOCKA subgroup each possess an SH3 domain, helical region, DHR1, DHR2, PBR, and proline rich motif. DOCKB subgroup each possess an SH3 domain, DHR1, DHR2, and proline rich motif. DOCKC subgroup each contain only the DHR1 and DHR2 domains. DOCKD subgroup are the only DOCK proteins to contain a PH domain in addition to DHR1 and DHR2 domains.

1.4.5.1 The DOCK atypical GEF activity

The DOCK atypical GEFs bear a mechanism of Rho GTPase activation that is distinct from the Dbl GEFs (as described in section 1.4). The DHR2 domain of DOCK proteins contain a conserved nucleotide sensor region with an essential valine residue within an insert in the α10 helix of the DHR2 domain. The specific valine residue binds to its target GDP-bound Rho GTPase and drives exclusion of an Mg^{2+} ion from the nucleotide pocket. The nucleotide free Rho GTPase can then bind a GTP molecule, in addition to activating the Rho GTPase this also induces conformational changes to the DOCK GEF through displacement of the DOCK a10 helix insert resulting in the release of the activated GTPase (Yang et al., 2009; Gadea and Blangy, 2014).

DOCK180-related proteins can be further classified by their domain organisation and sequence similarity into four sub-groups (see figure 1.-10): DOCKA (DOCK1, DOCK2, and DOCK5), DOCKB (DOCK3, and DOCK4), DOCKC (DOCK6, DOCK7, and DOCK8), and DOCKD (DOCK9, DOCK10, and DOCK11) (Cote and Vuori, 2007; Laurin and Côté, 2014).

The DOCKA (DOCK1, DOCK2, and DOCK5) and DOCKB (DOCK3 and DOCK4) subfamilies both possess a SH3 domain, DHR1 domain, and DHR2 domain. DOCKA and DOCKB proteins also have a proline rich region (PRR) at the carboxyl terminus, which binds Crk proteins (Gadea and Blangy, 2014). DOCKA proteins also have a polybasic region (PBR) and helical region. Both DOCKA and DOCKB have been identified as DOCK proteins able to drive RAC1 activation.

The DOCKC (DOCK6, DOCK7, and DOCK8), and DOCKD (DOCK9, DOCK10, and DOCK11) subfamilies lack both the SH3 domain and the proline-rich region but do have a pleckstrin homology domain at the amino-terminus. DOCKD subgroup of DOCK180 family proteins have been identified as CDC42 activating GEFs (Hiramoto-Yamaki et al., 2010; Côté and Vuori, 2002; Côté and Vuori, 2006). DOCKC subgroup of GEFs have been described as possessing dual specificity driving activation of both RAC1 and CDC42 (Harada et al., 2012;

Kulkarni et al., 2011; Miyamoto et al., 2013; Watabe-Uchida et al., 2006; Gadea and Blangy, 2014).

1.4.5.2 DOCK homology region1

The DHR1 domain of DOCK GEFs is approximately 200 amino acid residues and has been implicated in protein complex localisation to the plasma membrane. Côté et al. (2005) described the DHR1 domain of DOCK1 as capable of interacting with Phosphatidylinositol (3,4,5)-trisphosphate within the plasma membrane, driving localisation of a protein complex involved in RAC1 activation to the leading edge of migrating cells. Deletion of the DHR1 region of DOCK1 did not disrupt DHR2 domain RAC1 loading but prevented the localisation of DOCK1 to the leading edge of the cell, impeding cell migration (Côté et al., 2005).

1.4.5.3 DOCK homology region2

The DHR2 domain of DOCK GEFs are approximately 500 amino acid residues that bind in high specificity to either RAC1 or CDC42, driving Rho GTPase activation. Amino acid residue variances of the DHR2 domains between the different subgroups of DOCK GEFs facilitates the specificity in Rho GTPase targeting.

Crystal structural analysis of the DOCK2 (Kulkarni et al., 2011; Hanawa-Suetsugu et al., 2012; Ferrandez et al., 2017) and DOCK9 DHR2/GTPase complexes has demonstrated that the DHR2 is a symmetrical dimer comprised of three lobes: lobes A, B, and C. Lobe A of the DHR2 region was determined to be required for dimerisation of DOCK proteins. Lobe B and lobe C were seen to form the catalytic pocket which interact with the GTPase nucleotide-sensing switch. Lobe B and C were determined to bear unique functions in GTPase activation with lobe B binding to and opening switch 1 of the GTPase nucleotide sensing switch. Lobe C drives GDP dissociation by binding to switch 2 and inserting a nucleotide sensor loop into the nucleotide-binding site (Kulkarni et al., 2011; Hanawa-Suetsugu et al., 2012; Ferrandez et al., 2017; Yang et al., 2009).

Kulkami et al. 2011 described explicit differences between the amino acid sequences of RAC1 and CDC42, which enable specific binding of the DOCK2 DHR2 domain and DOCK9 DHR2 domain, respectively. A phenylalanine or tryptophan at Rho GTPase residue 56 of the β3 strand, and an alanine or lysine at residue 27 drives Rho GTPase interaction within a region of the GEF DHR2 domain called switch 1 (Kulkarni et al., 2011). This finding demonstrated that DOCK proteins bind to their target Rho GTPase in a highly specific manner that is determined by the amino acid sequence of their DHR2 domain and target Rho GTPase.

1.4.5.4 SH3 domain

The DOCKA and DOCKB subfamilies possess a SRC Homology 3 (SH3) domain at the amino-terminus. SH3 domains have been identified in approximately 250 proteins and are associated with aiding a large number of signalling pathways (Pollard et al., 2016). SH3 domains are short peptide sequences, approximately 60 amino acids, which drive weak and transient interactions with proline-rich regions of interacting proteins. Aromatic residues within the SH3 domain shallow grove bind polyproline regions of proteins which form left handed type II polyproline helices (Pollard et al., 2016).

The SH3 domain of DOCK1 acts in an auto-inhibitory mechanism through weak interaction with the protein's own DHR2 domain. The inhibitory conformation can be overcome through binding of the adaptor molecule, ELMO (Engulfment and Motility) (Gadea and Blangy, 2014). The SH3 domain of DOCK1 has been described as a site capable of binding the three isoforms of ELMO (Gadea and Blangy, 2014); ELMO acts as an adaptor molecule that couples RAC to specific downstream effectors (Katoh et al., 2006).

1.4.5.5 Pleckstrin-homology (PH) domains

Pleckstrin-homology (PH) domains are found in the DOCKD sub-group of DOCK GEFs and also within Dbl GEFs, downstream of the DH domain. PH domains form weak interactions with phosphoinositide of the plasma membrane. Within the context of Dbl GEFs, the binding of PH domain to phosphoinositide of the plasma membrane has been suggested to facilitate

allosteric changes within the DH–PH array instigating Rho GTPase nucleotide exchange. However, it is also plausible that PH domain-phosphoinositide binding may function to guide precise subcellular localisation of Dbl proteins and engagement of membrane-bound GTPases. PH domains of the DOCKD group of GEFs may also function in localisation of DOCKD proteins to the plasma membrane (Rossman et al., 2005).

1.4.5.6 Proline rich regions

Proline rich regions describe amino acid sequences with multiple proline residues within close proximity to one another (Yu et al., 1994; Alexandropoulos et al., 1995). Members of the DOCKA and B subfamilies possess a proline-rich region downstream of the DHR2 domain. DOCK9 was also determined to possess 11 PRRs with 9 of the 11 containing the typical PxxP or PxxxP motif which forms a continuous hydrophobic patch which preferentially binds to the amino acid sequence of SH3 domains.

1.4.5.7 PBR

A polybasic region (PBR) within DOCK1 and DOCK2 was initially thought to bind PIP_3, but more recent data suggest that it binds the signalling lipid phosphatidic acid (PA) (Kobayashi et al., 2001; Nishikimi et al., 2009; Sanematsu et al., 2013).

1.4.5.8 DOCK9

DOCK9 signalling has yet to be well characterised, but has thus far been identified as a CDC42 specific GEF (Meller et al., 2002), however a recent study characterising the phenotype driven by over expression of DOCK9 in HeLa cells implicated DOCK9 in inducing RAC1 activation and membrane ruffling (Ruiz-Lafuente et al., 2018). DOCK9 expression drives filopodia production when expressed within cells. DOCK9 activity has been described as necessary within neuronal development (Kuramoto et al., 2009), angiogenesis (Abraham et al., 2015), and has been implicated in a number of diseases. DOCK9 is also expressed in steady-state circulating human CD3+ T cells, although the function of this expression has not yet been described (Ruiz-Lafuente et al., 2018).

Variants in the DOCK9 gene have been implicated in bi-polar disorder (Detera-Wadleigh et al., 2007). *DOCK9* variant c.2262A>C has been associated in the development of the ocular degenerative disease Keratoconus (Karolak et al., 2016). DOCK9 has also been detected as a biomarker of tuberculosis (de Araujo et al., 2016). During the late stages of neuronal development DOCK9 is highly expressed in the hippocampus and cerebral cortex and activates CDC42, through which DOCK9 acts as a prominent regulator of dendritic growth in hippocampal neurons (Kuramoto et al., 2009). DOCK9 is able to homodimerise via the DHR2 domain (Meller et al., 2004) and is also able to auto-inhibit through binding of the DHR1 domain to the DHR2 domain, the mechanism through which DOCK9 overcomes auto-inhibition is not yet known (Meller et al., 2008). Within angiogenesis DOCK9 driven CDC42 activation is imperative for lateral filopodia of growing vascular sprouts (Abraham et al., 2015).

1.4.5.9 DOCK4

DOCK4 signalling is complex and has been described as an active component in multiple different cell signalling pathways within various cell types. DOCK4 activity has been termed as both pro and anti-oncogenic. DOCK4 has also been designated as required for correct growth of neuronal and ECs, with mutations within DOCK4 being implicated in a number of neurological diseases.

The pro-oncogenic potential of mutated DOCK4 was identified through a mouse model genetic based screening study (Yajnik et al., 2003). DOCK4 mutation Pro1718Leu was detected in prostate and ovarian cancers and led to DOCK4 being ineffective in activating Rap1 GTPase, however, the Pro1718Leu mutation led to an increase in RAC1 and CDC42 activation (Yajnik et al., 2003). The change in Rho GTPase signalling prompted by DOCK4 mutation Pro1718Leu, was seen to disrupt correct localisation of β-catenin to the sites of adherens junctions and resulted in the disruption of formation of intercellular junctions, leading to a loss of contact inhibition within cultured cells (Yajnik et al., 2003). In addition to

disrupting the formation of intercellular junctions, the DOCK4 Pro1718Leu mutation drove formation of filopodia protrusions (Yajnik et al., 2003). Together the characteristics driven by the DOCK4 mutation led to a tumour invasive phenotype which was also confirmed within a nude mouse model. Through this study, the tumour suppressor effect of wild type (WT) DOCK4 was also demonstrated through the use of a cancer invasion mouse model assay, during which cancer cells expressing WT DOCK4 were significantly less capable of invasion and metastasis when compared to tumours established from cell expressing DOCK4 Pro1718Leu mutant (Yajnik et al., 2003).

DOCK4 has also been described to have oncogenic potential within breast cancer, leading to an increased invasive potential of breast cancer cells. Hiramoto-Yamaki et al., (2010) established evidence describing a mechanism through which RhoG activation within breast cancer cells drives a complex formation at the tip of cortactin-rich protrusions between ELMO2, DOCK4, and a member of the Eph receptor family, EphA2. The formation of the ELMO2-DOCK4-EphA2 complex was seen to induce formation of protrusions within breast cancer cell, increasing cell mobility in a RAC1 dependent manner (Hiramoto-Yamaki et al., 2010).

Further evidence linking to the pro-ongogenic activity of DOCK4 was described by Jia-Ray Yu et al (2015) through investigation of TGF-β driven RAC1 activation via inducing an increase in DOCK4 expression. TGF-β initiated increase in DOCK4 expression occurs downstream of the Smad signalling pathway, prompting an increase in tumour cell extravasation and metastasis. TGF-β-induced DOCK4 expression within lung adenocarcinoma induces an epithelial to mesenchymal transition independent increase in cell protrusion, motility, and invasion (Yu et al., 2015).

Upadhyay et al have previously demonstrated *in vitro* that pro-oncogenic Wnt signalling may induce RAC1 activation via GSK3-β driven β-catenin stabilization, through interaction with and phosphorylation of DOCK4. Activity which led to DOCK4 driven

stabilisation of the cellular levels of β-catenin via DOCK4 interaction with the β-catenin degradation protein complex; Adenomatosis Polyposis Coli (APC), Axin, and GSK3-β proteins (Upadhyay et al., 2008).

While activation of Wnt signalling during cancer progression has been described as driving a more aggressive phenotype (Polakis, 2000), DOCK4 involvement within the Wnt signalling pathway was later established to have a tumour suppressor effect (Yajnik et al., 2003).

Debruyne et al. demonstrated that β-catenin induces an anti-proliferative mechanism via a feed forward loop to increase and accumulate its own nuclear activity through multiple mechanisms which regulate DOCK4 expression (Debruyne et al., 2018). GSK3-β activation and β-catenin transcriptional activity is required for DOCK4 mRNA and protein expressions (Debruyne et al., 2018). β-catenin directly binds to the 5' regulatory sequence of the DOCK4 gene, regulating transcriptional activity of DOCK4. DOCK4 is also required for expression and transcriptional activity of β-catenin, thus creating a β-catenin driven feed-forward loop. Interaction of active GSK3-β with, and phosphorylation of, DOCK4 induces β-catenin stabilisation and nuclear accumulation, activity which is driven by miR-302 (Debruyne et al., 2018). β-catenin/DOCK4/miR-302 regulatory circuitry has been described as promoting a non-proliferative state with higher levels of DOCK4 expression leading to repression of glioblastoma multiform (GBM) proliferation stemness markers. Thus, GBM patients with increased DOCK4 expression possess a better survival prognosis (Debruyne et al., 2018).

The DOCK4 isoform (DOCK4-Ex49) is expressed within the brain, eye, and inner ear. Within the inner ear, this DOCK4 isoform has been found to regulate actin cytoskeleton organisation in stereocilia, via a RAC-DOCK4-ABP harmonin-activated signalling pathway (Yan et al., 2006).

DOCK4 regulates essential processes during neural development and differentiation (Ueda et al., 2013; Xiao et al., 2013). DOCK4 driven RAC activation has also been proven to be imperative for the formation of dendritic spines within hippocampal neurons via DOCK4 interaction with the actin-binding protein cortactin (Ueda et al., 2013). During neuron differentiation, the SH3 domain of DOCK4, but not the proline-rich C-terminus, drives modulation of actin-enriched protrusions on the neurites leading to differentiation and extension and the establishment of the axon-dendrite polarity and the arborisation of dendrites (Xiao et al., 2013).

Further genetic based screening studies also identified DOCK4 as a candidate gene with mutations within the DOCK4 gene being associated with several neurological disorders, including autism (Pagnamenta et al., 2010), dyslexia (Pagnamenta et al., 2010) and schizophrenia (Alkelai et al., 2012). Microdeletion DOCK4 mutants lacking the GEF domain led to defective neuronal polarisation and neurite overgrowth, a phenotype which has been linked to autism and dyslexia (Xiao et al., 2013). A maternally inherited microdeletion encompassed chr7:110,663,978-111,257,682 leading to a *DOCK4-IMMP2L* fusion transcript was identified within people with autism spectrum disorder (Pagnamenta et al., 2010). Alkelai et al. (2012) identified a SNP (rs2074127) positioned within the *DOCK4* gene (intron 6) to be frequently present in a study group which represented schizophrenic people from within a Jewish population.

With the mounting evidence associated with DOCK4 functionality within multiple cell types, it is apparent that DOCK4 serves as a multi-functional protein important for numerous cell signalling pathways. However, evidence is still limited in the ability to decipher how, when, and under what context is DOCK4 expressed, activated, and regulated.

1.4.6   Role of DOCK4 in vascular patterning and interaction with DOCK9 and generation of

DOCK9 mutants in proline-rich regions

The function of the RAC1 GEF DOCK4 within EC biology was investigated by Dr.

Mavria's research group. This work published within Nature Communications (Abraham et

al., 2015) outlined the requirement of DOCK4 functionality for VEGF driven sprouting

angiogenesis. Within an organotypic angiogenesis model, EC depletion of DOCK4 lead to a

loss in stalk cell filopodia along the lateral edge of endothelial cords, but not filopodia

extending from the tip cells during VEGF stimulated angiogenesis. This loss of lateral filopodia

was accompanied by a reduction in branching and thus less dynamic endothelial structures.

DOCK4 depletion also reduced the ability for EC cords to form a lumen (Abraham et al., 2015).

Together these results suggest a role for DOCK4 in correct vascular patterning and formation

of new functional vessels through sprouting angiogenesis under VEGF stimulated

angiogenesis (Abraham et al., 2015). However, the role of DOCK4 activation of Rac1 within

FGF stimulated angiogenesis is unknown, as is the requirement for DOCK4 activity within

vascular biology *in vivo.*

In order to further explore the function of DOCK4 signalling within mammalian

biology the signalling context through which DOCK4 functions, and the protein complexes

formed with DOCK4 while the protein is active, will allow for a deeper understanding into

the relevance of DOCK4 for vascular biology. Investigating the effect of DOCK4 depletion

within a murine model will also generate insight into the requirement for DOCK4 in

mammalian physiology. However, a complete ablation of DOCK4 results in embryonic

lethality. Thus, a heterozygous deletion, resulting in a 50% reduction of DOCK4 expression,

would provide a robust model for exploring the biological effect of reduced DOCK4 bio-

availability.

As VEGFA and FGF2 signalling pathways are both capable of initiating angiogenesis,

yet both prompt growth of phenotypically different endothelial sprouts, and each control

angiogenesis under differing signalling context (i.e. during development and in response to hypoxia (Ucuzian et al., 2010; Simons et al., 2016) vs during wound healing (Ornitz and Itoh, 2015), respectively, elucidating the control mechanisms which regulate DOCK4 activity will deepen the current knowledge of the mechanisms through which ECs respond to growth cues, while also giving insight into the signalling context through which DOCK4 functions.

Abraham et al. (2015) also demonstrated a heterodimerisation between DOCK4 and the CDC42 specific GEF, DOCK9. The site of DOCK4 required for this interaction was determined to be the SH3 domain of DOCK4, indicating that DOCK4 binds a PRR of DOCK9, however, the PRR region of DOCK9 involved in this interaction was not determined.
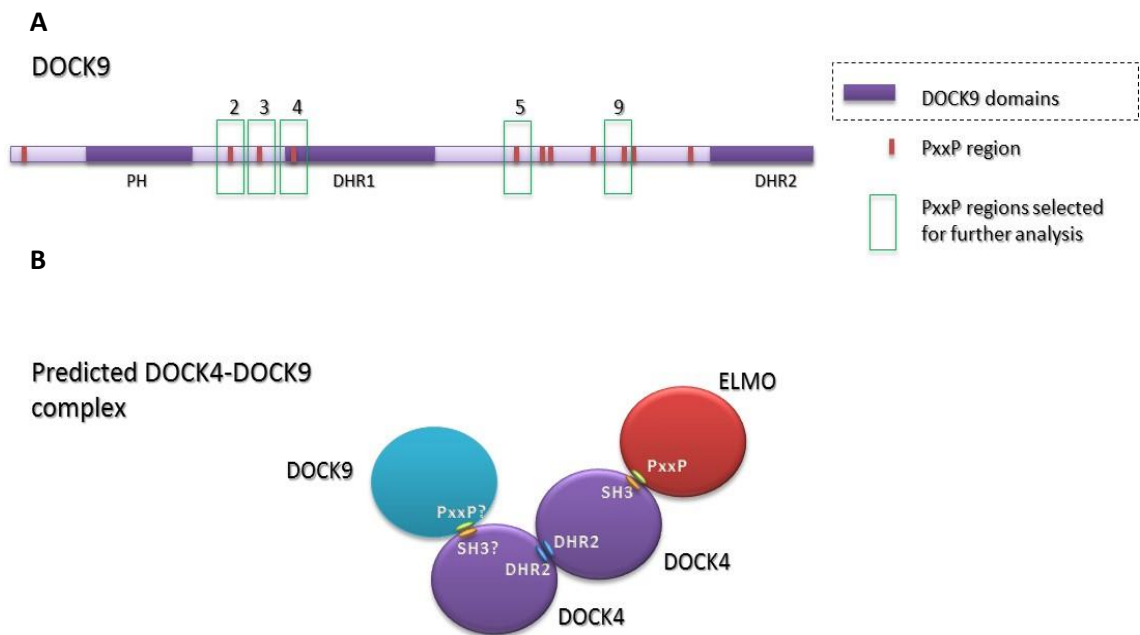
Figure 1-11 Identification of DOCK9 PRRs

(A) The GEF DOCK9 possess 11 proline PRR. Nine PRR have the typical PxxP or PxxxP motif. The small molecule QL-47 binds DOCK9 at the cysteine residue within PRR 3. **(B)** The predicted model of DOCK4 and DOCK9 interaction. The GEF DOCK4 homodimerises through bind of the DHR2 domains. DOCK4 SH3 domain also interacts with the adaptor protein, ELMO. DOCK4 and DOCK9 interact via the SH3 domain of DOCK4 and an unknown region of DOCK9, predicate to be one of nine typical PRRs.

1.5 Hypothesis

1. DOCK4 signalling is required for FGF2 driven angiogenesis.

2. The SH3 domain of DOCK4 interacts with a PRR of DOCK9.

3. DOCK4 expression is required for recovery from HLI in a murine model.

1.6 Aims

The overarching aim of this thesis is to understand the function of DOCK4 within pathological sprouting angiogenesis with consideration to the potential involvement of DOCK4 within FGF2 signalling. This thesis also investigates the mechanism of interaction between DOCK4 and DOCK9 within the RhoG signalling pathway (RhoG-DOCK4-RAC-DOCK9-CDC42) and its role in angiogenesis.

Aim 1. To investigate the role of DOCK4 in FGF2 signalling using an *in vitro* co-culture model.

Aim 2. To elucidate the molecular basis of the DOCK4-DOCK9 interaction using Co-IP and chromatography.

Aim 3. To investigate whether DOCK4 influences vascular response and recovery under conditions of ischemia in a Dock4+/- murine model.

2   Materials and methods

All materials used were purchased from Sigma-Aldrich or Thermo Scientific unless indicated otherwise in the text. Common laboratory standard solutions can be found in Table 2-1 at the end of this chapter.

All experimental work presented within this thesis was carried out by Leander Stewart, with the exception of the point mutagenesis generation of DOCK9 PxxP plasmids, as described in section 2.4 carried out by Ms. Anne Sanford. Hind limb surgical procedures, as described in section 2.28, were performed by Dr. Nadira Yuldasheva.

2.1   Primary cells and cell lines

Human Umbilical Vein Endothelial Cells (HUVECs) and Angiokit-tested (AGK) Human Dermal Fibroblasts (HDFs) were purchased from TCS cellworks. Human Embryonic Kidney Cells 293T (HEK 293T) cells were purchased from Clontech Laboratories.

2.2   Coating of tissue culture plates

Collagen I coating for the culture of HEK 293T cells after thawing: Plastic bottomed T-75cm^2 flasks were coated with 5mL of 50µg/mL Collagen I rat-tail (BD Biosciences); 5mg/mL stock of Collagen rat tail I was diluted in 0.02M glacial acetic acid. Coated plates were incubated at room temperature for 1 hour, and then washed three times with PBS.

Fibronectin coating for the culture HEK 293T in immunoprecipitation (IP) experiments: 100mm plastic plates were coated with 4ml of 10µg/mL fibronectin solution; 1mg/ml stock human plasma Fibronectin (Sigma-Aldrich) diluted in Phosphate Buffered Saline solution (PBS). Dishes were incubated at 37°C for 3 hours before excess solution was removed and plates washed 3 times with PBS.

2.3   Cell culture conditions

HEK 293T cells, stored in liquid nitrogen at passage 4 and passage 7, were thawed and seeded onto collagen I coated T-75 cm^2 flasks. HEK 293T were maintained in high glucose Dulbecco's modified eagle medium (DMEM) containing 10% v/v foetal bovine serum (FBS), supplemented with 1% v/v L-Glutamine, and 1% v/v penicillin-streptomycin.

Media was changed every 48 hours. Upon reaching 80% confluence cells were trypsinised, using 0.5% v/v Trypsin/EDTA, and split at a ratio of 1:6 and seeded onto T-150cm^2 flasks.

HUVEC were purchased at passage 2 and used in co-culture assays until passage 5. Cells were stored in liquid nitrogen and once thawed were seeded onto T-75cm^2 flasks and maintained in Large Vessel Endothelial Medium (LVEM, TCS cellworks) supplemented with 100µg/mL of penicillin and endothelial growth supplements. HUVEC LVEM was replenished every 48 hours. Upon reaching 80% confluence HUVEC were washed in PBS and trypsinised using 0.5% v/v Trypsin/EDTA. Cells were split in a 1:5 ratio onto T-75cm^2 flasks.

AGK HDF were cultured in high glucose DMEM containing 10% FBS, supplemented with 1% v/v L- Glutamine, and penicillin-streptomycin.

All cell culture work was carried out using aseptic techniques within a sterile HEPA filtration NuAire CellGuard class II biological safety cabinet and all cells were grown a humidified chamber at 37°C with 5% CO_2.

2.4   Plasmids

All plasmids used within this thesis are described in Table 2.2. Plasmid maps of each construct can be found in Appendix 7.1.2.

PEF4 Myc-Flag–DOCK9 (Meller et al., 2008) was obtained from Professor Martin Schwartz, University of Virginia, USA. pC3 EGFP-DOCK4 and pBABE puro Flag-DOCK4 were

obtained from Dr Vijay Yanik, Harvard Medical School, Massachusetts, USA. Plasmid pC3 EGFP-DOCK4 harbours a kanamycin resistance gene, for antibiotic selection in bacterial cultures. pEF4 Myc-Flag-DOCK9 and pBABE puro Flag-DOCK4 harbour an ampicillin resistance gene for antibiotic selection in bacterial cultures.

DOCK9 point mutants (proline-alanine) were previously developed in the laboratory (by Ms. Anne Sanford) using the pEF4 Myc-Flag–DOCK9 construct by means of the StratageneQuickchange II XL site- directed mutagenesis kit.

For expression of truncated DOCK4 proteins (as described table 2.1) human DOCK4 complementary DNA fragments were isolated from a pBABE puro Flag-DOCK4 plasmid and cloned into the pOPIN-F vector (Addgene). For the expression of full length or truncated DOCK9 proteins (as described table 2.1), fragments of the human DOCK9 complementary DNA was isolated from a pEF4 Myc-Flag-DOCK9-His plasmid and cloned into a pOPIN-F vector. Vector pOPINF harbours a C-terminal His tag, resulting in all expressed peptides being tagged at the C-terminal with the His tag. Constructs based on pOPIN-F harbor an ampicillin resistance gene for antibiotic selection. The pOPIN-F constructs also harbor a CMV enhancer, Chicken β -Actin promoter, T7 promoter/lac operator and ORFs Lef-2603 and 1629 for expression within mammalian cells, bacteria and insect cells. Primers used for sequencing confirmation of PCR amplified gene fragments can be found in Appendix 1 Tables 7.1 and 7.2.

DOCK4 primers	Forward primer sequences pOPIN vector sticky ends in lower case text	Reverse primer sequences pOPIN vector sticky ends in lower case text
SH3 1M-72K AT=51°C	5'-aagttctgtttcagggtacc ATGTGGATACCTACGG-3'	5'-Ctggtctagaaagcttaat TTTGTTCTTTACACAGGC-3'
SH3-CC 1M-174D AT=52°C	5'-aagttctgtttcagggtacc ATGTGGATACCTACGG-3'	5'-ctggtctagaaagcttaat GTCTTCCGGATCCACCATTGC G-3'
SH3-CC 1M-196Q AT=48°C	5'-aagttctgtttcagggtacc ATGTGGATACCTACGG-3'	5'-ctggtctagaaagcttaat CCGGTTAGTCACTCTCTAAA-3'
DHR2 1169M-1594A AT=56°C	5'-aagttctgtttcagggtacc ATGAAAATGGGAGAGG-3'	5'-ctggtctagaaagcttaa tAGCAGAGAACTCCTGTATCC C-3'
DOCK9 primers	Forward primer sequences pOPIN vector sticky ends in lower case text	Reverse primer sequences pOPIN vector sticky ends in lower case text
Full-length AT=54°C	5'-aagttctgtttcagggtacc ATGGAGGAATTTGTGCCCTGC-3'	5'-ctggtctagaaagctt AATCTGAGTATACACTGTAGA AACC-3'
PH-DHR1 AT=48°C	5'-aagttctgtttcagggtacc ATGGGTTCCCAGAAGGGTGGG-3'	5'-ctggtctagaaagctt AATCTGAGTATACACTGTAGA AACC-3'
PCIP-DHR1 AT=59°C	5'-aagttctgtttcagggtacc ATGTCGCAGCCGCCGCTGCTCCC-3'	5'-ctggtctagaaagctt TCATCCCAGCTGCTCATGC-3'

Table 2-1 Primers for nucleotide amplification for cloning of human DOCK4 and human DOCK9 gene sequences into plasmid constructs for protein expression. DOCK4 and DOCK9 gene sequences isolated from pBABE puro Flag-DOCK4 and pEF4 Myc-Flag-DOCK9, respectively. AT=Annealing temperatures used for each primer pair during PCR reaction.

Plasmid	Gene	Vector	Antibiotic selection gene
pC3 EGFP-DOCK4	DOCK4	pC3 EGFP	Kanamycin
pBABE puro Flag-DOCK4	DOCK4	pBABE puro	Ampicillin
pEF4 Myc-Flag-DOCK9	DOCK9	pEF4	Ampicillin
pOPINF DOCK4-SH3	DOCK4 SH3 domain	pOPINF HIS6-3C-POI	Ampicillin
pOPINF DOCK4-DHR2	DOCK4 DHR2 domain	pOPINF HIS6-3C-POI	Ampicillin
pOPINM DOCK9	DOCK9	pOPIN3SC HIS6-SUMO-3C-POI	Ampicillin
pOPINF PH-PCIP-DOCK9	DOCK9 PH-DHR1 domain	pOPINF HIS6-3C-POI	Ampicillin
pOPINF PCIP-DHR1-DOCK9	DOCK9 DHR1 domain	pOPINF HIS6-3C-POI	Ampicillin
pGIPz	Lentiviral packaging plasmid		Ampicillin
psPAX	Lentiviral packaging plasmid		Ampicillin
pMD2.G	VSV G	pMD2.G	Ampicillin

Table 2-2 List of plasmid construct used for experimental purposes

1.5   PCR

DOCK4 and DOCK9 DNA fragments were PCR amplified from the pBABE puro Flag-DOCK4 and pEF4 Myc-Flag-DOCK9, respectively, with a Q5 high-fidelity DNA polymerase and master mix (1x Q5 reaction buffer, 200μM dNTPs, 0.02U/μl Q5 high-fidelity polymerase, 1x Q5 high-fidelity enhancer, <1ng plasmid DNA, nuclease-free water). PCRs were carried using a Veriti™ 96-Well Thermal Cycler. Conditions are as follows: 30 sec denaturation at 98°C, 35 cycles of 5 sec, 30 sec annealing with temperature optimised for each primer pair (see table 2.1), elongation at 72°C for 4mins for full length DOCK9 constructs and 30 sec for all other constructs), 2 min final extension at 72°C.

2.5   PCR clean-up

15μl of PCR product per reaction was purified using a Monarch® PCR & DNA Cleanup Kit in accordance with manufacturer's protocol.

2.6   Cloning

DOCK4 SH3 domain amplified from pBABE puro Flag-DOCK4, DOCK9 PH-PCIP domain amplified from pEF4 Myc-Flag-DOCK9) and DOCK9 p.PCIP627-630 domain amplified from pEF4 Myc-Flag-DOCK9 by PCR were sub-cloned into a modified a pOPINF HIS6-3C-POI vector, which had been ligated by the restriction enzymes NcoI and MscI. Full length DOCK9 was sub-cloned into pOPIN3SC HIS6-SUMO-3C-POI. Sub-cloning was carried out using a NEB builder HiFi DNA assembly kit. All primers described within this section are listed within Table 2.1.

2.7   Bacterial transformation and plasmid preparation

BL21 pLYsS *E.coli* competent cells were quickly thawed on ice. 1μl of DNA was added to 50μl of *E.coli* then incubated on ice for 30 minutes. Cells were then heat shocked at 42°C

for 45 seconds then placed on ice for 2 minutes. Cells were supplemented with 250µl of super optimal broth and placed on a shaking incubator at 37°C for 1 hour. The pEF4 Myc-Flag–DOCK9 plasmids contain an ampicillin selectable marker thus were streaked onto lysogeny broth (LB) agar plates prepared with 100µg/ml of ampicillin. BC21 bacteria transformed with pC3 EGFP-DOCK4 and pC3 EGFP-EV (empty vector) plasmids were cultured on LB agar containing 50µg/mL of kanamycin; as these plasmids possess the kanMX cassette. Cultures were incubated overnight at 37°C. After 18 hours of growth one colony per plate was selected and inoculated into a 3ml aliquot of LB broth containing the antibiotics that corresponds with the plasmids selectable marker. The 3ml cultures were incubated at 37°C in a shaking incubator for 8 hours, following which the 3ml cultures were inoculated into antibiotic containing 100mL of LB broth and returned to the shaking incubator at 37°C for 18 hours.

DOCK9 point mutation plasmids were extracted and purified using PureLink® HiPure Plasmid Midiprep Kit (Invitrogen) according to manufacturer's protocol. Plasmid concentrations were determined using Nanodrop spectrophotometry.

2.8   Production of pOPINF-DOCK4 SH3, DOCK9 PH-PCIP, DOCK9 PCIP-DHR1, and pOPIN3SC-DOCK9 plasmids in *E.coli.*

E.coli strain DH5α were transformed, as previously described, using 500pg of the described plasmid constructs pOPINF-DOCK4 SH3, DOCK9 PH-PCIP, DOCK9 PCIP-DHR1, and pOPIN3SC-DOCK9. Cultures were streaked onto ampicillin agar plates and grown over 72 hours at 16°C. Colonies were selected using blue white screening and inoculated into 10ml of LB broth containing ampicillin and incubated overnight at 37°C. Plasmids were extracted from DH5α cells using the Wizard MagneSil plasmid purification system.

All constructs were sequenced using Sanger sequencing, incorporating multiple primers designed to complement the DNA sequence in 700 base pair increments. Sequencing was carried out by ThermoFisher.

2.9 Production and purification of Plasmids for mammalian cell expression

Plasmids pEF4 Myc EV Flag, pEF4 Myc-Flag–DOCK9, and pEF4 Myc-Flag–DOCK9 PRR mut2, pEF4 Myc-Flag–DOCK9 PRR mut3, pEF4 Myc-Flag–DOCK9 PRR mut4, pEF4 Myc-Flag–DOCK9 PRR mut5, pEF4 Myc-Flag–DOCK9 PRR mut9 were cultured from glycerol stocks and inoculated in BL21 (DES) competent cells (Invitrogen™, Carlsbad, California USA), in accordance with manufacturers protocol.

Transformed competent cells were cultured on agar plates in the presence of either ampicillin (pEF4 Myc EV Flag, pEF4 Myc-Flag–DOCK9, and pEF4 Myc-Flag–DOCK9 PRR mut2, pEF4 Myc-Flag–DOCK9 PRR mut3, pEF4 Myc-Flag–DOCK9 PRR mut4, pEF4 Myc-Flag–DOCK9 PRR mut5, pEF4 Myc-Flag–DOCK9 PRR mut9) or kanamycin (pC3 EGFP-DOCK4 and pC3 EGFP-EV) and cultured over night at 37°C. Individual colonies was inoculated into 15ml of LB, supplemented with the appropriate antibiotics, cultures for 6 hours in a shaking incubator at 37°C. 15ml start-up cultures were then inoculated into 50ml of LB supplemented with antibiotics and placed in a shaking incubator at 37°C overnight. Bacterial cultures were centrifuged at 5,000g for 15 minutes. Supernatant was discarded and pellet retained. Plasmids were extracted from bacterial pellets using a PureLink HiPure Plasmid Midiprep kit (Invitrogen™, Carlsbad, California USA), in accordance with manufacturers protocol.

2.10 Restriction Enzyme Digestion

Plasmids pEF-EV Flag pEF4 Myc EV Flag, pEF4 Myc-Flag–DOCK9, and pEF4 Myc-Flag–DOCK9 PRR mut2, pEF4 Myc-Flag–DOCK9 PRR mut3, pEF4 Myc-Flag–DOCK9 PRR mut4, pEF4 Myc-Flag–DOCK9 PRR mut5, pEF4 Myc-Flag–DOCK9 PRR mut9 were digested with NotI and

KpnI in NEB buffer 2.1 (New England Biosciences) according to the manufacturer's protocol. Plasmids pC3 EGFP-DOCK4 and pC3-EGFP were digested with BamHI in NEB buffer 3.1 in accordance with the manufacture's protocol. Digested plasmids were resolved on a 0.7% agarose gel using agarose gel electrophoresis.

2.11   Transformation of competent cells for protein expression

Optimal competent cells were selected through screening of a panel of competent cells (BL21 (DES), BL21 pLYsS (DES), BL21 (DES) RP, BL21 (DES) RIL, NiCo21), all competent cells produced in-house at the Protein Production Facility (Faculty of Biological Science, University of Leeds). Transformations of pOPINF and pOPIN3SC constructs were carried out as previously described. Transformed competent cells were streaked onto lysogeny broth (LB) agar plates prepared with selectable antibiotic markers (ampicillin 100µg/ml: BL21, NiCo21. Ampicillin plus chloramphenicol 34µg/ml: BL21 pLYsS (DES), BL21 (DES) RP, BL21 (DES) RIL). Cultures were incubated overnight at 37°C. Individual colonies were selected and inoculated into 1ml of LB supplemented with antibiotics and incubated overnight at 37°C. 20µl of overnight culture was inoculated into 2ml of LB plus antibiotic. Cultures were incubated in a shaking incubator at 37°C until reaching an optical density (OD) 600 of 0.6nm (measured using spectrophotometer). Once cultures reach 0.6nm cultures were treated with 0.2mM of Isopropyl β- d-1-thiogalactopyranoside (IPTG). Cultures were grown overnight at 18°C.

For large scale cultures 1 colony was selected per agar plate. Each colony was inoculated into 100ml of LB supplemented with antibiotics, cultures were grown overnight at 37°C. 100ml start-up culture was inoculated into 900ml of LB supplemented with antibiotics and placed in a shaking incubator at 37°C until reaching an optical density at 600nm (OD600) of 0.6 (measured using spectrophotometry). Once cultures reached OD600 0.6 cultures were treated with 0.2mM of IPTG. Cultures grown overnight at 18°C.

2.12   Bacterial culture lysis

Bacterial cultures treated with IPTG were centrifuged at 5,000g for 15 minutes. Supernatant was discarded and pellet retained and re-suspended in a His wash buffer (20mM Imidazole, 150mM NaCl, 20mM Tris ph7.6). Cultures were lysed by sonication with 10x 10 second sonication pulses with 30 second pauses in-between the pulses. All cultures were kept on ice during lysis protocols. Lysed cell cultures were then centrifuged at 17,000g for 35 minutes. Supernatants were retained and pellets discarded.

2.13   Transfection of plasmid DNA

Plasmid DNA was transfected into HEK 293T cells using Lipofectamine 2000 (Invitrogen) in accordance with manufacturer's protocol. $3x10^6$ HEK 293T cells were plated onto fibronectin coated 100mm plates in 10ml of DMEM supplemented with 10% v/v FBS, L-Glutamine, and antibiotics. Cells were cultured overnight at 37°C after which time the DMEM medium was removed and cells were washed 4x with antibiotic-free DMEM with 10% v/v FBS and L-Glutamine and 10ml antibiotic-free medium was left on each plate.

For each 100mm plate 20µL of Lipofectamine 2000 was added to 480µL of reduced serum OptiMEM medium. 5µg of plasmid was suspended in reduced serum OptiMEM medium to a total volume of 500µL. Plasmid and Lipofectamine 2000 containing aliquots were combined, vortexed for 15 seconds, then incubated at room temperature for 30 minutes. The combined solution was then added dropwise onto the cells. Transfected cells were incubated at 37°C + 5% CO_2 for 48 hours without medium change.

2.14   Affinity chromatography

His-tagged proteins were purified from bacterial lysates using a nickel column on an ÄKTA pure system (GE healthcare). The His-column was washed with 70% v/v ethanol then

equilibrated with a His wash buffer (20mM Imidazole, 150mM NaCl, 20mM Tris ph7.6). The sample was loaded onto the column at a rate of 1ml/min. The protein loaded column was then washed with His wash. Sample was eluted from the column through application of an elution buffer (50mM Tris pH 7.6, 300mM NaCl, 300mM imidazole, 5% v/v glycerol, 0.075% v/v β-mercaptoethanol) that was diluted with His wash buffer at increasing concentrations until reaching 100% elution buffer. DOCK4-SH3 domain and DOCK9 PCIP-DHR1 proteins purified through using affinity chromatography were stored in 20mM Tris pH7.6, 150mM NaCl, and 1mM DTT.

2.15   Size exclusion chromatography

Affinity chromatography of purified peptides DOCK4-SH3 domain and DOCK9 PCIP-DHR1 were concentrated using a 3K MWCO Pierce™ Protein Concentrators PES for concentrating DOCK4-SH3 and 10K MWCO Pierce™ Protein Concentrators PES for concentrating DOCK9 PCIP-DHR1, prior to size exclusion chromatography (SEC).

Protein samples were purified according to size using a Superdex® 75 Gel filtration column (GE Healthcare). In order to test DOCK4-SH3 and DOCK9 PCIP-DHR1 domain interaction, approximately 1ml of 1mg/ml DOCK4-SH3 was loaded onto the Superdex® 75 Gel filtration column using a 2.5ml loop. Immediately afterwards, approximately 1ml of 1mg/ml DOCK4-SH3 was loaded onto the Superdex® 75 Gel filtration column using a 2.5ml loop. Equal concentrations of DOCK4-SH3 and DOCK9 PCIP-DHR1 were combined then loaded onto the Superdex® 75 Gel filtration column using a 2.5ml loop. All samples were collected and analysed using SDS PAGE gel separation and Coomassie staining.

2.16   Lentiviral shRNA particle generation

In order to knock down DOCK4 protein in HUVEC, two different DOCK4 shRNA and a non-silencing pGIPZ construct (Thermo Scientific, Open Biosystems) were used:

DOCK4 shRNA 3 mature antisense - CTCAGTATTTGCAGATATA

DOCK4 shRNA 4 mature antisense - CGCAAGGTCTCTCAGTTAT

Non-silencing pGIPZ - ATCTCGCTTGGGCGAGAGTAAG

HEK 293T cells were seeded onto poly-L-lysine coated 100mm dishes at a density of 3×10^6. Cells were washed with 5ml of Opti-MEM and maintained in 7ml of Opti-MEM per plate prior to transfection. Cells were transfected with lentiviral packaging plasmids pMD2.G (3 µg) and psPAX2 (7 µg), and DOCK4 shRNA (10 µg) with 40µl of transfection reagent Lipofectamine 2000 per tissue culture plate. DNA and Lipofectamine were prepared separately in 500µl of Opti-MEM then combined, vortexed, and added dropwise to confluent HEK 293T cells. Cells were incubated at 37°C with 5% CO_2 for 4 hours after which Opti-MEM media was replaced with high glucose DMEM containing 10% v/v FBS, supplemented with 1% v/v L- Glutamine. Cells were maintained at 37°C with 5% CO_2.

Media was removed and replaced with fresh DMEM 24 hours post transfection and returned to the incubation cabinet at 37°C with 5% CO_2.

Viral rich medium was removed and replaced with fresh media after 48 hours. The collected supernatant was centrifuged at 3000 x g for 20 mins then filtered through a 0.45 µM syringe filter and stored at 4°C for use within 7 days following particle production.

All cell culture work was carried out using aseptic techniques within a sterile HEPA filtration NuAire CellGuard class II biological safety cabinet and all cells were grown a humidified chamber at 37°C with 5% CO_2.

2.17   Lentiviral transduction

HUVEC were seeded onto 6 well flat bottom plastic culture plates at a density of 1.5x10^5 cells per well, using cell culture conditions described in section 1.3. Approximately 24 hours post seeding cells were treated with shRNA viral supernatant diluted in large vessel media in a 2:3 ratio.

2.18   Cell lysis for Co-immunoprecipitation (Co-IP)

Cells growing in 6 well plates or 100mm plates were washed with PBS and then lysed in 50µl or 400µl cold RAC lysis buffer (50mM TRIS pH 7.4, 10% v/v Glycerol, 1% v/v NP40, 5mM MgCl2, 100mM NaCl, 5X Complete Protease Inhibitor EDTA free (Roche Applied Science), 1mM dithiothreitol (DTT)) respectively. Lysates were cleared by centrifugation at 13,000g on a bench-top centrifuge for 30 minutes.

2.19   Co-immunoprecipitation assay

GFP-DOCK4   protein   was   extracted   from   total   cell   lysate   through immunoprecipitation using GFP-trap (Chromotek) beads. GFP-trap beads were prepared according to manufacturer's protocol. Cell lysates were added to 20µL of washed GFP-trap slurry and incubated with rotation at 4°C for 1 hour.

Samples were then centrifuged for 2 minutes at 12,000 g, the supernatants were removed and the beads were resuspended in RAC wash buffer (TBS, 10mM MgCl2, 5x EDTA free Complete Protease Inhibitor, 1mM DTT) and washed twice. After the final wash the pelleted beads with bound protein were resuspended in 40µl 4x Sodium dodecyl sulfate (SDS) sample buffer (Invitrogen) and 1.5µL of 1M DTT. The samples were then denatured at 95°C for 10 minutes.

2.20   SDS polyacrylamide gel electrophoresis

3-8% v/v 12 well Tris-Acetate NuPAGE Novex® Pre-Cast Gel (Invitrogen) was used for the electrophoretic separation of proteins in an XCell4 SureLockTM Midi-Cell electrophoresis tank (Invitrogen). 1 litre of 1x NuPAGE® MES SDS running buffer (Invitrogen) was used to fill the tank, along with 465µl of NuPAGE® antioxidant (Invitrogen). 40µL of prepared protein sample was used per well and 5µL of Precision Plus Protein™ All dual colour Standards (Bio-Rad) was dispensed into the 10µL wells provided on either ends of the gel. Electrophoretic separation of proteins was carried out at 150V for 120 minutes.

2.21   Western blotting

Proteins were transferred onto an Immobilon® polyvinylidine difluoride membrane (PVDF) (Sigma-Aldrich) in a TE42 Standard Transfer Tank (Hoefer) submerged in 6L of 1x Towbin buffer (25nM Tris, 193mM Glycine, pH 8.3, 20% v/v methanol). The tank was positioned in a 4°C cold-room and protein transfer was performed for 2 hours at 1A.

Target proteins were probed using HRP labelled antibodies (see figure 2.3) diluted in TBS+0.1% (v/v) Tween-20 (TBST) in accordance with manufacturers recommendations. An ECL detection kit (Amersham) was used to visualise target proteins.

2.22   Colorimetric quantification of Co-IP proteins

Western blots analysis of the GFP-trap Co-IP of EGFP-DOCK4 and Flag-DOCK9 proteins (WT; Proline rich regions 2, 3, 4, 5, and 9) were quantified using ImageJ colorimetric analysis software. GFP-tagged protein levels were detected through anti-GFP primary antibody and an appropriate HRP-labelled secondary antibody probing of the Western blots, followed by ECL detection, blot exposure and imaging. The concentration of GFP-tagged proteins was determined by the ratio of signal through ImageJ colorimetric analysis.

Quantification of GFP-DOCK4 was used as a control to depict the level of IP protein concentration. Quantification of Flag-tagged proteins was determined through anti-Flag primary antibody and an appropriate HRP-labelled secondary antibody probing of the Western blots, followed by ECL detection and blot exposure and imaging. The concentration of GFP-tagged proteins was determined through ImageJ colorimetric analysis and then normalised to the GFP-tagged DOCK4 concentration. Ratio of signal analyses was performed using GraphPad Prism 7.0a.

2.23   Stripping and blocking

PVDF membranes were washed with dH$_2$O for 10 minutes on a rocker at RT. Membranes were then submerged in 50ml of 0.5M NaOH and returned to the rocker for 10 minutes at RT. The washing step in dH$_2$O was then repeated. PVDF membranes were then blocked in TBST containing 5% w/v skimmed milk powder for 1 hour at RT.

No.	Primary antibody	Dilution	Reactivity	Cat No./ Source
1	Rabbit anti-CD31	1:30	Mouse, Human, Pig	Ab28364/ ABCAM
2	Mouse anti-CD31	1:20	Human	M0823/ DAKO
3	Mouse anti-CD31	1:400	Human	KC1004/ Caltag medical systems
4	Rabbit anti-DOCK4	1:100	Human, Mouse	A302-263A/ Bethyl Laboratories
5	Rabbit anti-DOCK9	1:1000	Human	A300-530A/ Bethyl Laboratories
6	Mouse anti Flag-M2	1:1000	Human	F1804/ Sigma Aldrich
7	Rabbit anti-GFP	1:1000	Human	sc-8334/ Santa Cruz
8	Mouse anti-RFP Ab	1:1000	Mouse	GTX82561/ GeneTex
No.	Secondary antibody	Dilution	Reactivity	Cat No./ Source
1	ImmPRESS™ HRP Anti-Rabbit IgG	1:1000	Rabbit	MP-7401/ Vector lab
2	ImmPRESS™ HRP Anti-mouse IgG	1:1000	Mouse	MP-7402/ Vector lab
3	Alkaline phosphatase conjugated anti-mouse IgG1	1:500	Goat	KC1005 Caltag medical systems

Table 2-3 List of primary and secondary antibodies.

2.24 Organotypic angiogenesis assay

Human dermal fibroblasts (Caltag Medsystem) were seeded onto 24 well plastic tissue culture plates at a density of $2x10^4$ cells per well. Fibroblasts cells were maintained in DMEM, as described in section 2.3. Fibroblasts were incubated at 37°C +5% CO_2 for 7 days. After 7 days of fibroblasts growth the medium was removed. $1x10^4$ HUVEC were seeded on top of confluent fibroblasts per well. Where required, cells were stimulated with either 10ng/mL FGF2 (Peprotech) or 25ng/mL of recombinant human VEGFA (Sigma-Aldrich) on days 4 and 6 post HUVEC seeding. On day 7, all media was removed from cultures and cells were fixed in 70 % ice cold ethanol for later analysis.

2.25 Angiogenesis co-culture treatment with small molecule QL-47

QL-47 inhibitor reconstituted in DMSO, to a concentration of 10mM, was gifted from the Nathanael Gray Lab (Dana Farber Institute, USA). QL-47 was used to treat HUVEC within an organotypic angiogenesis assay. HUVEC and HDF co-cultures were treated with QL-47 at a concentration of 5μM, or with DMSO at a 1-1000 dilution on days 4 and 6. Co-cultures were also treated with 10ng/ml FGF2, 25ng/mL of recombinant human VEGFA, or cultured without supplementation of addition GFs. On day 7 media was removed from cultures and cells fixed for later analysis.

2.26 Hypoxic angiogenesis co-culture assay

Hypoxic angiogenesis co-culture assays were carried out in accordance with the organotypic co-culture assay previously described, with modification to the GF treatment protocol. Co-cultures were supplemented with 10ng/ml FGF2 4 days following HUVEC seeding and immediately placed into a hypoxic incubator at 1% O_2 and 5% CO_2. Cultures were removed from the hypoxic incubator on day 6 and supplemented with 10ng/mL FGF2.

Cultures were returned back to the hypoxic incubator for a further 24 hours. After the remaining 24 hours, cultures were removed from the incubator and immediately fixed in 70% ice cold ethanol for 30 minutes at RT.

2.27   Angiogenesis co-culture fixation and immuno-histochemical staining

24 well plated fibroblasts and HUVEC co-cultures were washed once using PBS then fixed in 70% ice cold ethanol for 30 minutes at RT. Cells were stained using a commercially available CD31 tubule staining kit supplied by TCS cell works (Caltag Med systems). Tubules were permanently stained through binding of anti-CD31 primary antibody coupled to an alkaline phosphatase conjugated secondary anti-IgG antibody. Insoluble chromogenic substrates nitro-blue tetrazolium (NBT) and 5- bromo-4-chloro-3'-indolyphosphate (BCIP) were used for colourmetric detection of CD31 expressing ECs.

2.28   *In vivo* mouse models

All *In vivo* experiments were conducted in accordance with the Animal (Scientific Procedures) Act 1986 Amended Regulations 2012 (ASPA 2012) and NCRI Guidelines approved by the University of Leeds Animal Welfare and Ethical Review Committee. The Dock4 conditional knockout line was generated and verified by Ozgene, Australia and the iVEC-Cre; Rosa26tdTomato line was kindly provided by Dr Karen Blyth, Beatson Institute, Glasgow. The two lines were maintained and intercrossed under Project license (PFE6DC80B) at the St James's Biological Services (SBS) animal facility unit.

The project and personal licenses used to carry out all animal research described within this thesis are as follows:

Project License: Stephen Wheatcroft P144DD0D6

Personal License: Leander Stewart I91EAEBOC

Personal License: Nadira Yuldasheva ICB059380

2.29   Mouse line breeding

For global heterozygous Dock4 deletion, heterozygous Dock4 mice (Abraham et al 2015) lacking exons 3, 4 and 5 were used (C57BL/6J background) as homozygous deletion is embryonic lethal (Abraham et al 2015). The line was maintained and experimental cohorts were generated through intercrossing with C57BL/6J mice (Appendix 3, Figure 7.13).

For conditional Dock4 deletion, the mouse line Dock4f/f (Dock4 exon 6 flanked by LoxP sites for recognition by Cre recombinase, depicted in Appendix 3, Figure 7.14) was intercrossed with the mouse line iVEC-Cre; mice. Rosa26tdTomato double transgenic line for Cre recombinase expressed under the control of the endothelial specific VE-cadherin promoter (Wang et al., 2010), for tamoxifen inducible Cre expression and Cre deletion of the loxP site flanked exon, and the tdTomato Cre reporter protein designed to have a loxP-flanked STOP cassette preventing transcription of a CAG promoter-driven red fluorescent protein (RFP) variant (tdTomato), all inserted into the Gt(ROSA)26Sor locus (originally from The Jackson Laboratory). The LoxP sites flank exon 6 of the Dock4 gene (Appendix 3, Figure 7.15), activation of Cre expression results in expression of an unstable truncated Dock4 peptide. Dock4 and tdTomato immunofluorescent staining of the hind limb tissues was used to confirm knockdown of Dock4 expression (Figure 5.10). Knockout of the Dock4 gene expression was further confirmed through tdTomato immunofluorescent staining of brain sections of iVEC-Cre; Rosa26tdTomato mice (Teklu Egnuni, Thesis 2018).

All pups produced for each mouse line were ear biopsied at 3 weeks old and genotyping was carried out by Transnetyx (TN, USA). Wild type littermates were used as an experimental control model. Both male and female mice were used during all experiments, as no difference in result was detected between the two genders. All mice were 21 weeks of age at the point of femoral artery ligation.

Primers used for conditional mouse model genotyping by Transnetyx (TN, USA):

2.30   *In vivo* ischemia model

Surgical procedures were carried out by Dr Nadira Yuldasheva. 24 hours prior to surgery the lower abdomen, groin, and legs of each mouse were depilated with hair removal cream (Veet, Reckitt Benckister UK). Mice were anaesthetised by inhalation of isoflurane-vet (Merial Animal Health Ltd, Essex, UK); initially isoflurane gas was delivered within a Perspex containment unit, then maintained via a nose cone mask. Each mouse was placed on a heating plane (Vettech, UK) in the supine position with the upper paws fixed on the mask and lower extremities abducted and extended. The surface area on and around the hind limbs were cleaned with providone-iodine 0.75% w/w (Vetasept animal care, York, UK).

The left femoral artery extending from the region under the inguinal ligament to the saphenous artery was exposed and the adipose pad with epigastric artery was cauterised. The iliac artery was encircled with 8.0 Vicryl suture (Ethicon, Belgium) then dissected. The femoral artery, proximally at the inguinal ligament and distally at the bifurcation to saphenous and popliteal vessels, was separated from the vein, encirculated with 8.0 Vicryl sutures, and the intervening arterial segment was excised.

Following surgery the mice were maintained at 38°C within a warm chamber (Thermal cage; Vettck, UK) until regaining consciousness and motility. The operation was performed with the assistance of the surgical microscope (Ziess, OPMI 1-FC) under the appropriate magnification (x7.2-x30).

2.31   Tamoxifen treatment

iVEC-cre+ve; Rosa26-lsl-tdTomato; Dock4 f/f mice (n=9) and iVEC-cre-ve; Rosa26-lsl-tdTomato; Dock4 f/f mice (n=8) underwent daily intraperitoneal injections of a 2mg dose of tamoxifen for 5 consecutive days. Seven days following the final tamoxifen dose all mice underwent a HLI operation to surgically ligate and transect the left femoral artery.

2.32   Laser Doppler Imaging techniques

Approximately one hour following surgery, superficial blood flow within the hind limbs was analysed using a moorLDI2-HIR Laser Doppler imager (Moor Instruments LTD). Mice were anaesthetised by inhalation of isoflurane-vet (Merial Animal Health Ltd); delivered within a Perspex containment unit. The anaesthetic was then maintained via a mask. Data readings of vascular perfusion were obtained via dynamic light scattering analysis of which is converted to a signal proportional to the tissue perfusion. From this data a color-coded perfusion image is generated by the moorLDI V6 PC Software (Moor Instruments LTD) which then generates a numerical value to represent the level of tissue perfusion of both hind legs. The region of hindlimb from the ankle to the foot was selected for comparative analysis, as this region of limb is the area most affected by the femoral artery ligation (Hellingman et al., 2010). The ratio of perfusion in the ischemic to non-ischemic limb was calculated to normalise the blood flow of the ischemic limb to that of the non-ischemic limb. Laser Doppler imaging (LDI) readings were taken 7, 14, and 21 days after surgical femoral artery ligation.

2.33   Muscle harvest and fixation

Approximately 2 hours after generating the final LDI reading mice were anaesthetised by inhalation of isoflurane-vet (Merial Animal Health Ltd); delivered within a Perspex containment unit. Mice were placed on a surgical table in a supine position on a heating plane (Vettech) with the upper paws fixed on the mask and lower extremities abducted and extended. Anaesthetic was then maintained via a nose mask.

Each mouse was exsanguinated via caudal vena cava transection and whole body perfused. Abdominal cavity and pericardial cavity were exposed through a lower abdominal longitudinal incision, approximately 2 cm long, and a 3cm ventral midline incision. The Caudal

vena cava was dissected free of surrounding fascia and cut. Whole body vasculature was flushed through with injection of 10ml of 10% v/v PBS into the cardiac left ventricle. Muscle was fixed via injection of 10ml of 4% v/v paraformaldehyde into the cardiac left ventricle.

All skin and fascia were removed from the lower extremities and the gastrocnemius and soleus muscles were surgically removed from both legs and placed together within a tissue storage cassette. All tissue samples were submerged in 4% v/v PFA for 24 hours then transferred to 70% v/v ethanol for approximately one week. Muscles were embedded in paraffin wax in a longitudinal orientation.

2.34   Muscle sectioning

Longitudinally orientated gastrocnemius and soleus embedded in paraffin wax were sectioned into 50x 5µm thick floating sections per block using a microtome (Leica Biosystem, Wetzlar, Germany). Initial 10 x 10µm sections of each muscles block were removed and discarded prior to selecting sections for mounting on non-frosted glass slides (Thermo Scientific).

2.35   Immunohistochemistry

2.35.1 Dewaxing and rehydration

Optimal slides were selected for immuno-histochemical (IHC) staining, with one slide selected after approximately every 10th slide. Slides were placed on a hotplate at 70°C for 20 minutes then transferred to 24-slide baskets. Slides were dewaxed in four separate consecutive Xylene containers for 5 minutes increments. Slides were then rehydrated in consecutive separate containers: absolute ethanol for 2x2 minutes, 90% v/v ethanol for 2 minutes, and 70% v/v for 2minutes. Slides were then thoroughly rinsed in running tap water for 1 minute.

2.35.2 Antigen retrieval and IHC staining

Slides were submerged and incubated in Antigen Unmasking Solution, Tris-Based (Vector Laboratory) within a pressure cooker reaching 125°C, then removed from Antigen Unmasking Solution and submerged in running water for 1 minute. Tissue section region was encircled using an ImmEdge™ Pen (H-4000) hydrophobic pen (Vector Laboratory). Slides were submerged in Tris buffered saline for 1 minute. Endogenous antibodies of tissue sections were incubated in BLOXALL Endogenous Peroxidase and Alkaline Phosphatase Blocking (Vector Laboratory) for 15 minutes followed by a 5 minute incubation in TBS-Tween. Tissue proteins were then blocked in 1/10 Casein Solution (Vector Laboratory) for 20 minutes. Antibodies prepared in Antibody Diluent (ThermoFisher) to their optimised concentration (see table 2.3) then dispensed onto slides and incubated at ambient temperature for 1 hour followed by 2x 5 minute washes in TBS-Tween. Slides were incubated in the appropriate secondary antibody (see table 2.3) for 30 minutes, then washed for 2x 5 minute washed in TBS. Slides were stained in ImmPACT DAB Peroxidase (HRP) (Vector Laboratory) prepared in ImmPACT DAB solution (Vector Laboratory).

Cell nuclei were counterstained with Mayer's haemotoxylin for 30 seconds, followed by a wash under running water and 1 minute immersion in Scott's Tap water. Slides were placed in lithium carbonate for 2 minutes then rinsed in running water then placed in Xylene.

2.35.3 Dehydration, clearing and mounting

IHC stained slides were dehydrated and cleared through submersion in 3 consecutive 20 second absolute ethanol washes. Slides were air dried for 5 minutes and cleared in 4 consecutive changes of Xylene. Glass slides were mounted onto slides with DEPEX (Sigma).

2.35.4 IHC quantitative image analysis

CD31 IHC stained tissue sections were scanned using Apeiro AT Virtual Slide scanner (Leica Biosystems, Wetzlar Germay) and area for analysis selected using Apeiro ImageScope software (Leica Biosystems, Wetzlar Germay). Eight randomly selected 500μm x 500μm

boxes were placed over each section image. ImageJ software (National Institutes of Health) was utilised for quantification of all visible CD31 stained vasculature within the 500μm x 500μm boxes. TVL and branch points within the defined areas were quantified within each box. RFP and DOCK4 IHC stained tissue sections were imaged at 20x using a Nikon light microscope (Nikon Instruments Inc, Edgewood NY).

2.36   Statistical analysis

All data within this thesis was collected and analysed by Leander Stewart. Data acquisition and analysis of organotypic co-cultures was blinded throughout. The genotypes of all mice to undergo HLI surgery were blinded from the outset and throughout the surgical procedure. However, genotypes of the mice utilised for the HLI was known during LDI data acquisition, and data analysis.

2.36.1 Organotypic angiogenesis assays

Organotypic angiogenesis assay cultures were imaged using an Olympus CKX41 light microscope with 9 images taken per well. Images were analysed manually using ImageJ software, generating a measurement of total vessel length (TVL), average vessel length, and branch point index (BPI) for each image.

Quantification of angiogenesis parameters (number of branches, tubules and tubule length) were performed as previously described (Hetheridge et al., 2011). The mean average of each data output was generated per experiment for each of the organotypic co-culture conditions. Gaussian distribution of calculated mean ± SD values of QL-47 treated organotypic co-cultures and DOCK4 shRNA knockout cultures were verified using Levene's and Bartlett's test and a Kruskal–Wallis one-way analysis of variance or One-way ANOVA analysis of variance were performed were appropriate using Origin 2015 software (OriginLab Corp., Northampton, MA) to assess significance.

2.36.2 Laser Doppler Imaging

Numerical values representing blood flow of tissues imaged by the Laser Doppler Imager Data were calculated as mean ± standard deviation. When comparing the ischemic limbs between experimental groups, the ratio of blood flow between the ischemic limb and non-ischemic limb was calculated, then the mean ± standard deviation ratio of blood flow of each experimental group was generated to compare hind limb perfusion between the different experimental groups using a One-way ANOVA with Tukey's multiple comparisons. For analysis of non-ischemic limb, mean ± standard deviation of the absolute value of the non-injured limbs were calculated and compared using One-way ANOVA with Tukey's multiple comparisons. Statistical analysis was performed with GraphPad Prism 7.0a.

Area under the curve was also measured using GraphPad Prism 7.0a, the software uses the trapezoidal rule algorithm for area under the curve calculations, values were compared between experimental groups using one-way ANOVAs, with LSD post-hoc analyses where appropriate. Statistical analysis was performed with GraphPad Prism 7.0a.

Linear regression and slope intersects of the blood flow recovery over time of each experimental group were also analysed using GraphPad Prism 7.0a. Statistical analysis comparing linear regression and slope intersects were performed using GraphPad Prism 7.0a.

2.36.3 Histological analysis

TVL of all CD31 stained vasculature within the defined areas were quantified and used to generate a mean value of TVL for each section. All branch points of all CD31 stained vasculature within the defined areas were quantified and used to generate a BPI (defined as total branch points/TVL). The mean value of total BPI of each box was used to calculate a mean BPI for each muscle section. Gaussian distribution of calculated mean ± SD values were verified using Levene's and Bartlett's test and a One-way ANOVA analysis of variance was performed using GraphPad Prism 5 to assess significance.

Sr.No.	Solution	Recipes or Cat. No
1	PBS	500ml dH$_2$0 + 2 PBS tablets (Cat.No. P4117, Sigma) + 1 PBS tablet (Ca.No. BR0014G, OXOID)
2	Lysis Buffer (PCR)	100 mM Tris (pH 8.5), 5 mM EDTA, 0.2% v/v SDS, 200 mM NaCl
3	Lysis buffer (WB)	50mM TRIS pH7.4, 10% v/v Glycerol, 1% v/v NP40, 5mM MgCl$_2$ 100mM NaCl
4	RAC Lysis buffer	50mM TRIS pH 7.4, 10% v/v Glycerol, 1% v/v NP40, 5mM MgCl$_2$, 100mM NaCl, 25x Complete Inhibitor (no EDTA) and 1mM DTT
5	10xTBS	100ml 1M Tris-Base pH 7.5 + 200ml 5M NaCl (900ml dH$_2$0 + 24 gm Tris Base + 88 gm NaCl)
6	1xTBS	900ml dH$_2$0 + 100ml 10xTBS
7	TBST	1xTBS + 0.1% v/v Tween-20 (900 ml dH$_2$0 + 200ml 10TBS + 1ml Tween-20)
8	Running Buffer	50ml 20xT.A + 950 ml dH$_2$0
9	Transfer Buffer	70% dH$_2$0, 20% v/v methanol and 10% v/v of 10XTBS
10	4% PFA	500 ml PBS + 20 g PFA powder + 200 ul 1M NaOH
11	5X DMEM	100ml dH$_2$0 + 6.74 g DMEM + 40g or 1.85 g or 0.37g NaHC0^3
12	Lysogeny Broth (LB) medium	20g LB powder in 1 litre dH$_2$0
13	LB agar	15g agarose powder in 1 litre LB medium
14	Tris-EDTA (TE) buffer (PCR)	5ml 1M Tris (pH8), 1ml 0.5M Na$_2$EDTA
15	Access Revelation (10x)	Antigen Retrieval (Cat.No. MP-607-X500, MenaPath)
16	TBS (20x)	Washing buffer (Cat. No. MP-945-X500, MenaPath)

Table 2-4 Common laboratory standard solutions.

3   Results chapter I: *In vitro* investigation of DOCK4 signalling during sprouting angiogenesis

3.1   Introduction

Healthy vascular growth capable of adequately providing the precise blood flow to the organs and tissues depends strongly upon the correct vascular patterning. Developing vasculature with adequate, but not excessive branching, along with the correct level of tubule elongation is imperative for healthy physiological function of the body's organs and tissues (Eilken and Adams, 2010).

The precise cellular mechanisms which underlie the coherent processes of vascular pattering during sprouting angiogenesis rely strongly upon an intricate repertoire of interplaying GFs. Stimulation of ECs by each GF potentially prompts differing intracellular events which induce different cellular responses. The GEF, DOCK4, has been described as required for the signalling events downstream of VEGFA driven angiogenesis, with depletion of DOCK4 leading to a loss in lateral filopodia and vascular branching; inducing growth of long thin but unbranched tubules (Abraham et al., 2015). As much of post developmental angiogenesis occurs in response to oxygen deprivation, it is important to consider this signalling mechanism within the context of hypoxia, while also considering the potential interplay of DOCK4 in the cellular response to grow factors other than VEGF. To further understand the functionality of DOCK4 within the signalling pathways which drive angiogenesis, *in vitro* techniques were conducted with inhibition of DOCK4, and the DOCK4 interaction partner DOCK9, through shRNA induced inhibition and small molecule inhibition, respectively; with consideration of hypoxic conditions. As FGF2 has previously been described as the predominant regulator of peripheral sprouting angiogenesis in response to ischemia (Ferraro et al., 2010), *in vitro* assays were carried out under VEGFA or FGF2 stimulation.

In order to study these signalling mechanisms *in vitro,* an organotypic co-culture model was employed (figure 3.1). The co-culture model creates a 3D culture environment with HDF grown to produce an extracellular matrix, through which the ECs may form dynamic cords; which more closely resemble physiological vasculature than other 3D angiogenesis models (Hetheridge et al., 2011).

QL-47, a DOCK9 binding small molecule inhibitor, was utilised as a tool for expanding upon the understanding of the DOCK4-DOCK9 signalling mechanism within angiogenesis. QL-47 is capable of covalently binding to p.C628 within the DHR1 domain of the DOCK9 protein (unpublished data Gray, N. Appendix 2); a cysteine residue which lies within a proline-rich region of DOCK9 identified as a potential interaction site of the DOCK4 SH3 domain.
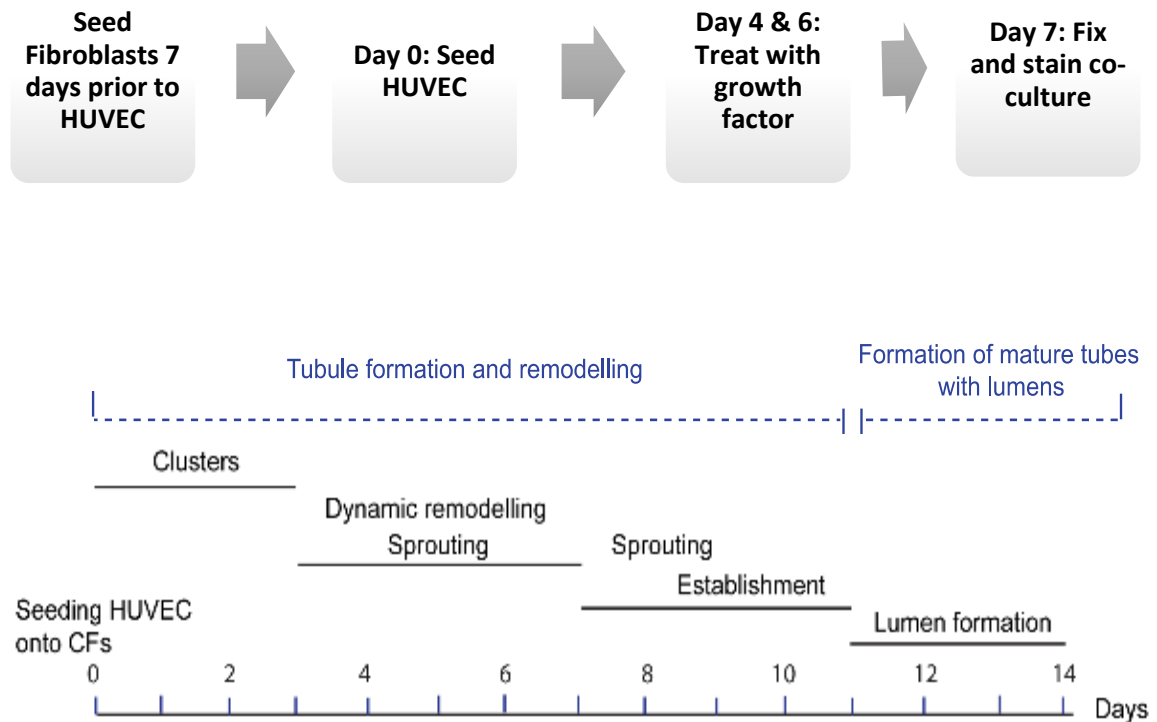
Figure 3-1 Schematic diagram of organotypic angiogenesis co-culture assay

An organotypic co-culture model was used to investigate sprouting angiogenesis within a 3D *in vitro* model. HDF cells were grown to form a confluent monolayer, forming a matrix through which ECs can sprout and develop into vascular structures. HUVEC were seeded on top of HDF, 7 days post HDF seeding. Where it was required, cells were stimulated with either 10ng/mL FGF2 or 25ng/mL of recombinant human VEGFA on days 4 and 6 post HUVEC seeding. The time point of co-culture fixation is adaptable according to the phenotypical readout of results required. Co-cultures described within this thesis were cultured until day 7, post HUVEC seeding, allowing for dynamic remodelled of cords of EC to form into more established tubules. CFs=Confluent fibroblasts.

Image adapted from Abraham et al (2015), with author permission.

3.2 Results

3.2.1 Effect of FGF2 stimulation on EC sprouting and elongation during tubule formation in the co-culture assay

The organotypic angiogenesis co-cultures were carried out to investigate the phenotypical difference in sprouting angiogenesis stimulated by the GF VEGFA when compared to the GF FGF2 (figure 3.2). Co-culture assays were supplemented with VEGFA, FGF2, or no GF on days 4 and 6 following HUVEC seeding onto a HDF monolayer. Following 7 days of endothelial growth within the co-culture model, cultures were fixed in ice cold 70% ethanol and IHC stained using an anti-CD31 antibody. Each co-culture condition was grown in duplicate (with two wells per condition) and each organotypic assay was repeated three times, as such n=6 per co-culture condition. Nine images per co-culture well, at random locations, were obtained using an inverted light microscope (example images given in figure 3.2). Of the nine images, five were randomly selected. All visible tubules within the field of view were quantified, with tubules measuring below 20µm being excluded. ImageJ software was employed to analyse a number of quantifiable characteristics of the formed tubules, indicative of the total amount of tubule formation, tubule elongation and branching: number of tubules, total tubule length, mean tubule length, longest tubule length, branch points, and BPI. Quantified data sets were analysed comparing data of each culture condition using a One-way analysis of variance (ANOVA). Data presented in figure 3.3.

(A) No GF **(B) VEGFA** **(C) FGF2**
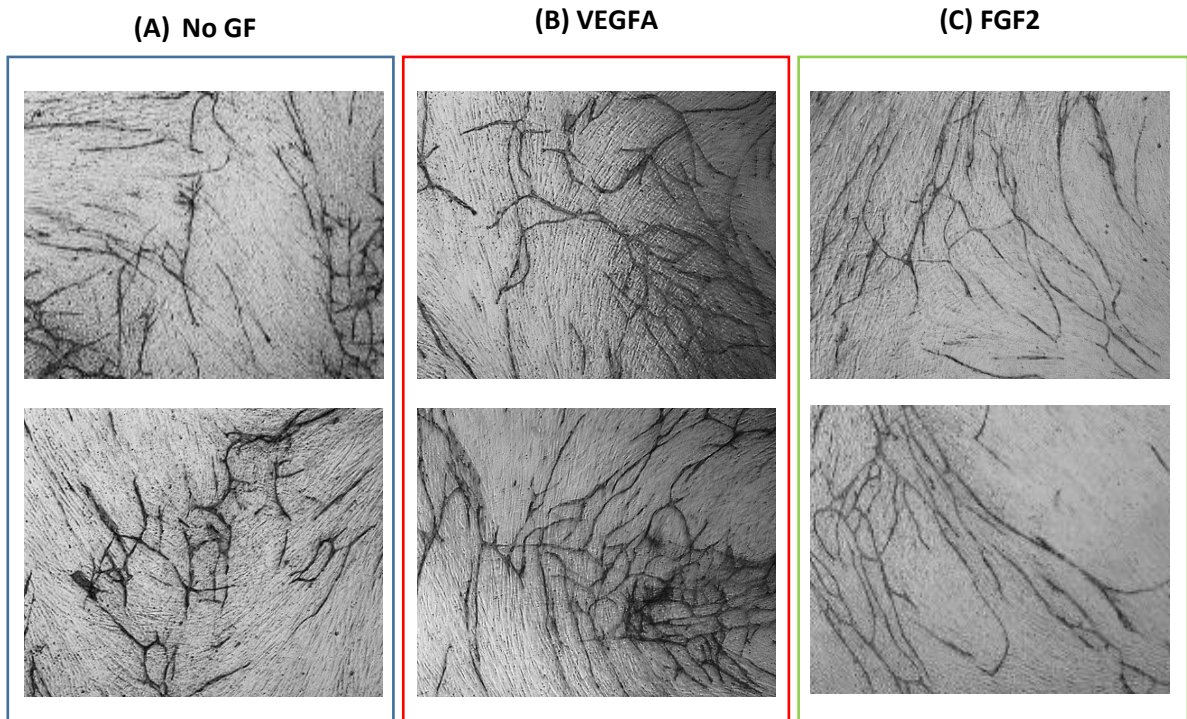
Figure 3-2 Growth factor stimulation of blood tubule growth within an organotypic angiogenesis co-culture assay

HUVECs were seeded onto a confluent monolayer of HDFs. Co-cultures were either (A) not treated with GF, (B) stimulated with VEGFA (25ng/ml) or (C) FGF2 (10ng/ml) on days 4 and 6 post HUVEC seeding. Co-cultures were fixed on day 7 with 70% ethanol and stained by IHC with an antibody against CD31. Images were taken under a light microscope (4x objective).

3.2.1.1 Mean tubule length

Mean tubule length values represents the average length of all tubules measured within each individual image, representative images given in figure 3.2. Mean value from each image were combined to generate the mean values for each condition (figure 3.3). Analysis of the mean tubule length demonstrated that addition of VEGFA or FGF2 to culture media led to an increase in mean tubule length, when compared to the control (non-GF supplemented). The mean tubule length of VEGFA supplemented cultures increased from 118μm, the mean measurement of the control cultures, to 142μm, this difference was not found to be statistically significant. Cultures supplemented with FGF2 developed an even larger increase in mean tubule length, to 193.1μm, with a significant difference 0.00005 when compared to the control.

3.2.1.2 Total tubule length

Total tubule length readings depict the overall growth of endothelial tubules, without consideration of the number of tubules or individual tubule length (figure 3.3). Representative images given in figure 3.2.

In cultures supplemented with VEGFA, total tubule length (10291μm) was increased, but the increase was not found to be statistically significant when compared to cultures without additional GF supplement (6863μm; figure 3.3). FGF2 supplemented cultures also developed a greater total tubule length (8985μm) when compared to control, however, this was also not found to be statistically significant.

3.2.1.3 Number of tubules

The number of tubules reading depicts how many tubules (defined as an elongated cord of CD31 positive cells) were detected within each co-culture image, with mean values for each condition used for statistical comparison (figure 3.3). Representative images given in figure 3.2.

The number of tubules detected in the VEGFA supplemented culture (75.25) increased when compared to the control (59.62), this increase was not statistically significant. FGF2 supplemented cultures had a slight reduction in the number of detected tubules, although this difference was not significant when compared to the control. However, statistical comparison between the number of tubules in VEGFA treated co-cultures to FGF2 treated cultures found that VEGFA treated cultures had develop a statistically significant increase in the number of detected tubules (p=0.01004).

3.2.1.4 Longest tubule length

As FGF2 stimulation of co-cultures led to an observed increase in tubule lengths, the longest detected tubule from each co-culture image were used to generate a mean value of longest tubule length for each co-culture condition (figure 3.3). Representative images given in figure 3.2.

The measure of the longest detected tubules (average of 6 wells, with 5 images per well) of FGF2 supplemented cultures (548.8µm) was significantly higher compared to control cultures (219.4µm), with a p value greater than 0.0001. FGF2 supplemented cultures showed a significant increase in the longest detected tubules (548.8µm) when compared to VEGFA supplemented cultures (436.8µm) in respect to control (219.4µm) with a p value of 0.018. VEGFA supplemented cultures also developed an increase in length of the longest detected tubule with a p value of 0.0013 when compared to the control cultures.

3.2.1.5 Branch points

Branch points were counted within each co-culture image and a mean per well was generated. Mean values were then compared between the three GF conditions, to demonstrate how branched endothelial tubules were within the co-cultures (figure 3.3). Representative images given in figure 3.2.

Supplementation of culture media with VEGFA led to a significant increase in the number of detected branch points (51.86) when compared to the control (31.93) but not

FGF2 supplemented cells (33.38). FGF2 supplemented cultures had a level of branching similar to the control cultures (figure 3.3).

3.2.1.6 Branch point index

Calculation of the BPI (number of branch points/total tubule length) for each co-culture image depicts the ratio of branch points to TVL (figure 3.3). With representative images of co-culture given in figure 3.2. Comparative analysis of the BPI of co-cultures under no-GF, VEGFA, or FGF2 treatment demonstrates how branched tubules are between the different co-culture conditions (no-GF=0.0045; VEGFA=0.0057; FGF2=0.00369). Supplementing culture media with FGF2 led to a decrease in BPI , while this was not found to be significantly different between the co-culture conditions, the trend of reduced BPI of FGF2 supplemented cultures indicates a reduction in the number of branches of FGF2 supplemented cultures in comparison to the outgrowth of tubules; a measurement which reflects the observed phenotype of FGF2 supplemented cultures as longer and less branched in comparison to the control and VEGFA supplemented cultures.

To summarise the data accumulated through comparison of FGF2 to VEGFA stimulation, sprouting angiogenesis within the organotypic co-culture model shows a different phenotype dependent on the angiogenic GF used to supplement the growth medium. FGF2 stimulation induces an increase in endothelial cord elongation with less branching and a trend for reduced number of tubules when compared to VEGFA supplemented cultures.
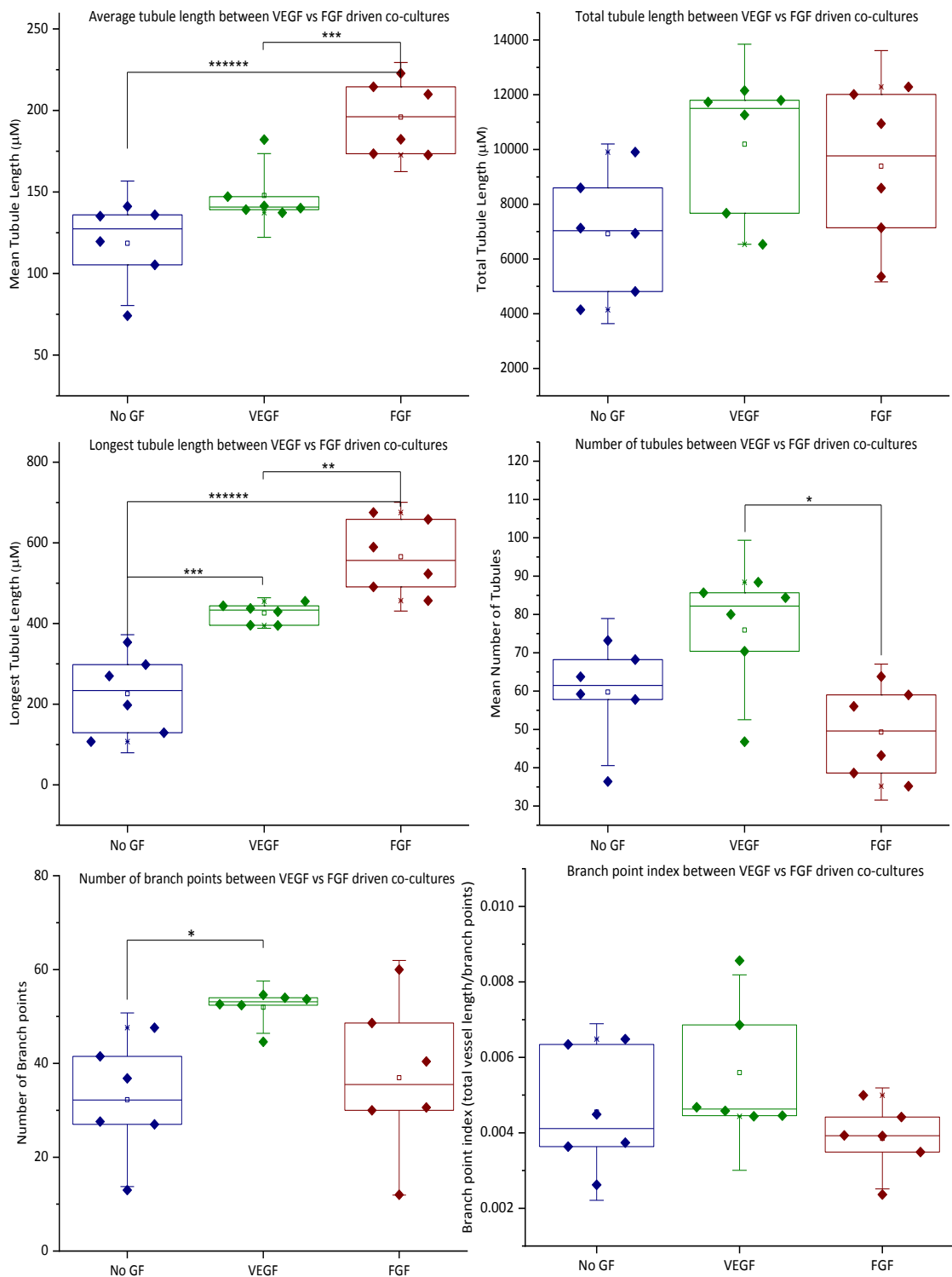
Figure 3-3 Comparative quantification of VEGFA vs FGF2 stimulated endothelial tubule growth within an organotypic angiogenesis co-culture assay

HUVEC were seeded onto confluent monolayer of HDFs. Co-cultures were grown within a humidified chamber at 37°C with 5% CO_2. On days 4 and 6 post HUVEC seeding,

cultures were stimulated with VEGFA (25ng/ml), FGF2 (10ng/ml), or no GF. On day 7 cultures were fixed with 70% ethanol and stained using IHC with an antibody against CD31. N= number of wells analysed. Five images were taken per well under a light microscope, with 3 independent experiments and 2 wells per condition, per experiment (n=6). Total tubule length, mean tubule length, number of tubules, and number of branch points, were measured manually per image using ImageJ software. Calculated values of each image were used to generate mean values and standard deviation per co-culture with readouts for: mean tubule length; total tubule length; longest detected continuous tubule; number of branch points; and BPI (branch points/TVL). Mean values of each co-culture well were analysed using a one-way analysis of variance (ANOVA) through Origin 2015 Software (OriginLab). Error bars signify standard deviation. Significant differences indicated by asterisks: *=P value equal to or lower than 0.05; **=P value equal to or lower than 0.01; ***=P value equal to or lower than 0.001; ****=P value equal to or lower than 0.0001; *****=P value equal to or lower than 0.00001.

3.2.2   The impact of FGF2 stimulation on tubules with shRNA mediated DOCK4 depletion within an organotypic angiogenesis co-culture assay

A DOCK4 Kd organotypic co-culture assay was utilised to investigate whether DOCK4 expression is required during FGF2 stimulated angiogenesis, in normoxia and hypoxia (representative images in figure 3.4 and data analysis in figure 3.5).

DOCK4 expression was attenuated in HUVEC by a method previously validated in Dr Mavria's laboratory via transduction of a lentivirus harbouring a shRNA oligonucleotide targeting DOCK4 (figure 3.4A). Two DOCK4 shRNA lenti-viruses were selected to induce DOCK4 Kd in HUVEC, the two shRNAs were selected on the basis of previous optimisation (Gary Grant, Thesis 2016). Successful shRNA Kd of DOCK4 within HUVECs was determined through western blot (figure 3.4 A). The DOCK4 specific shRNA labelled shRNA 4 was found to proficiently deplete DOCK4 expression, the shRNA labelled shRNA 3 was not found to successfully deplete DOCK4 expression. Therefore cells transduced with the DOCK4 shRNA 4 were used for the DOCK knockdown co-culture assays.

HUVEC transduced with the DOCK4 shRNA and control non silencing (NS) shRNA lentiviruses were seeded on a monolayer of HDF and co-cultured for a duration of 4 days at 20% O_2 with GF supplementation of either FGF2 (10ng/ml), or in the absence of additional GF, after which time cultures were placed in a hypoxic incubator in 1% O_2. On day 6 post HUVEC seeding, cultures were briefly removed from the hypoxic incubator and the media and FGF2 supplement were changed before being returned to the hypoxic incubator for a further 24 hours. Co-cultures were fixed and stained for CD31. For each well, 5 selected regions were imaged using brightfield microscopy, for each of the following conditions: HUVEC with DOCK4 shRNA, or control NS shRNA, supplemented with 10ng/ml FGF2 and cultured in hypoxic conditions; HUVEC with DOCK4 shRNA, or control NS shRNA, without FGF2 supplement and cultured in hypoxic conditions; HUVEC with DOCK4 shRNA, or control NS shRNA, supplemented with 10ng/ml FGF2 and cultured in normoxic conditions; HUVEC

with DOCK4 shRNA, or control NS shRNA, without additional FGF2 supplement and cultured within normoxic conditions. The impact of FGF2 stimulation of shRNA mediated DOCK4 knockdown on angiogenesis, in the organotypic co-culture assay, was assessed under hypoxic conditions and compared to normoxic conditions. As this co-culture assay contains only 2 wells for each condition from a single experiment, statistical analysis could not be performed. However trends detected in this assay gave preliminary data which indicate a potential role for DOCK4 function during angiogenesis within a hypoxic environment. Light microscope images of the CD31 stained co-cultures (5 images X 2 wells per condition) were analysed using ImageJ software to characterise a number of quantifiable read outs: mean tubule length; total tubule length; number of tubules; longest tubule length; branch points; and BPI.
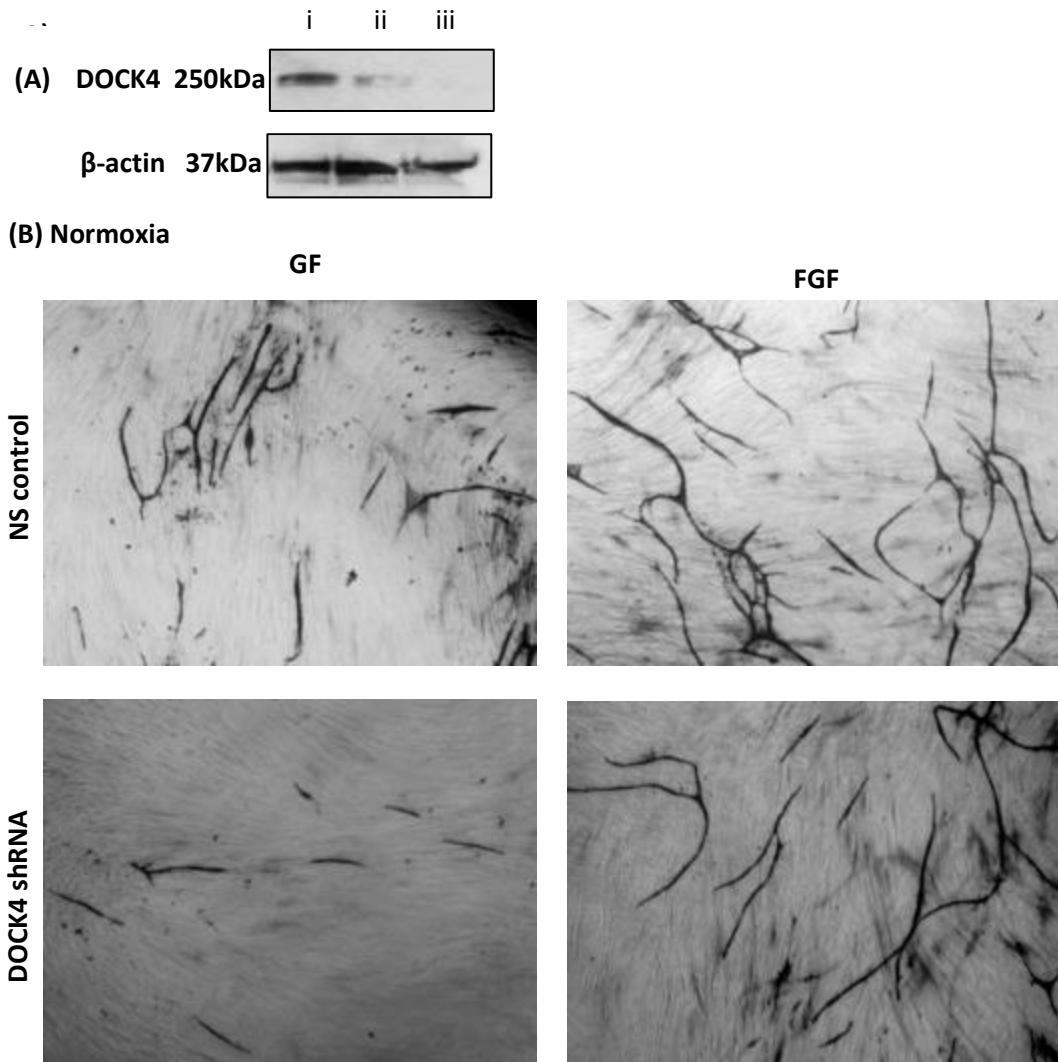
Figure 3-4 FGF2 stimulation of DOCK4 depleted ECs within an organotypic angiogenesis co-culture assay

(A) Anti-DOCK4 Western blot analysis of HUVECs transduced with either a **(i)** NS shRNA expressing lentivirus, or **(ii)** DOCK4 targeting shRNA lentivirus 3, or **(iii)** or DOCK4 targeting shRNA lentivirus 4. Successful DOCK4 shRNA driven DOCK4 knockdown was determined through absence of a detectable band at 250kDa. **(B)** DOCK4 shRNA 4 depleted HUVEC and Non-silencing shRNA HUVEC, each co-cultured with HDF, were grown in a humidified chamber at 37°C with 20% O_2 and 5% CO_2. On days 4 and 6 post HUVEC seeding cultures were stimulated with FGF2 (10ng/ml), or no GF. Immediately following FGF2 supplementation, the cell-culture plate with both FGF2 treated co-cultures and non-GF treated cells was placed back into the humidified chamber at 37°C with 20% O_2 and 5% CO_2. On day 7 cultures were fixed with 70% ethanol and stained by IHC with an antibody against CD31. Five images per well were taken under a light microscope.

Hypoxia

	No GF	FGF2
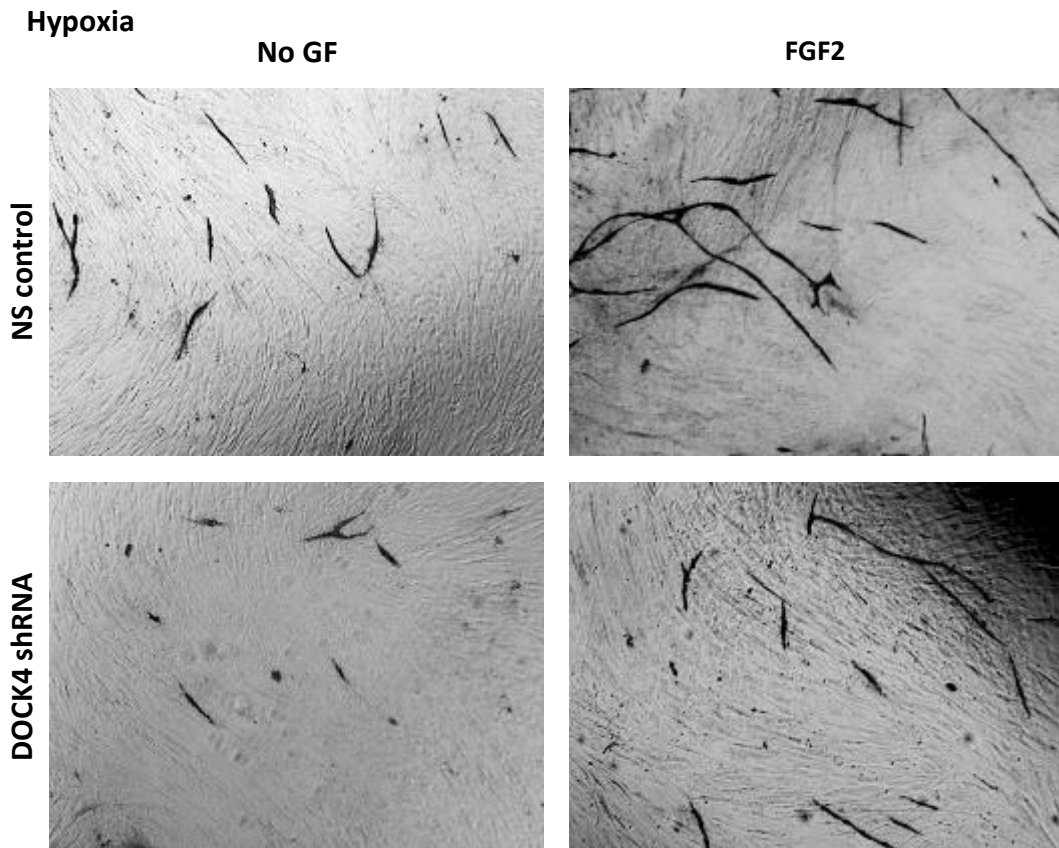
Figure 3-5 FGF2 stimulation of DOCK4 depleted ECs under hypoxia within an organotypic angiogenesis co-culture assay

DOCK4 shRNA 4 depleted HUVEC were seeded onto confluent monolayer of HDF. Non-targeting shRNA HUVEC were also seeded onto a confluent monolayer of HDF to produce control co-cultures as a point of comparison. Co-cultures were initially grown in a humidified chamber at 37°C with 20% O_2 and 5% CO_2. On days 4 and 6, post HUVEC seeding, cultures were stimulated with FGF2 (10ng/ml), or no growth factor. Immediately following FGF2 supplementation one cell culture plate with both FGF2 treated co-cultures and non-growth factor treated cells was placed within a hypoxic humidified chamber at 37°C with1% O_2 and 5% CO_2. On day 7 cultures were fixed with 70% ethanol and stained by IHC with an antibody against CD31. Five images per well were taken under a light microscope.

3.2.2.1 Mean tubule length

The mean tubule length analysis demonstrated that the average length of measured tubules within NS co-cultures, under all 4 condition, were similar in measurements NS non-hypoxic no GF=134.70µm; NS non-hypoxic FGF2=129.50µm; NS hypoxic no GF=128.50µm; NS hypoxic FGF2=153.95µm; figure 3.4, 3.5 and 3.6), with FGF2 treatment of cultures grown in hypoxia leading to an increase in average tube length.

DOCK4 depleted co-cultures demonstrated a reduction in mean tubule length (DOCK4 non-hypoxic no GF=122.35µm; DOCK4 non-hypoxic FGF2=160.23µm; DOCK4 hypoxic no GF=74.17µm; DOCK4 hypoxic FGF2=133.87µm). The reduction in mean tubule length of DOCK4 depleted tubules, when compared to NS tubules, was most pronounced in hypoxic conditions without FGF2 treatment. Within non-hypoxic conditions, FGF2 treatment lead to a strong increase in average tubule length. While FGF-treatment of hypoxic DOCK4 depleted co-cultures grew tubules of a similar average length as NS co-cultures without GF treatment in hypoxia, and with FGF2 treatment of normoxic cultures.

To summarise, FGF2 treatment appears to lead to an increase in average tubule length in hypoxia. DOCK4 depletion in ECs leads to a slight reduction in mean tubule length that becomes more pronounced under hypoxia. FGF2 treatment overcame this reduction of mean tubule length of DOCK4 deficient tubules, in both normoxia and hypoxia, with FGF2 treatment of DOCK4 depleted cultures in normoxia leading to a strong increase in average tube length.

3.2.2.2 Total tubule length

The total tubule length of NS co-cultures were found to develop a similar level of overall tubule growth within non-GF treated cultures, grown in both hypoxia and normoxia, as well as FGF-supplemented co-cultures grown in hypoxia. However, NS co-cultures treated with FGF, but grown in normoxia, had a near 2-fold increase in total tubule length (NS non-

hypoxic no GF=3991.42µm; NS non-hypoxic FGF2=6621.10µm; NS hypoxic no GF=3025.51µm; NS hypoxic FGF2=3643.37µm; figure 3.4, 3.5 and 3.6).

In contrast, DOCK4 depleted cultures had an overall decrease in total tubule length across all conditions (DOCK4 non-hypoxic no GF=1286.12µm; DOCK4 non-hypoxic FGF2=5723.86µm; DOCK4 hypoxic no GF=1651.09µm; DOCK4 hypoxic FGF2=300.2224µm). FGF2 treatment of DOCK4 depleted co-cultures, grown in hypoxia, had a strong decrease in total tubule length.

To summarise, FGF2 treatment greatly increase overall tubule length in normoxic conditions but does not impact on total tubule length under oxygen deprivation. DOCK4 depletion leads to a reduction in total tubule length. This reduction in total tubule length is over-come by treatment with FGF2, within normoxic conditions. The FGF2 driven increase in total tubule length is strongly diminished in DOCK4 depleted cultures grown in hypoxic conditions. This result suggests DOCK4 signalling within FGF2 driven angiogenesis differs depending on oxygen availability. The total tubule length analysis demonstrated high variation in the overall growth of sprouting HUVEC when comparing the 8 different culture conditions (figure 3.5 and 3.6).

3.2.2.3 Mean number of tubules

Analysis of the number of detected tubules within NS co-cultures found a slight decrease in number of tubules under FGF2 stimulation (NS non-hypoxic no GF=30.2; NS non-hypoxic FGF2=23.4; NS hypoxic no GF=30.2; NS hypoxic FGF2=23.2; figure 3.4, 3.5 and 3.6), normoxic and hypoxic NS co-culture were found to have a similar number of tubules.

In DOCK4 depleted co-cultures, non-GF treatment led to a 3-fold decrease in the number of tubules of cultures grown in normoxia, and an almost 10-fold decrease in the number of detected tubules in cultures grown under hypoxia. Within FGF2 supplemented cultures, the number of tubules increased when compared to the NS cultures. This increase in tubule numbers was strongly decreased under hypoxia, with almost half the average

number of tubules detected in the FGF2 treated DOCK4 deficient co-cultures grown within hypoxia (DOCK4 non-hypoxic no GF=10.5µm; DOCK4 non-hypoxic FGF2=35.7; DOCK4 hypoxic no GF=3.9; DOCK4 hypoxic FGF2=12.5µm).

To summarise, FGF2 treatment appeared to have little impact on the number of tubules which develop during sprouting angiogenesis. In the absence of DOCK4, the number of tubules were greatly decreased, a phenotype that was rescued by FGF2 treatment. Under hypoxic conditions FGF2 treatment was seen to be less effective in prompting the growth of new sprouts.

3.2.2.4 Longest tubule length

Longest tubule length measurements were used to detect the difference in tubule lengths between GF treatment conditions (figure 3.4, 3.5 and 3.6) as FGF2 treated cultures were observed to have obviously longer tubules than the non-GF treated cultures. All tubules were measured and the longest tubule per image was selected, the longest tubule lengths from each image were averaged per well. The numbers given are the mean average longest tubule length per well.

Analysis of the longest tubule length of NS co-cultures demonstrated that tubule length was increased in the presence of FGF2, and was further increased within hypoxic conditions (NS non-hypoxic no GF=364.88µm; NS non-hypoxic FGF2=401,36µm; NS hypoxic no GF=336.32µm; NS hypoxic FGF2=603.48µm; figure 3.5 and 3.6).

DOCK4 Kd led to a slight reduction in the longest tubule length of non-GF treated co-cultures under normoxia. This decrease was overcome with FGF2 treatment of DOCK4 depleted cultures, resulting in an increase in the average lengths of longest tubules compared to the NS co-cultures. DOCK4 depleted co-cultures grown with hypoxia developed shorter vessels, with FGF2 treated DOCK4 Kd cultures developing the tubules with a similar length to the non-GF treated NS cultures from in hypoxia (DOCK4 non-hypoxic no

GF=247.44µm; DOCK4 non-hypoxic FGF2=519.91µm; DOCK4 hypoxic no GF= 101.10µm; DOCK4 hypoxic FGF2=339.10µm).

To summarise, FGF2 treatment appeared to have little impact on the number of tubules which develop during sprouting angiogenesis. In the absence of DOCK4, the number of tubules were decreased, a phenotype that was reversed by FGF2 treatment. Under hypoxic conditions FGF2 treatment was seen to be less effective in prompting the growth of new sprouts.

3.2.2.5 Branch points

Mean values of all branch points within each co-culture image (figure 3.5 and 3.6) determined that FGF2 treatment of co-cultures prompted a strong increase in branching. This increase was greatly reduced under the conditions of hypoxia, with non-growth factor treated co-cultures developing slightly less branch points, and FGF2 treated co-cultures developing a 3-fold decrease in the number of branch points (NS non-hypoxic no GF=9.7; NS non-hypoxic FGF2=33.9; NS hypoxic no GF=7.2; NS hypoxic FGF2=9.1; figure 3.5 and 3.6).

DOCK4 depletion led to a decrease in overall branching detected in non-growth factor supplemented and FGF2 supplemented co-cultures grown in normoxia; with non-growth factor supplemented co-cultures showing a much higher reduction in branching. The growth of DOCK4 depleted co-cultures supplemented with FGF2 under hypoxic conditions led to a decrease in detected branch points similar to that of the DOCK4 depleted non-FGF2 supplemented co-cultures, grown in both normoxia and hypoxia (DOCK4 non-hypoxic no GF=1.5; DOCK4 non-hypoxic FGF2=13.7; DOCK4 hypoxic no GF=0.3; DOCK4 hypoxic FGF2=2.5). DOCK4 depleted co-cultures supplemented with FGF2 and grown within normoxia develop a level of branch points similar to the number of branch points seen in in NS FGF2 supplemented and non-growth factor supplemented co-cultures grown in hypoxia, and non-growth factor supplemented NS co-cultures grown in normoxia.

To summarise, FGF2 treatment induces a higher number of branch points. This increase in branch point numbers greatly reduced by DOCK4 depletion and is almost diminished by culture of DOCK4 depleted cells in hypoxia.

3.2.2.6 Branch point index

Calculation of the BPI for each co-culture image (figure 3.5 and 3.6) demonstrated that supplementing culture media with FGF2 in normoxic conditions led to an increase in BPI when compared to the no GF, thus reflecting the increase in the number of branches in comparison to total tubule length of FGF2 supplemented co-cultures; a result in contradiction with the previous findings within this chapter (3.2.1.6). All other NS co-culture conditions were found to have very similar BPI, indicating no difference in the number of branch points per vessel length under hypoxia when compared to normoxia (NS non-hypoxic no GF=0.0024; NS non-hypoxic FGF2=0.005; NS hypoxic no GF=0.0021; NS hypoxic FGF2=0.0025; figure 3.5 and 3.6).

The BPI was slightly reduced in DOCK4 depleted, no GF treated, non-hypoxic co-cultures. However, the BPI was unaffected in the hypoxic equivalent; suggesting a lower level of branching in the cells grown in normoxia. Within hypoxia this result was reversed, with no GF treated co-cultures having the same ratio of branch points to tubule length as the NS co-culture. However, DOCK depleted hypoxic co-cultured treated with FGF2 had a marked decrease in BPI, indicating much fewer branches per vessel length (DOCK4 non-hypoxic no GF=0.0012; DOCK4 non-hypoxic FGF2=0.002; DOCK4 hypoxic no GF=0.0023; DOCK4 hypoxic FGF2=0.0005).

In summary, the comparison of FGF2 stimulation in normoxic and hypoxic conditions showed that under normoxic conditions within this assay, sprouting angiogenesis was enhanced with FGF2 stimulation leading to an increase in the overall length of tubules and number of branch points. However, culture under hypoxic conditions abolished this FGF2

driven stimulation, with the exception of average tubule length which was higher in the presence of FGF2 in hypoxic conditions.

DOCK4 depletion had little impact on FGF2 stimulated cultures when grown under normoxia, leading to an increase in the length of the longest detected tubules while reducing the number of branch points; suggesting DOCK4 depletion had induced the phenotype described by Abraham et al. (2015) whereby DOCK4 depletion drove growth of endothelial cords that were elongating yet less branched.

FGF2 stimulated DOCK4 depleted ECs grown under hypoxic conditions showed impairment in both tubule elongation and branching, with profoundly fewer tubules, total tubule length, and number of branch points.
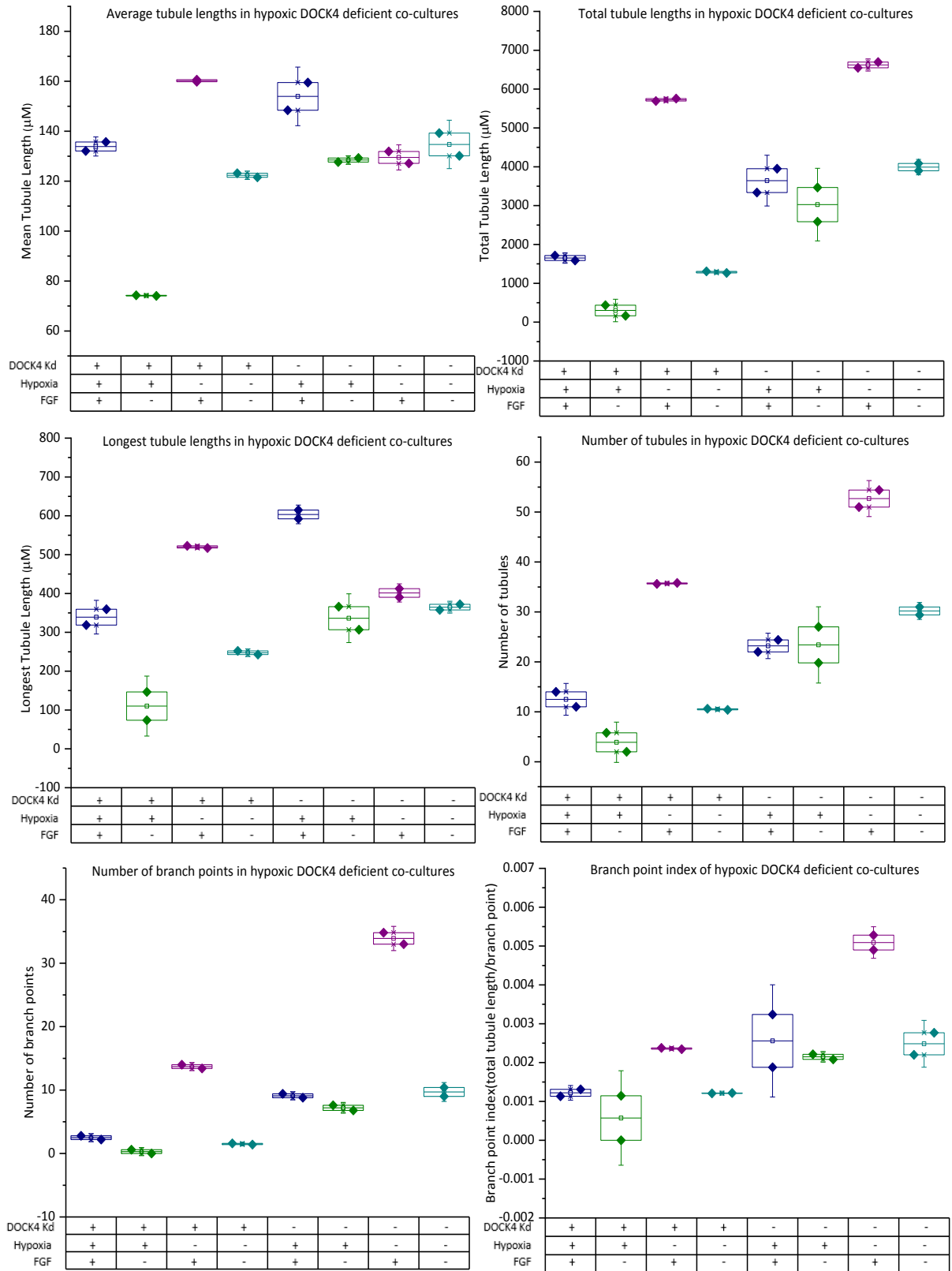
Figure 3-6 Comparative analysis of DOCK4 depleted HUVEC within a hypoxic organotypic angiogenesis co-culture assay

DOCK4 Kd or DOCK4 NS HUVECs were seeded onto confluent monolayer of HDFs. Co-cultures were initially grown with in a humidified chamber at 37°C with 20% O_2 and 5%

CO_2. On days 4 and 6 post HUVEC seeded cultures were stimulated with FGF2 (10ng/ml), or no GF. Immediately following FGF2 supplementation one cell culture plate with both FGF2 treated co-cultures and non-GF treated cells placed within a hypoxic humidified chamber at $37^{o}C$ with 1% O_2 and 5% CO_2, a second co-culture plate also possessing FGF2 treated co-cultures and non-GF treated co-cultures were placed within a humidified chamber at $37^{o}C$ with 20% O_2 and 5% CO_2. On day 7 cultures were fixed with 70% ethanol and stained by IHC with a CD31 targeting antibody. N= number of wells analysed. Five images per well were taken under a light microscope, with 2 co-cultures per condition (n=2). Total tubule length, mean tubule length, number of tubules, and number of branch points, were measured manually per image using ImageJ software. Calculated values of each image were used to generate mean values and standard deviation per co-culture with readouts for: mean tubule length; total tubule length, longest detected continues tubule; number of branch points; and BPI (branch points/TVL). Graphs representing the mean values of each co-culture were generated through Origin 2015 Software (OriginLab). Error bars signify standard deviation.

3.2.3　The effect of QL-47 treatment on blood vessel tubule growth in an organotypic angiogenesis co-culture assay

QL-47 is a small molecule inhibitor which has been demonstrated to inhibit Cd42 activation (Appendix 2). QL-47 binds DOCK9 at p.C628, a cysteine residue of DOCK9. In-order to test whether QL-47 has anti-angiogenic potential, an organotypic angiogenesis co-culture assay was carried as previously described with incorporation of QL-47 treatment at a 5μM concentration, or DMSO as a treatment control, on days 4, and 6 post seeding, control co-cultures were treat with DMSO in place of QL-47. Working concentrations of QL-47 used within this study were based on previously determined concentrations (Wu et al., 2014). It must be noted that QL-47 was found to aggregate once added to media and cell culture. This became apparent through observation of QL-47 treated cell cultures using light microscopy; where QL-47 was easily observed within cell culture plates. In order to properly dissolve the compound, QL-47 was diluted in warm media and vortexed for approx. 5 mins. Successful solubilisation of the compound was confirmed through loss of visible aggregates on cells within tissue culture. On day 7 post seeding co-cultures were fixed in 70% ethanol and staining using CD31 tubule staining kit. Cultures were imaged using light microscopy.

In co-cultures treated with a combination 5μM QL-47 and VEGFA, endothelial growth was ablated (figure 3.7). The ablation of ECs was not observed within co-cultures treated with 5μM QL-47 in the absence of additional GF supplementation, or in cultures treated with 5μM QL-47 and supplemented with FGF2 (figure 3.8). Treatment of co-culture with 5μM of QL-47 led to a reduction in overall sprouting angiogenesis. In co-cultures without additional GF or FGF2 stimulation, QL-47 treatment also inducing a slight tortuous phenotype of the observed vascular cords, with tubules displaying a more curved appearance (figure 3.8).

3.2.4   The effect of QL-47 treatment on sprouting angiogenesis within an organotypic angiogenesis co-culture assay following VEGFA or FGF2 stimulation

To further understand the effect of QL-47 on sprouting angiogenesis, the co-culture model was carried out in the presence of QL-47 with supplementation of either VEGFA or FGF2, to determine if the small molecule elicited a GF signalling specific effect. The organotypic angiogenesis co-cultures treated with either DMSO or QL-47 and supplemented with VEGFA, FGF2, or no GF were imaged using light microscopy. ImageJ software was employed to analyse a number of quantifiable characteristics which represent sprouting angiogenesis: mean tubule length; total tubule length; number of tubules; longest tubule length; branch points; and BPI. Quantified data were analysed using a one-way test of variance (Anova) test comparing data sets between each culture condition.

No Growth factor + DMSO

VEGFA + DMSO

No Growth factor + 5µM QL-47

VEGFA + 5µM QL-47
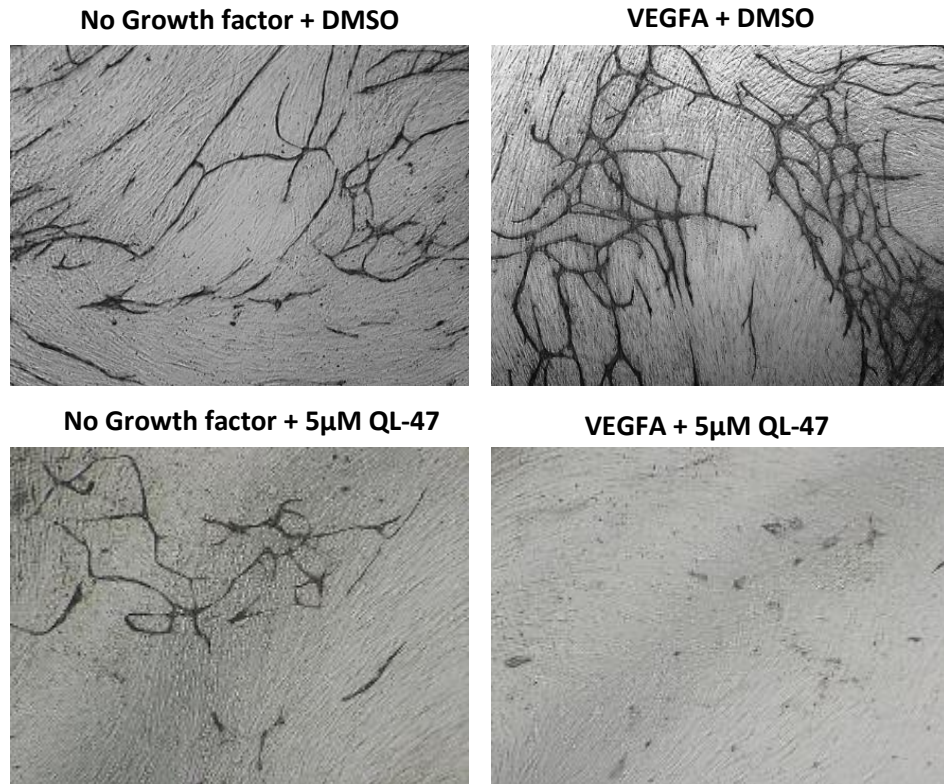
Figure 3-7 Comparative quantification of VEGFA vs no growth factor supplemented ECs treated with the small molecule QL-47 within an organotypic angiogenesis co-culture assay.

HUVECs were seeded onto a confluent monolayer of HDFs. Co-cultures were stimulated with VEGFA (25ng/ml) on days 4, and 6 post HUVEC seeding. Cells were treated with QL-47 at concentrations of 5µM on days 4 and 6 post HUVEC seeding. Co-cultures were fixed on day 7 with 70% ethanol and stained by IHC with a CD31 targeting antibody. Images were taken under a light microscope (4x magnification).

No Growth factor + DMSO

FGF2 + DMSO

No Growth factor + 5µM QL-47

FGF2 + 5µM QL-47
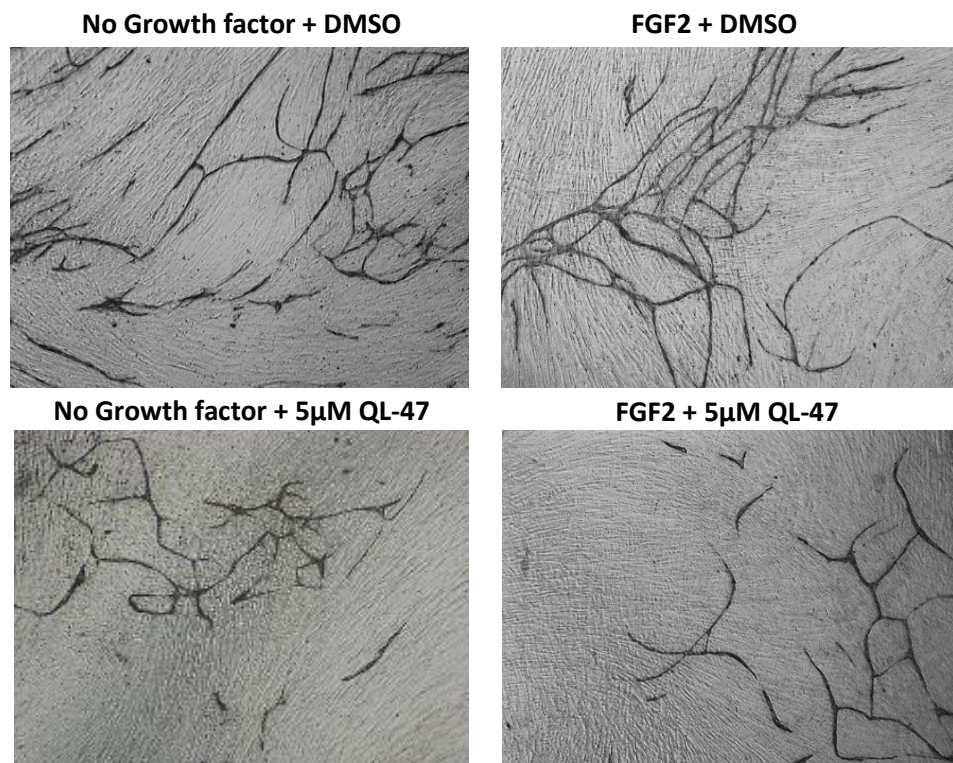
Figure 3-8 The effect of QL-47 treatment on EC tubule growth in an organotypic angiogenesis co-culture assay following FGF2 stimulation

HUVECs were seeded onto confluent monolayer of HDFs. Co-cultures were stimulated with FGF2 (10ng/ml) on days 4 and 6 post HUVEC seeding. Cells were treated with QL-47 at concentration of 5µM on days 4 and 6 post HUVEC seeding. Co-cultures were fixed on day 7 with 70% ethanol and stained by IHC with a CD31 targeting antibody. Images were taken under a light microscope.

3.2.4.1 Mean tubule length

Mean tubule length values represents the average length of all tubules measured within each individual image. Mean value from each image was then used to calculate mean values for each condition (figure 3.9).

Analysis of the mean tubule length in untreated control co-cultures followed the trend seen in previously described co-cultures, with no significant increase in mean tubule length of VEGFA supplemented co-cultures (over all mean=149µm) when compared to non-GF supplemented control cultures (over all mean=140.5µm). FGF2 supplemented untreated control co-cultures developed a statistically significant increase in mean tubule length (overall mean=196.9µm) when compared to both non-GF and VEGFA supplemented control co-cultures.

Co-cultures treated with QL-47 saw an overall reduction in mean tubule length in all three GF conditions (No GF=133.7µm; VEGFA=17.47µm; FGF2=107.5µm), with VEGFA experience the most significant reduction in mean tubule length following QL-47 treatment due to ablation of the majority of ECs within the VEGFA and QL-47 treated co-cultures.

3.2.4.2 Total tubule length

Total tubule length readings depicted the overall growth of endothelial cords of cells, without consideration of the number of tubules or length of individual tubules (figure 3.9).

In control cultures, non-QL-47 treated cultures supplemented with VEGFA total tubule length (12822µm) was significantly increased when compared to cultures without additional GF supplement (8529µm) with a p value of <0.001 (figure 3.9). In FGF2 supplemented control cultures there was also a significant increase in total tubule length (10720µm; p<0.01).

Treatment of cultures with the small molecule QL-47 lead to significant decrease in total tubule length within all three GF conditions (no-GF=3843µm; VEGFA=42.28µm; FGF2=1678µm), with the non-GF treated cultures total length being the least reduced of the

three conditions and VEGFA having the largest decrease in total tubule length; with a p value of <0.001 when compared to the non-GF supplemented QL-47 treated cultures. FGF2 supplemented QL-47 treated cultures also had a significantly lower total tubule length when compared to the non-GF treated co-cultures (0.0025; p<0.01).

3.2.4.3 Mean number of tubules

Mean number of tubules lengths were measured within each individual image (figure 3.9). Mean value from each image was then used to calculate mean values for each condition.

Within control co-cultures, VEGFA stimulation lead to a highly significant increase in the number of tubules (89.95), with a p value <0.01 when compared to the non-GF treated cultures (64.9), and a p value of <0.001 when compared to FGF2 treated cultures (56.06). QL-47 treatment of co-cultures significantly reduced the number of tubules within all three GF conditions (no GF=26.68; VEGFA=0.625; FGF2=12.94). Cultures stimulated with VEGFA experienced a near total loss of sprouted ECs (figure 3.7 and figure 3.9). While both non-GF cultures and FGF2 supplemented cultures experienced a reduction in the number of tubules (figures 3.8 and 3.9), the trend between the two GF conditions reflected that of the control co-cultured cells (with p<0.01), with a slight decrease in the number of tubules grown when stimulated with FGF2.

3.2.4.4 Longest tubule length measurements

Longest tubule length measurements were used to detect the difference in tubule lengths between GF treatment conditions (figure 3.9). Mean value from each image were then used to calculate mean values for each condition.

Co-culture experiments with culture media supplemented with either VEGFA or FGF2 demonstrated how the two GFs impact differently upon tubule length, with FGF2 stimulation inducing growth of longer tubules with a p value of <0.0001 when compared to non-GF stimulated cultures, and p < 0.01 when compared to VEGFA stimulated cultures.

Treatment of co-cultures with QL-47 lead to a marked decrease in branch points within VEGFA supplemented cultures, primarily due to an almost complete loss of sprouting ECs. QL-47 treatment led to a significant decrease in branch points in non-GF treated compared to FGF2 treated cultures (p<0.01).

3.2.4.5 Mean branch point number

The mean branch point number were measured (figure 3.9) to reflect how branched and dynamic the co-culture endothelial tubules between GF treatment conditions. Mean value from each image was then used to calculate mean values for each condition.

In control co-cultures, supplementation of culture media with VEGFA led to a significant increase in the number of branch points (VEGFA=55.15), when compared to the control non-GF co-culture (No GF=34.75; p<0.01; figure 3.9). This trend was not observed in FGF2 treated cells (FGF2=47.5), however FGF2 treated cultures did have a slight increase in the number of branch points when compared to the non-GF supplemented cultures. Within QL-47 treated co-cultures, the overall trend for a reduction in the number of observed branch points was seen across all three GF conditions (No GF=14.95; VEGFA=0.00 FGF2=6.889). Non-GF supplemented cultures branch point numbers were the least affected by QL-47. The almost total ablation of ECs within the QL-47 treated VEGFA stimulated cultures led to no detectable branch points within any of the co-culture wells. FGF2 and QL-47 treated cultures experienced a substantial reduction in the presence of branch points.

3.2.4.6 Branch point index

The BPI were measured to reflect how many branches tubules produce within the angiogenic co-cultures (figure 3.9) and thus how dynamic the co-culture endothelial tubules between GF treatment conditions. BPI defined as the number of branch points per co-culture image divided by the total tubule length per image. Mean value from each image was then used to calculate mean values for each condition.

Within the VEGFA supplemented control cultures total tubule length measurements and number of branch points were increased when compared to the non-GF stimulated control cultures, leading to an increase in the BPI of the VEGFA stimulated control cultures (BPI=0.007774; figure 3.9) when compared to the non-GF controls (BPI= 0.00391) with a p value of <0.01. FGF2 supplemented control cultures also saw a slight increase the BPI (BPI= 0.005408) when compared to the non-treated cultures, however this was not statistically significant.

Treatment of cultures with QL-47 saw a slight reduction in BPI detected within the non-GF supplemented culture images, with a mean of 0.00254. As VEGFA supplemented cultures grew little to no EC sprouts, the BPI of these cultures was 0, yielding a significant difference of <0.05 when compared to the non-GF treated cultures. The FGF2 supplemented QL-47 treated cultures had a reduction in BPI following QL-47 treatment (BPI=0.00254), however there was no significant difference in the mean BPI when compared to the non-GF supplemented cultures.

To summarize the overall effect of QL-47 treatment on sprouting angiogenesis *in vitro*; the small molecule inhibitor led to an angiogenic impairment, reducing the number of endothelial cords formed, and the elongation of these endothelial cords, while driving a more tortuous phenotype. Reduction in tubule growth resulting in fewer sites of tubule branching, however, this reduction was relative to the reduction in the amount of overall tubule growth within non-GF stimulated cultures (figure 3.7 and figure 3.8). The anti-angiogenic effect of QL-47 was greatly amplified in the presence of the angiogenic GF VEGF; leading to an almost complete ablation of ECs at a 5µM concentration of QL-47. Endothelial cultures supplemented with FGF2 were less affected by QL-47 treatment than VEGFA supplemented cultures. However, in comparison to the non-GF supplemented cultures the FGF2 supplemented cultures experienced a greater loss of endothelial cord elongation, a

reduction in average tubule length, and, unlike the non-GF supplemented cells, a reduction

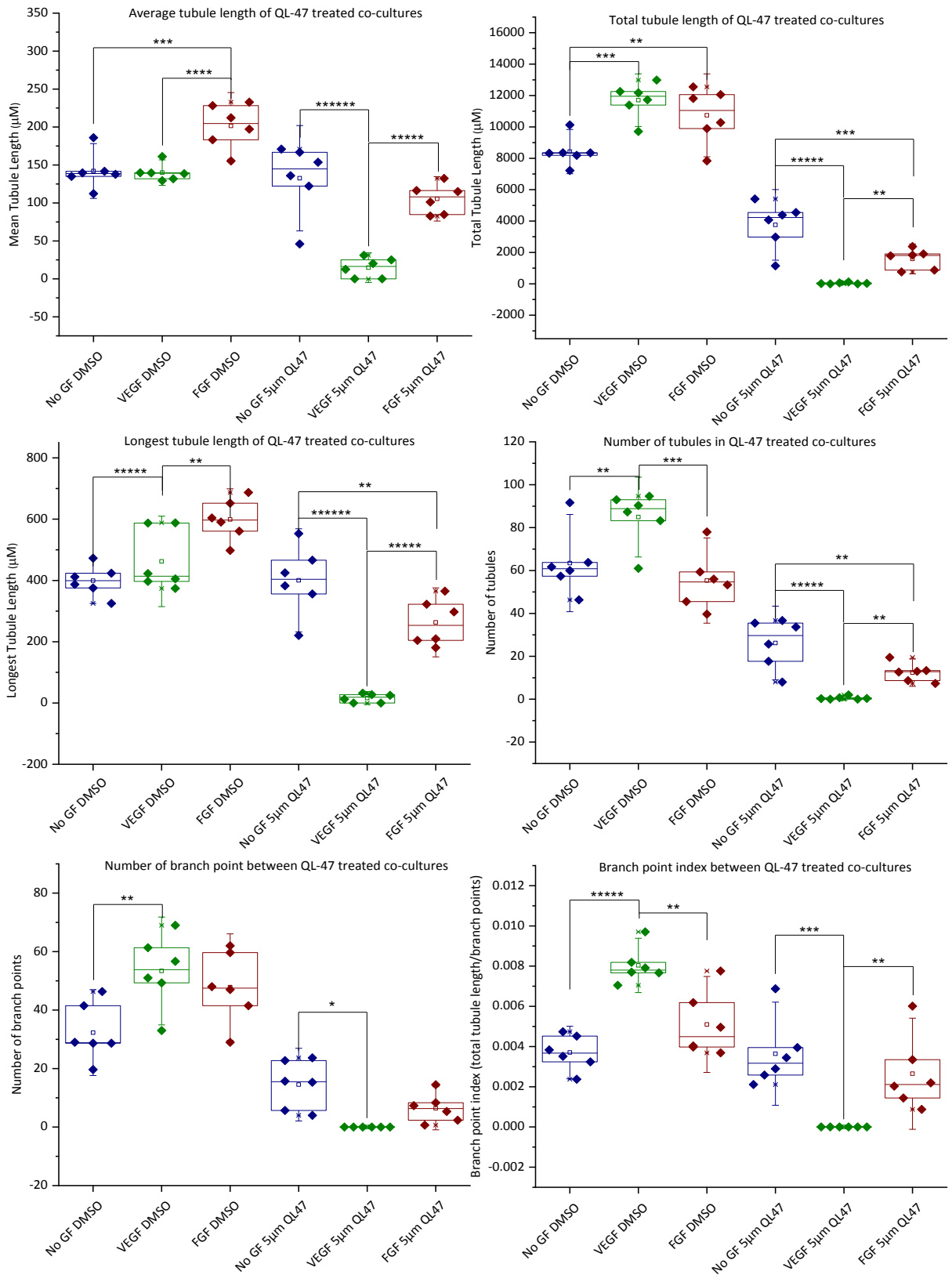in the relative number of branch points in relation to the overall level of tubule growth.

Figure 3-9 Comparative quantification of VEGFA vs FGF2 supplemented ECs treated with

QL-47 within an organotypic angiogenesis co-culture assay.

HUVECS were seeded onto confluent monolayer of HDFs. Co-cultures were grown

within a humidified chamber at 37°C with 5% CO_2. Co-cultures were cultured with either non-

GF supplemented or stimulated with FGF2 (10ng/ml) on days 4 and 6 post HUVEC seeding. Cells were treated with QL-47 at concentrations of 5µM on days 4 and 6 post HUVEC seeding. Co-cultures were fixed on day 7 with 70% ethanol and stained by IHC with a CD31 targeting antibody. N= number of wells analysed. 2 independent experiments were carried out, with 3 wells per condition, 5 images per co-culture well were taken under a light microscope (n=6). Total tubule length, number of tubules, and number of branch points, were measured manually per image using ImageJ software. Calculated values of each image were used to generate mean values and standard deviation per co-culture, with readouts for: mean tubule length; total tubule length, longest detected continues tubule; number of branch points; and BPI (branch points/TVL). Mean values of each co-culture were analysed using a one-way analysis of variance (ANOVA) through Origin 2015 Software (OriginLab). Error bars signify standard deviation. Significant differences indicated by asterisks: *=P value equal to or lower than 0.05; **=P value equal to or lower than 0.01; ***=P value equal to or lower than 0.001; ****=P value equal to or lower than 0.0001; *****=P value equal to or lower than 0.00001.

3.3   Discussion

To expand upon the understanding of DOCK4 function within sprouting angiogenesis DOCK4 signalling was investigated under FGF2 stimulation. In order to adequately establish the distinct characteristics between FGF2 driven angiogenesis compared to VEGFA driven angiogenesis, an organotypic angiogenesis co-culture model was employed and assays were set up with either FGF2 or VEGFA stimulation (figure 3.2). This investigation showed differences in sprouting angiogenesis phenotypes between the two GFs (figure 3.3) and served as a model for investigating any differences in DOCK4 signalling under the stimulation conditions.

Lentiviral DOCK4 targeting shRNA transduced ECs were incorporated into the co-culture assay under both normoxic and hypoxic conditions (figure 3.4-3.6). DOCK4 was found to not be required for sprouting angiogenesis under FGF2 stimulation in normoxia. However, the preliminary results indicated DOCK4 may be required for FGF2 driven angiogenesis within a hypoxic environment.

3.3.1   Comparison of VEGFA vs FGF2 stimulated sprouting angiogenesis *in vitro*

To further understand the downstream mechanisms of FGF2 signalling within ECs, an organotypic co-culture assays was employed. The organotypic angiogenesis assay, adapted to incorporate FGF2 within the growth culture media, demonstrated how FGF2 stimulation of sprouting angiogenesis induces growth of fewer number of tubules, however, the cords of ECs produced were more elongated and less branched than the VEGFA stimulated counterparts (figure 3.6). Thus implying that FGF2 signalling either directly, or indirectly, induces an intracellular response within the ECs which stimulates signalling to drive cord elongation, or cell proliferation of the forming cord.

The accumulated data within this study was unable to distinguish whether elongation of the endothelial cords were due to elongation of the individual cells within the tubules or due to an increase in cell proliferation of growing tubules. Distinguishing between

the two potential characteristics would lead to insight into the EC response to FGF2 stimulation. The potential of FGF2 signalling to impact on both cell proliferation and cell elongation has been demonstrated in previous studies (Ware and Simons, 1997; Ornitz and Itoh, 2001). It has been established that FGF2 promotes EC proliferation, migration and physical organisation of ECs into tube-like structures (Ware and Simons, 1997; Ornitz and Itoh, 2001). FGF2 stimulated endothelial activation of PI 3-kinase induces the reorganization of actin cytoskeleton to the cortex and stimulates changes in cell morphology to induce an elongated phenotype in a Rho GTPase dependent manner (Lee and Kay, 2006). Thus lending evidence to the concept that the observed FGF2 driven phenotype has potential to be driven by an increase in EC proliferation and recruitment to elongating vascular cords, as well as elongation of the individual cells within each cord of cells. This does not however explain the loss of branching observed within the FGF2 stimulated cultures (figure 3.6). Interestingly, it could suggest that FGF2 signalling acts to inhibit VEGF-driven branching. It would be interesting to test this hypothesis in future studies. It would also be interesting to analyse the number of nuclei, and individual cell length and orientation, of growing cords within the organotypic co-culture during FGF2 stimulation to determine whether the FGF driven phenotype is due to cell proliferation or elongation.

It must also be noted that the DOCK4 Kd organotypic angiogenesis assays found a slight increase in the branching of tubules under FGF2 stimulation, when compared to no GF, which directly contradicts the finding of the VEGFA vs FGF2 co-culture result (figure 3.2-3.3 and 3.4-3.6). Further repeats of both assays would be required to determine if loss of branching is a true characteristic of FGF2 stimulated angiogenesis.

While a difference in the characteristics of sprouting angiogenesis was observed when comparing FGF2 to VEGFA stimulated phenotype, the limitations of the experimental model need to be taken into consideration when attributing the observed results to physiological function. When comparing the two GF conditions it must be noted that

experiments were conducted *in vitro*, within an environment without the presence of the physiological variables found *in vivo*, such as: inflammatory factors, immune cell influence of angiogenesis, tissue specific signalling, the presence of pre-existing vasculature, and other signalling molecules within the tissue environment (Bishop et al., 1999; Stryker et al., 2019; Vailhé et al., 2001). Another limitation of the co-culture model lies within the lack of the GF gradient which would exist *in vivo* (Hetheridge et al., 2011). Growth factor gradients that induce angiogenesis drive polarisation of ECs, and guide directional growth of newly forming sprouts (Hetheridge et al., 2011). It must also be noted that all experiments were conducted using a single batch of commercially purchased angiogenesis tested HDF and a single batch of pooled HUVEC; in-order to reduce variability and maintain reproducibility. To confirm the robustness of the observed result, in demonstrating a physiological difference between angiogenesis stimulation between VEGFA and FGF2, these results should be replicated in HDF and HUVEC from other sources, to demonstrate that the observed results are not specific to the batch of cells (Abo et al., 1992).

In order to fully evaluate the findings of this study, it is also necessary to consider potential elements of the culture conditions which may confound the results. A limitation of this assay is the presence of different angiogenic factors in the LVEM, which makes the delineation of GF specific effects challenging, as it is not possible to eliminate other GFs in the system as such factors are required for EC survival (Huttala et al., 2015).

The growth serum present in the LVEM and additional FBS used to supplement the Dulbecco's Modified Eagle Medium, within all co-culture studies, possess a composition of proteins and hormones required for culture of both the HUVEC and HDF, respectively. The exact composition of proteins and hormones are unknown but have been equally maintained in all co-culture experiments in-order to establish a basal level of growth from which the growth characteristics, prompted by the two GFs, were investigated. It is however known that the media used contain a very small concentration of FGF2. Further to this, it must be

considered that VEGFA is produced by the HDFs in the assay, levels of which may not be equal across each experiment (Mavria et al., 2006). However, each assay was treated equally to reduce variability, and as such produced quantifiable results that served as a baseline from which an in-depth analysis was carried out.

FGF2 has been demonstrated, in part, to act on EC-associated fibroblasts and prompt fibroblasts to secrete VEGF; which in turn stimulates an angiogenic response within ECs leading to an increase in angiogenesis. However the results of this study demonstrate stimulation of angiogenesis by the two GFs induce different growth characteristics of sprouting angiogenesis, thus suggesting a role for FGF2 signalling in angiogenesis which acts independently from VEGFA signalling in driving a unique phenotype. Further dissection of each growth factor pathways involved in angiogenesis will expand our understanding of the complex mechanisms which drive the growth of new vasculature and offer insight in to potential therapeutic targets for manipulating how the new vasculature grows and develops.

3.3.2 DOCK4 function within sprouting angiogenesis

The small RhoGTPase RAC1 serves as an important component in the intracellular EC response to FGF2, inducing changes to the actin cytoskeleton required for the elongation of the individual cells. DOCK4 is a GEF involved in endothelial RAC1 activation downstream of VEGFA (Abraham et al., 2015) but has not yet been described as a component in the FGF2 angiogenic response. DOCK4 depletion within an organotypic angiogenesis co-culture model indicated that loss of endothelial DOCK4 expression leads to a loss in lateral branch points and less branching, without impacting endothelial cord elongation (Abraham et al., 2015), a phenotype similar to that of the FGF2 stimulated sprouting. Thus is possible to hypothesis that DOCK4 may act in RAC1 activation within a FGF2 driven sprouting angiogenesis context.

To investigate whether DOCK4 was involved in FGF2 stimulated sprouting angiogenesis, a preliminary co-culture was conducted incorporating lentiviral DOCK4 targeting shRNA transduced HUVEC into the organotypic angiogenesis co-culture model,

with FGF2 stimulation, along with lentiviral NS shRNA transduced HUVEC to serve as a control (figures 3.4-3.6). The results of this single experiment indicated that DOCK4 depletion led to a reduction in overall tubule growth when growth medium had no additional GF supplement, resulting in loss in total tubule length, the number of tubule, and the number of branch points. Supplementing growth medium with FGF2 rescued the loss in total tubule length, increasing mean tubule length, and inducing growth of the number of tubules and BPI back to the level of non-GF stimulated control cultures (figure 3.5 and 3.6). This finding indicates that in the absence of DOCK4, FGF2 stimulation of sprouting angiogenesis may overcome growth deficiencies prompted by loss of DOCK4 expression. Thus indicating that DOCK4 may not be required for FGF2 driven sprouting angiogenesis.

It must be noted, as previously mentioned, that within this experiment FGF2 treatment led to an increase in BPI (figure 3.6), a result which contradicts previous experiments. Further repeats of the experiment would be required to determine if this finding was an anomaly of this singular experiment. It should be considered that the variables, introduced by the conditions involved in treating cells with the NS shRNA, may have impacted upon branching, and would require further investigation to confirm the NS shRNA control cultures reflect the growth of non-transduced co-cultures.

Also, further investigation would be required to attribute the observed phenotype to loss of DOCK4 driven RAC1 activation, under FGF2 signalling. It would be necessary to measure changes in RAC1 activity within the cellular assay, to attribute the changes in phenotype to changes in RAC1 regulation. Measuring changes to RAC1 activation within the DOCK4 depleted co-cultures may prove challenging, as RAC1 may be involved in non-DOCK4 related activity within the same ECs during FGF2 driven sprouting angiogenesis (Shin et al., 2004). Investigating changes between DOCK4 depleted vs NS control ECs through observing any differences between the level of RAC1 activation, changes to RAC1 localisation within

the ECs, and changes to activation of RAC1 targets, may offer insight into DOCK4 involvement in RAC1 regulation during FGF2 vs VEGFA driven sprouting angiogenesis.

3.3.3 DOCK4 signalling in sprouting angiogenesis within hypoxia

FGF2 has been strongly linked to the angiogenic response within ischemia (Unger et al., 2000; Laham et al., 1999; Comerota et al., 2002; Nikol et al., 2008). As gene expression and cellular response within a hypoxic environment can differ greatly to a normoxic environment, it was imperative to also investigate the effect of DOCK4 functionality within FGF2 signalling under hypoxic conditions. For this purpose, the previously described culture was also conducted with co-cultures incubated in a hypoxic incubator (1% 0_2) following GF stimulation 4 days following HUVEC seeding to the HDF monolayer.

The culture of FGF2 stimulated NS HUVEC, within a hypoxic environment, led to a sprouting response similar to that of the non-GF supplemented cells grown in normoxia (figures 3.4-3.6), with only the FGF2 driven increase in mean length being maintained and longest tubule increasing. Thus indicating that FGF2 stimulation maintains the proliferative phenotype of ECs when experiencing oxygen deprivation. Conversely this phenotype was reversed when DOCK4 expression was depleted. Co-cultures of DOCK4 depleted HUVEC produced significantly fewer sprouts, resulting in loss in overall tubule length and fewer branch points than the NS FGF2 stimulated co-cultures also grown within hypoxia (figures 3.4-3.6). This result indicates a potential requirement for DOCK4 expression within FGF2 induced angiogenesis under oxygen deprivation.

While this experiment demonstrates a distinct response, a number of elements need to be evaluated when interpreting the results, and for use in optimising future investigations. It must be noted that the hypoxic environment will have been disrupted during the opening and closing of the incubator, and during additional GF treatments. Thus leading to some intermittent hypoxia during the sprouting angiogenesis. Using a hypoxia chamber, such the Modular Incubator Chamber manufactured by Billups-Rothenberg, Inc. (San Diego, CA USA),

would reduce instances of intermittent oxygen exposure and potentially provide more reproducible experimental results. Also, further confirmation must be carried out to ensure no off-target effect have been introduced by the NS shRNA or conditions which occur during treatment of the HUVECs with the shRNA lentiviral particles.

While this experiment was purely a preliminary test (with only 2 replicates within a single assay) to evaluate whether DOCK4 is relevant for FGF2 stimulation of sprouting angiogenesis, the outcome of the hypoxic DOCK4 depleted co-cultures indicates a potential role of DOCK4 within FGF2 driven sprouting angiogenesis within hypoxia. Implicating DOCK4 is required for the proliferation and branching of tubules within these conditions.

3.3.4   QL-47 treatment of organotypic angiogenesis co-cultures

It has been established that DOCK4 is required for development of functional vascular structures through sprouting angiogenesis. The interaction of DOCK4 with the CDC42 GEF DOCK9 has also been implicated in conferring the angiogenic response to VEGFA stimulation. To further understand the functionality of the SGEF-RhoG-DOCK4-RAC1-DOCK9-CDC42 signalling module, the interaction between DOCK4 and DOCK9 was investigated. Previous evaluation by Abraham et al. (2015) confirmed that the SH3 domain of DOCK4 is required for interaction with DOCK9, implicating a PRR of DOCK9 as important for DOCK4-DOCK9 interaction. Evaluation of the amino acid sequence of DOCK9 detected 11 potential PRRs of DOCK9, with 8 possessing the typical PxxP or PxxxP motif of a PRR. During the course of this study a DOCK9 binding small molecule inhibitor, QL-47, was gifted to the Mavria research group by Prof. Nathaniel Grey's research group (Dana-Farber Cancer Institute, MA USA).

QL-47 had been demonstrated to specifically bind to p.C628, a cysteine located within the 4th identified PRR of DOCK9. While the specific site of DOCK9 which binds DOCK4 had not been established, QL-47 offered the opportunity to utilise the compound to investigate whether the PRR4 of DOCK9 was a DOCK4 binding site. Before utilising the

compound to investigate DOCK4-DOCK9 interaction it was imperative to establish whether QL-47 possessed the ability to impact on angiogenesis.

3.3.4.1 The effect of QL-47 on sprouting angiogenesis

The organotypic co-culture model was adapted to include the covalently binding small molecule QL-47. As it had been established that angiogenic response to VEGFA and FGF2 stimulation differed, and that DOCK4 function may differ between VEGFA and FGF2 stimulated sprouting angiogenesis. For this reason co-cultures were carried out either in the absence of additional GF or under either VEGFA or FGF2 stimulation. This experiment strongly validated that QL-47 induced an anti-angiogenic effect under all three GF conditions, reducing both the number of endothelial cords formed and the elongation of these endothelial cords, while also driving a more tortuous phenotype (figures 3.7-3.9). Reduction in tubule growth resulted in fewer sites of tubule branching, however this reduction was relative to the reduction in the amount of overall tubule growth within non-GF stimulated cultures (figure 3.9). QL-47 induced a much more profound anti-angiogenic response when cultures were also supplemented with VEGFA; with an almost complete ablation of the ECs. Co-cultures grown without additional GF stimulation experienced a less profound anti-angiogenic affect (figures 3.7 and 3.9). The small molecule inhibitor led to an angiogenic impairment in all GF culture conditions.

Endothelial cultures supplemented with FGF2 were less affected by QL-47 treatment than VEGFA supplemented cultures, however, FGF2 supplemented cultures experienced a greater loss of endothelial cord elongation, a reduction in average tubule length, and, unlike the non-GF supplemented cells, a reduction in the relative number of branch points in relation to the overall level of tubule growth.

Within non-GF supplemented cultures the mean tubule length was not impacted, but did result in a reduction in total tubule length and the number of tubules, potentially indicating that that the inhibitor does not affect the outgrowth of endothelial cords but

impacts the overall proliferation of ECs and number of cords developed (figure 3.9). Branch point index was also unaffected, indicating that, while there was no reduction in the number of branch points tubules developed in comparison to overall length of tubules (figure 3.9).

The accumulated data investigating QL-47 indicate that the small molecule stimulates an apoptotic response under VEGFA signalling mechanisms, and also impairs correct FGF2 induced angiogenesis. While the DOCK9 binding molecule activity reflects the DOCK4 depleted cultures within VEGFA driven sprouting angiogenesis, and, to a lesser degree, DOCK4 within FGF2 driven sprouting angiogenesis, these results can only indicate a correlation but not causation. Investigation of the non-DOCK9 binding activity of QL-47 within ECs would be required to validate the anti-angiogenic phenotype as being a DOCK9 specific response. It would also be imperative to validate whether QL-47 disrupts DOCK4 interaction with DOCK9, a subject which will be discussed in results chapter 2.

QL-47 was originally developed as an inhibitor of the non-receptor tyrosine kinase BTK (Bruton's tyrosine kinase). BTK is not expressed within ECs, however, the BTK Family Tyrosine Kinase BMX (bone marrow tyrosine kinase gene on chromosome X) is expressed within endothelia and is targeted by QL-47; with QL-47 binding inducing a reduction in the tyrosine kinase activity of BMX (Wu et al., 2014). BMX is a cytoplasmic tyrosine kinase expressed within endocardium and in arterial endothelia and has been indicated as required for angiogenesis under inflammatory conditions not physiological angiogenesis (He et al., 2006; Luo et al., 2010). BMX is not expressed within capillaries and in not required for angiogenesis during development; with BMX null mice developing normal health vasculature (He et al., 2006; Luo et al., 2010). As the organotypic angiogenesis co-culture model is not designed to reflect the conditions of pathological angiogenesis it is unlikely BMX would be expressed within the experimental ECs used within the organotypic angiogenesis co-culture system employed within this study.

However, expression of BMX should be determined within the organotypic co-culture model, in-order to eliminate this protein as the QL-47 target driving the observed phenotype. Future experiments should also be carried out to confirm the observed phenotype is not due to BMX inhibition, through repeating QL-47 treatment of co-cultures with added BMX inhibition.

The findings of these studies establish the phenotypical differences in sprouting angiogenesis between VEGFA and FGF2 driven angiogenesis *in vitro*. DOCK4 has been implicated as a potential component in FGF2 signalling under hypoxic conditions, and to a much lesser degree under normoxic conditions. The small molecule inhibitor QL-47 is a potent anti-angiogenic compound, with VEGFA stimulated ECs being particularly sensitized to QL-47, however it cannot be concluded that the anti-angiogenic effects are due to inhibition of the CDC42 GEF DOCK9 or disruption of the DOCK4-DOCK9 interaction.

4 Results chapter II: Elucidating the site of DOCK4-specific binding to DOCK9

4.1 Introduction

The VEGFA-SGEF-RhoG-DOCK4-RAC1-DOCK9-CDC42 signalling module is required for correct vascular patterning and lumenisation during sprouting angiogenesis (Abraham et al., 2015). As part of this signalling module, DOCK4 has been demonstrated to heterodimerise with DOCK9, and is the first time a DOCKB subfamily protein has been seen to interact with a DOCKD subfamily protein (Abraham et al., 2015). Abraham et al. (2015) found the DOCK4 SH3 domain was the site of DOCK9 interaction. SH3 domains are short peptide sequences with aromatic residues that drive weak and transient interactions via their shallow groove, with PRR of interacting proteins to form left handed type II polyproline helices (Pollard et al., 2016). A PRR is a sequence of amino acids with multiple proline residues within close proximity of one another (Yu et al., 1994; Alexandropoulos et al., 1995). DOCK9 possesses 11 PRRs with 5 of them containing the typical PxxP or PxxxP motifs which form a continuous hydrophobic patch that preferentially binds to the amino acid sequence of SH3 domains.

In order to examine further the site of interaction between DOCK4 and DOCK9, five DOCK9- N-terminal Flag-tagged mutants had been cloned previously in the lab by Ms. Anne Sanford, each with a single point mutation within one of the five typical PRR regions (figure 4.1). DOCK9 mutant expression vectors were co-transfected together with an N-terminal GFP-tagged DOCK4 expression vector into HEK 293T cells and Co-IP assays were carried out analysing the DOCK4-DOCK9 interaction in the presence of the DOCK9 PRR mutations. A DOCK9 binding small molecule compound, QL-47, which binds within one of the PRR regions (figure 4.1), was used to determine whether it was capable of disrupting the DOCK4-DOCK9

interaction. SEC was also utilised to investigate the direct interaction between the DOCK4-

SH3 domain and the DOCK9 DHR1 domain.
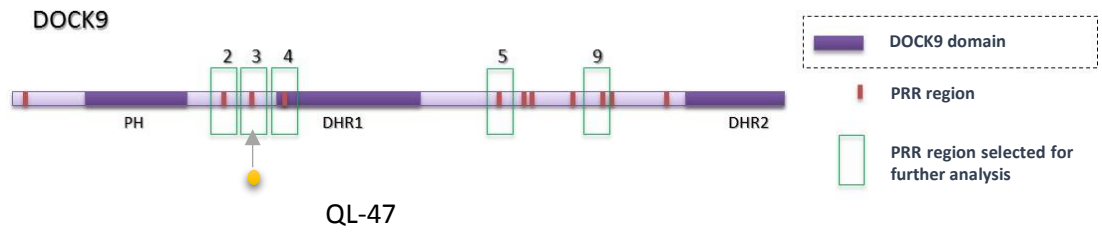
Figure 4-1 Identification of DOCK9 PRRs and site of QL-47 binding

The GEF DOCK9 possess 11 PRR. Five PRR have the typical PxxP or PxxxP motif. The small molecule QL-47 binds DOCK9 at the cysteine residue p.C628 within PRR 3.
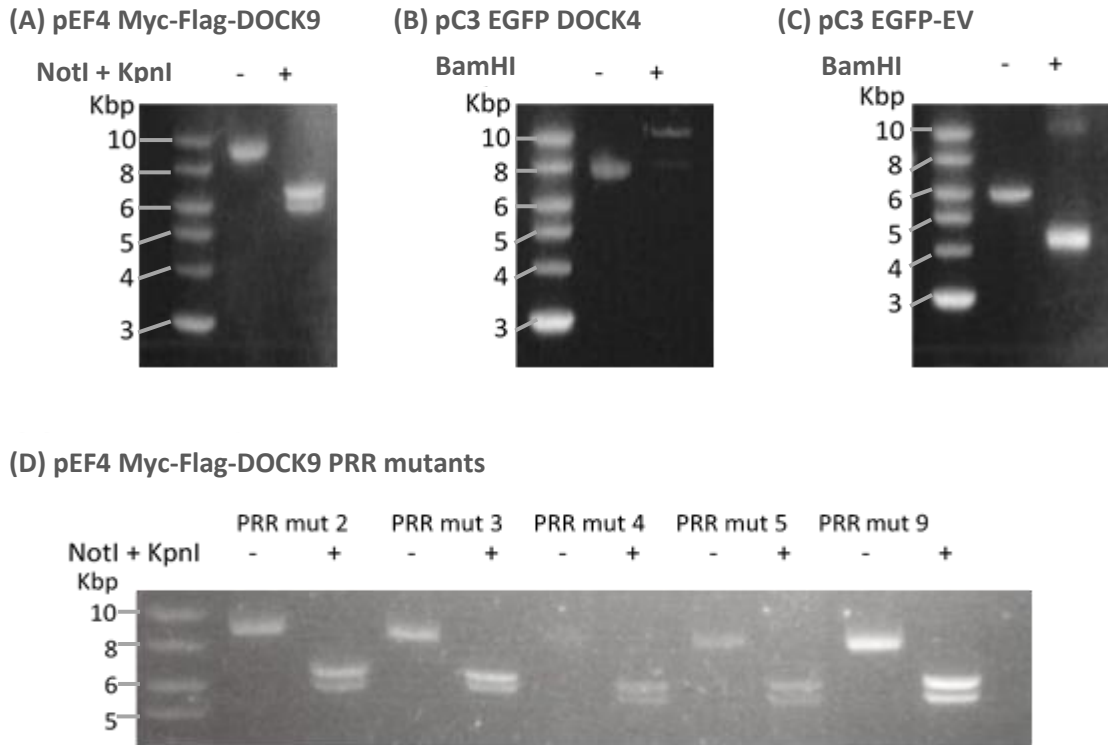
(A) pEF4 Myc-Flag-DOCK9

NotI + KpnI   -   +

(B) pC3 EGFP DOCK4

BamHI   -   +

(C) pC3 EGFP-EV

BamHI   -   +

(D) pEF4 Myc-Flag-DOCK9 PRR mutants

Figure 4-2 DNA plasmid preparation and restriction enzyme digestion.

(A) DNA plasmid pEF4 Myc-Flag-DOCK9, non-digested (12.3kbp), and digested with restriction enzymes NotI and KpnI, cutting out the Flag-DOCK9 insert (6.4kbp) from the pEF4 myc vector (5.9kbp). (B) DNA plasmids pC3 EGFP DOCK4 (12.4kbp) (C) and pC3 EGFP-EV (4.7kbp) were linearized using restriction enzyme BamHI. (D) Enzymes NotI and KpnI were used to separate Flag-DOCK9 insert (6.4kb) from the pEF4 vector (5.9kb) of the mutation variants of pEF4 Myc-Flag-DOCK9 (mutants 2, 3, 4, 5, and 9). Linearized plasmid fragments were resolved on a 0.7% agarose gel containing ethidium bromide. Kbp= Kilo base pairs. PRR= Proline rich region.

4.2.1 Plasmid preparation and verification of DOCK9 mutant plasmids

DNA plasmids to be used for overexpression of EGFP-DOCK4 (pC3 EGFP-DOCK4), Flag-DOCK9 proteins (pEF4 Myc-Flag-DOCK9), EGFP-EV (pC3 EGFP), and five Flag-DOCK9 constructs with mutated PRR 2, 3, 4, 5, and 9 (pEF4 Myc-Flag-DOCK9 PRR mut 2, pEF4 Myc-Flag-DOCK9 PRR mut 3, pEF4 Myc-Flag-DOCK9 PRR mut 4, pEF4 Myc-Flag-DOCK9 PRR mut 5, pEF4 Myc-Flag-DOCK9 PRR mut 9), were purified from *E. coli* cultures (as described in methods 2.9). Confirmation of extraction of the correct plasmid was determined through restriction enzyme digestion.

Each construct was confirmed based on kilobase pair size. Flag-DOCK9 plasmids (including all five Flag-DOCK9 mutants) were digested with restriction enzymes NotI and KpnI, cutting out the DOCK9-Flag insert (6.4kbp) from the pEF vector (5.9kbp). EGFP DOCK4 (12.4kbp) and EGFP-EV (4.7kpb) were linearized using restriction enzyme BamHI. Linearised plasmid fragments were resolved on a 0.7% agarose gel containing ethidium bromide. Agarose gel electrophoresis demonstrated that digestion of the plasmids, with the appropriate enzymes, yielded the expected DNA fragment sizes (figure 4.2). Non-digested constructs were determined to be supercoiled and thus detected as having a lower molecular weight than the linearized counterparts.

4.2.2   Confirming the presence of a complex between the RAC GEF DOCK4 and CDC42 GEF DOCK9 in HEK 293T.

The ability for DOCK4 and DOCK9 to interact and form a complex has previously been demonstrated (Abraham et al., 2015). This interaction was successfully reproduced through Co-IP of overexpressed DOCK4 and DOCK9 proteins, purified from HEK 293T cell lysates (figure 4.3). This condition formed the baseline for interaction between DOCK4 and DOCK9 in-order to investigate the loss of interaction through point mutation of prolines within identified PRR of DOCK9.

HEK 293T cells were transfected with EGFP-DOCK4 and Flag-DOCK9. Immunoblotting of total cell lysate was used for confirmation of successful expression of over-expressed proteins (figure 4.3). 48 hours after transfection, cells were lysed under mild conditions and GFP-DOCK4 and Flag-DOCK9 were precipitated in complex from TL using a GFP-trap (Chromotek). IP and Co-IP proteins were resolved by Western blot, and presence of Flag-tagged and GFP-tagged proteins was determined using HRP-conjugated anti-EGFP and anti-Flag antibodies and ECL detection as described in Materials and Methods (section 2).
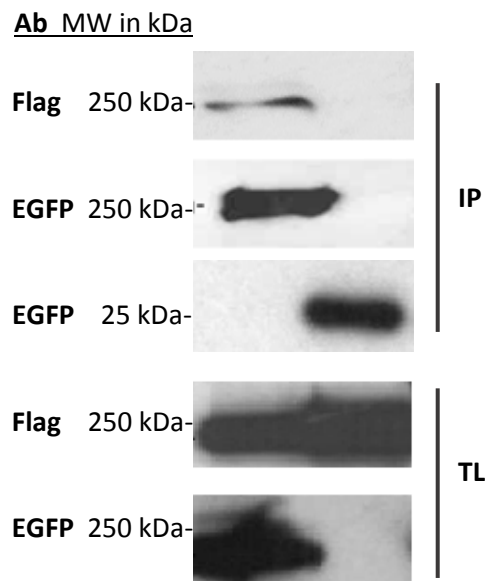
Figure 4-3 EGFP-DOCK4 overexpression and interaction with Flag-DOCK9

EGFP-DOCK4, pEF4-DOCK9, and EGFP-EV expression vectors were co-transfected into confluent HEK 293T. 48 hrs post transfection cells were lysed under mild lysis conditions. GFP-tagged proteins and interacting proteins were precipitated out of TL using a GFP-trap (Chromotek). TL and Co-IP products were resolved using Western blot and the ECL system. Representative Western blots depicts precipitated EGFP-DOCK4, Flag-DOCK9, EGFP-EV, and TL Flag-DOCK9 and EGFP-DOCK4

Ab=Antibody; MW=Molecular weight; kDa= kilodalton; IP=Immunoprecipitated; TL=Total lysate

4.2.3 Investigation of the DOCK4 interaction site of DOCK9

Once the ability for DOCK4-DOCK9 to form a complex was established, the regions of DOCK9 required for the interaction were investigated. Previous work in the laboratory (by Ms. Anne Sanford, unpublished) had led to selection of 5 proline-rich regions of DOCK9 as potential candidates as the site of DOCK4 binding. Five pEF4 Myc-Flag-DOCK9 plasmids had then been generated using a Stratagene Quickchange II XL site-directed mutagenesis kit (by Ms. Anne Sanford), each with a mutation of proline to alanine within each of the five identified PRRs. Each of the DOCK9 mutants was co-expressed together with GFP-DOCK4 in HEK 293T (figure 4.4-4.6), and precipitated from whole cell lysates using a GFP Trap.

Immunoblotting of Co-IP proteins was used to identify potential disruption of the DOCK4-DOCK9 complex, this was determined through the presence or absence of the DOCK9 mutant protein, following anti-Flag probing.

Co-IP of DOCK4 and DOCK9 mutant 2 consistently showed that a mutation within the 2nd PRR had no obvious effect on the complex, as can be seen by the presence of a strong band in the representative blot imagine in figure 4.4 and colourimeteric analysis in figure 4.7. This results indicates that this point mutation does not disrupt binding between overexpressed DOCK4 and DOCK9.

In initial experiments with samples derived from cells expressing DOCK9 mutant 3, anti-Flag probed Western blot bands yielded a much weaker, if not absent, signal than that of the positive control, suggesting this PRR may be necessary for DOCK4 binding. However, probing for GFP showed that this could be due to less IP of EGFP-DOCK4. Repeats of this experiment yielded conflicting results, with DOCK9 mutant 3 successfully precipitated with GFP-DOCK4, giving a signal equal to the positive control in Western blot analysis (figure 4.4) This variability has been demonstrated through combined colorimetric analysis (figure 4.7).

Analysis of lysates derived from DOCK9 mutant 4 initially yielded a weaker Western blot signal, when compared to the positive control in two out of four repeat experiments,

with the latter two repeat experiments showing a DOCK4 interaction with DOCK9 mutant 4 which was equivalent to that of the control (figure 4.4, 4.5, 4.7). DOCK9 mutant 4 consistently had a lower level of detectable protein within TL samples, something not seen with the other four DOCK9 mutant expression vectors, which further supported the conclusion that the reduction in the DOCK9 mutant 4 Co-IP product was likely due to a lower level of protein expression. Interaction of DOCK4 was also detected with DOCK9 mutant 5 (figure 4.5 and 4.7).

In initial experiments, DOCK9 mutant 5 also appeared to have less interaction with DOCK4, as the Western blot signal of Co-IP product were less pronounced than the positive control. However, this result was not reproducible in 3 out of 4 repeat experiments, which all yielded results which indicated that the interaction between DOCK4 and DOCK9 mutant 5 was equal to that of DOCK4 with WT DOCK9 (figure 4.5 and 4.6), and thus an unlikely site of direct DOCK4-DOCK9 interaction.

Co-IP product of DOCK9 mutant 9, with GFP-DOCK4, consistently yielded results equal to that of WT DOCK9 (figure 4.6 and 4.7). The results suggest that DOCK9 PRR 9 is unlikely to be involved in a direct interaction with DOCK4.

DOCK9 mutant 2 (figure 4.4) and mutant 9 (figure 4.6) both consistently gave a strong signal, which was comparable to the positive control, indicating the interaction between DOCK4 and DOCK9 was maintained in the presence of mutation within these PPR regions. DOCK9 mutant 5 Co-IP results were less consistent, but as 3 out 4 Co-IP experiments led to a strong level of DOCK9 mutant 5 pull down, the DOCK9 PRR 5 may not be required for direct interaction. Thus, it could be hypothesised that the PRR regions mutated in these experiments are unlikely to be required for the direct interaction of DOCK4 with DOCK9.

The Co-IP results obtained through analysis of DOCK4 interaction with DOCK9 PRRs 3 and 4 were non-conclusive. While initial experiments indicate a potential loss of DOCK4 interaction, the loss of these points of interaction between DOCK4 and DOCK9 PRR mutants

3 and 4 in these Co-IP experiments were not reproducible and thus a conclusion cannot be drawn from these experiments.

The conflicting results obtained in these assays suggest that DOCK9 PRR 3 and 4 may be involved in interaction between DOCK4 and DOCK9, however, the Co-IP model used within this chapter may not be a proficient method to elucidate if the selected PRR are involved in the interaction between the DOCK4 SH3 domain and DOCK9.
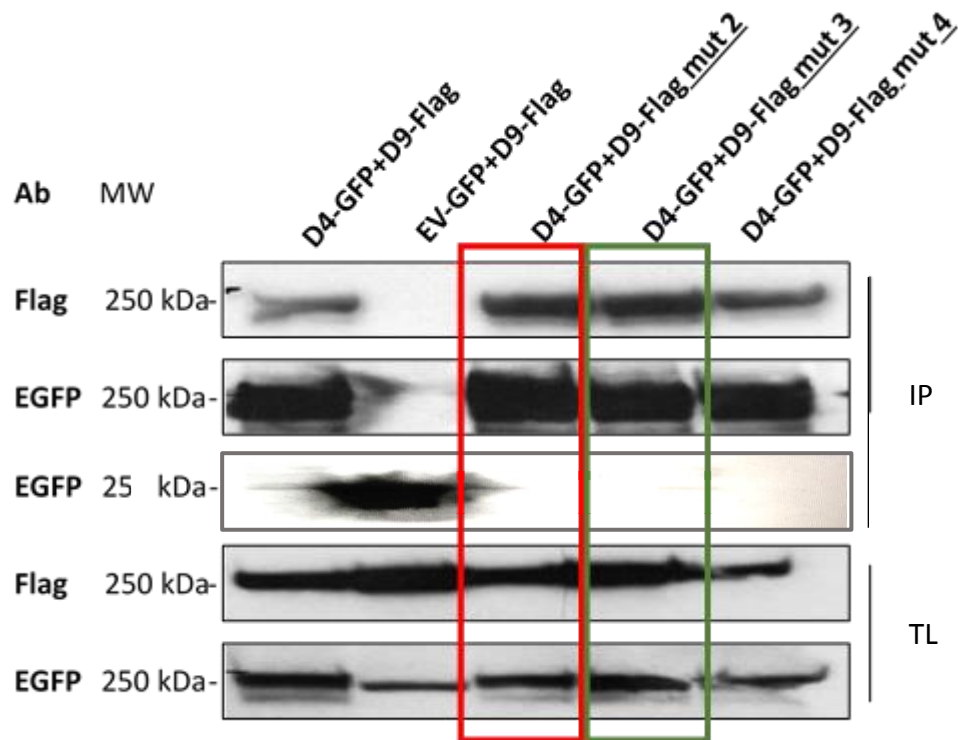
Figure 4-4 Co-IP EGFP-DOCK4 and Flag-DOCK9 mutants 2 and 3

Analysis of DOCK9 PRR through Co-IP of proteins overexpressed in HEK 293T cells. EGFP-DOCK4 was over expressed with one Flag-DOCK9 mutant 2 (green box) or mutant 3 (red box), mutant 4 also depicted. Flag-DOCK9 was also overexpressed with EGFP-EV. 48 hrs post transfection cells were lysed under mild lysis conditions. GFP-tagged proteins were precipitated out of total cell lysates using a GFP-trap (Chromotek). Co-IP and TL were resolved through Western blot and presence of Flag-tagged and GFP-tagged proteins were determined through targeted HRP conjugated antibody binding and ECL detection analysis.

Ab=Antibody; MW=Molecular Weight; kDa= kilodalton; IP=Immunoprecipitation; TL= Total lysate; D4=DOCK4; D9=DOCK9; EV=Empty vector.

Figure 4-5 Co-IP of EGFP-DOCK4 and Flag-DOCK9 mutants 4 and 5

Analysis of DOCK9 PRR through Co-IP of proteins overexpressed in HEK 293T cells. EGFP-DOCK4 was over expressed with one Flag-DOCK9 mutant 4 (green box) or mutant 5 (red box). Flag-DOCK9 was also overexpressed with EGFP-EV. 48 hrs post transfection cells were lysed under mild lysis conditions. GFP-tagged proteins were precipitated out of total cell lysates using a GFP-trap (Chromotek). Co-IP and TL were resolved through Western blot and presence of Flag-tagged and GFP-tagged proteins were determined through targeted HRP conjugated antibody binding and ECL detection analysis.

Ab=Antibody; MW=Molecular Weight; kDa= kilodalton; IP=Immunoprecipitation; TL= Total lysate; D4=DOCK4; D9=DOCK9; EV=Empty vector.
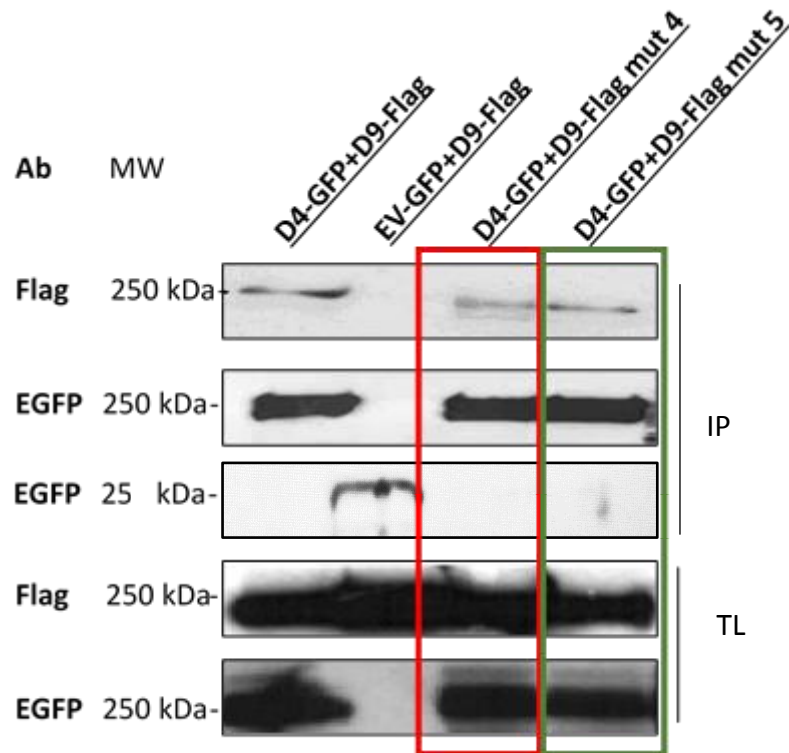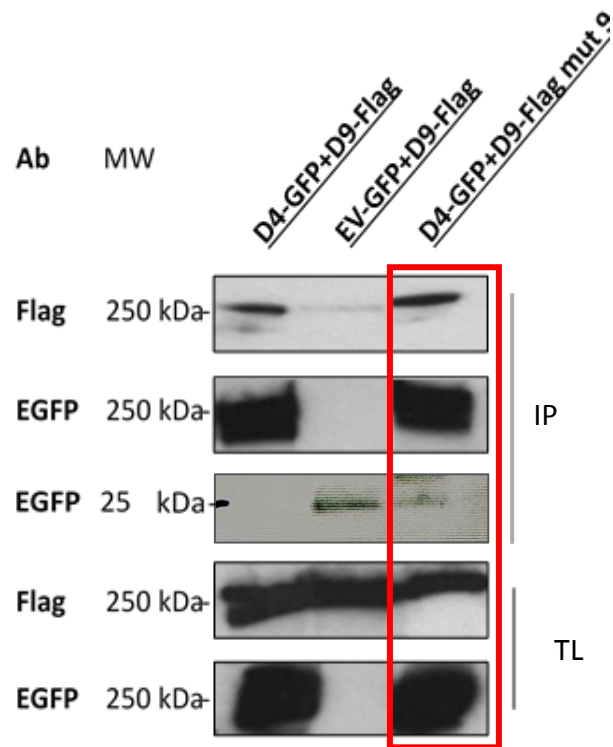
Figure 4-6 Co-IP EGFP-DOCK4 and Flag-DOCK9 mutant 9

Analysis of DOCK9 PRR through Co-IP of proteins overexpressed in HEK 293T cells. EGFP-DOCK4 was over expressed with either Flag-DOCK9, or Flag-DOCK9 mutant 9. Flag-DOCK9 was also overexpressed with EGFP-EV. 48 hrs post transfection cells were lysed under mild lysis conditions. GFP-tagged proteins were precipitated out of TL using a GFP-trap (Chromotek). Co-IP and TL were resolved through Western blot and presence of Flag-tagged and GFP-tagged proteins were determined through targeted HRP conjugated antibody binding and ECL detection analysis.

Ab=Antibody; MW=Molecular Weight; kDa= kilodalton; IP=Immunoprecipitation; TL= Total lysate; D4=DOCK4; D9=DOCK9; EV=Empty vector.
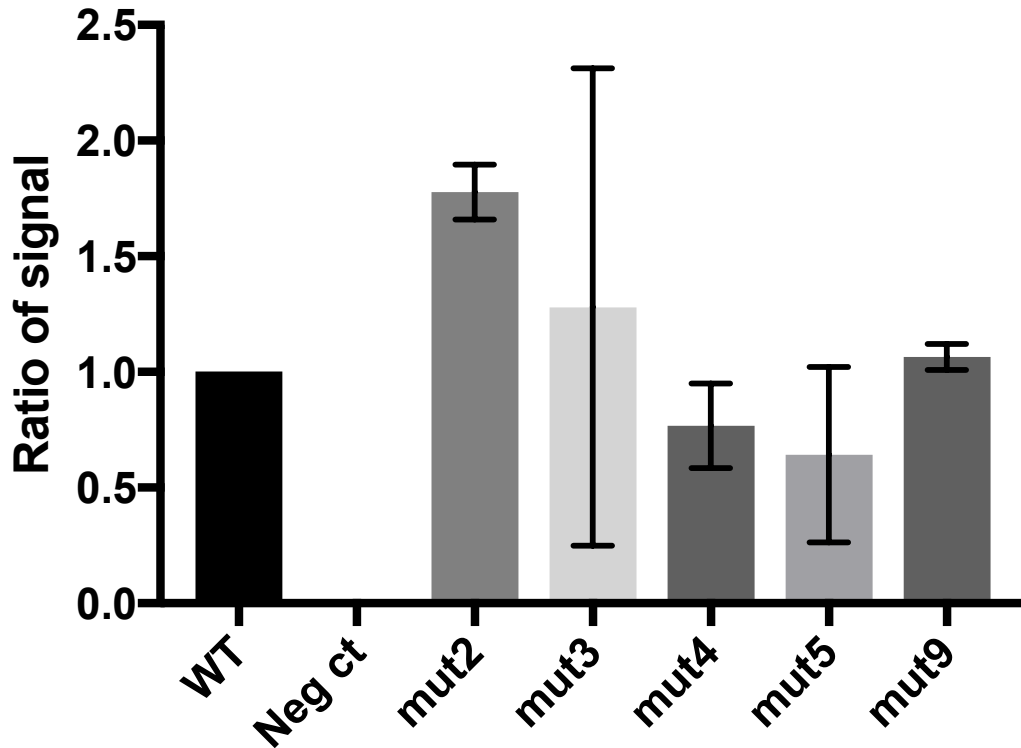
Figure 4-7 Quantitative colorimetric analysis of DOCK4 interaction with DOCK9 PRR mutant during Co-IP

Western blots of GFP-trap Co-IP experiments following co-transfection of EGFP-DOCK4 and Flag-DOCK9 proteins (WT or mutant PRRs 2, 3, 4, 5 and 9) were quantified from independent repeats of the experiments shown in figures 4.6 (n=3 for each PRR mutant co-culture) using Image J software. The values of each column represents the mean+SD of the ratio of Western blot signal when compared to a positive WT-Flag-DOCK9 Western blot signal, which was given a value of 1. Western blot band signal representing a mutant PPR DOCK9 complex with GFP-DOCK4. Data graph generated using GraphPad Prism 7.0a software. WT=Flag-DOCK9 expressed with EGFP-DOCK4; Neg ct=EGFP-EV negative control expressed with Flag-DOCK4; mut2=Flag-DOCK9 mutant 2 expressed with EGFP-DOCK4; mut3=Flag-DOCK9 mutant 3 expressed with EGFP-DOCK4; mut4=Flag-DOCK9 mutant 4 expressed with EGFP-DOCK4; mut5=Flag-DOCK9 mutant 5 expressed with EGFP-DOCK4; mut9=Flag-DOCK9 mutant 9 expressed with EGFP-DOCK4.

4.2.4   Effect of the DOCK9 binding small molecule inhibitor QL-47 on disruption of the DOCK4-

DOCK9 complex

QL-47 is a small molecule inhibitor which has been demonstrated to inhibit Cd42

activation and disrupt VEGFA driven angiogenesis (appendix 2, figure 7.10). QL-47 binds

DOCK9 at p.C628, a cysteine residue which lies within PRR 3 (p.PCIP627-630) of DOCK9

(figure 4.1). When considering DOCK4-DOCK9 PRR mutant 3 Co-IP experimental results,

which indicated a potential role for PRR 3 in disrupting DOCK4-DOCK9 interaction, QL-47

served as a potential tool for investigating whether this region serves as the site of DOCK4-

DOCK9 binding (figure 4.1).

Immunoprecipitation experiments of over expressed GFP-DOCK4 and Flag-DOCK9

from cell lysates of HEK 293T were carried out following treatment of 293T for 24 hours with

5µM of QL-47; a previously determined concentration (Wu et al., 2014) that was found to

also disrupt angiogenesis in an organotypic angiogenesis co-culture model (Chapter 3.

figures 3.7-3.9).

Western blot analysis of TLs of QL-47 treated cells showed an initial mild disruption

of DOCK4-DOCK9 interaction (figure 4.8), however this could not be demonstrated through

repeat experiments. Review of literature describing use of QL-47 in cell culture treatment

(Wu et al., 2014) indicated QL-47 was unable to infiltrate cells to successfully bind the target

protein (Wu et al., 2014). The lack of solubility of QL-47 had been apparent during use of the

compound within the co-culture assays (Chapter 3, figures 3.7-3.9), this was overcome by

adding QL-47 to warm media and vortexing for approx. 5 minutes. While this approach

overcame the solubility issues within the co-culture, proper entry into the cell could not be

determined within the transfected HEK 293T cells. Wu et al (2014) addressed this issue by

treating cell lysates as opposed to cultured cells, therefore QL-47 treatment was carried out

on TLs and cultured cells in order to overcome any issues of uptake by the cells. Western blot

analysis of Co-IP proteins treated with QL-47 established that QL-47 was unable to disrupt

the DOCK4-DOCK9 interaction in either pre-treated cells or cell lysate experiments.
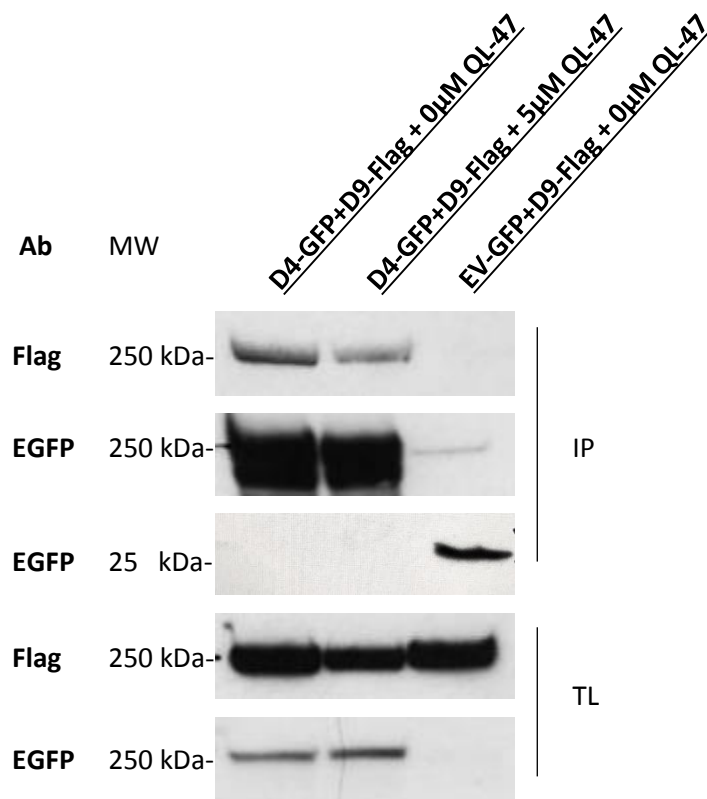
Figure 4-8 Co-IP of overexpressed EGFP-DOCK4 and Flag-DOCK9 following treatment of HEK 293T cells with the compound QL-47

Analysis of the effect of QL-47 treatment on the DOCK4-DOCK9 interaction through Co-IP of proteins overexpressed in HEK 293T cells. EGFP-EV and Flag-DOCK9, or EGFP-DOCK4 and Flag-DOCK9, expression vectors were co-transfected into HEK 293T cells. 24 hours post transfection cells were treated with 5μM QL-47. Cells were lysed 24 hrs post QL-47 treatment. Co-IP of protein complexes from TL was performed using a GFP-trap (Chromotek). Precipitated proteins and proteins of TL were resolved through Western blot and presence of Flag-tagged and GFP-tagged proteins were determined through targeted HRP conjugated antibody binding and ECL detection analysis.

Ab=Antibody; MW=Molecular Weight; kDa= kilodalton; IP=Immunoprecipitation; TL= Total lysate; D4=DOCK4; D9=DOCK9; EV=Empty vector.

4.2.5   Size exclusion analysis of DOCK4 SH3 domain and DOCK9 PCIP-DHR1 domain

interaction

The SH3 domain of DOCK4 has already been established as the domain which drives

DOCK4 interaction with DOCK9 (Abraham et al., 2015). Co-IP analysis of DOCK9 PRR mutants

indicated PRR 3 (p.PCIP627-630), which lies just upstream of the DHR1 domain, and PRR 4,

which lies within the DHR1 domain (figure 4.1) may be involved in the DOCK4-DOCK9

binding. Hence, a DOCK9 construct was generated to include a nucleotide sequence which

encompasses the p.PCIP627-630 residues and the DHR1 domain.

Nucleotide sequences for DOCK4 SH3 domain and DOCK9 PCIP-DHR1 domain were

cloned into pOPIN-F expression vectors with inclusion of a His-tag (figure 7.4; figure 7.5).

DOCK4 SH3-His (figure 4.9) and DOCK9 PCIP-DHR1-His peptides (figure 4.10) were produced

in BL21 (DE3) competent cells and purified using affinity chromatography, then both further

purified using SEC (figure 4.11). All protein lysates were concentrated to approximately

100μM/ml. Purified DOCK4 SH3 His-tagged peptides were diluted in a 1:1 ratio with elution

buffer and aliquoted into 2ml fractions. Diluted peptides were further purified and separated

according to size using SEC (figure 4.12).

The concentration of peptide particles within each 1ml fractions were determined

by UV light spectroscopy (mAU), generating a line graph which indicates concentration of

each fraction, with peaks indicating the UV absorbance and therefore hydrodynamic volume

of the molecules. Fractions represented by the large peak in figure 4.12 A.1 were then

resolved using a SDS PAGE gel and confirmed as DOCK4 SH3 moieties through Coomassie

blue staining of the gel based on the molecular weight of the detectable band by comparison

to a Bio-Rad molecular weight ladder (Figure 4.12 B, well 1). Purified DOCK9 PCIP-DHR1

peptides were then further purified and separated according to size using the same

methodology as the DOCK4 SH3 domain peptides. Fractions represented by the large peak

in figure 4.12 A.2 were then resolved using a SDS PAGE gel and confirmed as DOCK9 PCIP-

DHR1 through Coomassie blue staining of the gel (Figure 4.12 B, well 2).

A

B

C

D

Figure 4-9 Expression vectors of DOCK4 truncated peptide regions of interest.

POPINF DOCK4-SH3-HIS construct was cloned to express DOCK4-SH3 peptides. His-tagged

DOCK4-SH3 peptides expressed in BL21 (DE3) competent cells were purified using affinity

chromatography and a His Trap HP column, connected to an ÄKTA pure protein purification

system (GE Lifesciences). **(A)** PCR agarose gel of DOCK4 SH3 gene fragment isolated from a

pBabe puro DOCK4-Flag expression vector, and amplified through PCR amplification. DOCK4

SH3 domain nucleotide sequence (216 bp,) confirmed through Sanger sequencing

(ThermoFisher), was cloned into a pOPINF-HIS vector using cloning NEBuilder® HiFi DNA

Assembly Cloning Kit. Correct gene insert was determined by agarose gel DNA separation.

(B) Graph depicting an affinity chromatography elution profile of DOCK4 SH3 domain

peptides. DOCK4 SH3 domain peptide purification from a BL21 (DES) competent cell lysate. mAU= Milli absorbance units; ml=Millilitre of eluted sample, collected in 1ml aliquots on a 96 well collection plate; UV1_280= UV absorbance at 280 nm and represents protein concentration within lysate samples as they are eluted from the His-column; Cond= Conductivity monitor used to follow column equilibration; Cond B= Conductivity monitor used to monitor salt gradient formation. **(C)** Coomassie stained SDS-Page gel of affinity chromatography purified DOCK9 PCIP-DHR1 domain peptide. pOPINF DOCK4-SH3-His plasmid was transformed into BL21 (DE3) competent cells, grown in 1l cultures, lysed, and purified using affinity chromatography. C.1= Whole bacterial culture sample. C.2= Bacterial pellet sample. C.3= Sample of initial elution of the His-column wash of DOCK4-SH3 domain peptide containing lysate, during affinity chromatography. C.4= Second sample of elution of the His-column wash of DOCK4-SH3 domain peptide containing lysate, during affinity chromatography. C.5-11=Samples of affinity chromatography eluents corresponding to the eluted purified proteins in ml samples 63-68ml of the given chromatography elution peak. (D) Anti-His Western blot of DOCK4 SH3 proteins purified through affinity chromatography. Western blot lane 1-3 correspond to lanes labelled 8 and 9 of the Coomassie stained SDS-Page gel (C), respectively. AB=Antibody; BP=Base pair; MW=Molecular Weight; kDa= Kilodalton
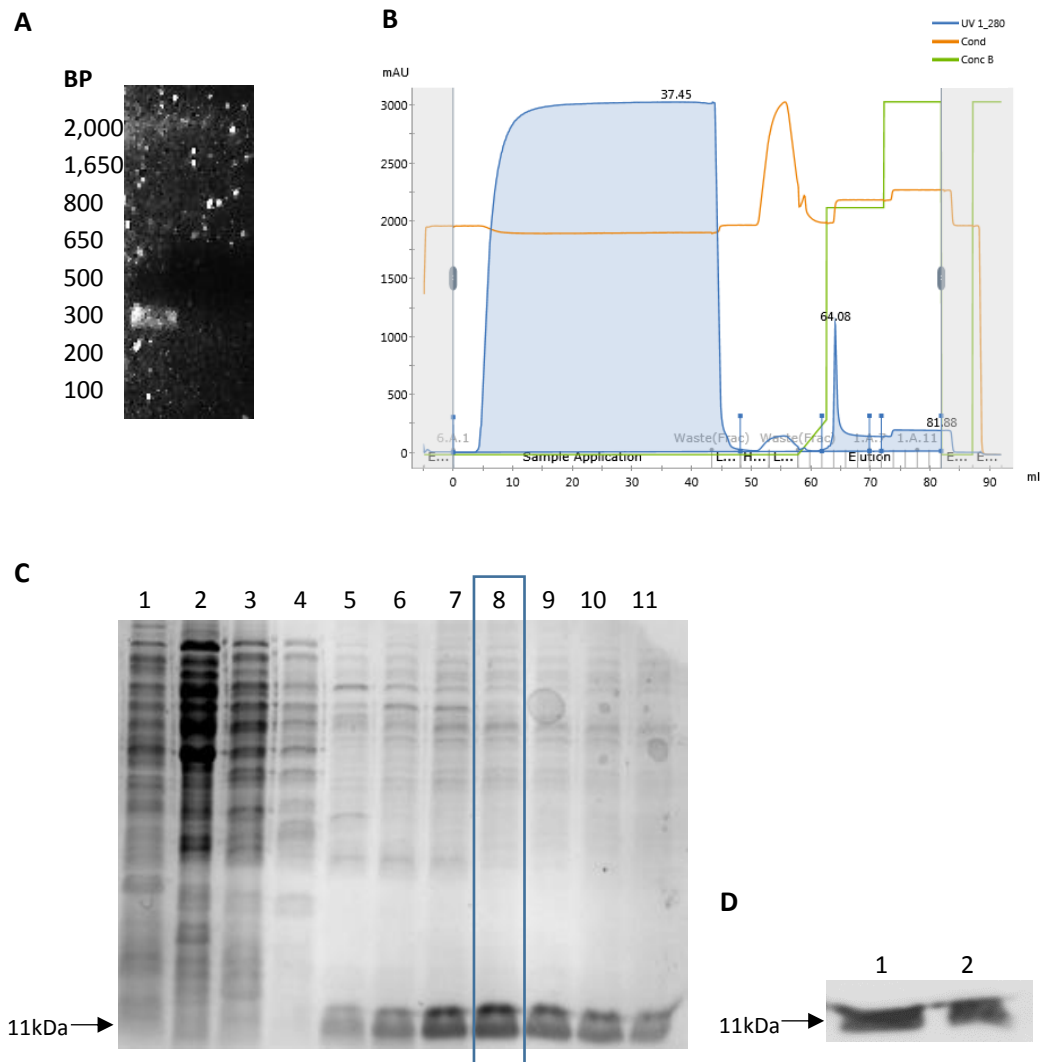
Figure 4-10 Expression vectors of DOCK9 truncated peptide regions of interest.

pOPINF DOCK9 PCIP-DHR1-His construct was cloned to express DOCK9 PCIP-DHR1 peptides. His-tagged DOCK9 PCIP-DHR1 peptides expressed in BL21 (DE3) competent cells were purified using through affinity chromatography using a using a His Trap HP column connected to an ÄKTA pure protein purification system (GE Lifesciences). **(A)** PCR agarose gel of DOCK9 PCIP-DHR1 gene fragment (well 2; BP 663) was isolated from a Flag-DOCK9 expression vector and amplified through PCR amplification. DOCK9 PCIP-DHR1 domain nucleotide sequence was cloned into a pOPINF-HIS vector using cloning NEBuilder® HiFi DNA Assembly Cloning Kit. Correct gene insert was determined by agarose gel DNA separation. **(B)** Affinity chromatography peak of DOCK9 PCIP-DHR1 domain peptide purification from a BL21 (DES) competent cell lysate. mAU= Milli absorbance unit; ml=Millilitre of eluted sample,

collected in 1ml aliquots on a 96 well collection plate; UV1_280= UV absorbance at 280 nm represents concentration of protein within lysate samples as they are eluted from the His-column; Cond=Conductivity monitor used to follow column equilibration; Cond B=Conductivity monitor used to monitor salt gradient formation. **(C)** Coomassie stained SDS-Page gel of affinity chromatography purified DOCK9 PCIP-DHR1 domain peptide. pOPINF DOCK9 PCIP-DHR1-His construct was transformed into BL21 (DE3) competent cells, grown in 1l cultures, lysed, and purified using affinity chromatography. C.1=Sample of initial elution of the His-column wash of DOCK9 PCIP-DHR1 domain peptide containing lysate, during affinity chromatography. C.4=Bacterial pellet sample. C.6-10=Samples of affinity chromatography eluents corresponding to the ml of eluted purified proteins in samples 118-122ml of the given chromatography elution peak. (D) Anti-His Western blot of DOCK9 PCIP-DHR1 proteins purified through affinity chromatography. Western blot lanes 1-3 represent affinity chromatography elutions detected on the Coomassie stained SDS-Page gel (C) lanes 6-8, respectively. AB=Antibody; BP=Base pair; MW=Molecular Weight; kDa= Kilodalton
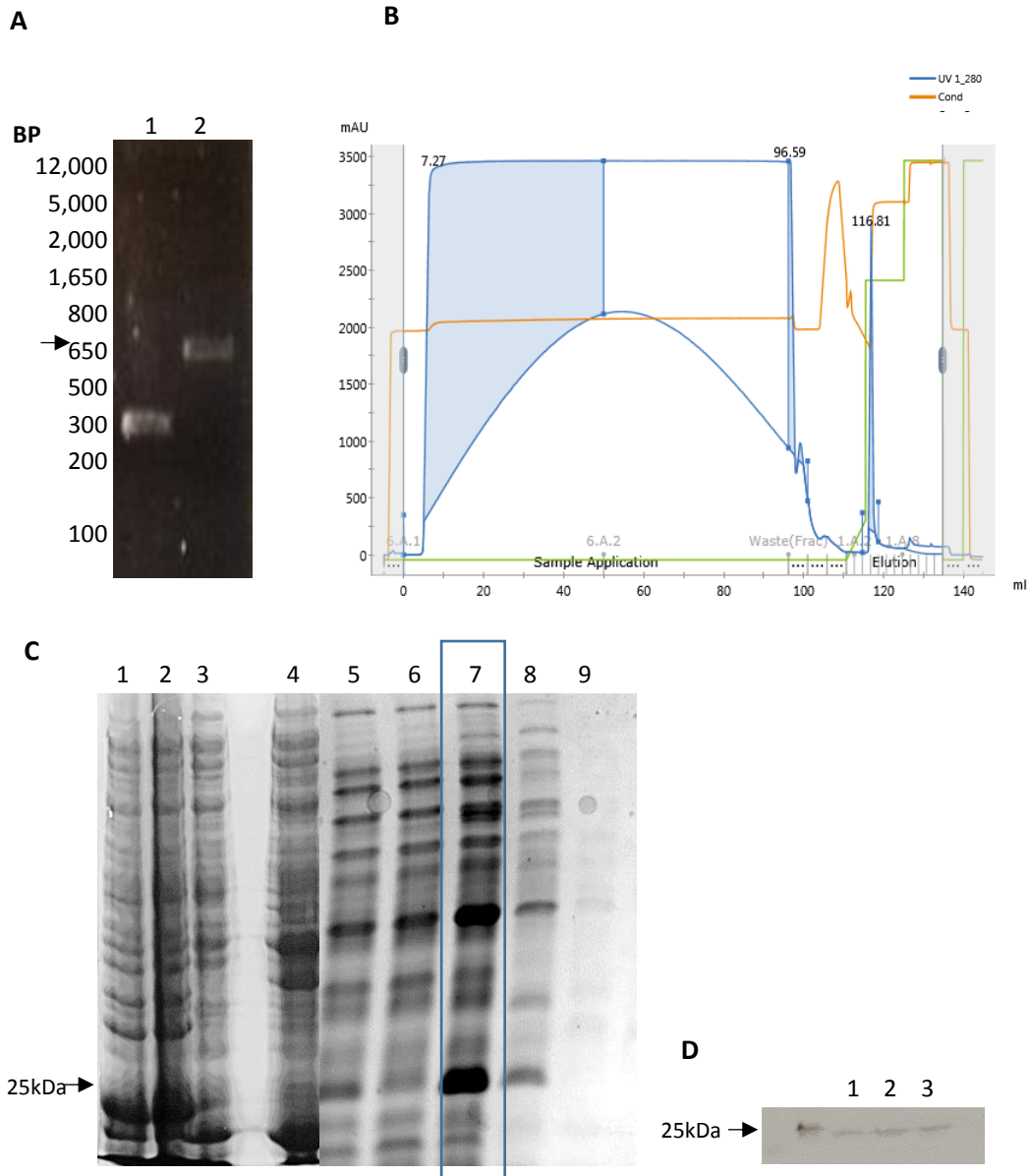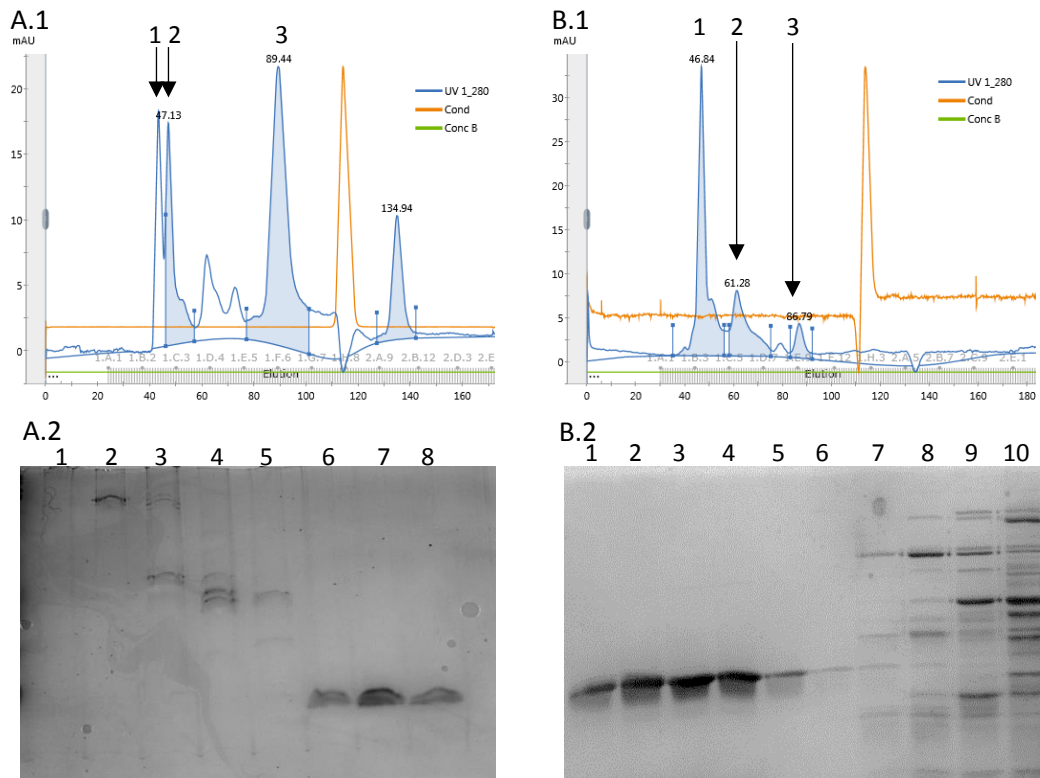
Figure 4-11 SEC purification of DOCK4-SH3 and DOCK9 PCIP-DHR1 peptides

His-tagged DOCK4-SH3 peptides and DOCK9 PCIP-DHR1 peptides expressed in BL21 (DE3) competent cells were purified from bacterial lysates using affinity chromatography and further purified through SEC using a Superdex® 75 10/300 GL column connected to an ÄKTA pure protein purification system (GE Lifesciences). **(A1)** DOCK4-SH3 peptide SEC elution peaks and **(B1)** DOCK9 PCIP-DHR1 peptide SEC elution peaks. mAU= Milli absorbance unit; ml=Millilitre of eluted sample, collected in 1ml aliquots on a 96 well collection plate; UV1_280= UV absorbance at 280 nm represents concentration of protein within lysate samples as they are eluted from the His-column; Cond= Conductivity monitor used to follow column equilibration; Cond B= Conductivity monitor used to monitor salt gradient formation. **(A2)** Coomassie stained SDS-Page gel of affinity chromatography purified DOCK4-SH3 domain peptide and **(B2)** DOCK9 PCIP-DHR1 domain peptide**. (A2 and B2)** Peptides purified using affinity chromatography were further purified using SEC **(A2)** SDS PAGE gel lanes correspond to specific 1ml DOCK4 SH3 SEC protein sample eluents as follows: A2 lanes 1-2 correspond to sample collected from A1 SEC peak 1. A2 lanes 3-5 correspond to sample collected from A1 SEC peak 2. A2 lanes 6-8 correspond to sample collected from A1 SEC peak 3. **(B2)** SDS PAGE gel lanes correspond to specific 1ml SEC DOCK9 PCIP-DHR1 protein sample eluents as follows B2 lanes 1-6 correspond to sample collected from A1 SEC peak 1. B2 lanes 7-9 correspond to sample collected from A1 SEC peak 2. B2 lane 10 corresponds to sample collected from A1 SEC peak 3.

To determine whether the DOCK4 SH3 domain binds directly to the DOCK9 PCIP residues and/or the DHR1 domain, 50μM of DOCK4 SH3-His peptides were combined with 50μM of DOCK9 PCIP DHR1-His peptides.

Combined peptides were diluted with non-denaturing elution buffer and fractionated through SEC into aliquots based on size, with larger proteins being eluted first. The concentration of peptide particles within each 1ml fractions was determined by UV light spectroscopy (mAU), generating a line graph that indicates concentration of each fraction with peaks signifying the UV absorbance and therefore hydrodynamic volume of the polymer molecules. Should the proteins interact and have formed a complex, the peak, currently indicated in figure 4.12 A3, would have shifted to the left; indicating complex of the two proteins resulting in a larger molecule, and an earlier elution of the proteins.. However, the peaks generated by elution of the combined lysates indicate lack of interaction between the two peptides, with each protein eluting separately with peaks that reflected the peaks generated by SEC of the individual peptides. Proteins collected in fractions represented by the two large peaks were resolved on an SDS PAGE gel and visualised with Coomassie blue. Peptides of the correct molecular weight for DOCK4 SH3-His and DOCK9 PCIP DHR1-His were confirmed (figure 4.12 B, wells 3 and 4). These results show lack of direct interaction between the DOCK4 SH3 domain and the DOCK9 p.PCIP627-630 residues encompassing PRR 3, nor the DOCK9 DHR1 domain encompassing PPR 4. This result also nullifies the hypothesis that the DOCK9 binding small molecule inhibitor QL-47 disrupts the DOCK4-DOCK9 interaction through binding to residue p.C628 which lies within the PPR region 3 of DOCK9.
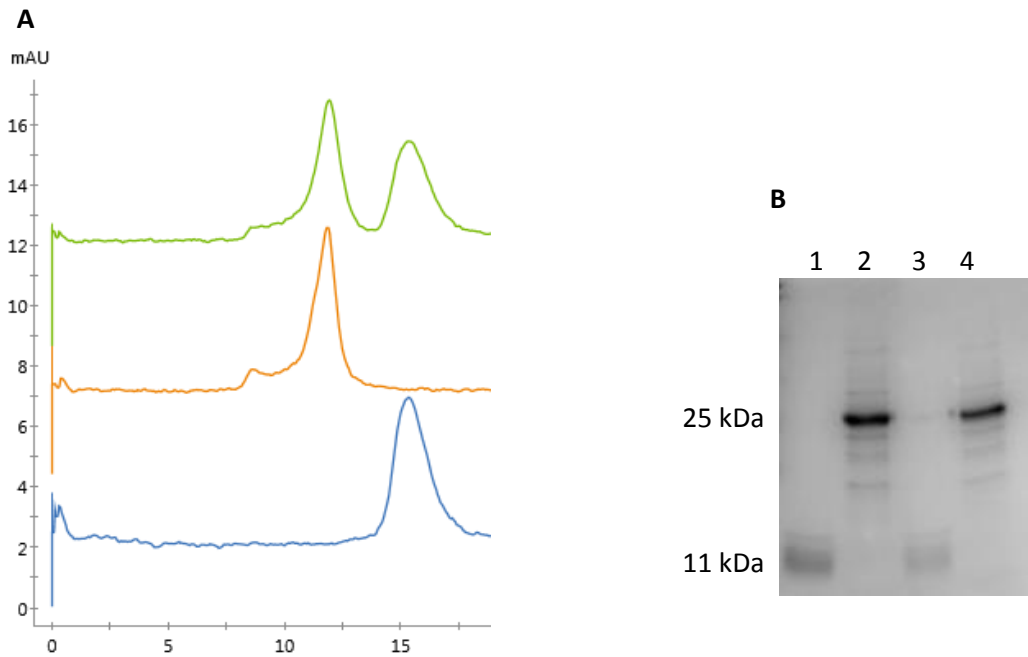
Figure 4-12 SEC interaction analysis of DOCK4 SH3 and DOCK9 PCIP-DHR1 purified peptides

Analysis of DOCK4 SH3 and DOCK9 PCIP-DHR1 interaction using SEC followed by confirmation using SDS PAGE gel confirmation. **(A)** Affinity chromatography purified DOCK4 SH3 and DOCK9 PCIP-DHR1 peptides were separated by size through SEC, using a Superdex® 75 10/300 GL column connected to an ÄKTA pure protein purification system (GE Lifesciences). (Blue line) 100µM of DOCK4 SH3 peptides in 1ml of lysate were loaded onto a Superdex® 75 10/300 GL column through a 500µl loop. Peptides were resolved through SEC and detected based on size. (Orange line) 100µM of DOCK9 PCIP-DHR1 peptides in 1ml of lysate were loaded onto a Superdex® 75 10/300 GL column through a 500µl loop. Peptides were resolved through SEC and detected based on size. (Green line) 50µM of DOCK4 SH3 and 50µM of DOCK9 PCIP-DHR1 peptides were combined to a volume of 1ml of lysate then loaded onto a Superdex® 75 10/300 GL column through a 500µl loop. Peptides were resolved through SEC and detected based on size. Right peak indicates DOCK4 SH3 domain peptides. Left peak indicated DOCK9 DHR1 peptides. **(B)** Peptides eluted by SEC were resolved on a SDS PAGE gel followed by Coomassie blue. Peptides in eluents corresponding to SEC peaks were confirmed as DOCK4 SH3 and DOCK9 PCIP-DHR1 peptides based on molecular weight: DOCK4 SH3 domain peptides (11kDa; blue line) indicated on Coomassie gel (B) lane 1. DOCK9 DHR1 domain peptides (25kDa; orange line) indicated on Coomassie gel (B) lane 2. DOCK4 SH3 domain peptides (right peak, green line) indicated on Coomassie gel (B) lane 3. DOCK9 DHR1 domain peptides (left peak, green line) indicated on Coomassie gel (B) lane 4.

4.3 Discussion

The interaction analysis carried out within this study were unable to elucidate the DOCK9 residues which serve as the binding site of the DOCK9 interaction with the DOCK4 SH3 domain (figures 4.3-4.7). The DOCK9 binding small molecule QL-47 was unable to disrupt the DOCK4-DOCK9 interaction within Co-IP assays, indicating that the p.C628 residue of DOCK9 may not be involved in a direct interaction between the two proteins (figures 4.8). Further to this, the truncated peptides DOCK4 SH3 and DOCK9 PCIP-DHR1 were found to not directly interact within SEC analysis (4.12).

The signalling pathways that are activated in ECs during angiogenesis are complex and not entirely understood. The ability to dissect and gain further understanding of the events that drive blood vessel growth, will give further insights into dysregulation of the process during pathological angiogenesis and may identify new therapeutic targets for those pathologies. This study has set out to further understand the RhoG-DOCK4-RAC1-DOCK9-CDC42 signalling pathway recently identified (Abraham et al., 2015). Previous work had demonstrated that the DOCK4-DOCK9 complex acts as an effector downstream of RhoG signalling (Abraham et al., 2015). Rho GEF proteins can heterodimerise as well as homodimerise. The ability of these proteins to form such complexes indicates their potential to act in-concert to finely tune Rho GTPase activity, throughout the highly organised and dynamic cellular events that take place during sprouting angiogenesis and lumen formation (Abraham et al., 2015). Different GEFs may modulate activation and inactivation of Rho proteins at key stages of blood vessel development, while also regulating other protein-protein interactions and protein localisation (Barlow and Cleaver, 2019). The function of DOCK4 and DOCK9 are required for the outgrowth of lateral filopodia along sprouting vessels in 3D tissue culture (Abraham et al., 2015). This function has been stipulated as necessary for lumenisation and therefore functionality of newly forming blood vessels (Abraham et al., 2015). The ability for DOCK4 and DOCK9 to heterodimerise during angiogenesis may be

required for signalling mechanisms involved in development of lateral filopodia. Elucidating how these two proteins interact will allow for further understanding of the signalling mechanisms involved in angiogenesis.

4.3.1 DOCK4-DOCK9 interaction

Purified GST-tagged DOCK4 SH3 domain has been demonstrated as capable of pulling down endogenous WT DOCK9 from HEK 293T cellular lysates (Abraham et al., 2015). Currently the specific DOCK9 site that interacts with the DOCK4 SH3 domain has not yet been determined. Initial attempts in this study to utilise the commercially available GFP-trap, to identify a putative PRR within DOCK9 that mediates the interaction with DOCK4, have been convoluted. DOCK9 mutations within PRRs identified as DOCK9 PRRs 2 and 9 demonstrated little effect on DOCK4-DOCK9 interaction, leading to the hypothesis that these PRRs are not required for the interaction (figures 4.4, 4.6, and 4.7). Mutations within the PRRs identified as DOCK9 PRRs 3, 4, and 5 were found to yield somewhat conflicting results via western blot analysis of the Co-IP of DOCK4 and DOCK9 proteins (figures 4.4, 4.5, and 4.7). Co-IP of EGFP-DOCK4 and Flag-DOCK9 PRR 3 and 4 mutants yielding the most varied results with EGFP-DOCK4 showing the least affinity for binding DOCK9 PRR 4 when compared to the control, and the other DOCK9 PRR mutants, however this result was not statistically significant through colorimetric analysis (figure 4.7); although it should be noted that the profoundly strong GFP signal detected through Western blot within the TL samples led to oversaturation which may not present a true representation of the level of GFP expression within the GFP TL samples, thus potentially confounding any differences in DOCK4 expression between samples. This may be corrected by testing repeat blots of decreasing concentration of loaded protein in-order to create a gradient, and a more true representation of protein concentration (Ghosh et al., 2014).

The variability of results indicates that Co-IP may not be sensitive enough to detect the loss of interaction between the two proteins. A number of elements within this model

should be considered and addressed, should this experiment be carried out for future purposes. Firstly, non-specific binding of the Flag-tag of the DOCK9 proteins should be investigated to determine if this epitope binds either the DOCK4 protein or GFP tag, as Flag-tags have been previously described to bind a number of proteins non-specifically (Free et al., 2009). Consideration should also be given to the level of protein expression of both DOCK4 and DOCK9, as both proteins are large proteins with similar sequence homology, and both capable of homodimerisation, there is potential that over-expression may lead to non-specific interaction. It should be noted that the GFP tag was determined to not bind the DOCK9 protein non-specifically, as seen in the EGFP-EV samples (figure 3.3, 3.4, and 3.5).

As both DOCK4 and DOCK9 proteins possess structural similarities, both with the ability to homodimerise, overexpression within HEK 293T cells may likely result in forced and non-sensitive interaction (Sommer et al., 2014; Marcotte and Tschansky, 2009). Through optimization of the Co-IP experiments, the concentration of transfected plasmid was tittered to reduce the level of protein expression, in-order to overcome false interaction. However, both the CMV promoter of the pC3 EGFP-DOCK4 plasmid and EF-1α promoter of the pEF4 Myc-Flag-DOCK9 plasmid both induce a high level of expression which may maintain too high a level protein expression (Xia et al., 2006), it may therefore be necessary to use expression vectors with a weaker, or less active, promoter in order to better control the level of expression. The Co-IP approach also lacks the ability to detect direct interaction, which may be overcome by purified fusion protein-pull down experiments or SEC of purified proteins (Hall, 2005). Further to this, detection of interacting proteins via Western blot lacks sensitivity and produces unreliable results that may not distinguish between genuine interaction and non-specific interaction (Zhu et al., 2017).

In an attempt to overcome the variability in results, the initial protocol TLs were also optimized to reduce detection of non-specific interaction. The TL buffer (RAC lysis buffer) was optimised with an increase in sodium chloride concentrations in an attempt to further

disrupt any non-specific binding of proteins. These experiments ultimately showed inconsistent results, with little or no difference in the binding ability of EGFP-DOCK4 to Flag-DOCK9 PRR 3 and 5 mutants when compared to the control, EGFP-DOCK4 binding to WT Flag-DOCK9 (figures 4.4, 4.5 and 4.7). In regards to the DOCK9 PRR 4 mutant, analysis of lysates from the optimised Co-IP experiment yielded results similar to the previous experiments, with EGFP-DOCK4 having a reduced affinity for binding DOCK9 PRR 4 mutant when compared to the WT and other DOCK9 mutants (figure 4.5 and 4.7), however this result was not significant and it was also noted that DOCK9 PPR 4 mutant appeared to express less total protein when compared to TL of HEK 293T transfected with the other 4 DOCK9 mutant constructs (figure 4.4 and figure 4.6). The variability within those results led to the consideration that the experimental design may not be suitable for demonstrating loss of DOCK4 and DOCK9 interaction, perhaps due to forced interaction of the two large overexpressed proteins (Sommer et al., 2014; Marcotte and Tschansky, 2009). Furthermore, the ability for mutations within 3 separate PRRs to show some level of disruption of the DOCK4-DOCK9 interaction may suggest that more than one PRR binding site may be required for the interaction, a concept which could be further explored through inclusion of wider protein domains within interaction analysis.

4.3.2   The effect of QL-47 on the DOCK4-DOCK9 interaction

Within the interim of the DOCK4-DOCK9 PRR mutant Co-IP experiments, a small molecule compound, QL-47, was identified by Nathanial Gray's research group as a DOCK9 binding compound. QL-47 specifically binds to the cysteine residue p.C628 within the PRR 3 (p.PCIP627-630). Experiments reported within the previous results chapter of this thesis (figure 3.8 and 3.9) established that QL-47 disrupts correct sprouting angiogenesis and promotes an angiogenic phenotype. For the aforementioned reasons, it was considered that the phenotypic effect of QL-47 may involve disruption of DOCK4 and DOCK9 interaction.

To test this hypothesis the EGFP-DOCK4 Flag-DOCK9 co-expression and Co-IP analysis was carried out in the presence of QL-47, at a concentration of 5µM, equal to the concentration required to induce a phenotypical effect on angiogenesis *in vitro*. In separate experiments cells were either treated with QL-47 before transfection with the EGFP-DOCK4 and Flag-DOCK9 expression vectors, or prior to cell lysis. Using anti-Flag and anti-GFP Western blot analysis it was not possible to conclusively demonstrate any disruption to the DOCK4-DOCK9 complex (figure 4.8).

The results of the DOCK4-DOCK9 PRR mutant Co-IP experiments in combination with the QL-47 supplemented DOCK4-DOCK9 Co-IP experiments substantiated that the Co-IP approach may not provide a reliable experimental model for investigating the interaction. To remedy the influence of potential variables within the live cell cultures, an experimental approach utilising only purified DOCK4 and DOCK9 peptides was carried out.

4.3.3 SEC analysis of DOCK4 SH3 domain interaction with the DOCK9 DHR1 domain

The previously mentioned experiments demonstrated that investigation of the wider domains of DOCK9 may be required to elucidate the binding site for DOCK4. In order to investigate this, SEC was carried out using specific domains of DOCK4 and DOCK9. SEC analysis of protein interactions is a robust and widely used technique for determining whether two proteins interact directly (Bloustine et al., 2003; Busch et al., 2017).

Constructs were generated with the gene sequence for expression of a truncated DOCK9 protein, cloned into a pOPINF expression vector (plasmid maps can be found in Appendix 7.1.2). A truncated portion of DOCK9 was cloned into the pOPINF expression vector, and included only the DHR1 region, which encompasses PRR4, and the PPR region directly upstream of the DHR1 binding domain, identified as PRR 3 (p.PCIP627-630). The DOCK4 SH3 domain gene sequence was also cloned into a pOPINF expression vector. Both the DOCK4 SH3 and DOCK9 PCIP-DHR1 construct incorporate a histidine tags. Both the DOCK4 SH3 and DOCK9 PCIP-DHR1 truncated proteins were successfully expressed in BL21

(DES) competent cells. Bacterial cultures were lysed and proteins purified using affinity chromatography (figures 4.9 and 4.10). Proteins were then further purified using SEC (figure 4.11)

To determine whether the SH3 domain of DOCK4 directly binds to either/or both of the DOCK9 PRRs 3 and 4 equal concentrations (approx. 50µM) of purified protein samples were resolved using SEC, under non-denaturing conditions (figure 4.11). In-order to establish a size-based peak, 100µM of each protein were first resolved individually, and then combined and resolved via SEC, under non-denaturing conditions. Proteins capable of binding one another would be expected to remain bound during SEC, however the results demonstrated that the DOCK4-SH3 domain does not bind DOCK9 PRR3-DHR1 peptides directly. SEC of DOCK4-SH3 and DOCK9 PCIP-DHR1 was repeated, in-order to confirm the absence of direct interaction (Figure 4.12). The repeat experiment yielded the same result, strongly suggesting that the DOCK9 PRR3 and PRR4 are not involved in a direct interaction between the DOCK4-SH3 domain and DOCK9. Furthermore, it is likely that the DOCK4-SH3 domain does not interact directly with the DHR1 domain of DOCK9.

While this experiment indicates that the DOCK4 SH3 domain residues do not bind directly to residues within the DOCK9 DHR1 domain, it does not give consideration to the requirement of secondary structures within the interaction, as the purified peptides may lack the correct folding of the native proteins. As the full structure of DOCK9 as not yet been determined

In consideration of the overall outcome of these experiments, it can be concluded that the experimental design for elucidating the site of DOCK9 which binds the DOCK4 SH3 domain would need to be further optimised in-order to yield a more reliable result. The acquired results indicate that the DOCK4-SH3 domain does not directly bind to the DOCK9 DHR1 domain, and is unlikely to interact with the DOCK9 PRRs 2, 3, 4, 5 and 9, however this cannot be considered a conclusive result. It can however suggest that it is likely that the small

molecule QL-47 does not disrupt DOCK4 and DOCK9 interaction, as there was no apparent binding of the DOCK4 SH3 domain to an individual residue of the DOCK9 p.C628. Therefore the phenotypic effects of QL-47 on sprouting angiogenesis *in vitro* are unlikely to be due to disruption of the interaction of DOCK4 with DOCK9.

Additional experiments will be required in-order to further understand the precise nature of the DOCK4-DOCK9 interaction. Generation of expression constructs which encompass wider regions of DOCK9 would be ideal for encapsulating which wider region of the protein truly binds DOCK4. Data of the DOCK4 and DOCK9 interaction partners, identified through previous work in the laboratory, could help elucidate how these two proteins interact potentially via an indirect mechanism (Abraham et al., 2015). Defining true binding partners of these two DOCK180 family members will afford a more in-depth understanding of their function, while also potentially shed more light into the purpose of the DOCK4-DOCK9 heterodimerisation.

5 Results chapter III: Dock4 genetic deletion impairs vascular recovery following an ischemic event *in vivo*

5.1 Introduction

The GEF DOCK4 is essential for correct vascular growth during sprouting angiogenesis *in vitro* (Abraham et al., 2015). Depletion of DOCK4 expression results in growth of less dynamic vascular structures *in vitro,* and impaired lumenisation both *in vitro* and *in vivo* (Abraham et al., 2015). The DOCK4 effector protein, RAC1, is a multifunctional dynamic Rho GTPase which has been implicated as an essential component for blood vessel growth, during development and post developmental sprouting angiogenesis (Ramo et al., 2016; Cao et al., 2017). RAC1 drives directional migration and correct vascular patterning via regulation of the actin polymerisation required for lateral filopodia production, during sprouting angiogenesis (Abraham et al., 2015). Understanding how blood vessels grow in response to oxygen deprivation is imperative for deciphering the mechanisms that underpin vascular pathologies, which result from inadequate angiogenic response (Ramo et al., 2016; Cao et al., 2017).

To expand upon current knowledge of the function of DOCK4 in angiogenesis, a global Dock4 heterozygous knockout C57BL/6J murine model (which will be referred to as Dock4 het throughout this chapter) was employed. This Dock4 het mouse model overcomes embryonic lethality of homozygous Dock4 deletion, and was used for analysis of Dock4 function *in vivo*. The Dock4 het murine model was previously demonstrated to express only 50% of the normal expression level of DOCK4 (Abraham et al., 2015). An EC specific conditional Dock4 knockout murine model, iVEC-cre+ve; Rosa26-lsl-Tomato; Dock4f/f mice, was also employed, to allow for inducible deletion of endothelial Dock4 (which will be referred to as EC Dock4 KO throughout this chapter).

To investigate how DOCK4 functionality influences vascular response and recovery, under pathological conditions of ischemia *in vivo,* the global heterozygous DOCK4 knockout model, and EC Dock4 KO model, were both employed in a HLI assay *in vivo*. The HLI model provides a model of arteriogenesis and angiogenesis within the hind limbs of mice, and is a widely performed and validated model of ischemia (Hellingman et al., 2010). All surgical procedures carried out by Dr Nadira Yuldasheva.

LDI was utilised to monitor vascular recovery and response, following removal of a portion of the femoral artery (figure. 5.1). The moorLDI2-HIR High Resolution Laser Doppler Imager allowed for deep penetrative imaging of small blood vessels, ideal for detecting blood flow within solid tissues.

Loss of blood flow through the femoral artery leads to redirection of blood flow via the pre-existing collateral arteries, and subsequent arteriogenesis and widening of the collateral arteries (van Royen et al., 2001; Limbourg et al., 2009). While blood flow through the collateral arteries allows some circulation to the lower appendage. Inadequate level of blood perfusion induces a strong angiogenic response within the muscles of the lower limb, the gastrocnemius and soleus (Limbourg et al., 2009; Niiyama et al., 2009). The strong angiogenic response within the gastrocnemius makes the muscle ideal for histological analysis of vascularity (Limbourg et al., 2009; Niiyama et al., 2009). Antibody staining of the endothelial specific surface protein, CD31, allows for visualisation of the blood vessels within the gastrocnemius and thus provides a method of comparative analysis of vascularisation of the gastrocnemius of the injured leg, compared to that of the un-injured leg (Hellingman et al., 2010).

Gastrocnemius and soleus muscles of the mouse hind limbs were harvested, embedded in paraffin wax, sectioned and stained for DOCK4, the vascular specific marker, CD31, and RFP (for confirmation of the Td Tomato reporter for EC DOCK4 deletion in the inducible DOCK4 KO mouse). IHC stained muscle sections were electronically scanned and

analysed using ImageJ, in-order to quantify the vascularity of the tissue and analyse key features of the vascular structures.

Numerical data generated through LDI detection of cell velocity, within the hind limbs of mice, was statistically analysed using a one-way analysis of variance (ANOVA), blood flow area under the curve, and linear regression and slope intersect analysis, to determine significant changes in vascular recovery.

Overall this chapter will provide evidence that the RAC1 GEF, DOCK4, is required for normal vascular recovery from severe HLI.
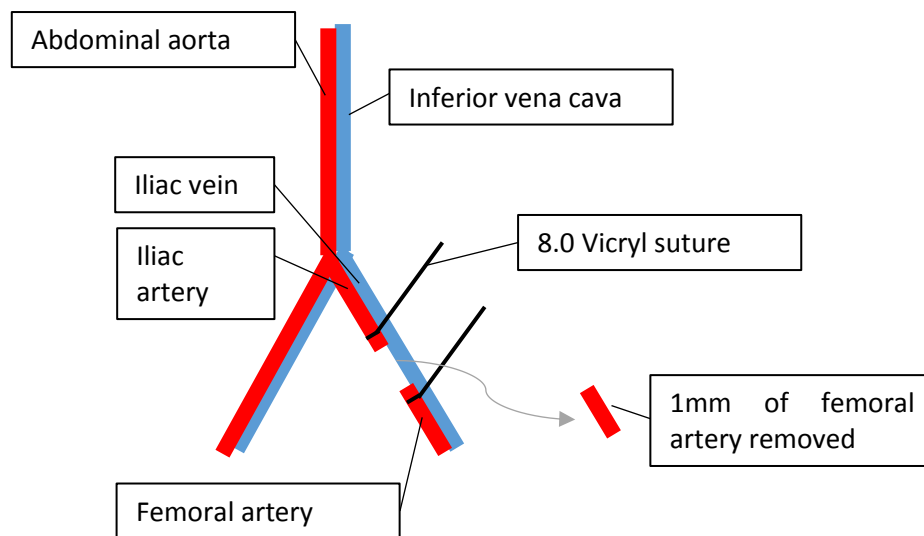
Figure 5-1 Schematic of the HLI model

The HLI surgery removes a portion of the left femoral artery. The femoral artery is separated from the iliac vein, encircled with 8.0 Vicryl sutures, and the intervening arterial segment is excised.

5.2   Results

5.2.1   Dock4 het mice have lower gross body weight compared to WT littermate control mice

Gross body weight of each mouse was tracked and recorded through-out the duration of the HLI experiment (table 5.1). Body weight was monitored to ensure each mouse was healthy and thriving throughout the duration of all murine experiments. Both male and female Dock4 het mice were found to have typically lower body weights, when compared to the WT littermate mice, at each time point. The reason for the lower body weight was not further investigated and has not yet been elucidated.

DOCK4 het					WT littermates			
ID	Day 0	Day 7	Day14	Day 21	ID	Day 0	Day 7	Day14	Day 21
608	16g	17g	18g	17g	611	16g	16g	17g	17g
609	16g	16g	17g	17g	631	19g	19g	20g	20g
610	18g	18g	20g	20g	632	17g	18g	19g	19g
630	17g	17g	17g	17g	641	20g	20g	20g	20g
638	16g	16g	16g	16g	642	19g	19g	20g	20g
645	15g	15g	15g	15g	643	19g	19g	19g	20g
614	22g	23g	24g	24g	612	26g	27g	29g	28g
633	24g	24g	25g	26g	613	22g	23g	24g	24g
634	20g	21g	22g	23g	635	27g	28g	29g	29g
636	20g	21g	22g	22g	637	25g	26g	29g	29g
639	23g	23g	23g	23g	640	27g	27g	27g	27g
646	23g	23g	24g	24g	647	26g	26g	26g	26g

Table 5-1 Weight of each mouse in grams

Table of the weight of each mouse, in grams. Each mouse was weighed directly before LDI was carried out. ID= Identification number of each mouse. Numbers highlighted in pink are female mice. Numbers highlighted in blue are male mice.

5.2.2   Dock4 het mice show reduced rate of hind limb mobility recovery compared to WT littermates

Response to HLI was studied in the Dock4 het mice, following surgical removal of a portion of the femoral artery. Hind limb mobility of each mouse was monitored following

surgery, in order to determine if any differences in loss of hind limb mobility and recovery could be observed between the experimental groups. Immediately following HLI both the WT mice and Dock4 het mice demonstrated substantial loss in left hind limb mobility (qualitative observations). Over 28 days post-surgery WT mice began to regain mobility of the injured hind limb, while Dock4 het mice were observed to have less mobility of the injured limb by comparison to the WT littermate controls. By day 21, WT mice regained full mobility of their hind limb, and no longer appeared to be physically impacted by loss of the portion of the femoral artery. Dock4 het mice continued to experience loss of full leg extension and flexibility, with the injured left hind limb being held in a retracted position with full manual extension of the hind limb not possible.

5.2.3   Dock4 het mice develop necrosis of the ischemic foot

Throughout the experiment all mice were monitored for any signs of necrosis of the ischemic limb, representative images and all recorded results are given in figure 5.2. Out of twelve Dock4 het mice, eleven experienced necrosis within the ischemic foot, which ranged from mild necrosis (blackening of the toe tips) to profound necrosis (auto-amputation of the ischemic foot). Three Dock4 het mice experienced auto-amputation of toe tips and an additional two Dock4 het mice experienced auto-amputation of toes. One Dock4 het mouse experienced auto-amputation of the affected foot (figure 5.2B). In summary, 5 out of 12 Dock4 het mice experienced some form of auto-amputation. There was no auto-amputation or evidence of necrosis observed in the WT littermate control mice.

A   B
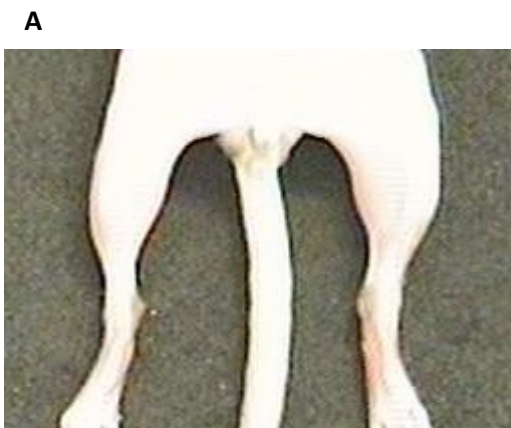
5.2.4 Dock4 het mouse hind limb blood flow is equal to the hind limb blood flow of WT littermates under physiological conditions

The hindlimb blood flow of the uninjured leg of both experimental groups were analysed through LDI, to determine whether any differences in hindlimb blood flow could be detected between the two experimental groups (figure 5.3 and 5.4). Blood flow of the uninjured limbs of both experimental groups followed the same trend (figure. 5.3 and 5.4), with blood flow appearing higher immediately following surgery, then decreasing each week post operation. Higher levels of post-operative blood flow were most likely due to mice being maintained on a heated surface prior to LDI.

Comparative analysis of blood flow to the non-injured limbs of Dock4 het mice to WT littermates determined there was no significant difference between the normal hind limb circulation of the two experimental groups before ligation of the left femoral artery (figure 5.3 and figure 5.4).
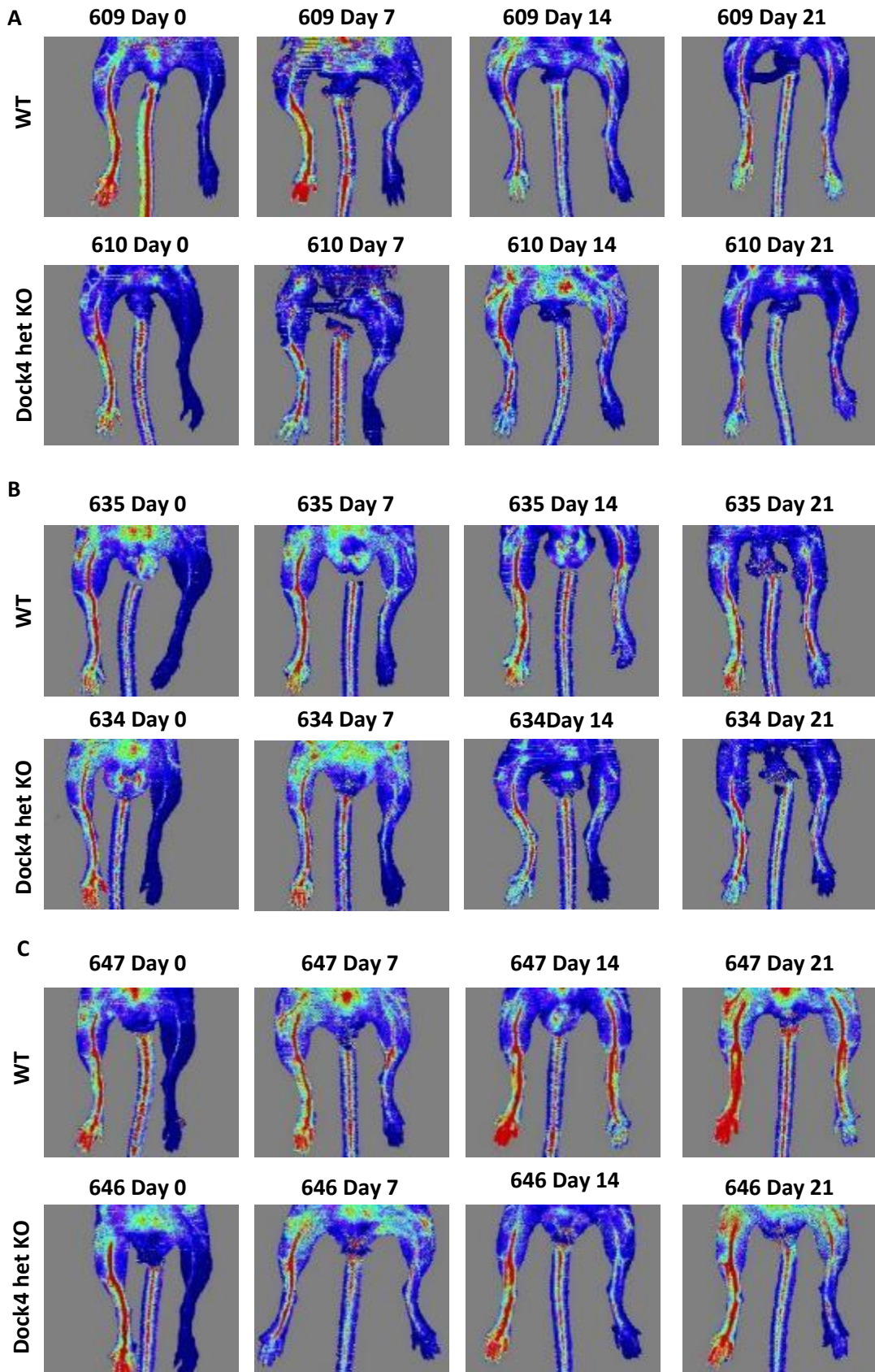
A

| 609 Day 0 | 609 Day 7 | 609 Day 14 | 609 Day 21 |

WT

| 610 Day 0 | 610 Day 7 | 610 Day 14 | 610 Day 21 |

Dock4 het KO

B

| 635 Day 0 | 635 Day 7 | 635 Day 14 | 635 Day 21 |

WT

| 634 Day 0 | 634 Day 7 | 634Day 14 | 634 Day 21 |

Dock4 het KO

C

| 647 Day 0 | 647 Day 7 | 647 Day 14 | 647 Day 21 |

WT

| 646 Day 0 | 646 Day 7 | 646 Day 14 | 646 Day 21 |

Dock4 het KO

Figure 5-3 Effect of Dock4 het deletion on hind limb vascular recovery following surgical ligation of the femoral artery

Representative images of LDI detected mean/area of blood flow perfusion in the hind limbs of Dock4 het mice and WT littermates, in a supine position, over a 21 day time period, following HLI surgery. Surgery to ligate and transect the left femoral artery was carried out to occlude blood flow to the left hind limb. Blood flow was analysed using LDI on day 0 (2 hours post-surgery), 7, 14, 21, and 28 following surgical ligation of the left hind leg femoral artery on day 0. **(A)** Experiment 1: WT mice (n=4) Dock4 het KO mice (n=4). **(B)** Experiment 2: WT mice (n=5); Dock4 het KO mice (n=4). **(C)** Experiment 3: WT mice (n=3) Dock4 het KO mice (n=4).
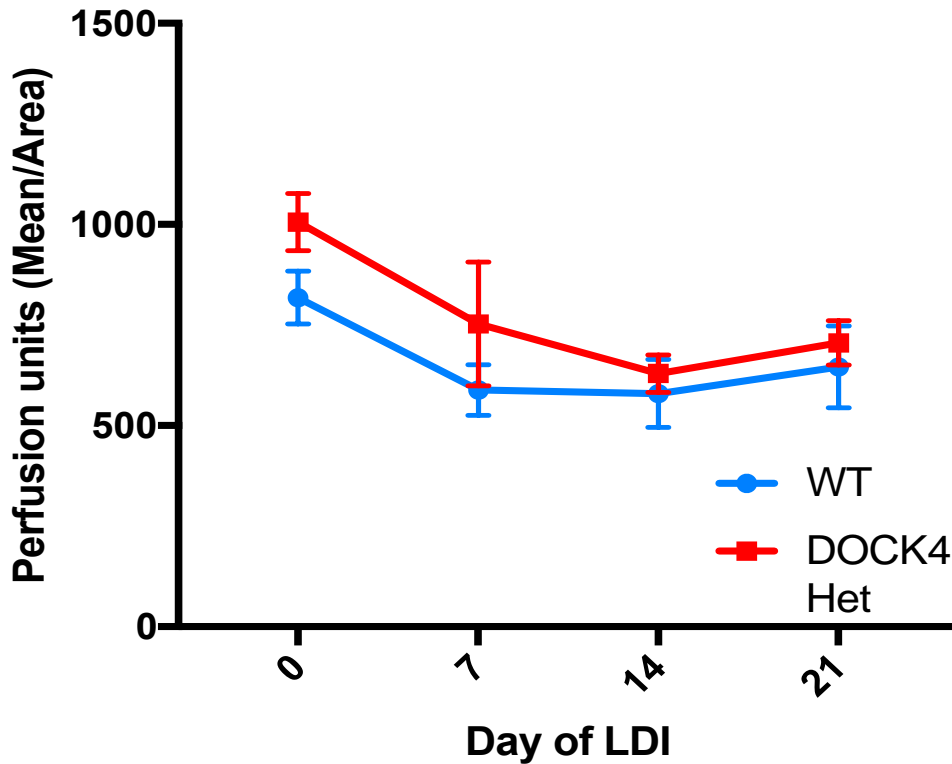
Figure 5-4 Quantification of LDI of non-injured hind limbs of Dock4 het KO mice during ischemia recovery

Combined data of blood flow perfusion detected by LDI in the hind limbs of WT mice (n=12) versus Dock4 heterozygous mice (n=12) following HLI surgery. A portion of the left femoral artery of each mouse was removed on day 0. Blood flow to the lower extremities of both injured and non-injured limbs of each mouse was monitored using LDI immediately following surgery, then every 7 days for a 21 day duration. Values plotted are mean blood flow perfusion divided by the area of each non-injured limb. Linear regression of Dock4 het mice was compared to the linear regression of the WT mice to detect differences in recovery over time. One-way ANOVA with Tukey's multiple comparisons was carried out to compare mean blood perfusion by area of Dock4 het mice to WT mice at each time point showed no significant differences at any time point.

5.2.5   Global heterozygous deletion of Dock4 resulted in a significant reduction in blood flow

recovery following HLI surgery.

Response to HLI was studied in the Dock4 het mice, following surgical removal of a

portion of the femoral artery. LDI was carried out to determine velocity of motile cells, and

thus blood perfusion, in the dermal tissue of the mouse hind limbs. Three separate HLI

experiments were conducted to compare blood flow recovery of Dock4 het mice to the WT

littermate controls, with a combined N number of 24 mice for each of the experimental

groups.

LDI data was generated over 3 separate HLI experiments, each for a duration of a 21

day time period, following femoral artery ligation of the left hind limb in order to monitor

the recovery of blood flow following femoral artery ligation (figure. 5.4, and figure. 5.5).

LDI of blood flow to the left (injured) hind limbs of the 12 Dock4 het mice and 12 WT

littermates immediately following hind limb surgery, on day 0, showed a loss of blood flow

to the left hind limb in all 12 Dock4 het mice and 12 WT mice (figure. 5.3 and figure. 5.5).

There was no significant difference in blood flow to the injured limbs of the Dock4 het mice

when compared to the WT littermates (figure. 5.3 and figure 5.5) immediately following HLI

surgery.

LDI analysis of injured hind limbs on day 7 showed no significant difference in blood

flow between the two experimental groups (figure. 5.4 and figure 5.5).

However, by 14 days post operation, the global Dock4 het mice had a significantly

lower level of blood flow to the ligated limbs when compared to the WT littermates

(P=0.0047) (figure. 5.4 and figure 5.5). The lower level of blood flow to the hind limbs, of

Dock4 het mice when compared to the WT, was also observed on day 21, however the

difference was not statistically significant.

The overall blood flow recovery following femoral artery ligation was reduced in the

Dock4 het mice when compared to WT littermate controls. Analysis of the area under the

curve demonstrates a significant difference (P<0.005) between the WT data set and the Dock4 het deletion data set, signifying a significant impact of reduced Dock4 expression on blood flow recovery following removal of a portion of the femoral artery.

Using linear regression analysis, the slope of the lines of best fit of the WT data set and the Dock4 het deletion data set are not significantly different, but only marginally not significant (P=0.056). However, the intercept of these two lines are significantly different (P=0.016). This signifies that the trend of vascular recovery between the WT and Dock4 het mice was similar, however the increase in blood perfusion over time was significantly higher in the WT mice when compared to the Dock4 het mice.

Overall the data generated through LDI analysis indicate an impairment in recovery from HLI surgery when global levels of Dock4 are reduced. This loss in Dock4 results in a delay in the recovery of blood flow to the affected limb.
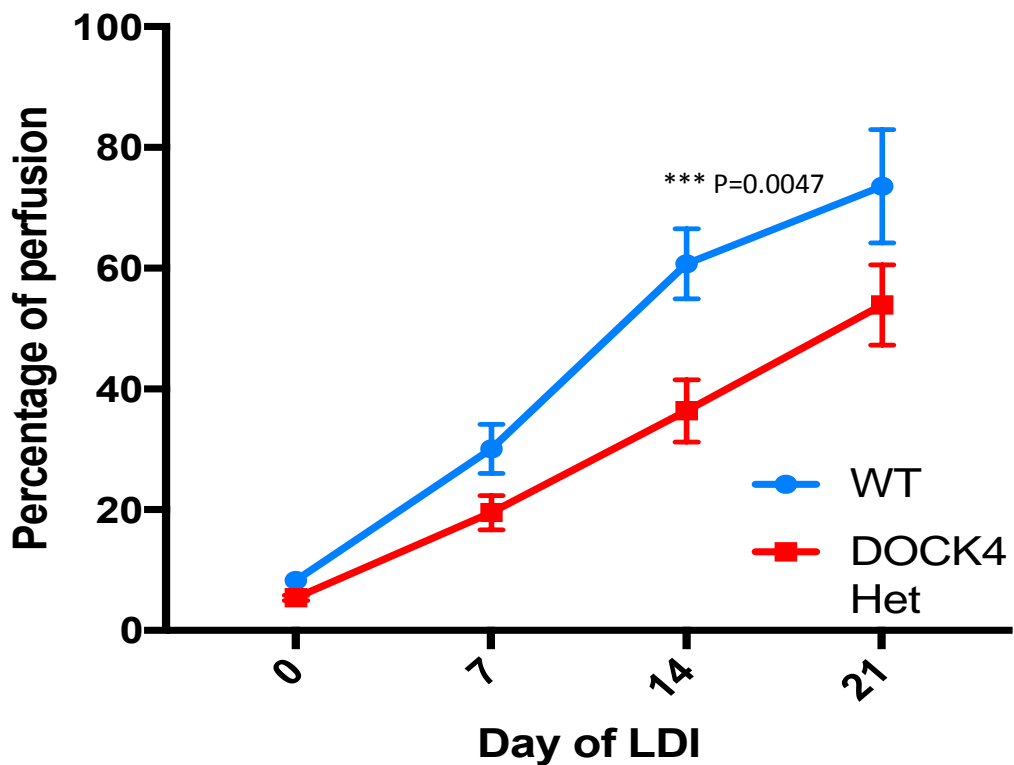
Figure 5-5 Quantification of LDI of injured hind limbs of Dock4 het KO mice during ischemia recovery

Combined data of LDI detection of blood flow perfusion in the hind limbs of WT mice (n=12) versus Dock4 het KO mice (n=12) following HLI surgery. A portion of the left femoral artery of each mouse was removed on day 0. Blood flow to the lower extremities of each mouse was monitored using LDI immediately following surgery, then every 7 days for a 21 day duration. Mean blood flow perfusion divided by the area of each injured limb was normalized to the non-injured limb, then calculated as a percentage. One-way ANOVA with Tukey's multiple comparisons were carried out to compare mean blood perfusion by area of Dock4 het mice to WT mice at each time point. Significant differences indicated by asterisks: ***=P value equal to or lower than 0.005.

5.2.6   IHC analysis of vasculature within the gastrocnemius tissue of Dock4 het mice following

HLI

The hindlimb muscles of all experimental mice were posthumously fixed and harvested for the purpose of analysing and comparing the vasculature of the hind limb tissues of each experimental group. One hour following the final LDI scan all mice were exsanguinated through ligation of the major vena cava. Whole animal fixation of each mouse was carried out through administration of 4% PFA through the left ventricle. The gastrocnemius and soleus muscles were harvested from both the injured and non-injured hind-limbs of each mouse and placed in 4% PFA for 24 hours before being transferred to 70% ethanol. Following fixation, gastrocnemius muscle tissue from both the injured and non-injured legs were imbedded in paraffin wax in a longitudinal orientation. The muscle was then section into 50 x 5μm thick sections using a floating sectioning technique.

Every 10th section from each muscle block was selected and IHC stained with an anti-CD31 antibody. Slides were electronically scanned and imaged. Imagescope software was utilised to randomly select 8 500μm x 500μm boxes per muscle section (figure. 5.8). ImageJ analysis software was employed to quantify the length of every detectable CD31 stained vessel and number of branch points per 500μm x 500μm area of analysis. The mean values of TVL and BPI (number of branch points/TVL) were then calculated per muscle section for both the injured and non-injured limbs of both Dock4 het mice and their WT littermates. Data was analysed using a One-way ANOVA with Tukey's multiple comparisons.

The TVL of non-injured gastrocnemius of the Dock4 het mice were compared to the mean values of TVL generated from the non-injured gastrocnemius of the WT littermates Statistical analysis demonstrated no significant difference between the TVL of CD31 stained vasculature of the non-injured limbs of the Dock4 het mice when compared to their WT littermates (figure. 5.4, 5.6, and 5.9).

Analysis of the gastrocnemius muscle sections from the injured legs of the two experimental groups demonstrated a significant increase in TVL within the muscle sections from the Dock4 het mice when compared to the WT littermates (p=0.043) (figure 5.5, 5.7, 5.9).

When comparing the BPI of the gastrocnemius sections from the non-injured limbs between the two experimental groups, there was a significant decrease in BPI of Dock4 het CD31 stained gastrocnemius sections compared to the WT littermates gastrocnemius sections (p=0.046), signifying a less branched vascular phenotype in the gastrocnemius of the non-injured Dock4 het mice (figure. 5.4, 5.6, and 5.10). However, in gastrocnemius of the injured limbs, there was no significance in the BPI between the two experimental groups (figure. 5.5, 5.7, 5.10).

To summarise the findings: IHC analysis detected differences between the pre-existing vasculature of the Dock4 het mice and the wild-type littermates. While the gastrocnemius of both experimental groups appeared to have a similar overall level of vascularisation, the reduction in branching of the Dock4 het experimental group indicates patterning differences in the pre-existing vasculature.

The vasculature within the gastrocnemius of the injured limbs also differed between the two experimental groups. However, following hind limb ischemia there was no significant difference between the BPI of the Dock4 het mice injured legs compared to the WT. Differences did however occur in the overall level of vascularisation between the two experimental groups, with the Dock4 het mice developing a much greater increase in TVL following vascular injury than was seen in the WT control group (figure. 5.7; figure. 5.9). These results were unexpected considering the reduction in blood flow to the injured hind limbs of the Dock4 het mice.
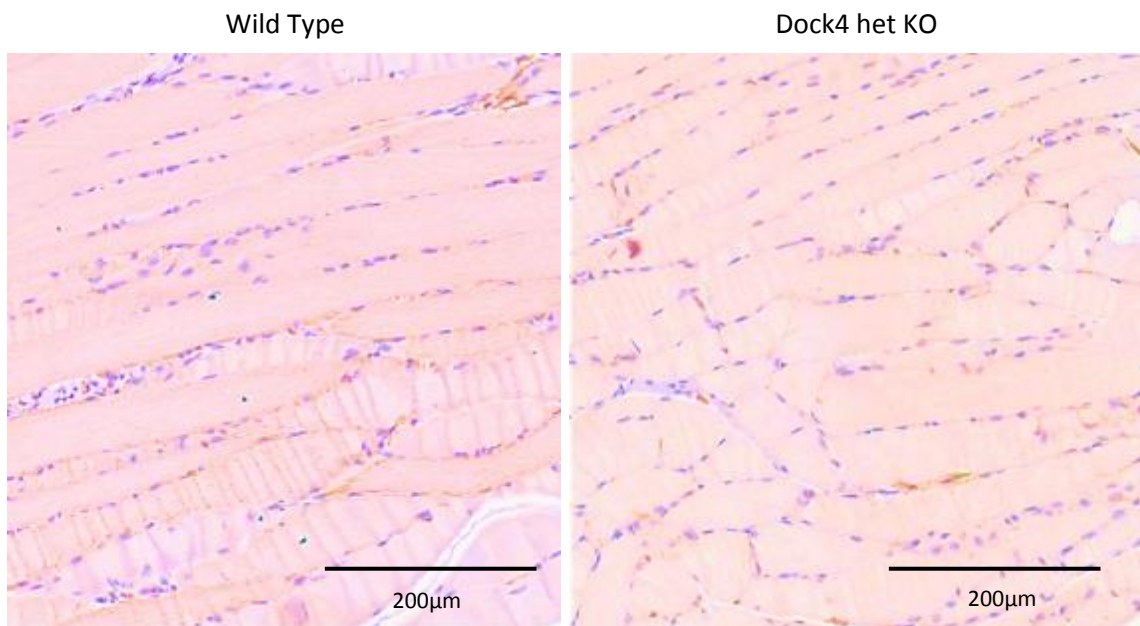
Figure 5-6 CD31 IHC staining of non-injured hind limb gastrocnemius muscle sections comparing DOCK4 het verses WT littermates.

Representative images of gastrocnemius muscle harvested from non-injured hind limbs of Dock4 het KO and WT littermates, 21 days post HLI operation. Muscle from 24 Dock4 het mice and 24 WT littermates were fixed in 4% paraformaldehyde, embedded in paraffin wax. 8 Dock4 het mice and 8 WT littermate muscle blocks were sectioned into 5µm floating sections and IHC stained using an antibody against CD31. Slides were scanned using an Apeiro AT Virtual Slide scanner and 500µm x 500µm boxes for analysis selected using Apeiro ImageScope software.
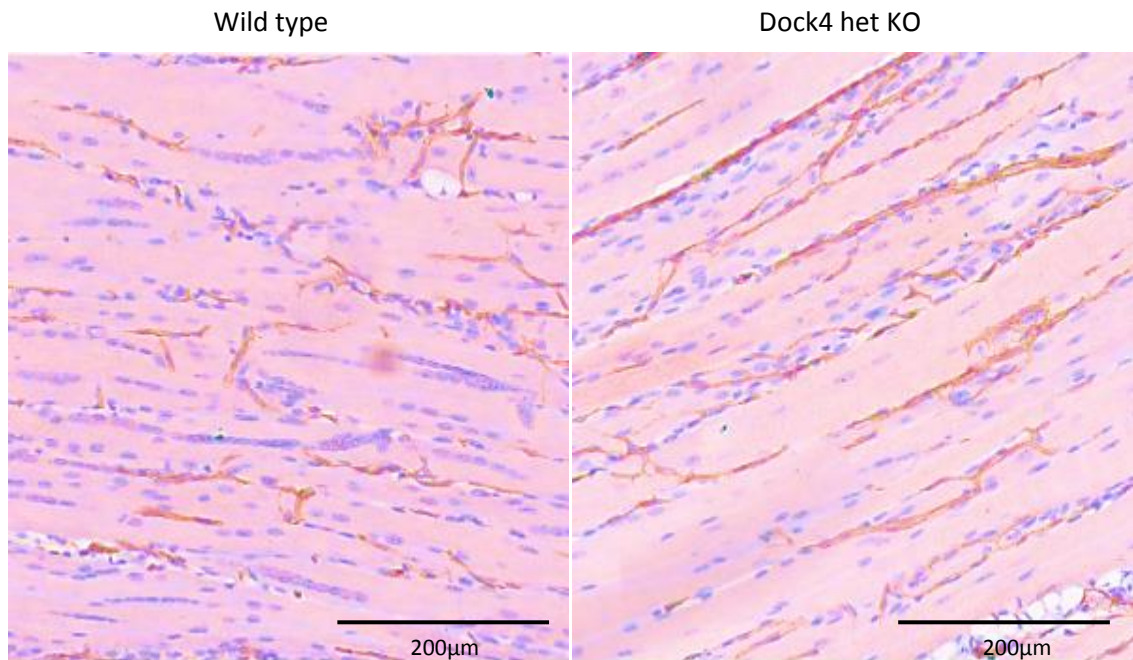
Wild type   Dock4 het KO

Figure 5-7 CD31 IHC staining of injured hind limb gastrocnemius muscle sections comparing DOCK4 het KO mice versus WT littermates.

Effects of het DOCK4 depletion on angiogenesis within the gastrocnemius following ligation and transection of the left femoral artery of global DOCK4 het deleted mice and WT littermates. Representative images of gastrocnemius muscle harvested from injured hind limbs of Dock4 het mice and WT littermates 21 days post HLI operation. Muscle from 24 Dock4 het mice and 24 WT littermates were fixed in 4% paraformaldehyde, embedded in paraffin wax. Muscle blocks of 8 Dock4 het mice and 8 WT littermates were sectioned into 5μm floating sections and IHC stained using an antibody against CD31. Slides were scanned using an Apeiro AT Virtual Slide scanner and 500μm x 500μm area for analysis were selected using Apeiro ImageScope software.
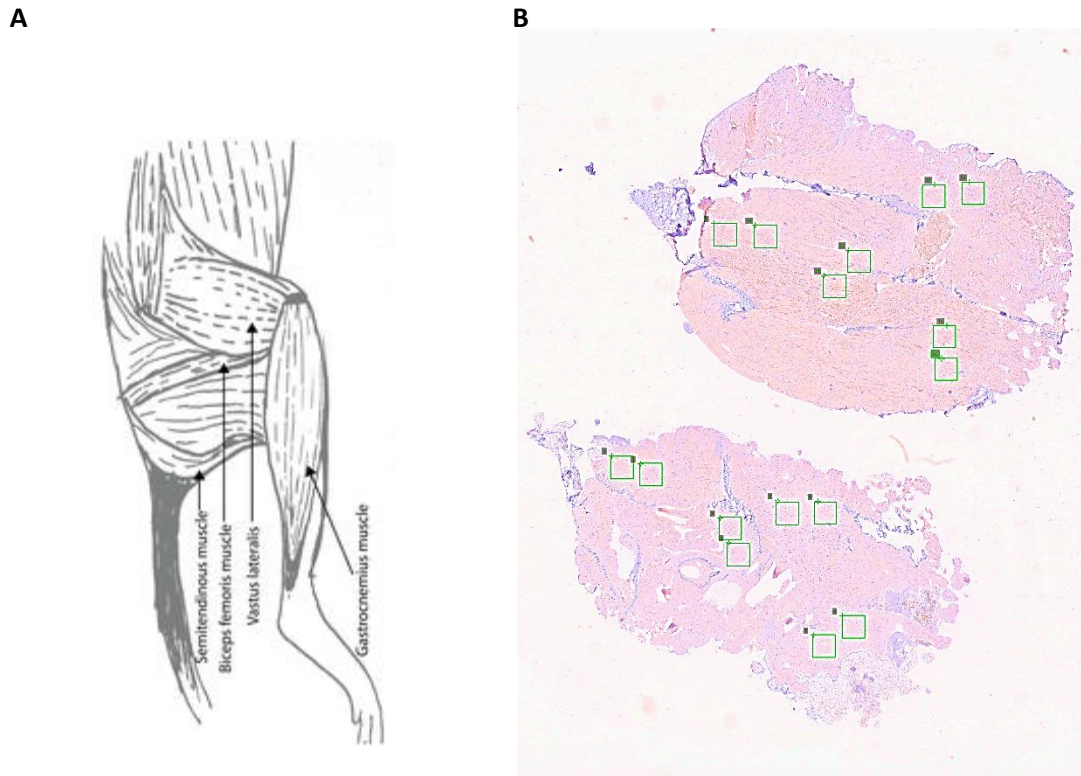
Figure 5-8 Selection for analysis and quantification of gastrocnemius section regions following anti-CD31 IHC staining.

(A) Representation diagram of anatomical location of gastrocnemius muscle in the hindlimb of mice. (B) Representative image of selection of area for analysis of IHC anti-CD31 immuno-stained 5μm thick floating sections of gastrocnemius muscle from injured and non-injured hind limbs of Dock4 het mice and WT littermate controls. Slides were electronically scanned using an Apeiro AT Virtual Slide scanner and characterised using Apeiro ImageScope software was utilized to randomly select 8 500x500μm boxes per muscle section.
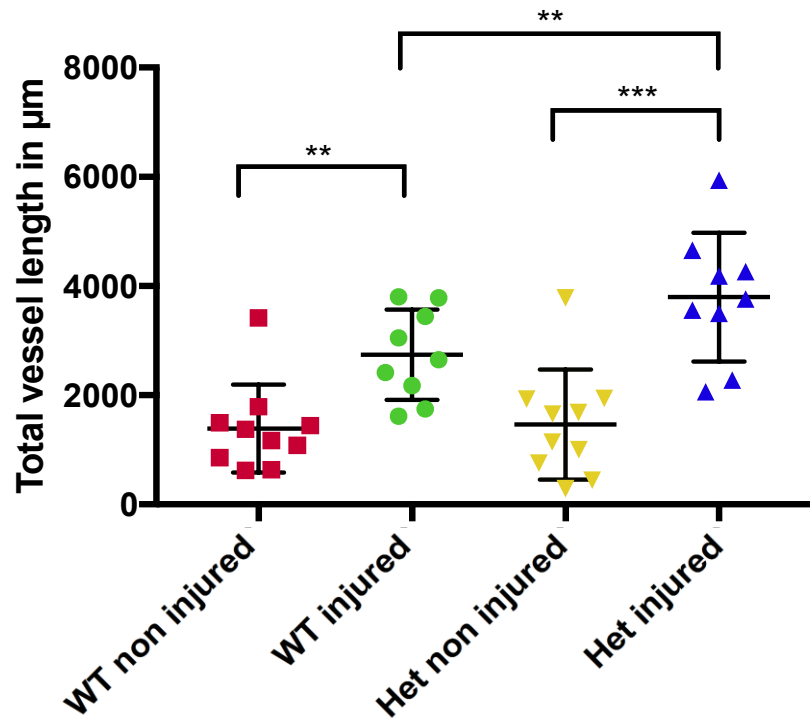
Figure 5-9 Quantification of CD31 IHC staining of hind limb gastrocnemius muscle sections comparing TL of WT versus DOCK4 het vessels detected in tissues sections

Combined data of quantification of total vessel length measured from anti-CD31 stained gastrocnemius muscle sections harvested from the injured and non-injured limbs of global DOCK4 heterozygote deleted mice and WT littermates 21 post HLI surgery. Gastrocnemius muscle fixed in 4% paraformaldehyde was harvested from non-injured and injured hind limbs of DOCK4 heterozygous and WT littermates, 21 days post HLI operation. Muscle was imbedded in paraffin wax and sectioned into 5μm floating section then immuno-stained using a CD31 antibody. IHC anti-CD31 sections were scanned using an Apeiro AT Virtual Slide scanner and characterised using Apeiro ImageScope software. Sixteen 500μm x 500μm areas of analysis were randomly selected. TVL of CD31 stained vessels within the 500μm x 500μm areas were quantified using ImageJ analysis. Histogram shows total vessel length per section ±SEM. N=3 sections per mouse with 4 mice per condition. *P<0.05; **P<0.01; **P<0.001 by one-way analysis of variance (ANOVA).
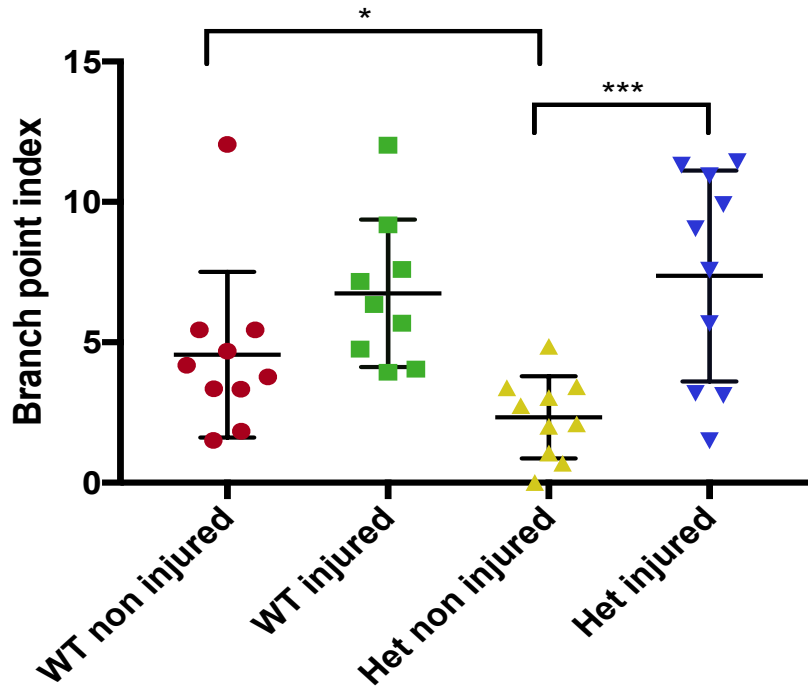
Figure 5-10   Quantification CD31 IHC staining of hind limb gastrocnemius muscle sections comparing BPI of WT versus DOCK4 het mouse.

Combined data of quantification of BPI (number of branch points/total vessel length) measured from anti-CD31 stained gastrocnemius muscle sections harvested from the injured and non-injured limbs of global DOCK4 heterozygote deleted mice and WT littermates 21 post HLI surgery. Gastrocnemius muscle fixed in 4% paraformaldehyde was harvested from non-injured and injured hind limbs of DOCK4 heterozygous and WT littermates, 21 days post HLI operation. Muscle was imbedded in paraffin wax and sectioned into 5μm floating section then IHC stained using a CD31 antibody. IHC anti-CD31 sections were scanned using an Apeiro AT Virtual Slide scanner and characterised using Apeiro ImageScope software. Sixteen 500μm x 500μm areas of analysis were randomly selected. CD31 stained vessels and vessel branch points within the 500μm x 500μm areas were quantified using ImageJ analysis software. Histogram shows BPI calculated as the number of total number of branches per section divided by the total tubule length ±SEM. N=3 sections per mouse with 4 mice per condition. *$P<0.05$; **$P<0.01$; **$P<0.001$ by one-way analysis of variance (ANOVA). Graphs generated using Graph Pad software.

5.2.7   Tamoxifen induced EC specific Dock4 deletion does not impact on blood flow recovery following HLI surgery.

In-order to analyse whether the reduction in blood flow recovery following femoral artery ligation, detected in the Dock4 het mice, was due to reduction in endothelial specific Dock4 expression, an EC Dock4 KO model was used within the HLI experiment. Two separate HLI experiments were conducted using EC Dock4 KO mouse model in-order to study the effect of an endothelial specific homozygote Dock4 deletion on the recovery of blood flow to the hind limb following femoral artery ligation. In-order to deplete Dock4 expression EC Dock4 KO mice (n=9), and, iVEC-cre-ve; Rosa26-lsl-Tomato; Dock4f/f mic (which will be referred to as Cre-negative mice from this point forward) (n=8), underwent daily intraperitoneal injections of a 2mg dose of tamoxifen for 5 consecutive days. Tamoxifen induced Cre expression, leading to targeted deletion of the Dock4 gene, which was flanked by the Cre targeted lox sites (Dock4$^{f/f}$). Seven days following the final tamoxifen dose, all mice underwent a HLI operation to surgically ligate and transect the left femoral artery. LDI was carried out immediately following surgery, then 7, 14, and 21 days post hind limb surgery. Comparative One-way ANOVA analysis of percentage of blood flow to the injured hind limb, normalised to the non-injured limb, was calculated for each weekly time point, in addition to linear regression analysis, and area under the blood flow curve.

LDI data was generated over 2 separate HLI experiments, each for a duration of a 21 day time period, following femoral artery ligation of the left hind limb. Each of the two experiments demonstrated no significant difference in blood flow of the non-injured hind limb of the 9 analysed EC Dock4 KO mice when compared to the 8 Cre negative control littermates (figure. 5.12). Each of the two experiments also demonstrated no significant difference in blood flow recovery of the injured hind limb of the 9 analysed EC Dock4 KO mice when compared to the 8 Cre negative control littermates (figure. 5.13) at any of the 4 time points.

From visual analysis of the linear regression of the rate of blood flow recovery between the analysed EC Dock4 KO mice and the 8 Cre negative control littermates (figure. 5.13) it can be noted that the level of detected blood flow of the mice with an inducible Dock4 deletion have a lower level of blood flow in comparison to the Cre negative control group. However, using linear regression analysis the slope of the lines of best fit, of the Cre negative data set and the EC Dock4 KO mice data set, were not significantly different (p=0.155). The intercept of the two lines representing the different data sets were also not significantly different (p=0.093). This signifies that while the Cre neg control group appear to recover marginally faster than the EC Dock4 KO experimental group, data analysis does not detect a significant difference between the rates of recover of the two experimental groups. Area under the blood flow curve analysis supported the linear regression analysis and found no significant difference between the data sets of the two experimental groups (p=0.179).
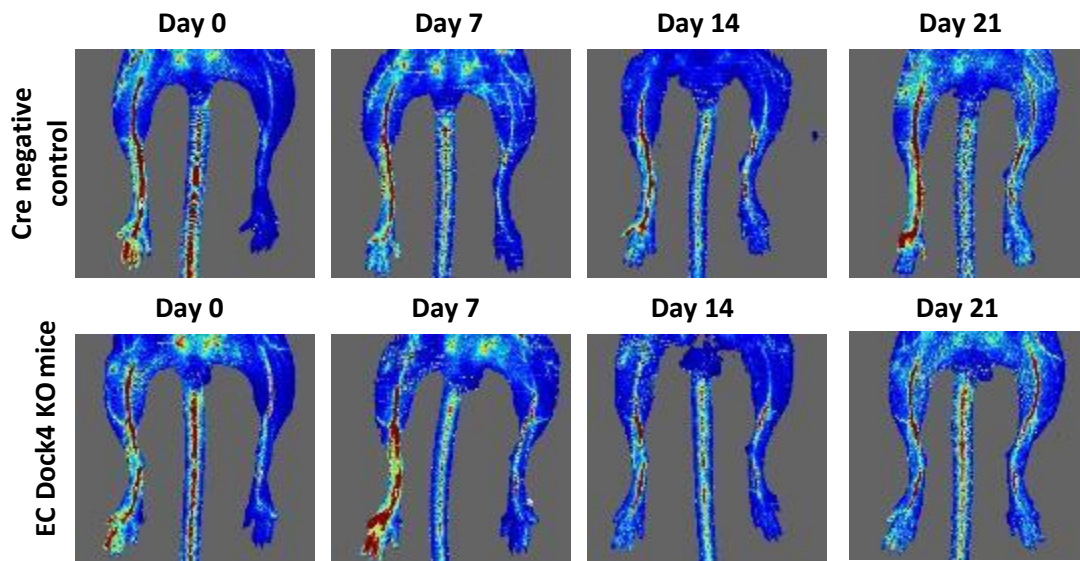
Figure 5-11 Effect of EC specific inducible Dock4 deletion on hind limb vascular recovery following surgically induced HLI

Representative images of Laser Doppler detected mean/area of blood flow perfusion in the hind limbs of tamoxifen Cre neg control and EC Dock4 KO mice, in a supine position, over a 21 day time period, following HLI surgery. EC Dock4 KO mice and cre-negative control mice were treated with once daily intraperitoneal injections of 2mg of tamoxifen for 5 consecutive days. Surgery to ligate and transect the left femoral artery of 9 mice was carried out 7 days prior to tamoxifen treatments to occlude blood flow to the left hind limb. Blood flow within the hind limbs was analysed using LDI on day 0, 7, 14, and 21, following surgical ligation of the left hind leg femoral artery on day 0. Cre negative control (n=8) EC Dock4 KO mice (n=9).
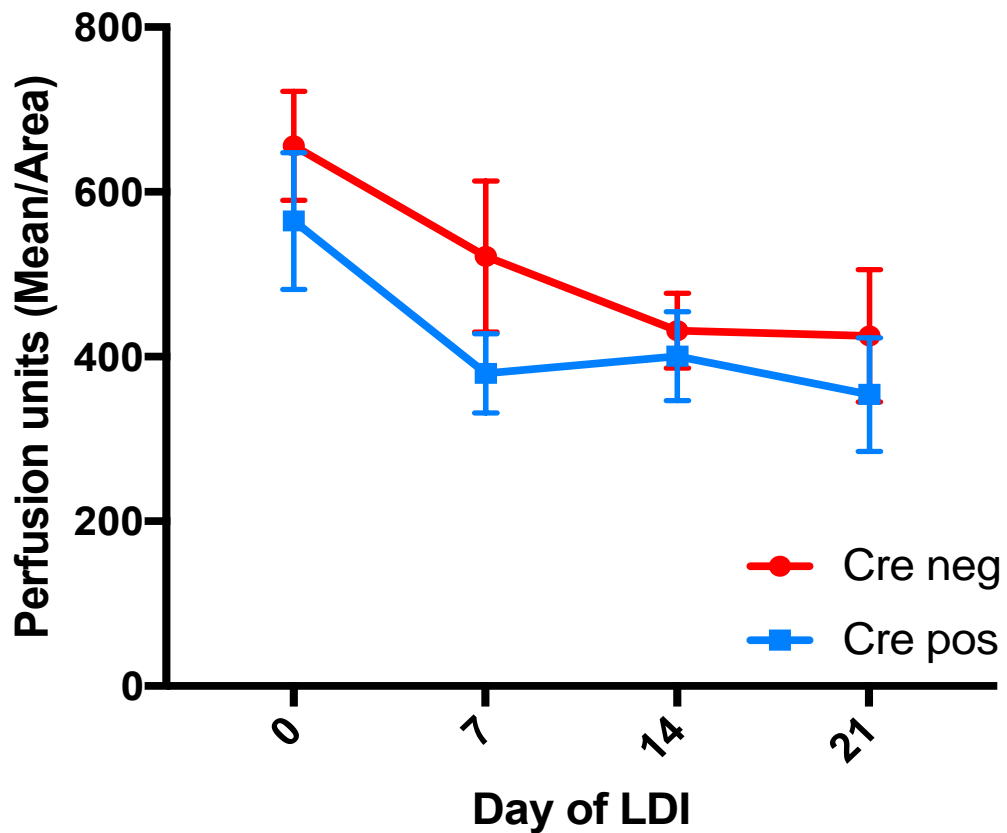
Figure 5-12 Quantification of LDI of EC Dock4 KO non-injured hind limbs during ischemia recovery

Combined data LDI detection of blood flow perfusion in the uninjured hind limbs of EC Dock4 KO mice (n=9) versus Cre-negative control littermates (n=8) following HLI surgery. EC Dock4 KO mice and Cre-negative control mice were treated with once daily intraperitoneal injections of 2mg of tamoxifen for 5 consecutive days. Surgery to ligate and transect the left femoral artery of 9 mice was carried out 7 days prior to tamoxifen treatments to occlude blood flow to the left hind limb. Blood flow within the hind limbs was analysed using LDI on day 0, 7, 14, and 21, following surgical ligation of the left hind leg femoral artery on day 0. (Cre neg) Cre negative control (n=8) (Cre pos) EC Dock4 KO mice (n=9).
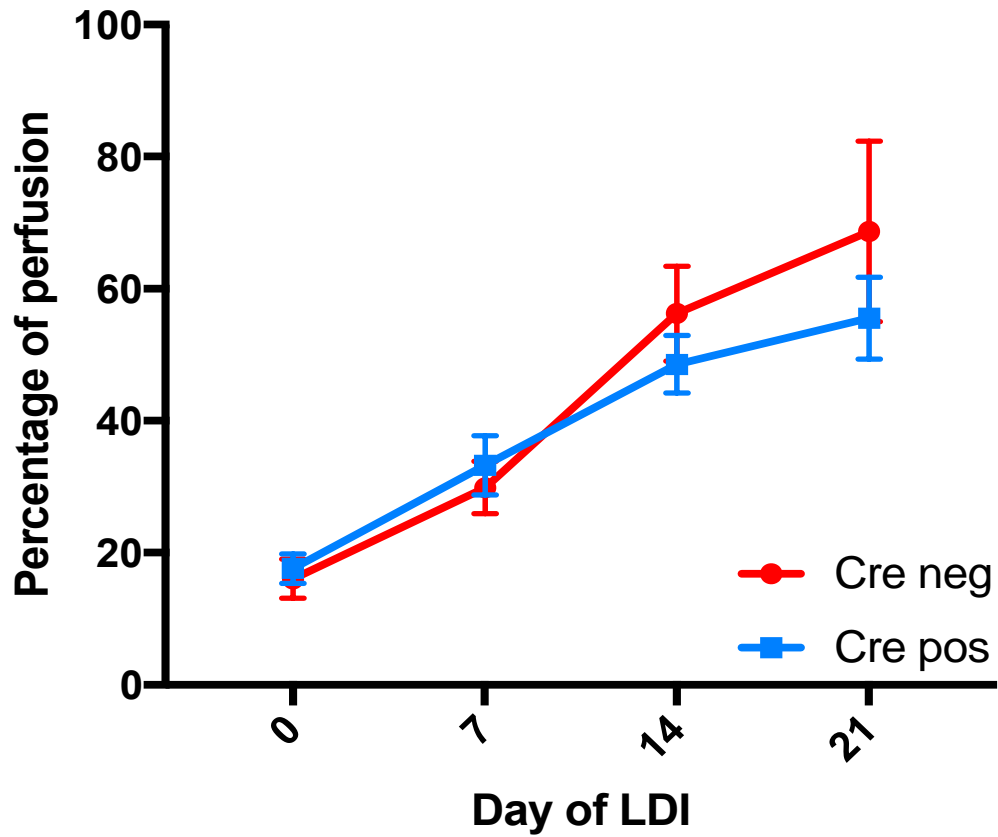
Figure 5-13 Quantification of LDI of EC Dock4 KO mice injured hind limbs during ischemia recovery

Combined data of LDI detection of blood flow perfusion in the injured hind limbs of EC Dock4 KO mice (n=9) versus Cre-negative control littermates (n=8) following HLI surgery. EC Dock4 KO mice and Cre-negative control mice were treated with once daily intraperitoneal injections of 2mg of tamoxifen for 5 consecutive days. Surgery to ligate and transect the left femoral artery of 9 mice was carried out 7 days following tamoxifen treatments to occlude blood flow to the left hind limb. Blood flow within the hind limbs was analysed using LDI on day 0, 7, 14, and 21, following surgical ligation of the left hind leg femoral artery on day 0. (Cre neg) Cre negative control littermates (n=8) (Cre pos) EC Dock4 KO mice (n=9).

5.2.8   Tamoxifen treatment of EC Dock4 KO mice successfully depleted Dock4 expression

The hindlimb muscles of all experimental mice were posthumously fixed and harvested, for the purpose of analysing and comparing the vasculature of the hind limb tissues of each experimental group. One hour following the final LDI scan, all mice were exsanguinated through ligation of the major vena cava. Whole animal fixation of each mouse was carried out by administration of 4% PFA, through the left ventricle. The gastrocnemius and soleus muscles were harvested from both the injured and non-injured hind-limbs of each mouse, and placed in 4% PFA for 24 hours, before being transferred to 70% ethanol. Following fixation, gastrocnemius muscle tissue from both the injured and non-injured legs, were imbedded in paraffin wax in a longitudinal orientation. The muscle was sectioned into 5µm thick sections using a floating sectioning technique.

Muscle section slides were selected from each experimental group and were IHC stained with an anti-DOCK4 antibody to detect presence of absence of Dock4 expression and RFP to detect the Td Tomato reporter; indicating successful tamoxifen induced depletion of DOCK4 (figure 5.14). Analysis of the anti-RFP stained muscle sections indicated Td Tomato expression within the vasculature of EC Dock4 KO mice, but not in Cre negative control littermates (figure 5.14). Dock4 expression was detected in the Cre negative mouse, anti-DOCK4 stained gastrocnemius muscle sections, but was not detected in the Cre positive muscle sections (figure 5.14).
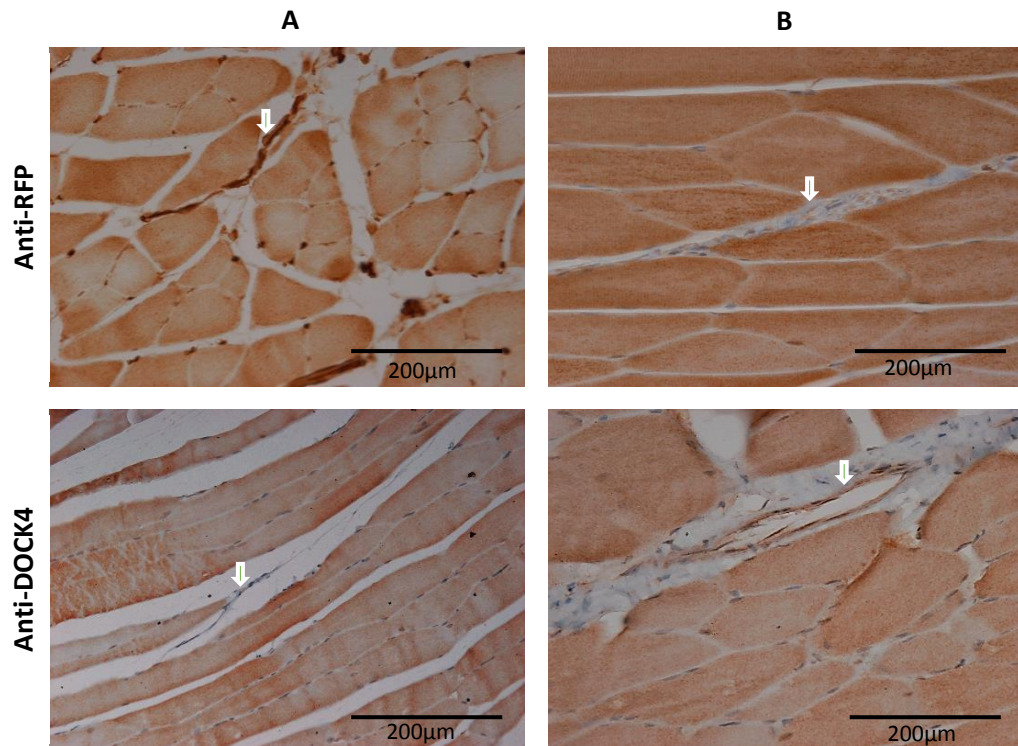
Figure 5-14 IHC staining of hind limb gastrocnemius muscle sections detecting vascular specific expression of DOCK4

Representative images of anti-RFP and anti-DOCK4 IHC stained gastrocnemius muscle sections of the hind limbs of tamoxifen treated **(A)** EC Dock4 KO mice and **(B)** Cre neg control littermates. Mice were treated with once daily intraperitoneal injections of 2mg of tamoxifen for 5 consecutive days. Muscles were fixed in 4% paraformaldehyde, embedded in paraffin wax, sectioned into 5µm floating sections and IHC stained using an antibody against RFP or DOCK4. Images were taken at 20x using a Nikon light microscope. White arrows indicate vessels of interest.

5.3   Discussion

Understanding the complex cellular signalling mechanisms which underlay the dynamic process of angiogenesis, in response to a hypoxic environment, is imperative for furthering the knowledge of vascular pathologies that relate to the dysregulation of angiogenesis, such as peripheral ischemia. The ability to identify proteins essential for the growth of fully functional, normal blood vessels, is key for understanding how blood vessels form and grow in response to oxygen deprivation and other extracellular cues. In addition to expanding the understanding of vascular cell signalling mechanisms, the identification of potential therapeutic targets may also lead to improvement in the approach to treating such vascular pathologies.

In the current study, global Dock4 het deletion severely impacted upon the vascular response to the loss of blood flow in a model of HLI, leading to inadequate vascular perfusion when Dock4 expression was reduced (figure 5.5). Reduction of Dock4 expression affected the mobility of the ischemic murine hind limbs, leading to necrosis of the toes and loss of the foot, in 2 out of 12 Dock4 het mice (figure 5.2). Thus, adequate levels of global Dock4 expression are important for functional blood vessel growth following an ischemic event.

Laser Doppler analysis of murine hind limbs following transection and removal of a portion of the femoral artery, inducing HLI, demonstrated that WT mice recovered from HLI within 21 days post operation (figure 5.5). This is in agreement with previous studies describing the expected normal response to HLI (Hellingman et al., 2010). However, global Dock4 het depleted littermates did not adequately recover from HLI (figure 5.5), as assessed by laser Doppler analysis of perfusion. Indicating that unlike controls, blood flow in the Dock4 het mice had not recovered by day 21.

When a conditional EC Dock4 KO model was employed, a trend towards reduced perfusion and vascular recovery from femoral artery ligation in response to HLI was

observed, however the level of reduction was not statistically significant (figure 5.13). This was unexpected as a complete ablation of Dock4 expression in ECs in the conditional knockout model had been hypothesised to re-capitulate, or exaggerate, the impaired recovery from HLI observed in the global het deletion model. This unexpected result may have been due to a number of different reasons: A potential inadequate knockdown of Dock4 expression, and the efficiency of the RFP reporter system, Td Tomato. Although IHC assessment did indicate a successful depletion of Dock4 expression and expression of Td Tomato, in the EC Dock4 KO model (5.14). Isolation and culturing of ECs from experimental mice, for example pulmonary ECs, could be utilised for genetic confirmation of DOCK4 KO via analysis of the level of DOCK4 RNA within the ECs (Fehrenbach et al., 2009). However, isolation of pulmonary ECs from the DOCK4 het and conditional KO mice, used within this thesis, had been attempted but found to be unsuccessful. This was likely due to the age of the mice used within this thesis (24 weeks at the point of sacrifice). It has previously been reported that isolated pulmonary ECs harvested from adult mice have a reduced ability to proliferate, with an increase in susceptibility for fibroblast overgrowth (Fehrenbach et al., 2009).

Consideration also needs to be given to any compensatory cellular mechanisms which occur in response to Dock4 depletion. Cells may evoke transcription and post-transcription mechanisms to overcome loss of an individual protein (El-Brolosy and Stainier, 2017). When comparing genetic knockout and knockdown, of the same protein within a mouse model, phenotypical differences can arise (De Souza et al., 2006). The differences observed between a knockout and a knockdown can be attributed, in part, to compensatory mechanisms of the cell in response to ablation of a protein (De Souza et al., 2006). Considering such evidence in light of the conditional EC specific Dock4 deletion, which experiences a knockout of Dock4 expression, there may be potential for an endothelial compensatory mechanisms to overcome the loss of Dock4 expression within the adult

mouse, thus caution should be used when interpreting the findings of the HLI results in comparison to the Dock4 het mouse.

Furthermore, global Dock4 het deletion affected Dock4 expression throughout the duration of development, unlike the conditional endothelial specific Dock4 deletion, which deletes Dock4 in the adult following tamoxifen treatment. The significant reduction in the vascular branching of the gastrocnemius of non-injured limbs of the Dock4 het mice (figure 5.10) supports this concept as this observation indicates that 50% reduction in global Dock4 expression, throughout development and post-developmental growth, impacts on vascular patterning.

However, it should be noted that the EC DOCK4 KO mice did experience a reduction in the rate of vascular recovery compared to the control littermates, however, the difference between the two experimental groups was not statistically significant (figure 5.13). Expanding this study to include larger number of mice may have been necessary for the experiment to reach statistical significance.

The significant difference in body weight between the global Dock4 depleted mice in comparison to their WT littermates indicates reduction in Dock4 expression has a greater over-all effect on the developing mouse, which may go beyond the vascular response to ischemia. This is also evident through many other studies which implicate DOCK4 dysregulation in a number of pathologies; such as neural developmental functions of DOCK4 (Ueda et al., 2013; Xiao et al., 2013) cancer (Yajnik et al., 2003; Hiramoto-Yamaki et al., 2010; Yu et al., 2015), and mental health related effects of DOCK4 mutations (Pagnamenta et al., 2010; Alkelai et al., 2012). Thus demonstrating that DOCK4 depletion affects more biological mechanisms than is currently understood.

It is also noteworthy that the heterozygous deletion is also global, unlike the conditional endothelial specific deletion. The potential involvement of non-endothelial Dock4 expression in driving the phenotypical effects seen in the global Dock4 KO model, but

not the EC DOCK4 KO mouse, should also be considered. Other requirements of DOCK4, such as for stromal cell paracrine signalling to the endothelium, or for the correct recruitment of perivascular cells, may also be relevant when considering the differences in impact of global versus EC Dock4 KO. However such functions have not yet been explored in relation to DOCK4, but may be of interest in fully understanding the function of DOCK4 in angiogenesis.

Within normal vascular models, ischemia prompts a significant increase in total amount of vasculature. IHC CD31 staining of gastrocnemius muscle harvested from the hind limbs of global Dock4 het depleted mice and WT littermates, 21 days post HLI surgery, indicated distinct difference in the vascular growth in both the injured and non-injured hind limbs of the Dock4 het deleted mice and the WT littermates (figures 5.3-5.7). Dock4 depleted mice were found to have a normal amount of pre-existing vasculature in tissue harvested from the non-injured limbs in comparison to the wildtype littermates, although there may potentially be differences in patterning of the vasculature in Dock4 het mice, as they were found to have a less branched vasculature phenotype (figures 5.6, 5.9). Angiogenesis in response to ischemia was increased significantly in Dock4 depleted mice when compared to the WT littermates, as Dock4 het mice were found to have an increase TVL in the gastrocnemius following HLI in comparison to the wildtype littermates (figures 5.7 and 5.9)

The findings indicate the DOCK4 depleted mice potentially experience differences in vascular patterning during development and/or during post developmental growth unrelated to HLI. The differences detected in vascular growth between the two experimental groups show that Dock4 depletion drives an increase in angiogenesis within the lower limbs. This may be due to blood vessel elongation as opposed to lateral branching, the latter of which is reduced by DOCK4 depletion *in vitro*(Abraham et al., 2015). However, BPI was not significantly impacted by Dock4 depletion following loss of blood flow. Similar phenotypes have been observed in other HLI model studies, which have investigated disruption of signalling mechanisms implicated in regulating angiogenesis that leads to an increase in

vascular structures but reduction in blood flow reperfusion (Ramo et al., 2016; Dor et al., 2002; Clayton et al., 2008; Herold et al., 2017).

Roma et al. found disruption of the MLK-JNK signalling pathway during development led to increased sprouting angiogenesis in conjunction with an inadequate response to HLI (Ramo et al., 2016). Interestingly, disruption of the signalling pathway in adult mice prior to hind limb surgery resulted in no significant difference in the recovery of hind limb blood flow. Impairment of hindlimb vascular of JNK deficient mice was only observed in mice which had experienced JNK protein depletion throughout development. This affect was attributed to the irregular growth of the collateral arteries during development, leading to loss of compensatory collateral blood flow in response to femoral artery ligation (Katoh et al., 2006). As the collateral arteries of either the Dock4 het or EC Dock4 KO experimental mice were not analysed, the findings of this study cannot be attributed to differences in vascular patterning or arteriogenesis of the collateral arteries. However, while this study investigates a non-Dock4 related pathway, their results demonstrate how a genetic depletion can impact on vascular recovery to hind limb ischemia, when the depletion is present throughout development and adulthood, but for the same genetic depletion to have no impact on vascular recovery when induced only during adulthood. This finding offers potential insight to the differences observed between the global Dock4 het mouse recovery to hind limb ischemia when compared to the inducible EC Dock4 KO model. Further exploration into the impact of Dock4 expression on the hindlimb vasculature would be of great interest in understanding the true role of Dock4 within vascular biology.

Data generated from LDI and IHC analysis together suggest reduction in Dock4 expression impacts upon functionality of the vasculature, which grows through angiogenesis in the lower limbs or arteriogenesis in the upper limbs, in response to loss of the femoral artery. Despite the increase in angiogenesis within the gastrocnemius of the injured limbs, the global Dock4 het deleted mice appeared more physically impacted by the femoral artery

ligation, resulting in limited mobility, differing levels of necrosis, and a reduced rate of blood flow recovery to the injured limb when compared to the WT mice.

The observation of increase in angiogenesis within the gastrocnemius, despite less blood flow to the hind limbs of Dock4 het mice compared to WT, may potentially be due to differences in the arteriogenesis within the collateral arteries. An investigation into the role of exogenous factor VII activating protein in vascular recovery, found application of exogenous factor VII activating protein inhibited arteriogenesis of the collateral arteries, resulting in an impairment in blood flow to the hind limbs and a pronounced increase in angiogenesis of the gastrocnemius. This effect was determined to be due to sustained hypoxia of the lower limbs due to a decrease in blood flow through the collateral arteries (Herold et al., 2017).

Considering the wider implications of the combined Dock4 het deletion data it is possible to speculate that Dock4 depletion impacts upon the development of the pre-existing vasculature of the hind limb. It is also possible to hypothesis that Dock4 depletion may impact on the ability to form functional vasculature in response to ischemia, leading to an overgrowth of less functional vasculature structures, as DOCK4 depletion *in vitro* results in loss of lumenisation of EC cords during angiogenesis (Abrahams et al. 2015). Abraham et.al (2015) demonstrated that Dock4 expression was found to be required for lumenisation and growth of functional vasculature. Abraham et.al described how Dock4 deletion within an organotypic angiogenesis co-culture *in vitro* resulted in long unbranched cords of ECs unable to form a lumen.

This current study therefore supports the findings that DOCK4 is required for formation of functional vasculature during blood flow recovery following ischemia. Investigation into Dock4 function during vasculogenesis and angiogenesis during development would be of key interest to understand how DOCK4 impacts upon the growth

of functional blood vessels. Further investigation into the patterning of the collateral arteries may also add further insight into the role of DOCK4 function.

The study demonstrates the requirement for Dock4 signalling in growth and formation of functional vasculature, with reduction in global Dock4 expression impacting on a functional angiogenic response to oxygen deprivation.

6   Overall Discussion

Sprouting angiogenesis describes the dynamic outgrowth of new blood vessels from existing vasculature in response to external stimuli. Chemotactic initiated sprouting angiogenesis integrates a dynamic repertoire of external stimuli, driving complex intracellular remodelling to permit growth of new vascular sprouts. The VEGFA driven small Rho GTPase signalling module SGEF-RhoG-DOCK4-RAC1-DOCK9-CDC42 is an important component for development of lateral filopodia and vessel lumenisation *in vitro*, and thus is likely to be required for correct patterning and functionality of newly sprouted vasculature (Abrahams et al., 2015). Depletion of the endothelial expression of RAC1 GEF, DOCK4, results in loss of filopodia along the lateral edge of newly forming vascular sprouts, leading to deficiencies in tube formation (Abraham et al., 2015). As dysregulation in vascular patterning and tube formation impairment are characteristics of some pathological angiogenesis driven disorders (Matucci-Cerinic et al., 2013; Maruotti et al., 2006; Maruotti et al., 2008; Cantatore et al., 2017), expanding upon the understanding of DOCK4 function within angiogenesis could lend insight into mechanisms affected during pathological angiogenesis. This study strove to expand upon the understanding of the DOCK4-DOCK9 interaction, while also investigating whether DOCK4 activity was required for pathological angiogenesis.

The small molecule inhibitor QL-47 was demonstrated to be a potent anti-angiogenic compound with VEGFA stimulated ECs being particularly sensitive to QL-47 (figures 3.7-3.9). However, it is highly unlikely that the anti-angiogenic effects are due to disruption of a direct DOCK4-DOCK9 interaction at this site, as in this study no evidence was obtained that the p.C628 cysteine residue was found to bind the DOCK4 SH3 domain (figure 4.12). It is largely plausible that the QL-47 inhibitor disrupts DOCK9 through non-DOCK4 specific mechanism; perhaps through disruption of localisation, or inhibition of interaction with other DOCK9 binding partners. Abraham et al (2015) described an extensive list of proteins which

specifically bind DOCK9. Repetition of the Abraham et al (2015) Co-IP with LC-MS/MS Orbitrap Elite mass spectrometer and MASCOT analysis of DOCK9 binding partners in the presence of QL-47 would potentially elucidate which DOCK9 interaction partners may be disrupted by the small molecule inhibitor.

The specific site of DOCK9 which interacts with the SH3 domain of DOCK4 was not elucidated during this study, the results suggested that DOCK9 PRRs identified as PRR 2,3,4, 5, and 9 were unlikely to serve as singular points of direct interaction between the two proteins (figures 4.3-4.12). Use of the Co-IP overexpression system and SEC of truncated peptides both present discrepancies which may have confound results. Forced interaction between the two large GEFs within an overexpression system within HEK 293T cells may have yielded non-specific interaction and a false positive pull down of Flag-DOCK9 due to non-specific interaction of the peptide tags (Free et al., 2009), excessively high level of protein expression due to overly active promoters (Xia et al., 2006), and also the lack of sensitivity of the Western blotting technique which lacks sensitivity, with the potential to produce unreliable results that may not distinguish between genuine interaction and non-specific interaction (Zhu et al., 2017).

Detecting an interaction between two truncated peptides using SEC may also prove difficult as the peptides may not provide a true representation of the secondary structures of the complete protein and thus they may lose the potential binding affinity between the site of interaction (Wingfield, 2015).

Use of a MultiBac™ system designed to co-express both DOCK4 and DOCK9, followed by trypsin digest to expose crosslinking residues, and cryoEM analysis would allow for detection of the interacting residues of the two large proteins, with cryoEM providing an optimal technique for structural analysis of two large proteins within a complex (Serna, 2019). Such an approach would offer a more highly sensitive approach for elucidating the site of interaction between the two proteins.

Through this study, DOCK4 was demonstrated as being a potential component of FGF2 stimulated angiogenesis under hypoxia *in vitro*, (figure 3.5 and 3.6) indicating DOCK4 as important for mechanisms involved in the angiogenic response to ischemia.

FGF2 has a protective effect during wound healing, and when used as a treatment improves outcomes of cardiac ischemia (Unger et al., 2000; Laham et al., 1999), and the peripheral circulation of people suffering from claudication (Lazarous et al., 2000). Such effects of FGF2 signalling may be attributed to the GFs function in EC proliferation and elongation in angiogenesis in response to vascular pathologies *in vivo* (Unger et al., 2000; Laham et al., 1999). The protective mechanisms of FGF2 has been indicated to occur in a RAC1 and CDC42 dependent mechanism (Lee and Kay, 2006). As DOCK4 is an activator of RAC1, it can be considered that DOCK4 may serve as a potential component in conferring the FGF2 protective response to pathological angiogenesis, a concept which has been supported by the results presented throughout this thesis.

This finding was further supported through *in vivo* analysis of blood flow recovery in the hind limbs of het global DOCK4 deleted mice following femoral artery ligation. LDI of injured mouse hind limbs demonstrated a reduction in global Dock4 expression results in impairment of blood flow recovery (Figures 5.3 and 5.5). The reduction in blood flow recovery of the EC Dock4 KO mice was also seen to be impaired, but to a much lesser and non-significant degree (figures 5.11 and 5.13). This finding may potentially indicate additional non-EC functions of DOCK4 during pathological angiogenesis. The data also indicates that Dock4 may be required for the growth and correct patterning of hind limb vasculature during development (figure 5.4 and 5.10), with Dock4 deficiencies leading to differences in pre-existing vasculature in the mature mice; findings which are similar to other proteins which are not required for normal vasculature but impact on an adequate vascular response to hind limb ischemia (Herold et al., 2017; Ramo et al., 2016).

The IHC analysis of muscle tissue from the ischemic hind limbs of DOCK4 deficient mice indicated DOCK4 depletion may impair vessel functionality, as an increase was observed in the overall abundance of vascular structures despite a reduction in blood flow (Figures 5.4 and 5.9). This finding was in line with *in vitro* analysis of the impact of DOCK4 depletion on sprouting angiogenesis, with loss of DOCK4 resulting in growth of less dynamic vascular structures with impaired tube formation (Abraham et al., 2015).

In light of previous studies, which highlight the importance of correct vascular patterning of the collateral arteries during development for a proficient response to HLI (Ramo et al., 2016; Dor et al., 2002; Herold et al., 2017), consideration should be given to the effect of Dock4 depletion on the correct vascular patterning of the collateral circulation. Pre-existing defects in the collateral vascular patterning, or arterogenesis response to ischemia, have both been observed to induce a similar phenotype to the global Dock4 depletion, in response to hind limb ischemia; with loss of blood flow recover to the hind limbs combined with an increase in angiogenesis detected in the gastrocnemius (Ramo et al., 2016; Dor et al., 2002; Herold et al., 2017). The detected difference in vascular recovery between the Dock4 het mouse model and the EC Dock4 KO mouse model may potentially indicate Dock4 vascular signalling as being required for developmental blood vessel development, but not adult angiogenesis. Thus the collateral arteries of the Dock4 deficient mice should be further explored in future experiments to determine whether DOCK4 may be involved in collateral artery development, patterning, and/or arteriogenesis.

MicroCT imaging of hind limb vasculature of both the DOCK4 het and EC Dock4 KO mouse lines, following HLI, would allow for analysis of intact whole leg vascular structures, including the collateral arteries, and would perhaps give insight into non-luminized structures when comparing Micro-fil perfused vessels to those detected through IHC analysis (Schaad et al., 2017). Comparison of Dock4 het mouse whole leg vasculature to that of non-

Dock4 depleted littermates whole leg vasculature, would lend an interesting insight into how vascular Dock4 impairs recovery of blood flow following an ischemic event.

The accumulated results of this thesis have strongly indicated that DOCK4 is a critical component of the vascular response to ischemia driven angiogenesis. Further investigation of DOCK4 function during development, formation of collateral arteries, correct lumenisation *in vivo*, and within the context of pathological angiogenesis during peripheral ischemia, would be required to determine how aberrant DOCK4 expression and regulation may underlie angiogenesis driven pathologies, such as peripheral ischemia. However, these finding highlight the importance of DOCK4 in growth of healthy vasculature that is capable of adequately responding to critical ischemia. Elucidating the vascular function of DOCK4 during development and within the response to ischemia may further our understanding of how blood vessels grow, and expand our understanding of how angiogenesis may differ during development in comparison to a pathological context.

7 Appendices

7.1 Appendix 1. Nucleotide sequences of primers for Sanger sequencing and Expression vector cloning

7.1.1 Primer design for Sanger sequencing

1	pBABE Flag-DOCK forward 1	5'-GTTCAGTGAATCAGAAC-3'
2	pBABE Flag-DOCK forward 2	5'-GGATGAAGGACGTGAAG-3'
3	pBABE Flag-DOCK forward 3	5'-TTTCTCATGGAGTATCC-3'
4	pBABE Flag-DOCK forward 4	5'-AGTAAAGTTTCTGCAGG-3'
5	pBABE Flag-DOCK forward 5	5'-AAGGACCTGATCATGTG-3'
6	pBABE Flag-DOCK forward 6	5'-CAGCCAGATCTTCGGAATG-3'
7	pBABE Flag-DOCK forward 7	5'-CCAGCAACGTCTTGAAC-3'
8	pBABE Flag-DOCK forward 8	5'-AGCTGATGCTTGAGCAG-3'
9	pBABE Flag-DOCK forward 9	5'-AGAACATGTCGGATAGTG-3'
10	pBABE Flag-DOCK forward 10	5'-AGTTGCTGATCTAAAACGC-3'

Table 7-1 Primer sequences for Sanger sequencing of the pBabe puro Flag-DOCK4 plasmid construct designed for expression of human DOCK4.

Human DOCK4 expression vector pBABE puro Flag- DOCK4; a plasmid gifted by Dr Vijay Yanik (Harvard Medical School, Massachusetts, USA) was sequenced using Sanger sequencing by GATC Biotech (Konstanz, Germany).

1	pEF4 Myc-Flag-DOCK9 forward 1	5'-ACTATAGGGAGACCCAAGCTG-3'
2	pEF4 Myc-Flag-DOCK9 forward 2	5'-CTGGCAAAGCCAAAGCTAATTGAG-3'
3	pEF4 Myc-Flag-DOCK9 forward 3	5'-CTTCCCTTACGATGACTTTCAGAC-3'
4	pEF4 Myc-Flag-DOCK9 forward 4	5'-AAACCTATAACTCTGACTGGCATC-3'
5	pEF4 Myc-Flag-DOCK9 forward 5	5'-AAAGTTCAGACTCTTCTAAGGTGG-3'
6	pEF4 Myc-Flag-DOCK9 forward 6	5'-CAAGGACATTGTTTAAGGATGC-3'
7	pEF4 Myc-Flag-DOCK9 forward 7	5'-GCTCAAGTTACTTGCAGACTTTCG-3'
8	pEF4 Myc-Flag-DOCK9 forward 8	5'-AAACTCCCATCACGTTTGAAG-3'
9	pEF4 Myc-Flag-DOCK9 forward 9	5'- GACCCAAAGACCCTCTTTGAATAC -3'
10	pEF4 Myc-Flag-DOCK9 forward 10	5'-GGGCATGACTGTGAAGGATG-3'

Table 7-2 Primer sequences for Sanger sequencing of the pEF4 Flag-DOCK9 plasmid construct designed for expression of human DOCK9.

Human DOCK9 expression vector pEF4 Myc-Flag–DOCK9 (Meller et al., 2008); a plasmid gifted by Professor Martin Schwartz (University of Virginia, USA) was sequenced using Sanger sequencing by GATC Biotech (Konstanz, Germany).
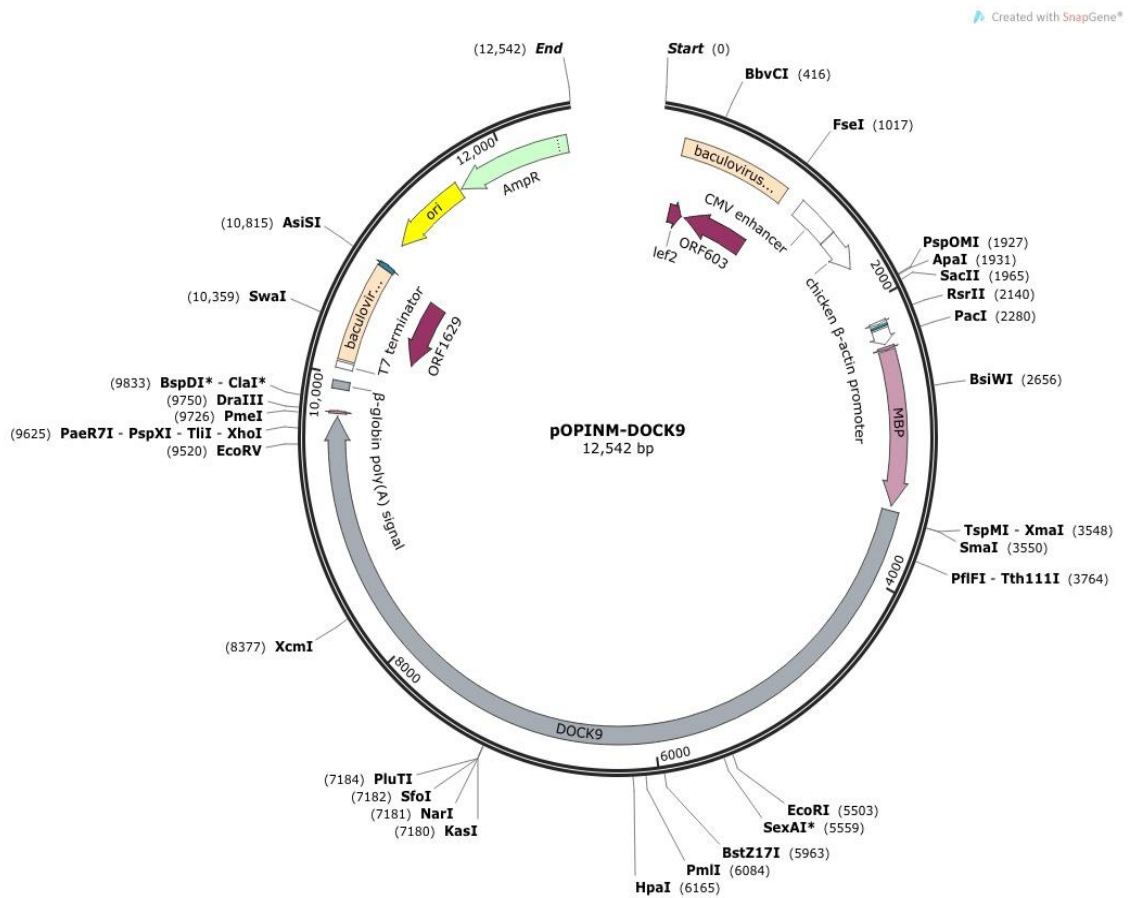
7.1.2   Plasmid maps

Figure 7-1 Plasmid vector map of pOPINM DOCK9

Full length DOCK9 was sub-cloned into pOPIN3SC HIS6-SUMO-3C-POI with ampicillin resistance gene sequence. Full length DOCK9 gene inserted in recombinant plasmid vectors designed for expression of full length DOCK9 was PCR amplified from the template plasmid pEF4 Myc-Flag–Dock9 (Meller et al., 2008) using the primer sequences described in Table 7.1. Plasmid map generated using Snapgene software.
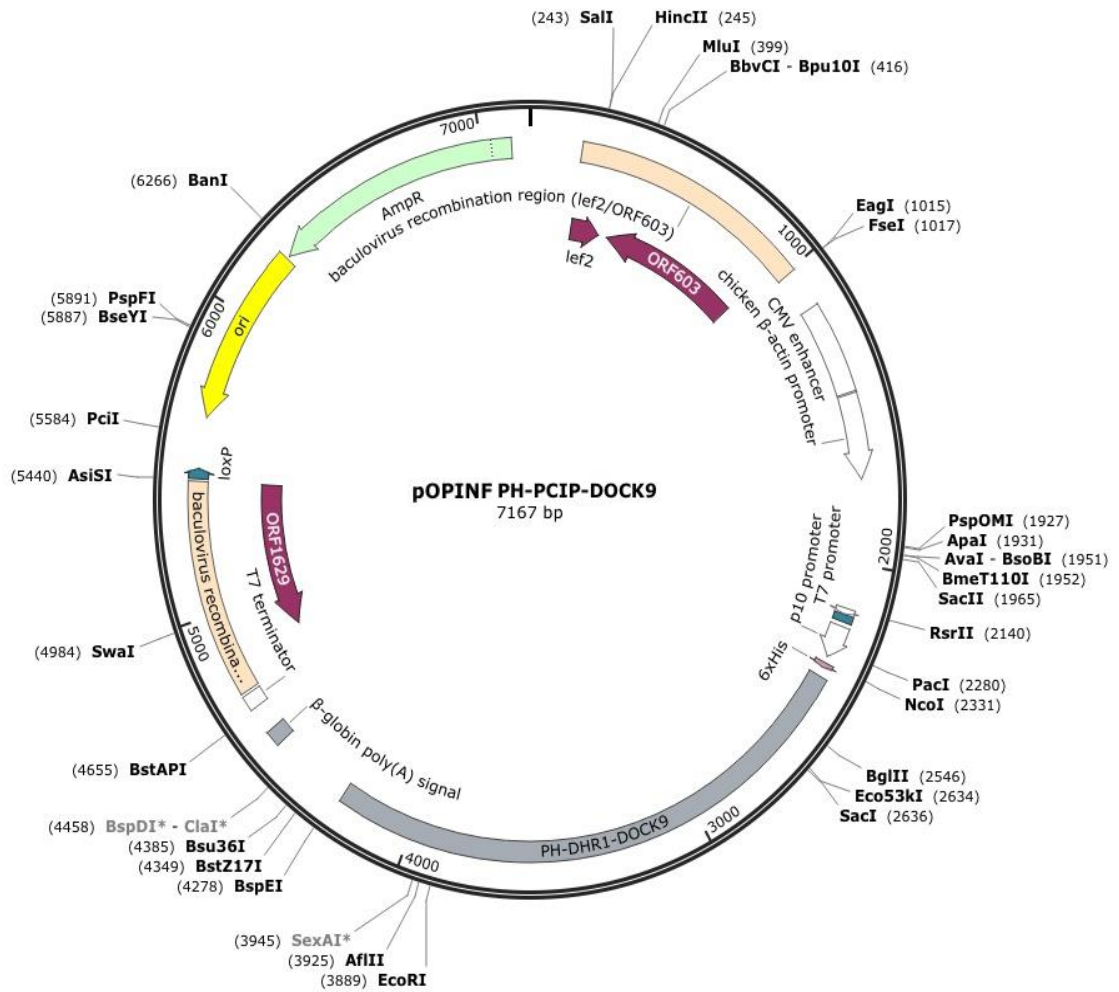
Figure 7-2 Plasmid vector map of pOPINF PH-PCIP-DOCK9

DOCK9 PH-PCIP-DHR1 domain PCR fragments were sub-cloned into a modified a pOPINF HIS6-3C-POI vector with ampicillin resistance gene sequence. DOCK9 gene fragments inserted in recombinant plasmid vectors designed for expression of full length DOCK9 was PCR amplified from the template plasmid pEF4 Myc-Flag–DOCK9 (Meller et al., 2008) using the primer sequences described in Table 7.1. Plasmid map generated using Snapgene software.
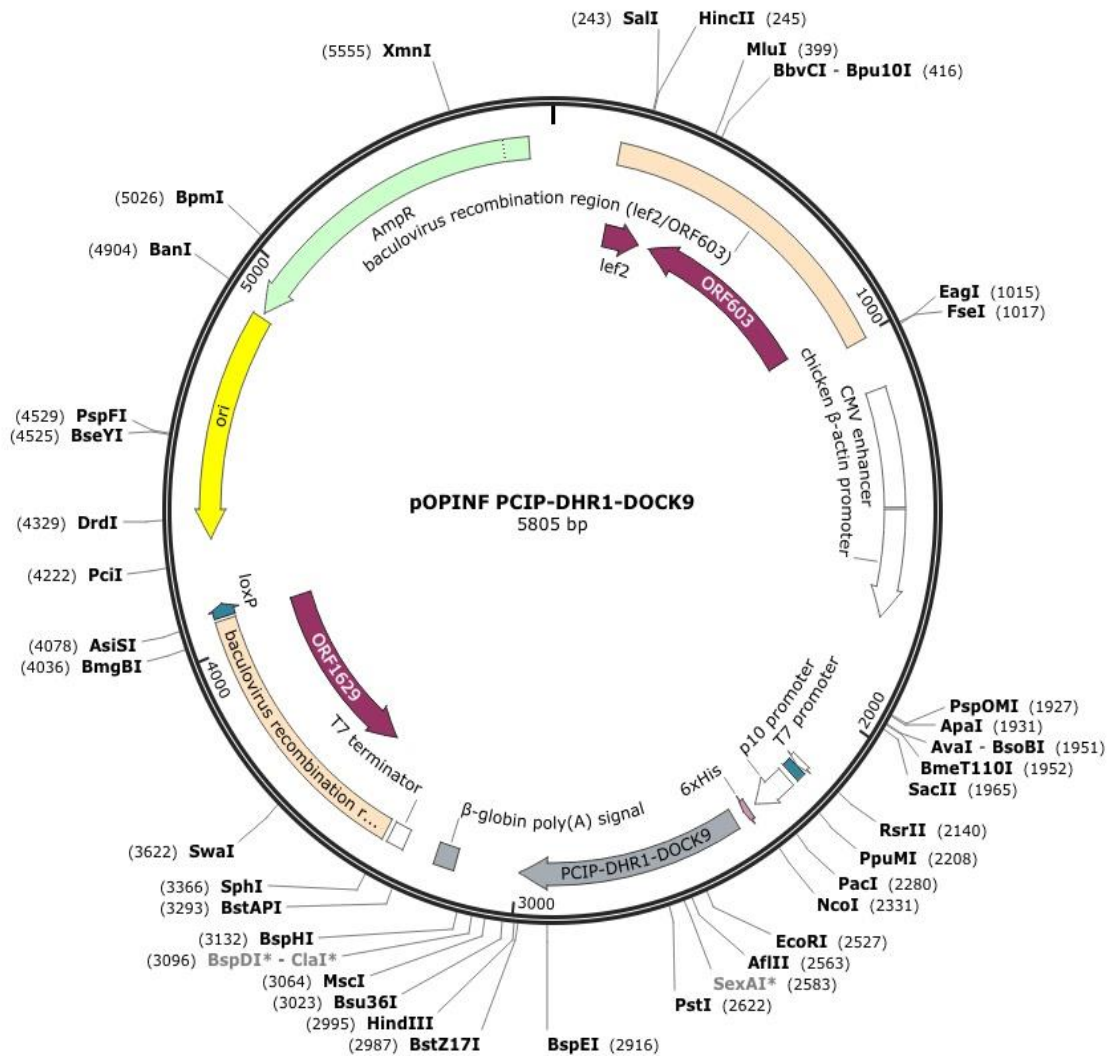
Figure 7-3 pOPINF PCIP-DHR1-DOCK9

DOCK9 PCIP-DHR1 domain PCR fragments were sub-cloned into a modified a pOPINF HIS6-3C-POI vector with ampicillin resistance gene sequence. DOCK9 gene fragments inserted in recombinant plasmid vectors designed for expression of full length DOCK9 was PCR amplified from the template plasmid pEF4 Myc-Flag-DOCK9 (Meller et al., 2008) using the primer sequences described in Table 7.1. Plasmid map generated using Snapgene software.
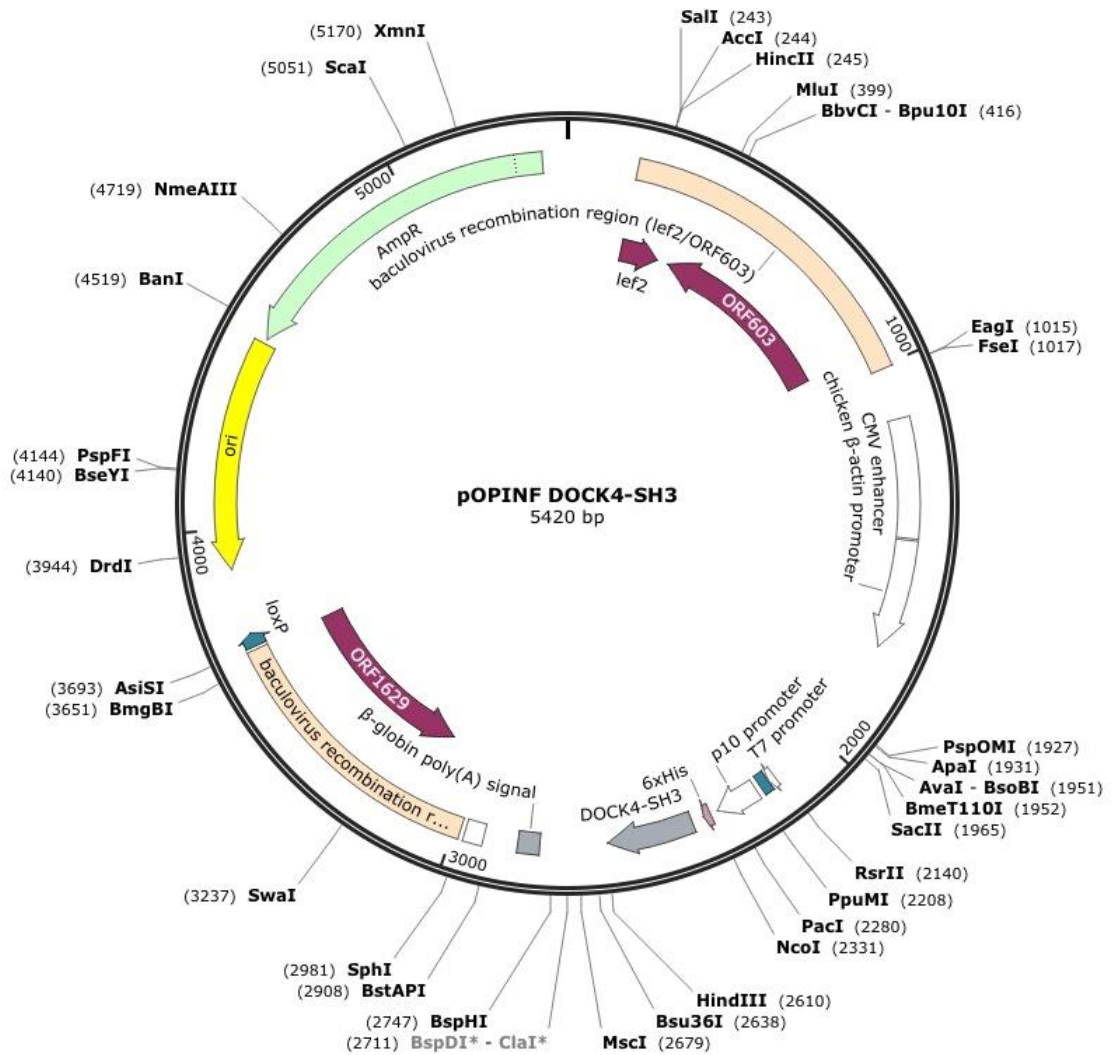
Figure 7-4 pOPINF DOCK4-SH3

DOCK4 SH3 domain PCR fragments were sub-cloned into a modified a pOPINF HIS6-3C-POI vector with ampicillin resistance gene sequence. DOCK4 gene fragments were PCR amplified, using the described primer sequences, from the template plasmid pBABE puro Flag- DOCK4; a plasmid gifted by Dr Vijay Yanik (Harvard Medical School, Massachusetts, USA). Plasmid map generated using Snapgene software.
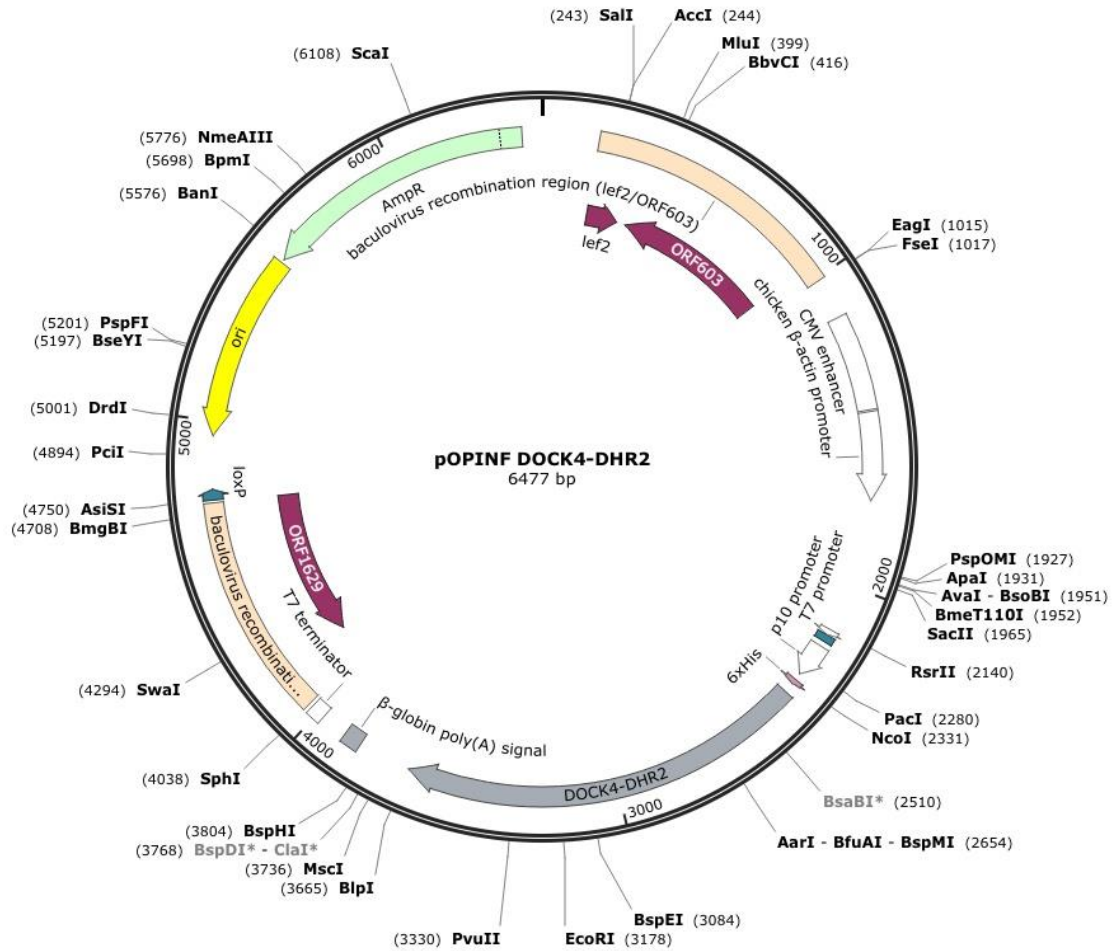
Figure 7-5 pOPINF DOCK4-DHR2

DOCK4 DHR2 domain PCR fragments were sub-cloned into a modified a pOPINF HIS6-3C-POI vector with ampicillin resistance gene sequence. DOCK4 gene fragments were PCR amplified, using the described primer sequences, from the template plasmid pBABE puro Flag- DOCK4; a plasmid gifted by Dr Vijay Yanik (Harvard Medical School, Massachusetts, USA). Plasmid map generated using Snapgene software.

Figure 7-6 pGIPz lenti viral plasmid for DOCK4 shRNA expression

Plasmid map of pGIPz lenti viral vector backbone with Dock4 SHRNA and non-silencing pGIPZ nucleotide sequence. Plasmid map generated using Snapgene software.
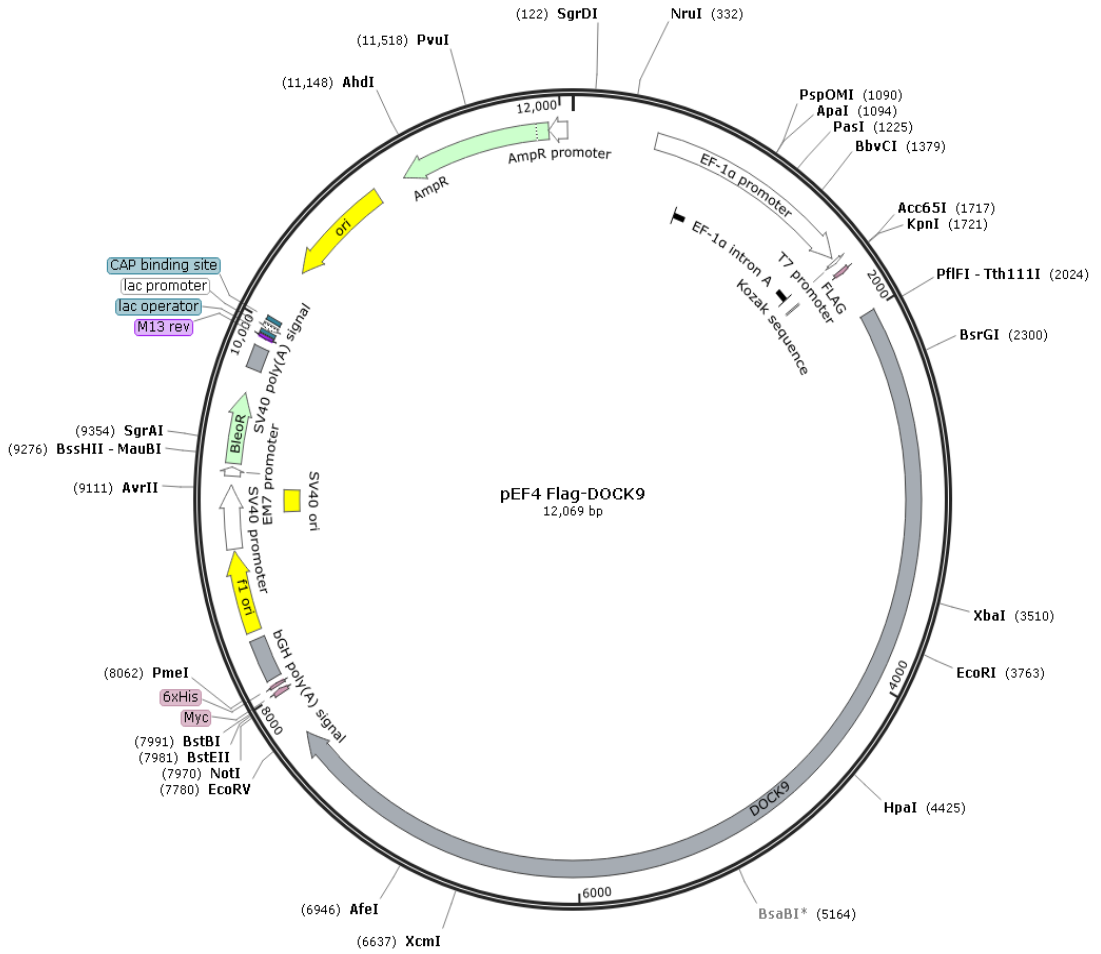
Figure 7-7 pEF4 Flag-DOCK9 plasmid map

PEF4 Myc-Flag–DOCK9 (Meller et al., 2008) was obtained from Professor Martin Schwartz (University of Virgina, USA). Plasmid map generated using Snapgene software.
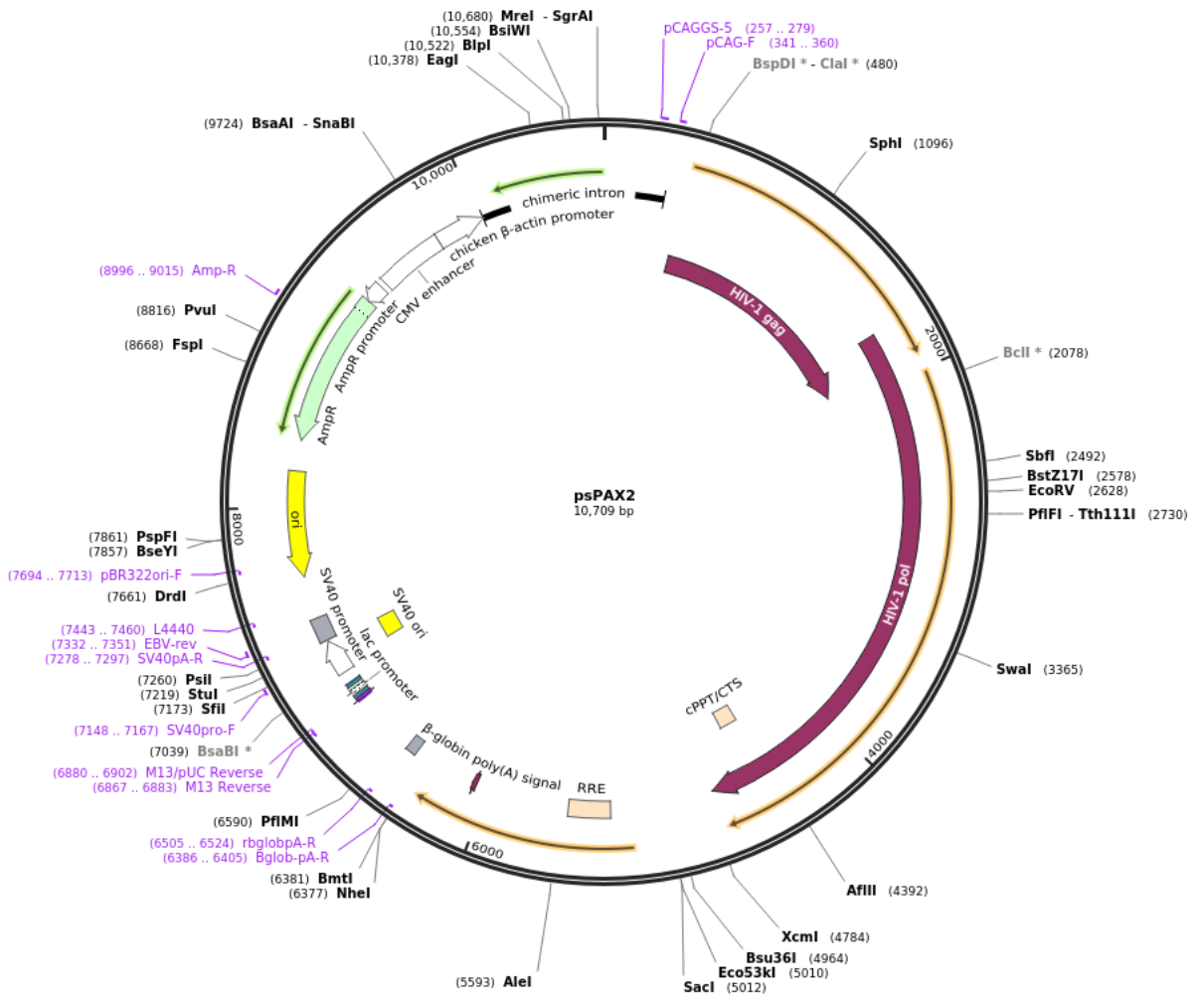
Figure 7-8 psPAX plasmid map

Plasmid psPAX plasmid map, generated by Snapgene software.
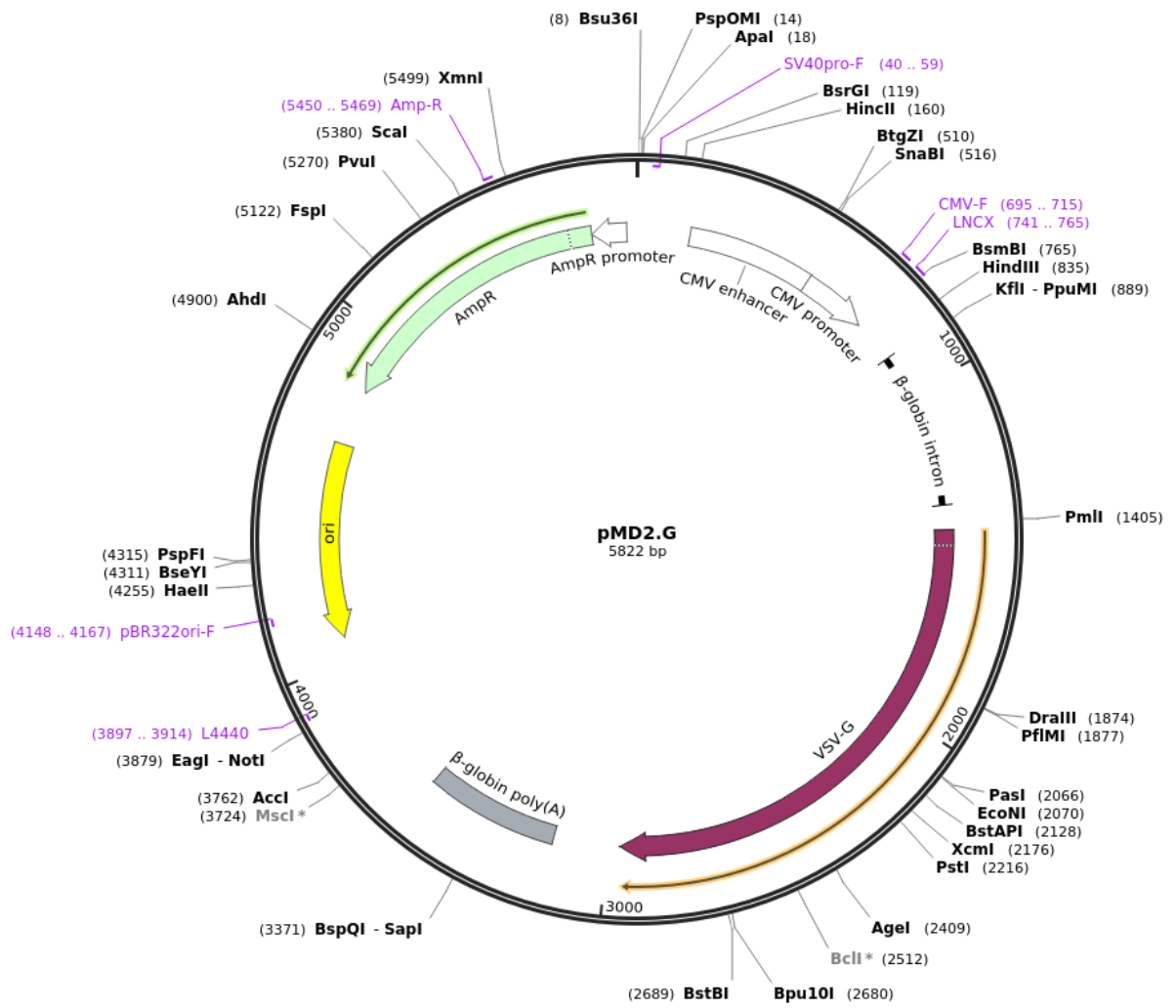
Figure 7-9 pMD2.G plasmid map

Plasmid map of pMD2.G plasmid map generated using Snapgene software.

7.2 Appendix 2. The small molecule QL-47 binds to c628 of DOCK9

Figure 7-10 The small molecule inhibitor QL-47 and YKL-04-126

Molecular structure of the (A) covalent small molecule inhibitor QL-47 and (B) a tagged form of the covalent QL-47 inhibitor YKL-04-126. QL-47 is a compound developed by Prof. Nathanael Gray's research group (Dana Farber Cancer Institute Harvard Medical School), MA).
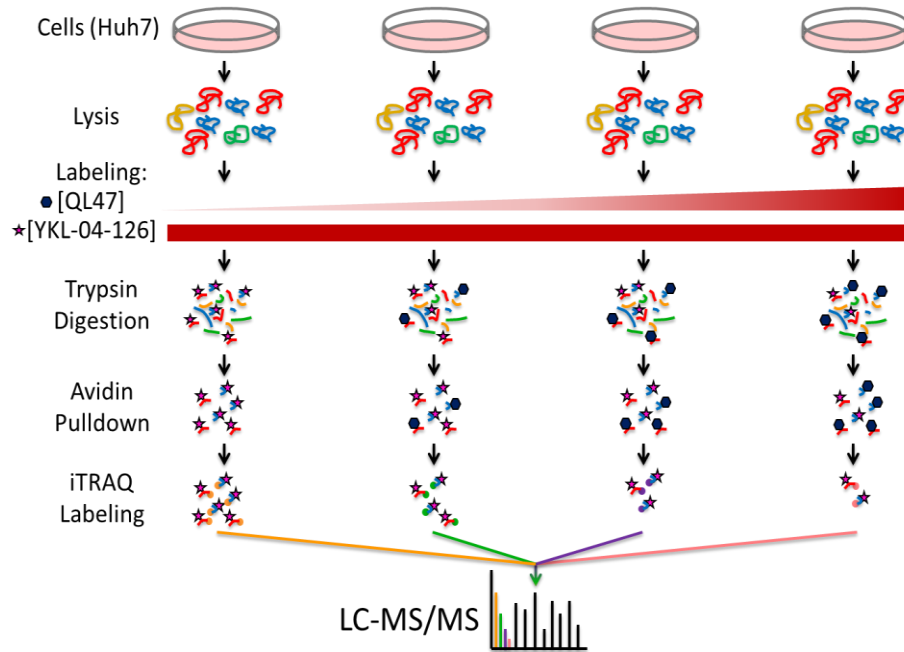
Figure 7-11 Covalent inhibitor target-site-identification and Liquid chromatography–mass spectrometry of QL-47 targeted proteins
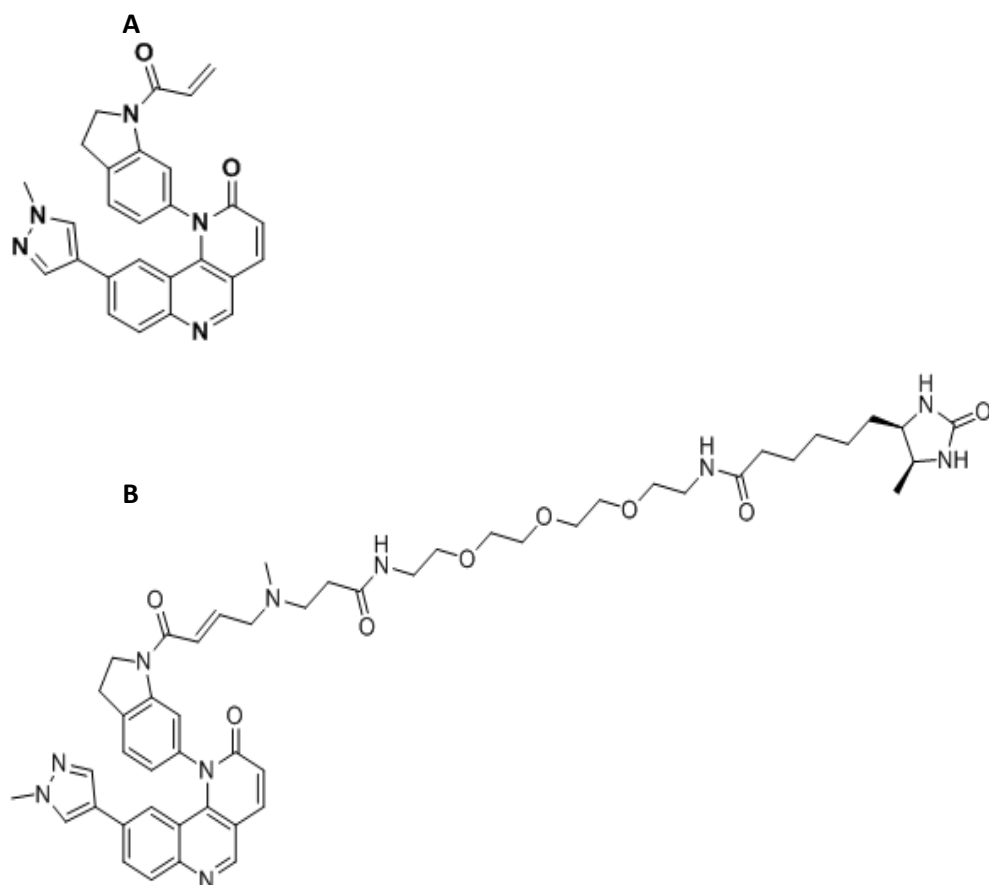
Inhibitor competition assay between a tagged (YKL-04-126) form of the covalent QL-47 inhibitor and QL-47. This assay screen 1656 proteins for QL-47 specific binding. Purified tagged inhibitor peptides were identified via Liquid chromatography–mass spectrometry (LC-MS/MS) to distinguish between true targets of QL-47 and non-specific interactions. DOCK9 was detected to have a very high degree of competitiveness for QL-47. QL-47 was determined to bind irreversibly to distinct cysteine residues on target proteins. For DOCK9 this residue is cysteine 628. Assays carried out and diagram generated by Dr Christopher Browne, of Prof. Nathanael Gray's research group (Dana Farber Cancer Institute Harvard Medical School, MA).
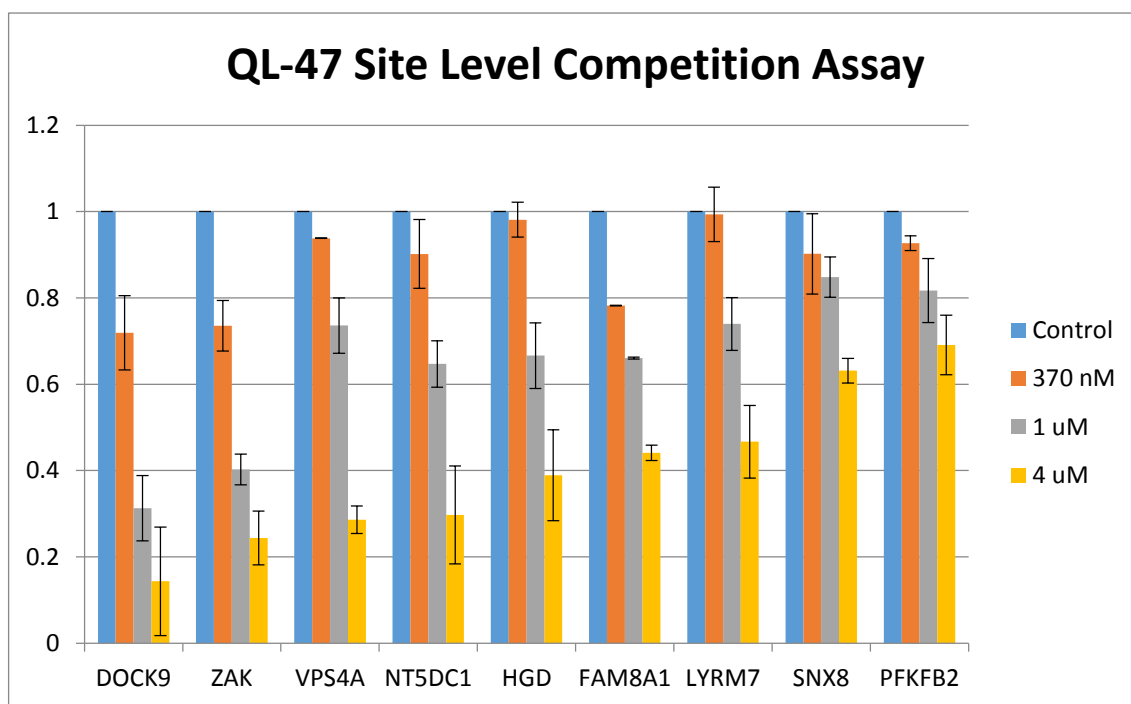
Figure 7-12 Proteins identified as targets of QL-47 through Covalent inhibitor target-site-identification and Liquid chromatography–mass spectrometry

Purified tagged inhibitor peptides were identified via Liquid chromatography–mass spectrometry (LC-MS/MS) following an inhibitor competition assay between a tagged (YKL-04-126) form of the covalent QL-47 inhibitor and QL-47; to distinguish between true targets of QL-47 and non-specific interactions. DOCK9 was detected to have a very high degree of competitiveness for QL-47. Of 1656 proteins screened, 9 were found as specific targets of QL-47. QL-47 was determined to bind irreversibly to distinct cysteine residues on DOCK9. Assays carried out by, and histogram generated by, Dr.Christopher Browne of Prof. Nathanael Gray's research group (Dana Farber Cancer Institute Harvard Medical School, MA).

7.3 Appendix 3. DOCK4 murine line genetic background
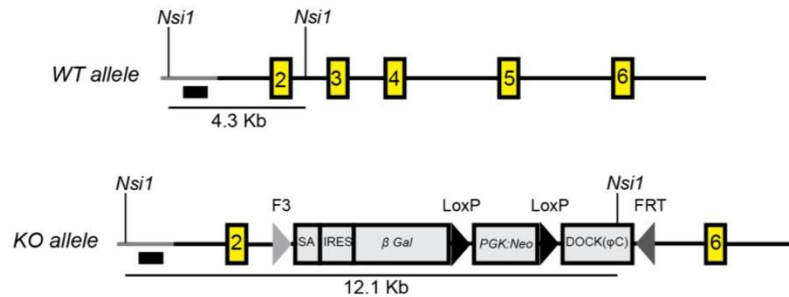
Figure 7-13 Retroviruses used in the in vivo tumour co-injection model and generation of the Dock4 het mouse line.

Schematic diagram showing the WT and the targeted KO Dock4 alleles. In the targeted allele, exons 3-5 were replaced by the targeting cassette for frameshift of the open reading frame. Yellow boxes show exons, main black lines show homology regions, grey lines show homology outside of the targeting vector. SA = Splice Acceptor, IRES = Internal Ribosomal Entry Site, β Gal= Beta galactosidase. Black boxes show position of the Southern probe that detects bands shown upon NsiI digestion for the purpose of genotyping. Figure provided by Dr. Georgia Mavria.

Figure 7-14 Schematic showing the EC Dock4 KO alleles and excision site of Dock4 exon 6.

Diagram depicting the targeted strategy for the EC Dock4 KO model, generated by Ozgene. Dock4$^{f/f}$ mice were crossed with VE-cadERT2-CreTd tomato gene carrying mice. FRT sites flanking, SA (splice acceptor), IRES (internal ribosomal entry site), β Gal (Beta galactosidase). Expression of FLP recombinase enzymes targets FRT sites, deleting the internal compartment. Cre recombinase expression, under the control of the VE-Cadherin reporter, targets and deletes the LoxP sites flank the Dock4 exon 6, and also Lox.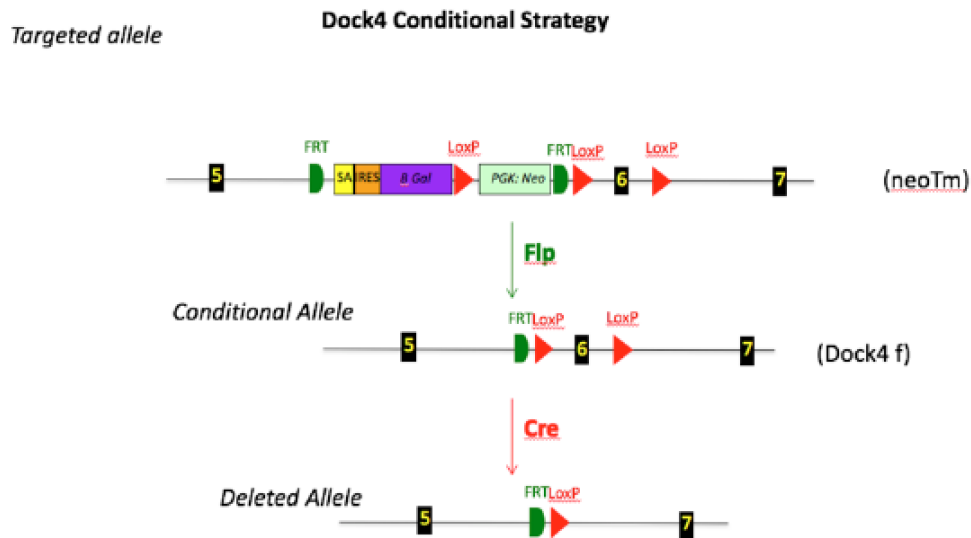 The Td Tomato gene lies downstream of a transcriptional/translational-floxed stop cassette, allowing for strong expression of the Td Tomato gene in the presence of Cre recombinase expression. The VE-cadERT2-CreTd tomato mouse line was originally generated by the lab of Prof. Ralf Adams (London Research Institute), and is commercially available via purchase from Taconic Biosciences (Germantown, NY USA). VE-cadERT2-CreTd tomato mouse line carries a gene for tamoxifen inducible Cre recombinase expression, under the control of the VE-Cadherin reporter. VE-cadERT2-CreTd tomato alleles not depicted within this diagram. Black boxes show exons, main black lines show homology regions. SA = Splice Acceptor; IRES = Internal Ribosomal Entry Site; B-gal = β-galactosidase; FR= FLP recombinase; PGK: Neo= Phosphoglycerine Kinase: neomycin resistance gene. Figure provided by Dr. Georgia Mavria.

8   References

Aaronson, P.I. et al. 2012. Mechanism of hydrogen sulfide mediated contraction in rat small pulmonary arteries. *The FASEB Journal.* **26**(1_supplement), pp.871.5-871.5.

Abo, A. et al. 1992. Reconstitution of neutrophil NADPH oxidase activity in the cell-free system by four components: p67-phox, p47-phox, p21rac1, and cytochrome b-245. *J Biol Chem.* **267**(24), pp.16767-70.

Abraham, S. et al. 2015. A Rac/Cdc42 exchange factor complex promotes formation of lateral filopodia and blood vessel lumen morphogenesis. *Nat Commun.* **6**.

Adair, T.H. and Montani, J.P. 2010. *Angiogenesis.* San Rafael (CA).

Adams, R.H. and Alitalo, K. 2007. Molecular regulation of angiogenesis and lymphangiogenesis. *Nat Rev Mol Cell Biol.* **8**(6), pp.464-78.

Alexandropoulos, K. et al. 1995. Proline-rich sequences that bind to Src homology 3 domains with individual specificities. *Proceedings of the National Academy of Sciences of the United States of America.* **92**(8), pp.3110-3114.

Alkelai, A. et al. 2012. DOCK4 and CEACAM21 as novel schizophrenia candidate genes in the Jewish population. *International Journal of Neuropsychopharmacology.* **15**(4), pp.459-469.

Andrianantoandro, E. et al. 2006. Synthetic biology: new engineering rules for an emerging discipline. *Molecular systems biology.* **2**, pp.2006.0028-2006.0028.

Antoniucci, D. et al. 2002. Relation between preintervention angiographic evidence of coronary collateral circulation and clinical and angiographic outcomes after primary angioplasty or stenting for acute myocardial infarction. *Am J Cardiol.* **89**(2), pp.121-5.

Arber, S. et al. 1998. Regulation of actin dynamics through phosphorylation of cofilin by LIM-kinase. *Nature.* **393**(6687), pp.805-809.

Aukland, K. and Reed, R.K. 1993. Interstitial-lymphatic mechanisms in the control of extracellular fluid volume. *Physiol Rev.* **73**(1), pp.1-78.

Aviles, R.J. et al. 2003. Testing clinical therapeutic angiogenesis using basic fibroblast growth factor (FGF-2). *Br J Pharmacol.* **140**(4), pp.637-46.

Barlow, H.R. and Cleaver, O. 2019. Building Blood Vessels-One Rho GTPase at a Time. *Cells.* **8**(6).

Barry, D.M. et al. 2015. Cdc42 is required for cytoskeletal support of endothelial cell adhesion during blood vessel formation in mice. *Development.* **142**(17), pp.3058-70.

Beenken, A. and Mohammadi, M. 2009. The FGF family: biology, pathophysiology and therapy. *Nat Rev Drug Discov.* **8**(3), pp.235-53.

Bennett, H.S. et al. 1959. Morphological classifications of vertebrate blood capillaries. *Am J Physiol.* **196**(2), pp.381-90.

Bishop, E. et al. 1999. An in vitro model of angiogenesis: Basic features. *Angiogenesis.* **3**, pp.335-44.

Blaber, M. et al. 1996. X-ray crystal structure of human acidic fibroblast growth factor. *Biochemistry.* **35**(7), pp.2086-94.

Blanco, R. and Gerhardt, H. 2013. VEGF and Notch in Tip and Stalk Cell Selection. *Cold Spring Harbor Perspectives in Medicine.* **3**(1), pa006569.

Bloustine, J. et al. 2003. Measurements of protein-protein interactions by size exclusion chromatography. *Biophysical journal.* **85**(4), pp.2619-2623.

Bobek, V. et al. 2006. Gene therapy of the ischemic lower limb--Therapeutic angiogenesis. *Vascul Pharmacol.* **44**(6), pp.395-405.

Bokoch, G.M. 1995. Regulation of the phagocyte respiratory burst by small GTP-binding proteins. *Trends Cell Biol.* **5**(3), pp.109-13.

Bosco, E.E. et al. 2009. Rac1 GTPase: a "Rac" of all trades. *Cell Mol Life Sci.* **66**(3), pp.370-4.

Brown, J.L. et al. 1996a. Human Ste20 homologue hPAK1 links GTPases to the JNK MAP kinase pathway. *Curr Biol.* **6**(5), pp.598-605.

Brown, K.J. et al. 1996b. A novel in vitro assay for human angiogenesis. *Lab Invest.* **75**(4), pp.539-55.

Brugnera, E. et al. 2002. Unconventional Rac-GEF activity is mediated through the Dock180-ELMO complex. *Nat Cell Biol.* **4**(8), pp.574-82.

Busch, F.M. et al. 2017. Analysis of proteins and protein interactions by size exclusion chromatography – high resolution mass spectrometry. *The FASEB Journal.* **31**(1_supplement), pp.926.9-926.9.

Byzova, T.V. et al. 2000. A mechanism for modulation of cellular responses to VEGF: activation of the integrins. *Mol Cell.* **6**(4), pp.851-60.

Cain, R.J. et al. 2010. The PI3K p110alpha isoform regulates endothelial adherens junctions via Pyk2 and Rac1. *J Cell Biol.* **188**(6), pp.863-76.

Caldwell, J.E. et al. 1989. Effects of CapZ, an actin capping protein of muscle, on the polymerization of actin. *Biochemistry.* **28**(21), pp.8506-14.

Cantatore, F.P. et al. 2017. Angiogenesis Dysregulation in the Pathogenesis of Systemic Sclerosis. *BioMed research international.* **2017**, pp.5345673-5345673.

Cao, J. et al. 2017. Polarized actin and VE-cadherin dynamics regulate junctional remodelling and cell migration during sprouting angiogenesis. *Nat Commun.* **8**(1), p2210.

Cao, R. et al. 2004. Comparative Evaluation of FGF-2–, VEGF-A–, and VEGF-C–Induced Angiogenesis, Lymphangiogenesis, Vascular Fenestrations, and Permeability. *Circulation Research.* **94**(5), pp.664-670.

Carmeliet, P. 2000. Mechanisms of angiogenesis and arteriogenesis. *Nat Med.* **6**(4), pp.389-95.

Carmeliet, P. 2003. Angiogenesis in health and disease. *Nat Med.* **9**(6), pp.653-60.

Caron, E. and Hall, A. 1998. Identification of two distinct mechanisms of phagocytosis controlled by different Rho GTPases. *Science.* **282**(5394), pp.1717-21.

Cheng, G. et al. 2006. Nox1-dependent reactive oxygen generation is regulated by Rac1. *J Biol Chem.* **281**(26), pp.17718-26.

Cheng, H. et al. 1996. Spinal cord repair in adult paraplegic rats: partial restoration of hind limb function. *Science.* **273**(5274), pp.510-3.

Cheng, H. et al. 2004. Spinal cord repair with acidic fibroblast growth factor as a treatment for a patient with chronic paraplegia. *Spine (Phila Pa 1976).* **29**(14), pp.E284-8.

Cherfils, J. and Zeghouf, M. 2013. Regulation of Small GTPases by GEFs, GAPs, and GDIs. *Physiological Reviews.* **93**(1), pp.269-309.

Chesarone, M.A. and Goode, B.L. 2009. Actin nucleation and elongation factors: mechanisms and interplay. *Curr Opin Cell Biol.* **21**(1), pp.28-37.

Chhabra, E.S. and Higgs, H.N. 2007. The many faces of actin: matching assembly factors with cellular structures. *Nat Cell Biol.* **9**(10), pp.1110-21.

Chiariello, M. et al. 2001. Regulation of c-myc expression by PDGF through Rho GTPases. *Nat Cell Biol.* **3**(6), pp.580-6.

Choi, K. et al. 1998. A common precursor for hematopoietic and endothelial cells. *Development.* **125**(4), pp.725-32.

Chrifi, I. et al. 2017. Cgnl1, an endothelial junction complex protein, regulates GTPase mediated angiogenesis. *Cardiovascular Research.* **113**(14), pp.1776-1788.

Cines, D.B. et al. 1998. Endothelial cells in physiology and in the pathophysiology of vascular disorders. *Blood.* **91**(10), pp.3527-61.

Clayton, J.A. et al. 2008. Vascular endothelial growth factor-A specifies formation of native collaterals and regulates collateral growth in ischemia. *Circ Res.* **103**(9), pp.1027-36.

Cleaver, O. and Melton, D.A. 2003. Endothelial signaling during development. *Nat Med.* **9**(6), pp.661-8.

Comerota, A.J. et al. 2002. Naked plasmid DNA encoding fibroblast growth factor type 1 for the treatment of end-stage unreconstructible lower extremity ischemia: preliminary results of a phase I trial. *J Vasc Surg.* **35**(5), pp.930-6.

Cook, D.R. et al. 2013. Rho guanine nucleotide exchange factors: regulators of Rho GTPase activity in development and disease. *Oncogene.* **33**, p4021.

Cooper, J.A. and Pollard, T.D. 1985. Effect of capping protein on the kinetics of actin polymerization. *Biochemistry.* **24**(3), pp.793-9.

Côté, J.-F. et al. 2005. A novel and evolutionarily conserved PtdIns (3, 4, 5) P 3-binding domain is necessary for DOCK180 signalling. *Nature cell biology.* **7**(8), p797.

Côté, J.-F. and Vuori, K. 2002. Identification of an evolutionarily conserved superfamily of DOCK180-related proteins with guanine nucleotide exchange activity. *Journal of Cell Science.* **115**(24), pp.4901-4913.

Cote, J.F. and Vuori, K. 2007. GEF what? Dock180 and related proteins help Rac to polarize cells in new ways. *Trends Cell Biol.* **17**(8), pp.383-93.

Côté, J.F. and Vuori, K. 2006. In Vitro Guanine Nucleotide Exchange Activity of DHR-2/DOCKER/CZH2 Domains. *Methods in Enzymology.*   Academic Press, pp.41-57.

Cuevas, P. et al. 1991. Hypotensive activity of fibroblast growth factor. *Science.* **254**(5035), pp.1208-10.

Cuevas, P. et al. 1996. Correction of hypertension by normalization of endothelial levels of fibroblast growth factor and nitric oxide synthase in spontaneously hypertensive rats. *Proc Natl Acad Sci U S A.* **93**(21), pp.11996-2001.

D'Amico, G. et al. 2009. Regulation of lymphatic-blood vessel separation by endothelial Rac1. *Development (Cambridge, England).* **136**(23), pp.4043-4053.

Dailey, L. et al. 2005. Mechanisms underlying differential responses to FGF signaling. *Cytokine Growth Factor Rev.* **16**(2), pp.233-47.

de Araujo, L.S. et al. 2016. Transcriptomic Biomarkers for Tuberculosis: Evaluation of DOCK9. EPHA4, and NPC2 mRNA Expression in Peripheral Blood. *Front Microbiol.* **7**, p1586.

De Souza, A.T. et al. 2006. Transcriptional and phenotypic comparisons of Ppara knockout and siRNA knockdown mice. **34**(16), pp.4486-4494.

Debidda, M. et al. 2006. Rac1 GTPase regulates cell genomic stability and senescence. *J Biol Chem.* **281**(50), pp.38519-28.

Debruin, E.J. et al. 2014. Podocalyxin regulates murine lung vascular permeability by altering endothelial cell adhesion. *PLoS One.* **9**(10), pe108881.

Debruyne, D.N. et al. 2018. DOCK4 promotes loss of proliferation in glioblastoma progenitor cells through nuclear beta-catenin accumulation and subsequent miR-302-367 cluster expression. *Oncogene.* **37**(2), pp.241-254.

DeLisser, H.M. 2011. Modulators of endothelial cell filopodia: PECAM-1 joins the club. *Cell Adhesion & Migration.* **5**(1), pp.37-41.

Detera-Wadleigh, S.D. et al. 2007. Sequence variation in DOCK9 and heterogeneity in bipolar disorder. *Psychiatr Genet.* **17**(5), pp.274-86.

Dor, Y. et al. 2002. Conditional switching of VEGF provides new insights into adult neovascularization and pro-angiogenic therapy. *Embo j.* **21**(8), pp.1939-47.

Drake, C.J. et al. 1998. Morphogenesis of the first blood vessels. *Ann N Y Acad Sci.* **857**, pp.155-79.

Egami, K. et al. 2006. Ischemia-induced angiogenesis: role of inflammatory response mediated by P-selectin. *J Leukoc Biol.* **79**(5), pp.971-6.

Egile, C. et al. 2005. Mechanism of filament nucleation and branch stability revealed by the structure of the Arp2/3 complex at actin branch junctions. *PLoS Biol.* **3**(11), pe383.

Ehrlich, J.S. et al. 2002. Spatio-temporal regulation of Rac1 localization and lamellipodia dynamics during epithelial cell-cell adhesion. *Dev Cell.* **3**(2), pp.259-70.

Eilken, H.M. and Adams, R.H. 2010. Dynamics of endothelial cell behavior in sprouting angiogenesis. *Curr. Opin. Cell Biol.* **22**, pp.617-625.

El-Brolosy, M.A. and Stainier, D.Y.R. 2017. Genetic compensation: A phenomenon in search of mechanisms. *PLoS genetics.* **13**(7), pp.e1006780-e1006780.

Elfenbein, A. et al. 2009. Suppression of RhoG activity is mediated by a syndecan 4-synectin-RhoGDI1 complex and is reversed by PKCalpha in a Rac1 activation pathway. *J Cell Biol.* **186**(1), pp.75-83.

Ellerbroek, S.M. et al. 2004. SGEF, a RhoG guanine nucleotide exchange factor that stimulates macropinocytosis. *Molecular biology of the cell.* **15**(7), pp.3309-3319.

Estrach, S. et al. 2002. The Human Rho-GEF trio and its target GTPase RhoG are involved in the NGF pathway, leading to neurite outgrowth. *Curr Biol.* **12**(4), pp.307-12.

Etienne-Manneville, S. 2004. Cdc42 - the centre of polarity. *Journal of Cell Science.* **117**(8), pp.1291-1300.

Etienne-Manneville, S. and Hall, A. 2002. Rho GTPases in cell biology. *Nature.* **420**(6916), pp.629-635.

Faber, J.E. et al. 2014. A brief etymology of the collateral circulation. *Arterioscler Thromb Vasc Biol.* **34**(9), pp.1854-9.

Fehrenbach, M.L. et al. 2009. Isolation of murine lung endothelial cells. *American journal of physiology. Lung cellular and molecular physiology.* **296**(6), pp.L1096-L1103.

Ferrandez, Y. et al. 2017. Allosteric inhibition of the guanine nucleotide exchange factor DOCK5 by a small molecule. *Scientific reports.* **7**(1), pp.14409-14409.

Ferraro, B. et al. 2010. Increased perfusion and angiogenesis in a hindlimb ischemia model with plasmid FGF-2 delivered by noninvasive electroporation. *Gene Ther.* **17**(6), pp.763-9.

Fischer, R.S. et al. 2009. Local Cortical Tension by Myosin II Guides 3D Endothelial Cell Branching. *Current Biology.* **19**(3), pp.260-265.

Fletcher, D.A. and Mullins, R.D. 2010. Cell mechanics and the cytoskeleton. *Nature.* **463**(7280), pp.485-492.

Fong, G.H. et al. 1995. Role of the Flt-1 receptor tyrosine kinase in regulating the assembly of vascular endothelium. *Nature.* **376**(6535), pp.66-70.

Free, R.B. et al. 2009. Identifying novel protein-protein interactions using co-immunoprecipitation and mass spectroscopy. *Current protocols in neuroscience.* **Chapter 5**, pp.Unit-5.28.

Frost, J.A. et al. 1996. Actions of Rho family small G proteins and p21-activated protein kinases on mitogen-activated protein kinase family members. *Mol Cell Biol.* **16**(7), pp.3707-13.

Fujii, T. et al. 2008. VEGF function for upregulation of endogenous PlGF expression during FGF-2-mediated therapeutic angiogenesis. *Atherosclerosis.* **200**(1), pp.51-7.

Gadea, G. and Blangy, A. 2014. Dock-family exchange factors in cell migration and disease. *Eur J Cell Biol.* **93**(10-12), pp.466-77.

Galan Moya, E.M. et al. 2009. PAKing up to the endothelium. *Cell Signal.* **21**(12), pp.1727-37.

Galley, H.F. and Webster, N.R. 2004. Physiology of the endothelium. *Br J Anaesth.* **93**(1), pp.105-13.

Gao, Y. et al. 2000. Synectin, syndecan-4 cytoplasmic domain binding PDZ protein, inhibits cell migration. *J Cell Physiol.* **184**(3), pp.373-9.

Gardner, A.W. and Poehlman, E.T. 1995. Exercise rehabilitation programs for the treatment of claudication pain. A meta-analysis. *JAMA.* **274**(12), pp.975-80.

Gebala, V. et al. 2016. Blood flow drives lumen formation by inverse membrane blebbing during angiogenesis in vivo. *Nat Cell Biol.* **18**(4), pp.443-50.

Gerhardt, H. et al. 2003. VEGF guides angiogenic sprouting utilizing endothelial tip cell filopodia. *J Cell Biol.* **161**(6), pp.1163-77.

Ghosh, R. et al. 2014. The necessity of and strategies for improving confidence in the accuracy of western blots. *Expert review of proteomics.* **11**(5), pp.549-560.

Gospodarowicz, D. et al. 1977. Control of proliferation of bovine vascular endothelial cells. *J Cell Physiol.* **91**(3), pp.377-85.

Govek, E.-E. et al. 2005. The role of the Rho GTPases in neuronal development. *Genes & Development.* **19**(1), pp.1-49.

Grant, M.A. and Karsan, A. 2018. Chapter 123 - The Blood Vessel Wall. In: Hoffman, R., et al. eds. *Hematology (Seventh Edition).*   Elsevier, pp.1843-1856.e6.

Guo, D. et al. 2007. A Rac-cGMP signaling pathway. *Cell.* **128**(2), pp.341-55.

Hall, A. 1998. Rho GTPases and the Actin Cytoskeleton. *Science.* **279**(5350), pp.509-514.

Hall, A. 2012. Rho family GTPases. *Biochemical Society Transactions.* **40**(6), pp.1378-1382.

Hall, R.A. 2005. Co-immunoprecipitation as a strategy to evaluate receptorreceptor or receptor-protein interactions. *G Protein-Coupled Receptor-Protein Interactions. John Wiley & Sons, New York.* pp.165-178.

Hanawa-Suetsugu, K. et al. 2012. Structural basis for mutual relief of the Rac guanine nucleotide exchange factor DOCK2 and its partner ELMO1 from their autoinhibited forms. *Proceedings of the National Academy of Sciences of the United States of America.* **109**(9), pp.3305-3310.

Harada, Y. et al. 2012. DOCK8 is a Cdc42 activator critical for interstitial dendritic cell migration during immune responses. *Blood.* **119**(19), pp.4451-61.

He, Y. et al. 2006. Critical function of Bmx/Etk in ischemia-mediated arteriogenesis and angiogenesis. *The Journal of clinical investigation.* **116**(9), pp.2344-2355.

Heil, M. et al. 2006. Arteriogenesis versus angiogenesis: similarities and differences. *J Cell Mol Med.* **10**(1), pp.45-55.

Hellingman, A.A. et al. 2010. Variations in Surgical Procedures for Hind Limb Ischaemia Mouse Models Result in differences in Collateral Formation. *European Journal of Vascular and Endovascular Surgery.* **40**(6), pp.796-803.

Hellstrom, M. et al. 2007. Dll4 signalling through Notch1 regulates formation of tip cells during angiogenesis. *Nature.* **445**(7129), pp.776-80.

Herold, J. et al. 2017. Factor VII activating protease (FSAP) influences vascular remodeling in the mouse hind limb ischemia model. *American journal of translational research.* **9**(6), pp.3084-3095.

Hetheridge, C. et al. 2011. Uses of the in vitro endothelial-fibroblast organotypic co-culture assay in angiogenesis research. *Biochem Soc Trans.* **39**(6), pp.1597-600.

Hiramoto-Yamaki, N. et al. 2010. Ephexin4 and EphA2 mediate cell migration through a RhoG-dependent mechanism. *The Journal of Cell Biology.* **190**(3), pp.461-477.

Hiratsuka, S. et al. 1998. Flt-1 lacking the tyrosine kinase domain is sufficient for normal development and angiogenesis in mice. *Proc Natl Acad Sci U S A.* **95**(16), pp.9349-54.

Hirschi, K.K. and D'Amore, P.A. 1996. Pericytes in the microvasculature. *Cardiovasc Res.* **32**(4), pp.687-98.

Hoang, M.V. et al. 2011. Cdc42-mediated inhibition of GSK-3beta improves angio-architecture and lumen formation during VEGF-driven pathological angiogenesis. *Microvasc Res.* **81**(1), pp.34-43.

Hoeppner, L.H. et al. 2015. RhoC maintains vascular homeostasis by regulating VEGF-induced signaling in endothelial cells. *J Cell Sci.* **128**(19), pp.3556-68.

Holmes, K.C. et al. 1990. Atomic model of the actin filament. *Nature.* **347**(6288), pp.44-49.

Hori, Y. et al. 2017. Functional Characterization of VEGF- and FGF-induced Tumor Blood Vessel Models in Human Cancer Xenografts. *Anticancer Res.* **37**(12), pp.6629-6638.

Horowitz, A. et al. 1999. Phosphatidylinositol-4,5-bisphosphate Mediates the Interaction of Syndecan-4 with Protein Kinase C. *Biochemistry.* **38**(48), pp.15871-15877.

Hutley, L. et al. 2004. Fibroblast growth factor 1: a key regulator of human adipogenesis. *Diabetes.* **53**(12), pp.3097-106.

Huttala, O. et al. 2015. Human vascular model with defined stimulation medium - a characterization study. *Altex.* **32**(2), pp.125-36.

Ichetovkin, I. et al. 2002. Cofilin produces newly polymerized actin filaments that are preferred for dendritic nucleation by the Arp2/3 complex. *Curr Biol.* **12**(1), pp.79-84.

Irani, K. et al. 1997. Mitogenic signaling mediated by oxidants in Ras-transformed fibroblasts. *Science.* **275**(5306), pp.1649-52.

Iruela-Arispe, L., Zovein, A. 2017. Angiogenesis Fetal and Neonatal Physiology (Fifth Edition). In: Polin, R.A. ed. *Fetal and Neonatal Physiology.* Elsevier, pp.85-89.e2.

Iruela-Arispe, M.L. and Davis, G.E. 2009. Cellular and molecular mechanisms of vascular lumen formation. *Dev Cell.* **16**(2), pp.222-31.

Iwakura, A. et al. 2000. Myocardial ischemia enhances the expression of acidic fibroblast growth factor in human pericardial fluid. *Heart Vessels.* **15**(3), pp.112-6.

Jakobsson, L. et al. 2010. Endothelial cells dynamically compete for the tip cell position during angiogenic sprouting. *Nat Cell Biol.* **12**(10), pp.943-53.

Javerzat, S. et al. 2002. The role of fibroblast growth factors in vascular development. *Trends in molecular medicine.* **8**(10), pp.483-489.

Jo, Y.J. et al. 2015. Actin-capping proteins play essential roles in the asymmetric division of maturing mouse oocytes. *J Cell Sci.* **128**(1), pp.160-70.

Joneson, T. and Bar-Sagi, D. 1998. A Rac1 Effector Site Controlling Mitogenesis through Superoxide Production. *Journal of Biological Chemistry.* **273**(29), pp.17991-17994.

Karolak, J.A. et al. 2016. Molecular Screening of Keratoconus Susceptibility Sequence Variants in VSX1, TGFBI, DOCK9, STK24, and IPO5 Genes in Polish Patients and Novel TGFBI Variant Identification. *Ophthalmic Genet.* **37**(1), pp.37-43.

Katoh, H. et al. 2006. Activation of Rac1 by RhoG regulates cell migration. *Journal of Cell Science.* **119**(1), pp.56-65.

Katoh, H. and Negishi, M. 2003. RhoG activates Rac1 by direct interaction with the Dock180-binding protein Elmo. *Nature.* **424**(6947), pp.461-4.

Keller, M. et al. 2008. Active caspase-1 is a regulator of unconventional protein secretion. *Cell.* **132**(5), pp.818-31.

Khurana, R. and Simons, M. 2003. Insights from angiogenesis trials using fibroblast growth factor for advanced arteriosclerotic disease. *Trends Cardiovasc Med.* **13**(3), pp.116-22.

Kitamura, M. et al. 2008. Periodontal tissue regeneration using fibroblast growth factor-2: randomized controlled phase II clinical trial. *PLoS One.* **3**(7), pe2611.

Kobayashi, S. et al. 2001. Membrane recruitment of DOCK180 by binding to PtdIns (3, 4, 5) P3. *Biochemical Journal.* **354**(1), pp.73-78.

Koh, W. et al. 2008. Cdc42- and Rac1-mediated endothelial lumen formation requires Pak2, Pak4 and Par3, and PKC-dependent signaling. *Journal of Cell Science.* **121**(7), pp.989-1001.

Kozma, R. et al. 1995. The Ras-related protein Cdc42Hs and bradykinin promote formation of peripheral actin microspikes and filopodia in Swiss 3T3 fibroblasts. *Molecular and cellular biology.* **15**(4), pp.1942-1952.

Krugmann, S. 2001. Cdc42 induces filopodia by promoting the formation of an IRSp53:Mena complex. *Curr. Biol.* **11**, pp.1645-1655.

Kulkarni, K. et al. 2011. Multiple factors confer specific Cdc42 and Rac protein activation by dedicator of cytokinesis (DOCK) nucleotide exchange factors. *J Biol Chem.* **286**(28), pp.25341-51.

Kumar, V.B. et al. 2007. Endothelial cell response to lactate: implication of PAR modification of VEGF. *J Cell Physiol.* **211**(2), pp.477-85.

Kuramoto, K. et al. 2009. Regulation of dendrite growth by the Cdc42 activator Zizimin1/Dock9 in hippocampal neurons. *J Neurosci Res.* **87**(8), pp.1794-805.

Laham, R.J. et al. 1999. Intracoronary and intravenous administration of basic fibroblast growth factor: myocardial and tissue distribution. *Drug Metab Dispos.* **27**(7), pp.821-6.

Lammert, E. and Axnick, J. 2012. Vascular lumen formation. *Cold Spring Harb Perspect Med.* **2**(4), pa006619.

Laurin, M. and Côté, J.-F. 2014. Insights into the biological functions of Dock family guanine nucleotide exchange factors. *Genes & development.* **28**(6), pp.533-547.

Lawson, N.D. et al. 2002. sonic hedgehog and vascular endothelial growth factor act upstream of the Notch pathway during arterial endothelial differentiation. *Dev Cell.* **3**(1), pp.127-36.

Lazarous, D.F. et al. 2000. Basic fibroblast growth factor in patients with intermittent claudication: results of a phase I trial. *J Am Coll Cardiol.* **36**(4), pp.1239-44.

Lee, J.G. and Kay, E.P. 2006. Cross-talk among Rho GTPases acting downstream of PI 3-kinase induces mesenchymal transformation of corneal endothelial cells mediated by FGF-2. *Invest Ophthalmol Vis Sci.* **47**(6), pp.2358-68.

Lim, K.B. et al. 2008. The Cdc42 effector IRSp53 generates filopodia by coupling membrane protrusion with actin dynamics. *J Biol Chem.* **283**(29), pp.20454-72.

Limbourg, A. et al. 2009. Evaluation of postnatal arteriogenesis and angiogenesis in a mouse model of hind-limb ischemia. *Nature Protocols.* **4**, p1737.

Lin, P.H. et al. 2005. Spinal cord implantation with acidic fibroblast growth factor as a treatment for root avulsion in obstetric brachial plexus palsy. *J Chin Med Assoc.* **68**(8), pp.392-6.

Lizama, C.O. and Zovein, A.C. 2013. Polarizing pathways: balancing endothelial polarity, permeability, and lumen formation. *Experimental cell research.* **319**(9), pp.1247-1254.

Luo, Y. et al. 2010. Endothelial-specific transgenesis of TNFR2 promotes adaptive arteriogenesis and angiogenesis. *Arteriosclerosis, thrombosis, and vascular biology.* **30**(7), pp.1307-1314.

Machacek, M. et al. 2009. Coordination of Rho GTPase activities during cell protrusion. *Nature.* **461**(7260), pp.99-103.

Maciag, T. et al. 1981. Serial propagation of human endothelial cells in vitro. *J Cell Biol.* **91**(2 Pt 1), pp.420-6.

Marcotte, E.M. and Tsechansky, M. 2009. Disorder, promiscuity, and toxic partnerships. *Cell.* **138**(1), pp.16-18.

Martin, K. et al. 2016. Spatio-temporal co-ordination of RhoA, Rac1 and Cdc42 activation during prototypical edge protrusion and retraction dynamics. *Sci Rep.* **6**, p21901.

Maruotti, N. et al. 2006. Angiogenesis in rheumatoid arthritis.

Maruotti, N. et al. 2008. Angiogenesis in vasculitides. **26**(3), p476.

Mattila, P.K. and Lappalainen, P. 2008. Filopodia: molecular architecture and cellular functions. *Nat Rev Mol Cell Biol.* **9**(6), pp.446-54.

Matucci-Cerinic, M. et al. 2013. Evidence that systemic sclerosis is a vascular disease. **65**(8), pp.1953-1962.

Mavria, G. et al. 2006. ERK-MAPK signaling opposes Rho-kinase to promote endothelial cell survival and sprouting during angiogenesis. *Cancer Cell.* **9**(1), pp.33-44.

Meller, N. et al. 2002. Zizimin1, a novel Cdc42 activator, reveals a new GEF domain for Rho proteins. *Nat Cell Biol.* **4**(9), pp.639-47.

Meller, N. et al. 2004. The novel Cdc42 guanine nucleotide exchange factor, zizimin1, dimerizes via the Cdc42-binding CZH2 domain. *J Biol Chem.* **279**(36), pp.37470-6.

Meller, N. et al. 2005. CZH proteins: a new family of Rho-GEFs. *J Cell Sci.* **118**(Pt 21), pp.4937-46.

Meller, N. et al. 2008. Function of the N-terminus of zizimin1: autoinhibition and membrane targeting. *Biochem J.* **409**(2), pp.525-33.

Merks, R.M. et al. 2006. Cell elongation is key to in silico replication of in vitro vasculogenesis and subsequent remodeling. *Dev Biol.* **289**(1), pp.44-54.

Miki, H. et al. 2000. IRSp53 is an essential intermediate between Rac and WAVE in the regulation of membrane ruffling. *Nature.* **408**(6813), pp.732-735.

Miller, D.L. et al. 2000. Compensation by fibroblast growth factor 1 (FGF1) does not account for the mild phenotypic defects observed in FGF2 null mice. *Mol Cell Biol.* **20**(6), pp.2260-8.

Mitola, S. et al. 2010. Gremlin is a novel agonist of the major proangiogenic receptor VEGFR2. *Blood.* **116**(18), pp.3677-80.

Miyamoto, Y. et al. 2013. Akt and PP2A reciprocally regulate the guanine nucleotide exchange factor Dock6 to control axon growth of sensory neurons. *Sci Signal.* **6**(265), pra15.

Movilla, N. and Bustelo, X.R. 1999. Biological and regulatory properties of Vav-3, a new member of the Vav family of oncoproteins. *Mol Cell Biol.* **19**(11), pp.7870-85.

Nagata, K. et al. 1998. The MAP kinase kinase kinase MLK2 co-localizes with activated JNK along microtubules and associates with kinesin superfamily motor KIF3. *EMBO J.* **17**(1), pp.149-58.

Niiyama, H. et al. 2009. Murine model of hindlimb ischemia. *Journal of visualized experiments : JoVE.* (23), p1035.

Nikol, S. et al. 2008. Therapeutic Angiogenesis With Intramuscular NV1FGF Improves Amputation-free Survival in Patients With Critical Limb Ischemia. *Mol Ther.* **16**(5), pp.972-978.

Nishikimi, A. et al. 2009. Sequential regulation of DOCK2 dynamics by two phospholipids during neutrophil chemotaxis. *Science.* **324**(5925), pp.384-387.

Nobes, C. and Marsh, M. 2000. Dendritic cells: new roles for Cdc42 and Rac in antigen uptake? *Curr Biol.* **10**(20), pp.R739-41.

Norgren, L. et al. 2007. Inter-Society Consensus for the Management of Peripheral Arterial Disease (TASC II). *Eur J Vasc Endovasc Surg.* **33 Suppl 1**, pp.S1-75.

Noritake, J. et al. 2005. IQGAP1: a key regulator of adhesion and migration. *J Cell Sci.* **118**(Pt 10), pp.2085-92.

Oda, T. and Maéda, Y. 2010. Multiple Conformations of F-actin. *Structure.* **18**(7), pp.761-767.

Olsen, S.K. et al. 2003. Fibroblast growth factor (FGF) homologous factors share structural but not functional homology with FGFs. *J Biol Chem.* **278**(36), pp.34226-36.

Olson, M.F. et al. 1995. An essential role for Rho, Rac, and Cdc42 GTPases in cell cycle progression through G1. *Science.* **269**(5228), pp.1270-2.

Ornitz, D.M. and Itoh, N. 2001. Fibroblast growth factors. *Genome Biol.* **2**(3), pREVIEWS3005.

Ornitz, D.M. and Itoh, N. 2015. The Fibroblast Growth Factor signaling pathway. *Wiley interdisciplinary reviews. Developmental biology.* **4**(3), pp.215-266.

Pagnamenta, A.T. et al. 2010. Characterization of a family with rare deletions in CNTNAP5 and DOCK4 suggests novel risk loci for autism and dyslexia. *Biological psychiatry.* **68**(4), pp.320-328.

Partovian, C. et al. 2008. Syndecan-4 regulates subcellular localization of mTOR Complex2 and Akt activation in a PKCα-dependent manner in endothelial cells. *Molecular cell.* **32**(1), pp.140-149.

Patel, M. et al. 2011. Opening up on ELMO regulation: New insights into the control of Rac signaling by the DOCK180/ELMO complex. *Small GTPases.* **2**(5), pp.268-275.

Pepper, M.S. and Skobe, M. 2003. Lymphatic endothelium: morphological, molecular and functional properties. *J Cell Biol.* **163**(2), pp.209-13.

Phng, L.K. et al. 2013. Filopodia are dispensable for endothelial tip cell guidance. *Development.* **140**(19), pp.4031-40.

Polakis, P. 2000. Wnt signaling and cancer. *Genes & Development.* **14**(15), pp.1837-1851.

Pollard, T.D. et al. 2016. *Cell Biology E-Book.* Elsevier Health Sciences.

Potente, M. et al. 2011. Basic and Therapeutic Aspects of Angiogenesis. *Cell.* **146**(6), pp.873-887.

Presta, M. et al. 2005. Fibroblast growth factor/fibroblast growth factor receptor system in angiogenesis. *Cytokine Growth Factor Rev.* **16**(2), pp.159-78.

Prieto-Sanchez, R.M. et al. 2006. Involvement of the Rho/Rac family member RhoG in caveolar endocytosis. *Oncogene.* **25**(21), pp.2961-73.

Ramo, K. et al. 2016. Suppression of ischemia in arterial occlusive disease by JNK-promoted native collateral artery development. *Elife.* **5**.

Ressad, F. et al. 1998. Kinetic Analysis of the Interaction of Actin-depolymerizing Factor (ADF)/Cofilin with G- and F-Actins: COMPARISON OF PLANT AND HUMAN ADFs AND EFFECT OF PHOSPHORYLATION. *Journal of Biological Chemistry.* **273**(33), pp.20894-20902.

Rissanen, T.T. et al. 2001. Gene therapy for therapeutic angiogenesis in critically ischaemic lower limb - on the way to the clinic. *Eur J Clin Invest.* **31**(8), pp.651-66.

Rizov, M. et al. 2017. Molecular regulation and role of angiogenesis in reproduction. *Taiwanese Journal of Obstetrics and Gynecology.* **56**(2), pp.127-132.

Robeer, G.G. et al. 1998. Exercise therapy for intermittent claudication: a review of the quality of randomised clinical trials and evaluation of predictive factors. *Eur J Vasc Endovasc Surg.* **15**(1), pp.36-43.

Rodrigues, S.F. and Granger, D.N. 2015. Blood cells and endothelial barrier function. *Tissue Barriers.* **3**(1-2), pe978720.

Rohatgi, R. et al. 1999. The interaction between N-WASP and the Arp2/3 complex links Cdc42-dependent signals to actin assembly. *Cell.* **97**(2), pp.221-31.

Rossman, K.L. et al. 2005. GEF means go: turning on RHO GTPases with guanine nucleotide-exchange factors. *Nat Rev Mol Cell Biol.* **6**(2), pp.167-80.

Ruan, G.X. and Kazlauskas, A. 2013. Lactate engages receptor tyrosine kinases Axl, Tie2, and vascular endothelial growth factor receptor 2 to activate phosphoinositide 3-kinase/Akt and promote angiogenesis. *J Biol Chem.* **288**(29), pp.21161-72.

Rucker, H.K. et al. 2000. Cellular mechanisms of CNS pericytes. *Brain Res Bull.* **51**(5), pp.363-9.

Ruiz-Lafuente, N. et al. 2018. DOCK9 induces membrane ruffles and Rac1 activity in cancer HeLa epithelial cells. *Biochem Biophys Rep.* **14**, pp.178-181.

Sadok, A. and Marshall, C.J. 2014. Rho GTPases: Masters of cell migration. *Small GTPases.* **5**, pe29710.

Sakurai, Y. et al. 2005. Essential role of Flk-1 (VEGF receptor 2) tyrosine residue 1173 in vasculogenesis in mice. *Proc Natl Acad Sci U S A.* **102**(4), pp.1076-81.

Sandoo, A. et al. 2010. The endothelium and its role in regulating vascular tone. *Open Cardiovasc Med J.* **4**, pp.302-12.

Sanematsu, F. et al. 2013. Phosphatidic acid-dependent recruitment and function of the Rac activator DOCK1 during dorsal ruffle formation. *Journal of Biological Chemistry.* **288**(12), pp.8092-8100.

Sase, H. et al. 2009. VEGFR2-PLCgamma1 axis is essential for endothelial specification of VEGFR2+ vascular progenitor cells. *J Cell Sci.* **122**(Pt 18), pp.3303-11.

Schaad, L. et al. 2017. Correlative Imaging of the Murine Hind Limb Vasculature and Muscle Tissue by MicroCT and Light Microscopy. *Scientific Reports.* **7**(1), p41842.

Schaper, W. 2009. Collateral circulation. *Basic Research in Cardiology.* **104**(1), pp.5-21.

Schmid-Schönbein, G.W. 1990. Mechanisms causing initial lymphatics to expand and compress to promote lymph flow. *Archives of histology and cytology.* **53**(Supplement), pp.107-114.

Scholz, D. et al. 2001. Arteriogenesis, a new concept of vascular adaptation in occlusive disease. *Angiogenesis.* **4**(4), pp.247-57.

Schuebel, K.E. et al. 1998. Phosphorylation-dependent and constitutive activation of Rho proteins by wild-type and oncogenic Vav-2. *EMBO J.* **17**(22), pp.6608-21.

Schumacher, B. et al. 1998. Induction of neoangiogenesis in ischemic myocardium by human growth factors: first clinical results of a new treatment of coronary heart disease. *Circulation.* **97**(7), pp.645-50.

Serna, M. 2019. Hands on Methods for High Resolution Cryo-Electron Microscopy Structures of Heterogeneous Macromolecular Complexes. *Front Mol Biosci.* **6**, p33.

Shalaby, F. et al. 1995. Failure of blood-island formation and vasculogenesis in Flk-1-deficient mice. *Nature.* **376**(6535), pp.62-6.

Shepherd, J. 1983. *Handbook of physiology, section 2, the cardiovascular system, Vol. III, peripheral circulation and organ blood flow*. Bethesda: American Physiological Society.

Shibuya, M. 2013. VEGFR and type-V RTK activation and signaling. *Cold Spring Harb Perspect Biol.* **5**(10), pa009092.

Shin, E.-Y. et al. 2004. Basic fibroblast growth factor stimulates activation of Rac1 through a p85 βPIX phosphorylation-dependent pathway. **279**(3), pp.1994-2004.

Shing, Y. et al. 1984. Heparin affinity: purification of a tumor-derived capillary endothelial cell growth factor. *Science.* **223**(4642), pp.1296-9.

Sigurbjornsdottir, S. et al. 2014. Molecular mechanisms of de novo lumen formation. *Nat Rev Mol Cell Biol.* **15**(10), pp.665-76.

Simons, M. and Eichmann, A. 2015. Molecular controls of arterial morphogenesis. *Circ Res.* **116**(10), pp.1712-24.

Simons, M. et al. 2016. Mechanisms and regulation of endothelial VEGF receptor signalling. *Nat Rev Mol Cell Biol.* **17**(10), pp.611-25.

Smallwood, P.M. et al. 1996. Fibroblast growth factor (FGF) homologous factors: new members of the FGF family implicated in nervous system development. *Proc Natl Acad Sci U S A.* **93**(18), pp.9850-7.

Sommer, F. et al. 2014. Identification and validation of protein-protein interactions by combining co-immunoprecipitation, antigen competition, and stable isotope labeling. *Stable Isotope Labeling by Amino Acids in Cell Culture (SILAC).* Springer, pp.245-261.

Stegmann, T.J. 1998. FGF-1: a human growth factor in the induction of neoangiogenesis. *Expert Opin Investig Drugs.* **7**(12), pp.2011-5.

Strilic, B. et al. 2009. The molecular basis of vascular lumen formation in the developing mouse aorta. *Dev Cell.* **17**(4), pp.505-15.

Stryker, Z.I. et al. 2019. Evaluation of Angiogenesis Assays. **7**(2), p37.

Sugihara, K. et al. 1998. Rac1 is required for the formation of three germ layers during gastrulation. *Oncogene.* **17**(26), pp.3427-3433.

Takahashi, T. and Shibuya, M. 1997. The 230 kDa mature form of KDR/Flk-1 (VEGF receptor-2) activates the PLC-gamma pathway and partially induces mitotic signals in NIH3T3 fibroblasts. *Oncogene.* **14**(17), pp.2079-89.

Takahashi, T. et al. 1999. VEGF activates protein kinase C-dependent, but Ras-independent Raf-MEK-MAP kinase pathway for DNA synthesis in primary endothelial cells. *Oncogene.* **18**(13), pp.2221-30.

Takahashi, T. et al. 2001. A single autophosphorylation site on KDR/Flk-1 is essential for VEGF-A-dependent activation of PLC-gamma and DNA synthesis in vascular endothelial cells. *The EMBO journal.* **20**(11), pp.2768-2778.

Tan, W. et al. 2008. An essential role for Rac1 in endothelial cell function and vascular development. *The FASEB Journal.* **22**(6), pp.1829-1838.

Teramoto, H. et al. 1996. Signaling from the small GTP-binding proteins Rac1 and Cdc42 to the c-Jun N-terminal kinase/stress-activated protein kinase pathway. A role for mixed lineage kinase 3/protein-tyrosine kinase 1, a novel member of the mixed lineage kinase family. *J Biol Chem.* **271**(44), pp.27225-8.

Thornton, S. et al. 1983. Human endothelial cells: use of heparin in cloning and long-term serial cultivation. *Science.* **222**(4624), pp.623-625.

Tkachenko, E. et al. 2004. Fibroblast growth factor 2 endocytosis in endothelial cells proceed via syndecan-4-dependent activation of Rac1 and a Cdc42-dependent macropinocytic pathway. *J Cell Sci.* **117**(Pt 15), pp.3189-99.

Trueb, B. et al. 2013. Role of FGFRL1 and other FGF signaling proteins in early kidney development. *Cellular and molecular life sciences.* **70**(14), pp.2505-2518.

Tsuchida, R. et al. 2008. Cisplatin treatment increases survival and expansion of a highly tumorigenic side-population fraction by upregulating VEGF/Flt1 autocrine signaling. *Oncogene.* **27**(28), pp.3923-34.

Ucuzian, A.A. et al. 2010. Molecular mediators of angiogenesis. *J Burn Care Res.* **31**(1), pp.158-75.

Udan, R.S. et al. 2013. Understanding vascular development. *Wiley Interdiscip Rev Dev Biol.* **2**(3), pp.327-46.

Ueda, S. et al. 2013. Rac GEF Dock4 interacts with cortactin to regulate dendritic spine formation. *Molecular biology of the cell.* **24**(10), pp.1602-1613.

Unger, E.F. et al. 2000. Effects of a single intracoronary injection of basic fibroblast growth factor in stable angina pectoris. *Am J Cardiol.* **85**(12), pp.1414-9.

Upadhyay, G. et al. 2008. Molecular association between beta-catenin degradation complex and Rac guanine exchange factor DOCK4 is essential for Wnt/beta-catenin signaling. *Oncogene.* **27**(44), pp.5845-55.

Uriel, S. et al. 2006. Sustained low levels of fibroblast growth factor-1 promote persistent microvascular network formation. *Am J Surg.* **192**(5), pp.604-9.

Vailhé, B. et al. 2001. In Vitro Models of Vasculogenesis and Angiogenesis. *Laboratory Investigation.* **81**(4), pp.439-452.

van Royen, N. et al. 2001. Stimulation of arteriogenesis; a new concept for the treatment of arterial occlusive disease. *Cardiovascular Research.* **49**(3), pp.543-553.

Vanlandewijck, M. et al. 2018. A molecular atlas of cell types and zonation in the brain vasculature. *Nature.* **554**, p475.

Vasioukhin, V. et al. 2000. Directed actin polymerization is the driving force for epithelial cell-cell adhesion. *Cell.* **100**(2), pp.209-19.

Wacker, A. and Gerhardt, H. 2011a. Endothelial development taking shape. *Curr. Opin. Cell Biol.* **23**, pp.676-685.

Wacker, A. and Gerhardt, H. 2011b. Endothelial development taking shape. *Current Opinion in Cell Biology.* **23**(6), pp.676-685.

Wang, S. et al. 2008. Control of endothelial cell proliferation and migration by VEGF signaling to histone deacetylase 7. *Proceedings of the National Academy of Sciences of the United States of America.* **105**(22), pp.7738-7743.

Wang, Y. and Becker, D. 1997. Antisense targeting of basic fibroblast growth factor and fibroblast growth factor receptor-1 in human melanomas blocks intratumoral angiogenesis and tumor growth. *Nat Med.* **3**(8), pp.887-93.

Wang, Y. et al. 2010. Ephrin-B2 controls VEGF-induced angiogenesis and lymphangiogenesis. *Nature.* **465**(7297), pp.483-6.

Ware, J.A. and Simons, M. 1997. Angiogenesis in ischemic heart disease. *Nat Med.* **3**(2), pp.158-64.

Watabe-Uchida, M. et al. 2006. The Rac activator DOCK7 regulates neuronal polarity through local phosphorylation of stathmin/Op18. *Neuron.* **51**(6), pp.727-739.

Wennerberg, K. et al. 2002. RhoG signals in parallel with Rac1 and Cdc42. *J Biol Chem.* **277**(49), pp.47810-7.

West, X.Z. et al. 2012. Integrin beta3 crosstalk with VEGFR accommodating tyrosine phosphorylation as a regulatory switch. *PLoS One.* **7**(2), pe31071.

Weston, L. et al. 2012. Actin nucleators in the nucleus: an emerging theme. *Journal of cell science.* **125**(Pt 15), pp.3519-3527.

Westwick, J.K. et al. 1997. Rac regulation of transformation, gene expression, and actin organization by multiple, PAK-independent pathways. *Mol Cell Biol.* **17**(3), pp.1324-35.

Wilkinson, S. et al. 2005. Cdc42-MRCK and Rho-ROCK signalling cooperate in myosin phosphorylation and cell invasion. *Nat Cell Biol.* **7**(3), pp.255-61.

Wingfield, P.T. 2015. Overview of the purification of recombinant proteins. *Current protocols in protein science.* **80**, pp.6.1.1-6.1.35.

Wu, H. et al. 2014. Discovery of a potent, covalent BTK inhibitor for B-cell lymphoma. *ACS Chem Biol.* **9**(5), pp.1086-91.

Wu, X. et al. 2008. Rac1 activation controls nuclear localization of beta-catenin during canonical Wnt signaling. *Cell.* **133**(2), pp.340-53.

Wu, Y. et al. 2006. The vascular endothelial growth factor receptor (VEGFR-1) supports growth and survival of human breast carcinoma. *Int J Cancer.* **119**(7), pp.1519-29.

Xia, P. et al. 1996. Characterization of vascular endothelial growth factor's effect on the activation of protein kinase C, its isoforms, and endothelial cell growth. *J Clin Invest.* **98**(9), pp.2018-26.

Xia, W. et al. 2006. High levels of protein expression using different mammalian CMV promoters in several cell lines. *Protein Expression and Purification.* **45**(1), pp.115-124.

Xiao, Y. et al. 2013. The atypical guanine nucleotide exchange factor Dock4 regulates neurite differentiation through modulation of Rac1 and actin dynamics. *Journal of Biological Chemistry.*

Xiong, Y. et al. 2009. Vascular endothelial growth factor (VEGF) receptor-2 tyrosine 1175 signaling controls VEGF-induced von Willebrand factor release from endothelial cells via phospholipase C-gamma 1- and protein kinase A-dependent pathways. *J Biol Chem.* **284**(35), pp.23217-24.

Yajnik, V. et al. 2003. DOCK4, a GTPase activator, is disrupted during tumorigenesis. *Cell.* **112**(5), pp.673-684.

Yan, D. et al. 2006. An isoform of GTPase regulator DOCK4 localizes to the stereocilia in the inner ear and binds to harmonin (USH1C). *J Mol Biol.* **357**(3), pp.755-64.

Yanagisawa-Miwa, A. et al. 1992. Salvage of infarcted myocardium by angiogenic action of basic fibroblast growth factor. *Science.* **257**(5075), pp.1401-3.

Yang, J. et al. 2009. *Activation of Rho GTPases by DOCK Exchange Factors Is Mediated by a Nucleotide Sensor.*

Yu, H. et al. 1994. Structural basis for the binding of proline-rich peptides to SH3 domains. *Cell.* **76**(5), pp.933-45.

Yu, J.-R. et al. 2015. TGF-β/Smad signaling through DOCK4 facilitates lung adenocarcinoma metastasis. *Genes & Development.* **29**(3), pp.250-261.

Zhao, Z. and Manser, E. 2015. Myotonic dystrophy kinase-related Cdc42-binding kinases (MRCK), the ROCK-like effectors of Cdc42 and Rac1. *Small GTPases.* **6**(2), pp.81-88.

Zhu, X. et al. 2017. Visualization of Protein-protein Interaction in Nuclear and Cytoplasmic Fractions by Co-immunoprecipitation and In Situ Proximity Ligation Assay. *Journal of visualized experiments : JoVE.* (119), p55218.

Zhuang, G. et al. 2013. Phosphoproteomic analysis implicates the mTORC2-FoxO1 axis in VEGF signaling and feedback activation of receptor tyrosine kinases. *Sci Signal.* **6**(271), pra25.

Zihni, C. and Terry, S.J. 2015. RhoGTPase signalling at epithelial tight junctions: Bridging the GAP between polarity and cancer. *The international journal of biochemistry & cell biology.* **64**, pp.120-125.